2013-4

Polystyrene: A Potential Standard for Developing In Vitro Cellular Tracking Methods for Nanotoxicology

Jennifer Dorney
Technological University Dublin

Polystyrene: A Potential Standard for Developing *In Vitro* Cellular Tracking Methods for Nanotoxicology

By

Jennifer Dorney BSc Hons

A thesis submitted to Dublin Institute of Technology

For the degree of Doctor of Philosophy

School of Physics

Dublin Institute of Technology

Kevin Street, Dublin 8.

April 2013

Declaration

I certify that this thesis which I now submit for examination for the award of doctor of philosophy, is entirely my own work and has not been taken from the work of others save and to the extent that such work has been cited and acknowledged within the text of my work.

This thesis was prepared according to the regulations for postgraduate study by research of the Dublin Institute of Technology and has not been submitted in whole or in part for an award in any other Institute or University.

The work reported on in this thesis conforms to the principles and requirements of the Institute's guidelines for ethics in research.

The Institute has permission to keep, or lend or to copy this thesis in whole or in part, on condition that any such use of the material or the thesis be duly acknowledged.

Signature

_____ Date ____/____/____

Acknowledgements

There are many people who I would like to thank for their support and assistance throughout my project.

Gordon, if it wasn't for you I would have fallen at the first hurdle. Thank you for always sticking by me and believing in me. Your advice and support kept me on the straight and narrow and always helped me overcome anything. Thank you for everything from the bottom of my heart.

I would also like to extend a massive thank you to Prof. Hugh Byrne, for not only helping to get me over that final hurdle, but for all his help throughout my project. Thank you also for affording me this opportunity to complete my studies in an area which I love, to PhD level and for not throwing away my cv! Your knowledge and support had been invaluable and I sincerely thank you for everything.

Mam I don't think you know how much you have been my rock and how much you have done for me over the last, let's say, 10 years of my college life! I would not have gotten through all the ups and downs over the last four years without you. Thank you with all my heart and I hope someday I can begin to repay back everything you've done for me. I'm so lucky to have a best friend like you.

To my brothers Gregory, Ciarán and my sister Rachel, my siblings and best friends in equal measures. And Shelly! Thank you for everything and thanks for always reminding me how long it's taken for me to get here! And a big thank you to my Daddy, Greg, for not only putting up with all of us, but also for always making me laugh. I can't forget Dec and Jen either!

I would like to say a huge thank you to Franck for all his help and knowledge and most importantly, patience, which was tested many times, over the course of the last 4 years. From the bottom of my heart, thank you for all of your help.

I would also like to thank some special friends in my life. Sean, you have stuck with me the whole way through, from that first day in second year to right now! Thank you for being my best friend, and for always being you. You know what you mean to me and thank you for reminding me to always have fun! Tina, your advice, support and

friendship are invaluable. Thank you for always being there for me and I know how lucky I am to have a friend like you.

Dr. Aoife Power (!!!), thank you for always being someone I could turn to in the lab and for our quirky friendship that I cherish so much. Alan O Rourke, thank you for bring some fabulousness into my life! John Brady, our chats are legendary and you'll always listen to me giving out. Marian, thank you for all of your support and guidance. Auds, we've come a long way from school!! Thank you all. Love all you guys and I couldn't have gotten through the last few years without you!

To my fellow 'Nanolabers', Niall and Sanchalli, thank you for making the nanolab a great place to work. Thank you both for your help and advice over the last four years. Niallo, we'll always have Miami.

Rach, Sandar and Lollipops (Rachel, Sandra and Laura!), thank you for adopting me and helping me to get over the final hurdle. You made the tough times easier for me and helped me more than you all could know. I'm so glad to have made such beautiful, fun friends for life.

My special thanks go to Ms Amaya Garcia and Prof Alfonso Blanco for their help, knowledge and expertise.

And finally, I would like to acknowledge the help of the following people over the last few years; Prof Fiona Lyng, Anne Shannan, Dr. Luke O Neill, Dr. Kelvin Poon, Mark Keating and last, but certainly not least, George.

I would like to end with a quote that has helped me through the tough times over the last couple of years;

"Nothing is permanent in this wicked world, not even our troubles".

-Charlie Chaplin.

Abstract

Nanotoxicology has emerged as a discipline of a result of the revolution of nanotechnology. While nanotoxicology is in its infancy, there is a lack of toxicological data for nanoparticles, naturally occurring or commercially produced. The need for information regarding mechanisms associated with nanoparticle uptake by biological cells, as well as internalisation and accumulation of nanoparticles once penetrating cell membranes, is imperative. This project will focus on the internalisation studies of surface modified polystyrene nanoparticles. An *in vitro* lung model consisting of A549 (ATCC No: CRL185), a carcinogenic lung epithelial cell line, was employed to investigate the biocompatibility of nano scaled polystyrene particles in pulmonary systems. Biological effects of 40nm and 100nm carboxylated surface modified nanopolystyrene, 50nm and 100nm neutral nanopolystyrene and 60nm aminated nanopolystyrene were monitored. Prior to cellular studies, a full particle size characterisation was carried out using Dynamic Light Scattering, Atomic Force Microscopy, Zeta Potential and Electronic Spectroscopy. The cytotoxic effects of nano scale 40nm and 100nm carboxylated, 50nm and 100nm neutral nanopolystyrene and 60nm aminated nanopolystyrene were then evaluated using four cytotoxic endpoints, namely the Neutral Red, Alamar Blue, Comassie Blue and MTT assays, with both neutral and carboxylated modified particles exhibiting no cytotoxic effect at any of the concentrations or timepoints examined. Aminated nanoparticles were observed to elicit some toxic effects in cells, over certain test concentrations and exposure times. Cellular internalisation of the fluorescently labelled particles was monitored with the aid of fluorescent confocal microscopy. Nanoparticle internalisation and accumulation within specifically labelled cell organelles was then monitored and verified with the aid of commercially available

transfection labelling kits. Raman microscopy was then employed to spectroscopically image biological cells previously exposed to fluorescently labelled 50nm and 100nm polystyrene nanoparticles. The use of K-means clustering and principal component analysis (PCA), demonstrated that the technique was capable of localising the nanoparticles and identifying the subcellular environment based on the molecular spectroscopic signatures.

List of Abbreviations

3-(4,5-Dimethylthiazol-2-yl)-2,5-diphenyltetrazolium bromide Assay .....MTT

Alamar Blue™ ..... AB

American Type Culture Collection ..... ATCC

Atomic Force Microscopy ..... AFM

Coomassie Brilliant Blue ..... CB

Dulbecco's Modified Eagles Medium ..... DMEM

Dynamic Light Scattering ..... DLS

Foetal Calf Serum ..... FCS

Nanometres ..... nm

Neutral Red ..... NR

Phosphate Buffered Saline ..... PBS

Polystyrene ..... PS

Royal Park Memorial Institute Medium ..... RPMI

Scanning Electron Microscopy ..... SEM

Transmission Electron Microscopy ..... TEM

Zeta Potential ..... ZP

Endoplasmic Reticulum..... ER

Fluorescein-5-isothiocyanate ..... FITC

Principle Component Analysis .....PCA

Surface Enhanced Raman Spectroscopy ..... SERS

Coherent anti-Stokes Raman Spectroscopy ..... CARS

Table of Contents

Chapter 3 Experimental Techniques and Procedures

Chapter 4 Characterisation of Nanopolymers

Chapter 5 Toxicology of Nanopolymers

Chapter 6 Confocal Fluorescent Microscopy

Chapter 8 Discussions and Conclusions

Chapter 1

Introduction to Nanotechnology

1.1 Introduction to Nanotechnology

At a conference on precision engineering in 1974 in Tokyo Science University, Professor, Norio Taniguchi, first used the term "*nanotechnology*" [1].

The concept, however, was previously presented by physicist Richard Feynman at an American Physical Society in 1959. In Feynman's lecture, *"There's Plenty of Room at the Bottom"*, he describes the possible manipulation of atoms and molecules in order to create new materials and devices with a vast range of applications [2]. The massive potential of these materials later became evident, having applications in areas such as medicine, biomaterials and electronics, promising denser computer circuitry, and microscopes with higher resolution than before. His ideas were later realised in the middle of the 1980's, when nanoscience was born with the invention of the Scanning Tunnelling Microscope, eventually leading to many important "nanomaterial" discoveries [3] [4] [5]. Today, nanotechnology has evolved into a highly competitive multidisciplinary research area encompassing an exceptional range of subdivisions from fuel cells [6] to food technology [7] and medical applications [8].

The word "nano" itself refers to the length scale (one nanometre is one billionth of a metre), that is one thousand times smaller than the micro scale, the scale that was traditionally associated with the electronics industry. Viruses and DNA are examples of natural objects on the nanoscale; in contrast to which a human cell can appear enormous. The term nanotechnology refers to the engineering, measurement and understanding of nano-scaled materials and devices. Manipulating matter atom by atom and creating features on the atomic or "nano" scale is now a proven technology and there is an ever growing catalogue of industries that utilise nanotechnology.

Although variations in the exact definition of the term nanotechnology exist, the International Standards Organization, ISO, has defined the area of science as;

'Understanding and control of matter and processes at the nano-scale, typically, but not exclusively, below 100 nanometres in one or more dimensions where the onset of size dependent phenomena usually enables novel applications where one nanometre is one thousand millionth of a metre.' [9]

Sizes at the nano level are incredibly small. To conceptualise, if the distance between the Earth and the Sun was one metre, then the length of one nanometre would be equivalent to the size of a football field. Figure 1.1 attempts to put into context the macro, micro and nano scale. It can be seen from figure 1.1 that there are both manmade and natural nanostructures. Nanostructures have existed in nature since the dawn of time, examples including molecular structures, volcanic ash particles and indeed some proteins and viruses [10] . It is also important to note that such natural structures have existed alongside humans throughout their evolution. Manmade or engineered nanoparticles, are however a relatively new entity in the environment and, due to their undefined bioactivity, pose a potential risk to human and environment health. Examples include self-assembled nanostructures, diesel combustion particles, and structures such as carbon nanotubes [11] [12] [13].

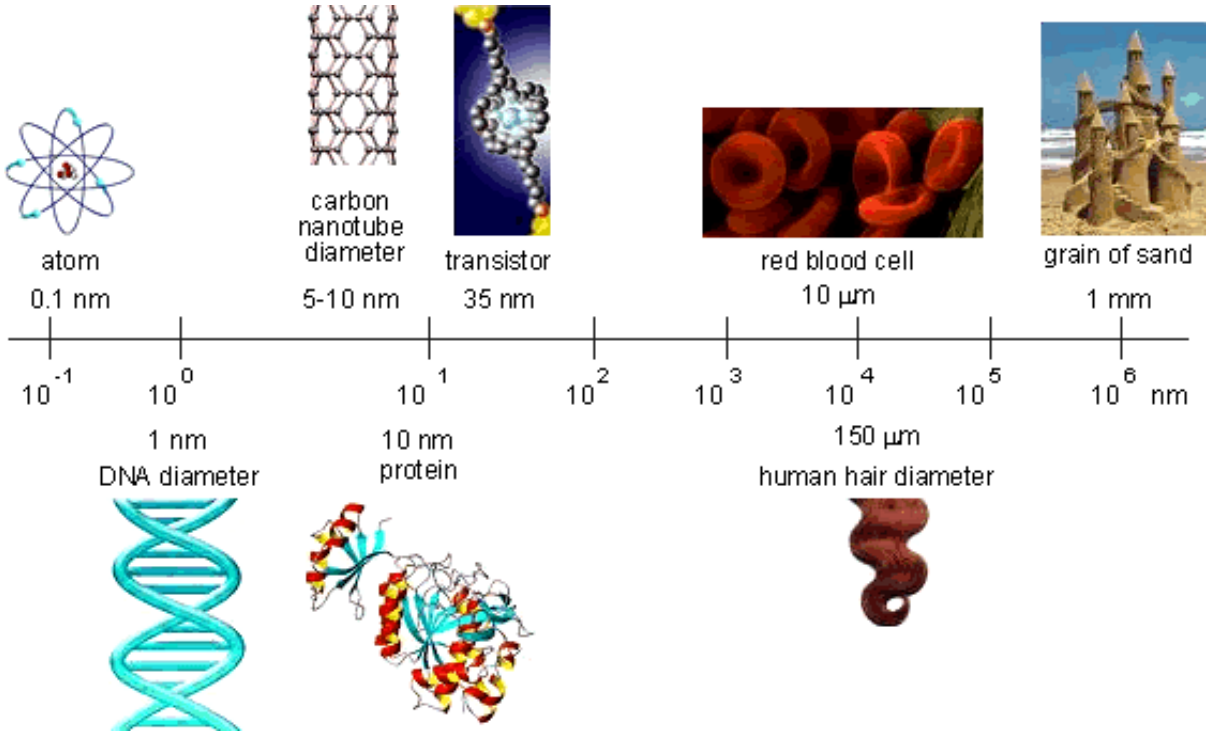

Figure 1.1 The nano-scale, highlighted is the progress from the macro world down to the nano-world with examples of both manmade and natural structures [14].

There are many uses and applications of nanomaterial technology that are not possible using conventional materials. For applications that use a substance's chemical properties, substantially less nanomaterial may be required to do the job of a conventional material. The chemical reactivity of a material is related to its surface area compared to its volume and the surface area for a nanoparticle per unit volume is significantly higher. Figure 1.2 illustrates how surface area increases when a material is dissected into nano sized particles.

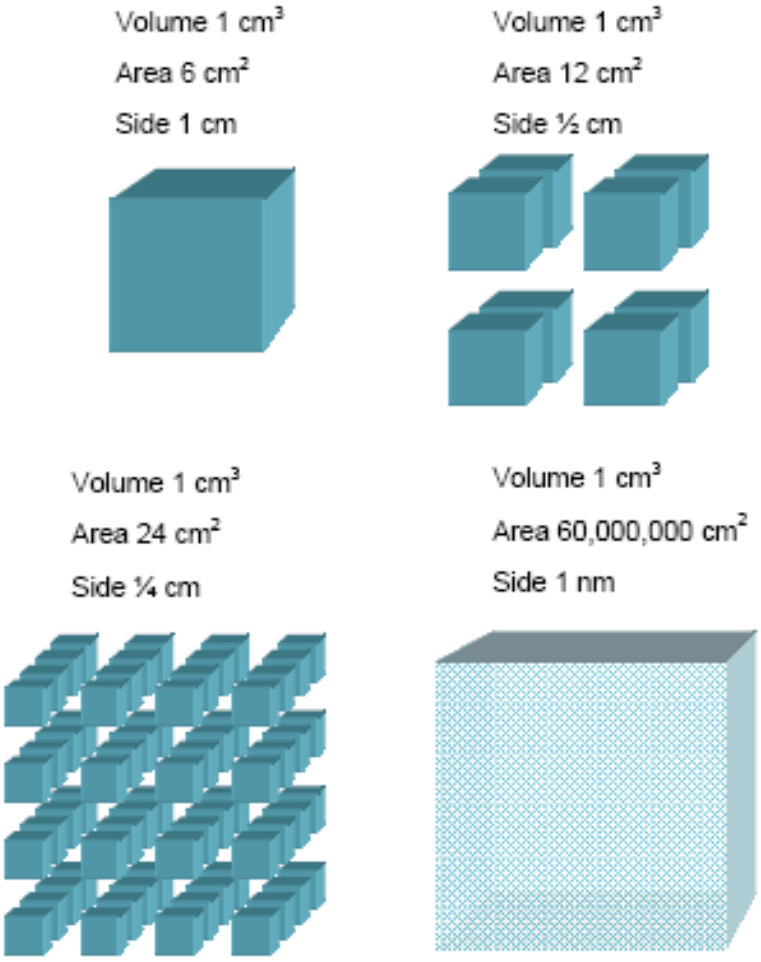

Figure 1.2 Example of how surface area increases with increased dissection of a $1cm^3$ cube into $1nm^3$ cubes [15].

1.2 Engineered Nanoparticles

The production of nanomaterials is one of the main areas in which the nanotechnology sector holds its focus. There are numerous synthetic methods for the production of nanomaterials including physical, chemical and biological approaches. However, most can be divided into either 'top-down' or 'bottom-up' methods. The top down method of fabrication generally involves physical approaches such as lithography and milling. Often described as the traditional approach to nanofabrication, it involves essentially the breaking down of a material

into nano-components [16]. The Bottom-up approach, in contrast to the top down method, is often emphasized in nanotechnology literature, though bottom-up is nothing new in materials synthesis. Typically, in material synthesis a structure is built atom by atom on a very large scale, and has been in industrial use for over a century. Examples include the production of salt and nitrate in chemical industry, the growth of single crystals and deposition of films in the electronics industry [17]. The Bottom-up approach can thus be defined as simply building-up a material atom-by-atom or molecule-by-molecule. The bottom-up approach plays an important role in the fabrication and processing of nanostructures and nanomaterials [18] [19].

1.2.1 Classification of Engineered Nanoparticles

Engineered Nanoparticles, or man-made nanoparticles, have been classified in various ways, according to different academies or agencies. The OECD, for example, have a published a list of representative manufactured nanomaterial of interest, of which the listed nanomaterials may be classified into four different groups;

- Fullerenes and carbon nanotubes
- Metals
- Polymeric
- Semiconductors (quantum dots)

Fullerenes are molecular forms of carbon and constitute 28 to more than 100 atoms, forming a hollow sphere. Carbon nanotubes (CNTs) are crystalline forms of pure carbon, and exist in many sizes. CNTs are composed of cylinders of graphite sheets wound around themselves in one or more layers. The diameter of a CNT can be as small as 0.7 nm and be several mm in length. Fullerenes and CNTs are similar, as

both can be bonded with organic or inorganic groups to form various products. Fullerenes are used in solar and lithium batteries, electronics, storage of gases, such as methane and oxygen and additives to rubber and plastics [20] [21]. CNTs have also been investigated for use in drug delivery. CNT's can be functionalised with various functional groups to improve their solubilisation and to carry simultaneously several moieties for targeting, imaging, and therapy [22]. These moieties can then be delivered into the cytoplasm or the nucleus [23] making antibiotic, antiviral and anti-cancer drug delivery possible [23].

Metallic nanoparticles and oxides are based on inorganic materials such as metals, and derivatives of silicon. These materials differ from molecular or bulk species with their high surface areas and unique optical, magnetic, and electronic properties [24]. They find many uses in high technology areas right down to food storage devices. Examples of inorganic nanoparticles are nZnO, nAg [25]. Examples of metal nanoparticles include nanogold, nanosilver and nanocopper. Their biocompatibility have found use in biomedical sector and can be functionallised as specifically probes of intracellular processes and have been used for targeted drug delivery, vehicles for gene and drug delivery and more importantly diagnostic imaging [26]. For example, with the use of Surface Enhanced Raman Spectroscopy (SERS), nanosilver and nanogold have been used to detect unlabeled DNA [27].

Polymeric nanoparticles are prepared from polymers and are considered potential drug delivery devices due to recent applications in drug targeting to particular organs and tissues. These nanoparticles are also used as DNA in gene therapy and delivery of proteins, peptides and genes through oral route administration. Dendrimers are a type of polymeric nanoparticles constructed by the successive addition of layers of branching groups. The properties of dendrimers are dominated by the functional

groups on the molecular surface [25] [28]. Dendrimers have been proposed to act as artifical proteins, due to their similar shape and size of various proteins, and have also been proposed as nano-scale containers for drug delivery [29] [30].

A quantum dot is a nanoparticle made of any semiconductor material such as silicon, cadmium selenide, cadmium sulfide, or indium arsenide. They are small enough to display quantum mechanical properties; specifically the excitons are confined in all three spatial dimensions. The electronic properties of these materials are intermediate between those of bulk semiconductors and of discrete molecules [31] [32]. Quantum dots have specifically been developed as intracellular probes, as an alternative to conventional stains based on organic dyes [33] [34].

1.3 Potential of Nanotechnology

Countries such as the United States and Japan are investing heavily in the area of nanotechnology with groups not only identifying high-impact application properties, but also carrying out research in all aspects of the nano area, including nano-medicine and nano-electronics. With forecasts of US$2.6 trillion markets by 2015 and estimated employment rates upwards of 2 million people [35], it is not surprising that there are many other nations with strong research centres, including China, Denmark, France, Germany, Russia, Sweden, and the United Kingdom. Nanotechnology is already enhancing everyday products such as sunscreens, golf clubs, clothing, and cell phones [36] [37] [38]. Within the next decade, it is likely to be commonplace in drug therapies, water filters, fuel cells, power lines, computers, and a wide range of other applications [15]. According to the Royal Society:

“Nanotechnologies are widely seen as having huge potential in areas as diverse as healthcare, IT and energy storage.”

Widespread commercial adoption of nanotechnology is growing rapidly. Examples of areas in which nanotechnology is expected to have a high commercial impact include; [39]

- *Embedded nanotechnology* (electronics, optoelectronics, building materials, sports equipment),
- *Films and coatings* (self-cleaning coatings, waterproofing, antimicrobial coatings e.g. medical equipment, food containers and appliances),
- *Biological nanotechnology* (nano-sized motors, medical diagnostics),
- *Manufactured particles* (food and cosmetic additives including sunscreens, anti-microbial uses, pollution clean-up)
- *Nano-electrical mechanical systems (NEMS)* (Drug delivery and diagnostics, smart sensors).

1.4 Concerns Raised

Materials with well known properties and documented toxicity values can exhibit entirely different characteristics when moving from their bulk to their nano state. When a material approaches the nanoscale, certain properties become scale-dependent, particularly in particles below 20nm diameter. These include capillary forces, optical effects/colour, melting points, conductivity, ionization potential, electron affinity, magnetism, and, significantly, surface energy and reactivity [40]. It is generally considered that the smaller the particle, because of the greater surface area to volume ratio, the higher its chemical reactivity and biological activity. In biological cells, it has been shown that the greater chemical reactivity of nanomaterials results in increased production of reactive oxygen species (ROS),

including free radicals among other effects [41]. The large number of variables influencing toxicity means that it is difficult to generalise about health risks associated with exposure to nanomaterials, which brings to light the urgency for each new nanomaterial to be assessed individually and a full toxicological profile assembled with material properties taken into account.

In 2004, the Royal Society and the Royal Academy of Engineering in the UK released a report which recommended a review of existing regulations to assess and control workplace exposure to nanoparticles and nanotubes [42]. The report expressed particular concern for the inhalation of large quantities of nanoparticles by workers involved in the manufacturing process. Assessment of health risks arising from exposure to chemicals or other substances requires understanding of the intrinsic toxicity of the substance, the levels of exposure that may occur (by inhalation, by ingestion or through the skin) and any relationship between exposure and health effects. Concerns about the lack of knowledge and possible risks arising from exposure to nanoparticles led the UK Government to request advice from the Royal Society and Royal Academy of Engineering, resulting in the formation of their Nanoscience and Nanotechnology Working Group. However, with a growing number of nanoparticles being used in consumer products from cosmetics to food and beverage packaging, it is important that the public's perception be guided in the right direction with correct information. Unfortunately the rapid growth in the production and use of nanoparticles has left regulating bodies behind, due to the lack of knowledge of toxicological data. This highlights the need for full characterisation and toxicological study of nanoparticles [42].

1.5 This Thesis

The use of model nanoparticles is imperative when attempting to gain a general understanding of the toxicity of nanoparticles, mechanisms of uptake of nanoparticles by cells as well as identifying particles localised within cells. However, from batch to batch, commercially produced nanoparticles often exhibit variable physical characteristics such as particle sizes, shapes, surface functionality, etc. The consideration of such information is important when choosing model nanoparticles for establishing structural activity relationships between particles and cells.

For these reasons, this study examines three types of surface modified fluorescently labelled polystyrene model nanoparticles, of five different sizes, namely 40nm and 100nm carboxylated nanopolystyrene, 50nm and 100nm neutral nanopolystyrene and 60nm aminated nanopolystyrene. It will explore the preliminary toxicity of these materials using *in vitro* cell culture techniques and will fully characterised the physicochemical properties of each particle in order to investigate any potential link to the any perceived toxicity. The thesis will also aim to obtain information about the possible internalisation of nanopolystyrene particles within lung cells. With the insufficient information provided about nanoparticles internalisation using conventional *in vitro* assays, here a conventional fluorescent microscopic method (confocal microscopy) will be used to explore the internalisation and localisation of fluorescently labelled nanoparticles and their possible internalisation within specific organelles. Also in this thesis, Raman spectroscopy is proposed and investigated as a potential label free method for the verification of generic nanoparticle internalisation and for tracking the intracellular trafficking, local environment and cellular metabolism.

References

1. Taniguchi, N. *On the basic concept of nanotechnology* in *Proceedings of the International Conference on Precision Engineering*. 1974.
2. Feynman, R.P., *There's Plenty of Room at the Bottom* in *Engineering and Science* 1960, California Institute of Technology.
3. Odom, T.W., et al., *Atomic structure and electronic properties of single-walled carbon nanotubes.* Nature, 1998. **391**(6662): p. 62-64.
4. Hafner, J.H., C.L. Cheung, and C.M. Lieber, *Direct Growth of Single-Walled Carbon Nanotube Scanning Probe Microscopy Tips.* Journal of the American Chemical Society, 1999. **121**(41): p. 9750-9751.
5. Mikkelsen, A., et al., *Direct imaging of the atomic structure inside a nanowire by scanning tunnelling microscopy.* Nat Mater, 2004. **3**(8): p. 519-523.
6. Danilov, M. and G. Kolbasov, *Nanocomposites based on chromium oxide and carbon nanotubes for oxygen electrodes of power cells.* Russian Journal of Applied Chemistry, 2010. **83**(6): p. 1010-1014.
7. Chaudhry Q, S.M., Blackburn J, Ross B, Boxall A, Castle L, Aitken R, Watkins R., *Applications and implications of nanotechnologies for the food sector.* Food Additives and Contaminants. , 2008. **25**(3): p. 241-58.
8. Maneerung, T., S. Tokura, and R. Rujiravanit, *Impregnation of silver nanoparticles into bacterial cellulose for antimicrobial wound dressing.* Carbohydrate Polymers, 2008. **72**(1): p. 43-51.
9. ISO, *BUSINESS PLAN, ISO/TC 229, NANOTECHNOLOGIES*. 1997, British Standars Institution.
10. Yuan, G., *Environmental Nanomaterials: Occurrence, Syntheses, Characterization, Health Effect, and Potential Applications.* Journal of Environmental Science and Health, Part A: Toxic/Hazardous Substances and Environmental Engineering, 2005. **39**(10): p. 2545 - 2548.
11. Fendler, J.H., *Self-Assembled Nanostructured Materials.* Chemistry of Materials, 1996. **8**(8): p. 1616-1624.
12. Revell, P.A., *The biological effects of nanoparticles.* Nanotechnology Perceptions 2006. **2**: p. 283–298.
13. Ajayan, P. and O. Zhou, *Applications of Carbon Nanotubes*, in *Carbon Nanotubes*, M. Dresselhaus, G. Dresselhaus, and P. Avouris, Editors. 2001, Springer Berlin / Heidelberg. p. 391-425.
14. Chambers, G., *DIT Lecture Notes Year 1*. 2008.
15. Lloyds, *Risks: Lloyds Emerging Risks Team Report*. 2007.
16. Xia, D., et al., *Top-Down Approaches to the Formation of Silica Nanoparticle Patterns.* Langmuir, 2007. **23**(10): p. 5377-5385.
17. Jimsher N. Aneli, A.J., Stephan Kubica, *Chemistry and Physics of Modern Materials*. 2013: Apple Academic Press Inc.
18. Shimomura, M. and T. Sawadaishi, *Bottom-up strategy of materials fabrication: a new trend in nanotechnology of soft materials.* Current Opinion in Colloid & Interface Science, 2001. **6**(1): p. 11-16.
19. Verma, S., R. Gokhale, and D.J. Burgess, *A comparative study of top-down and bottom-up approaches for the preparation of micro/nanosuspensions.* International Journal of Pharmaceutics, 2009. **380**(1–2): p. 216-222.

20. Dresselhaus, M.S., G. Dresselhaus, and P.C. Eklund, *Science of fullerenes and carbon nanotubes: their properties and applications*. 1996: Academic Press.
21. Thostenson, E.T., Z. Ren, and T.-W. Chou, *Advances in the science and technology of carbon nanotubes and their composites: a review.* Composites science and technology, 2001. **61**(13): p. 1899-1912.
22. Prato, M., K. Kostarelos, and A. Bianco, *Functionalized Carbon Nanotubes in Drug Design and Discovery.* Accounts of Chemical Research, 2007. **41**(1): p. 60-68.
23. Bianco, A., K. Kostarelos, and M. Prato, *Applications of carbon nanotubes in drug delivery.* Current Opinion in Chemical Biology, 2005. **9**(6): p. 674-679.
24. Schrand, A.M., et al., *Metal-based nanoparticles and their toxicity assessment.* Wiley Interdiscip Rev Nanomed Nanobiotechnol, 2010. **2**(5): p. 544-68.
25. Moreno-Vega, A.-I., et al., *Polymeric and Ceramic Nanoparticles in Biomedical Applications.* Journal of Nanotechnology, 2012. **2012**: p. 10.
26. Mody, V.V., et al., *Introduction to metallic nanoparticles.* Journal of Pharmacy and Bioallied Sciences, 2010. **2**(4): p. 282.
27. Papadopoulou, E. and S.E.J. Bell, *Label-Free Detection of Nanomolar Unmodified Single- and Double-Stranded DNA by Using Surface-Enhanced Raman Spectroscopy on Ag and Au Colloids.* Chemistry – A European Journal, 2012. **18**(17): p. 5394-5400.
28. Mukherjee. S, L.F., Garcia. A, Davorena. M, Byrne. H. J. , *Mechanistic studies of in vitro cytotoxicity of Poly(amidoamine) dendrimers in mammalian cells.* Toxicology and Applied Pharmacology, 2010. **Paper accepted. Awaiting Publication.** .
29. Svenson, S. and D.A. Tomalia, *Dendrimers in biomedical applications—reflections on the field.* Advanced Drug Delivery Reviews, 2012. **64, Supplement**(0): p. 102-115.
30. Lee, C.C., et al., *Designing dendrimers for biological applications.* Nat Biotech, 2005. **23**(12): p. 1517-1526.
31. Bawendi, M.G., M.L. Steigerwald, and L.E. Brus, *The Quantum Mechanics of Larger Semiconductor Clusters ("Quantum Dots").* Annual Review of Physical Chemistry, 1990. **41**(1): p. 477-496.
32. Leutwyler, W.K., S.L. Bürgi, and H. Burgl, *Semiconductor clusters, nanocrystals, and quantum dots.* Science, 1996. **271**: p. 933.
33. Resch-Genger, U., et al., *Quantum dots versus organic dyes as fluorescent labels.* Nat Meth, 2008. **5**(9): p. 763-775.
34. Michalet, X., et al., *Quantum dots for live cells, in vivo imaging, and diagnostics.* Science, 2005. **307**(5709): p. 538-544.
35. Peter J M Bartos, J.J.H., Pavel Trtik, Wenzhong Zhu. , *From nanotechnology to new production systems: the EU perspective*, J.J.H. P. J. M. Bartos, P. Trtik, W. Zhu, Editor. 2004, RSC.
36. Stern, S.T. and S.E. McNeil, *Nanotechnology Safety Concerns Revisited.* Toxicological Sciences, 2008. **101**(1): p. 4-21.
37. Benn, T.M. and P. Westerhoff, *Nanoparticle Silver Released into Water from Commercially Available Sock Fabrics.* Environmental Science & Technology, 2008. **42**(11): p. 4133-4139.
38. Vaitheki, K. and R. Tamijetchelvy, *A State Variables Analysis for Emerging Nanoelectronic Devices*, in *Information and Communication Technologies*,

V.V. Das and R. Vijaykumar, Editors. 2010, Springer Berlin Heidelberg. p. 632-637.
39. Walter Klöpffer, *Nanotechnology and Life Cycle Assessment,*. 2007, Woodrow Wilson International Centre for Scholars.
40. Jones, C.a.G., D.W. , *In vitro assessments of nanomaterial toxicity* Advanced Drug Delivery Reviews, 2009. **61**(6): p. 438-456.
41. Nel, A., et al., *Toxic Potential of Materials at the Nanolevel.* Science, 2006. **311**(5761): p. 622-627.
42. Engineering, T.R.S.T.R.A.o., *Nanoscience, and Nanotechnology: Opportunities and Uncertainties*. 2004, The Royal Society & The Royal Academy of Engineering: London

Chapter 2

Introduction to Nanotoxicology

Chapter 2

2.1 Introduction

Despite the huge benefits of nanotechnology, there are concerns regarding the potential toxicity of engineered materials on the nano scale [1]. Indeed the knowledge gaps in assessing and determining the potential toxicity of nanomaterials and nanoparticles may ultimately undermine the area by impacting on public confidence and acceptance of the technology in general [2].

Since the dawn of time, humankind has been routinely exposed to natural ambient or background nanoparticles in the environment, for example SiO_2 in food and water [3]. However, the concentration of natural nanoparticles is generally relatively small, with only occasional increases in the background due to, for example, a volcanic eruption [4]. In contrast, as engineered or manmade nanoparticles become increasingly prevalent in consumer goods and find ever more applications, human exposure to nanoparticles is expected to grow significantly. However, it is unclear whether nanoparticles can cause adverse environmental or health effects. Literature reports have begun to emerge in recent years indicating that some engineered nanoparticles can cause acute toxicity , when compared to their larger counterparts [5] [6]. However, issues with respect to dosing, methodology and indeed basic understanding of mechanisms of nanotoxicity make it difficult to truly identify whether a nanomaterial is toxic or not. Indeed, several international bodies, both governmental and nongovernmental, have highlighted the concerns in appropriately measuring nanotoxicity and have set as a priority the examination of nanoparticles with respect to a number of end points. The most vocal of these bodies has been the Organisation for Economic Co-operation and Development (OECD) which has listed a number of toxicological endpoints as key [7] (Table 2.1).

Table 2.1 List of toxicological endpoints for physical-chemical characterisation of nanoparticles [7].

Physical-Chemical Properties and Material Characterization	***Mammalian Toxicology***
• Agglomeration/aggregation • Water solubility • Representative TEM picture(s) • Particle size distribution • Specific surface area • Zeta potential (surface charge) •Surface chemistry	• Acute toxicity • Repeated dose toxicity • Chronic toxicity • Reproductive toxicity If available: • Developmental toxicity • Genetic toxicity • Experience with human exposure

The focus of this study is on the clear and unambiguous identification of the uptake of model nanopolystyrene particles by human lung cells, the intracellular effects forming the underlying theme. Hence, many of the endpoints listed by the OECD are crucially important when examining the effects of model particle systems on cells in ensuring consistency of nanoparticle physical-chemical properties. To aid later discussion, this chapter will give a brief introduction to toxicology and attempt to develop the concept of nanotoxicology in particular. As part of this study is to focus on particle uptake, a discussion on the mechanisms behind particles entering cells will be given as well as any possible interactions between nanoparticles and biological systems. A discussion of the relevance and choice of nanopolystyrene as a material for this study will also be given, along with its current applications.

2.2 Nanotoxicology

"*Toxicology is the study of the adverse effects of chemical, physical or biological agents on living organisms and the ecosystem, including the prevention and amelioration of such adverse effects*" [8]. Toxicology is an inter-disciplinary science that integrates the principles and methods of many fields. These include chemistry, biology, pharmacology, molecular biology, physiology and medicine. For example, by combining the study of the physiological effects of certain chemical structures and the molecular mechanisms underpinning those effects with their toxicology, a better understanding of the actions of an entire class of chemical substances can evolve.

Nanotoxicology is a new and emerging sub-discipline of toxicology, which is concerned with looking at the toxicological effects caused by particles or materials with at least one dimension less than 100nm. Much of the current understanding of nanotoxicology has evolved from ultra fine particle toxicology performed in the latter part of the last century. Indeed particle toxicology has progressed from the 20th century, when coal and silica induced diseases were discovered, to currently, where the focus has moved to the decreased size of particles as a cause of increased toxicity [9].

However, unlike particle toxicology, nanotoxicology faces a number of challenges and opportunities in the near future. These challenges include to:

- generate an understanding of the biological action of nanomaterials,

- use, communicate and adapt current particle toxicology paradigms,

- bridge know-how between different application areas of nanomaterials,

- communicate findings to the broad public in an increasing relevant society.

To meet these challenges, a number of basic research questions need to be answered. The most relevant ones to this thesis being

1. Can poorly soluble nanoparticles penetrate cell membrane and organelles?
2. What are the properties of nanoparticles that help them to internalise and accumulate within cells (e.g. size, solubility, reactivity) and how do these properties have an effect on particle uptake or toxicity?
3. What are the mechanisms by which cells take up nanoparticles and what mechanisms govern nanoparticle transportation once they have been internalised?
4. How can fluorescent and non fluorescently labelled nanoparticles be tracked or identified within cells?

It is proposed that these questions will be answered over the course of this thesis.

2.2.1 Possible Exposure Pathways of Nanoparticles

Although current knowledge about the exact pathways taken by nanoparticles once inside the body is relatively scant, there is no reason to expect external exposure pathways would vary from the traditional or normal exposure routes.

There are thus three main routes of expose for nanoparticles as follows;

- *Inhalation*: where nanoparticle translocation from the lung into the bloodstream may cause direct effects on the central nervous system, and have the capacity to invoke inflammatory responses in the lung with subsequent effects [10].

- *Dermal contact*: where, upon contact through exposure from products such as sunscreen, nanoparticles penetrate the outer layer of human skin [11].

- *Ingestion*: where nanoparticles may be absorbed through the intestinal lining and translocate into the blood stream and may cause liver damage [12] [13] [14].

Due to potential occupational risks, the examination of nanoparticles through the inhalation pathway has been the subject of much attention and literature reports on this type of exposure far outweigh the other two exposure routes.

The work reported in this thesis is no exception to this and focuses on a lung cell line. The A549 cell line was first developed by D.J Giard in 1972 [15] through the removal and culturing of cancerous lung tissue in the explanted tumour of a 58-year-old Caucasian male. A549 cells are human alveolar basal epithelial cells. These are squamous in nature and responsible for the diffusion of substances, such as water and electrolytes, across the alveoli of lungs. The cells grow adherently, as a monolayer, *in vivo* [16].

Following inhalation, nanoparticles must cross cellular barriers to further enter the body. The walls, or epithelium, of the respiratory tract contain mucous or serous lining fluid. Therefore, depending on the solubility of the nanoparticle, it may remain in the mucous lining for 1 – 2 days, where they may possibly be removed by coughing or to the larynx where they may be swallowed [17]. However, nanoparticles may also be deposited in the pulmonary alveolar region of the lungs, which is the region of the lungs responsible for gas exchange with the blood. This region also forms the termination point of the respiratory tract. Insoluble nanoparticles deposited in this region may be taken up by specialised defence cells called macrophages,

which are located in the alveoli. Remaining particles, not ingested by macrophages, will interact with the cells of the epithelium and be transported into the interstitial spaces. As a result, it is possible for nanoparticles to remain in the lungs for months or even years [17] [18]. While specific sites of contact with nanoparticles are of great interest when examining exposure pathways into the human body, so too are the portal entry of nanoparticles into cells.

2.2.2 Mechanisms of Particle Uptake and Internalisation

The information on mechanisms by which a cell may take-up a particle is vital in order for nanotoxicologists to develop a better understanding of how nanoparticles interact with cells [19]. In order for a substance to enter a cell interior, it must first pass through the plasma membrane. The plasma membrane is a dynamic structure that functions to segregate the chemically distinct intracellular milieu (the cytoplasm) from the extracellular environment by regulating and coordinating the entry and exit of small and large molecules. The uptake of substances is accomplished via a variety of processes that can be described as passive or active (energy requiring). Essentially small molecules, such as amino acids, sugars and ions, can cross the plasma membrane through *diffusion* or *facilitated diffusion*. Diffusion of small molecules across the plasma membrane results in selective permeability to low molecular weight substances and requires the action of essential membrane protein pumps or channels, that drive an electrochemical or concentration gradient [20].

Larger macromolecules must be carried into the cell in membrane-bound vesicles by the folding inward and pinching-off of pieces of the plasma membrane in a process termed *endocytosis*. Endocytosis is a collective term that describes the energy-dependant internalisation of substances which gain entry into a cell without passing

through the cell membrane [21]. Endocytosis occurs by multiple mechanisms that can be divided into two broad subdivisions: *'phagocytosis'* or *'pinocytosis'.*

In the process of phagocytosis, the cell changes shape by sending out projections which are called pseudopodia (false feet). A phagocytic cell, such as a macrophage, may be attracted to a particle such as a bacteria or virus by chemical attractants. This process is called chemotaxis (movement toward a source of chemical attractant). The phagocytic cell sends out membrane projections that make contact with a particle. A receptor – ligand interaction occurs between the phagocytic cell surface and the particle that will be ingested. The pseudopodia then surround the particle and when the plasma membrane sections of the projection meet, membrane fusion occurs. This results in the formation of an intracellular vesicle [22] [23].

Phagocytosis is typically restricted to specialized mammalian cells, whereas pinocytosis occurs in all cells by at least four basic mechanisms: macropinocytosis, caveolae-mediated endocytosis, clathrin-mediated endocytosis (CME) and clathrin- and caveolae-independent endocytosis. These diverse and highly regulated endocytic pathways function to control complex physiological processes such as hormone-mediated signal transduction and immune surveillance. Figure 2.1 displays the pathways of the different mechanisms by which particle uptake into a cell occurs. The endocytic pathways differ with regard to the size of the endocytic vesicle, the nature of the cargo (ligands, receptors and lipids) and the mechanism of vesicle formation [24].

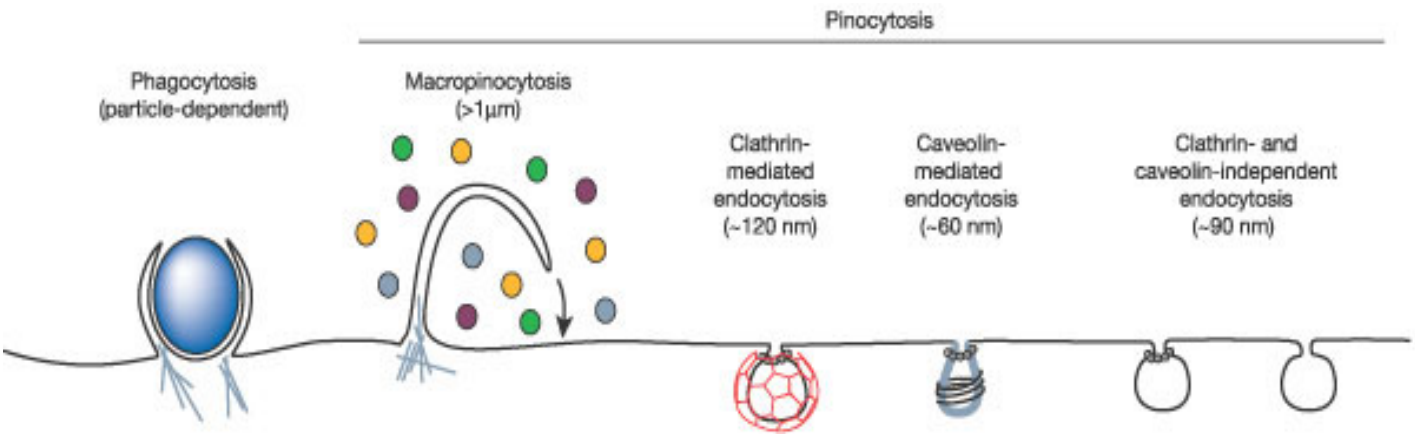

Figure 2.1 Multiple portals of entry into a mammalian cell [24].

In the process of *macropinocytosis,* the plasma membrane forms an invagination, which then pinches off into the cell to form a vesicle filled with a large volume of extracellular fluid and is usually 0.5–5 μm in diameter. Whatever substance is found within the area of the invagination is brought into the cell. In general this material will be dissolved in water and thus this process is also referred to as "cellular drinking", to indicate that liquids and material dissolved in liquids are ingested by the cell [24].

Caveolae are the most common reported non-clathrin coated plasma membrane buds, which exist on the surface of many, but not all cell types. They consist of the cholesterol-binding protein caveolin (Vip21) with a bilayer enriched in cholesterol and glycolipids. Caveolae are small (approx. 50 nm in diameter) flask-shape pits in the membrane which have several functions in signal transduction. They are also believed to play a role in oncogenesis and the uptake of pathogenic bacteria and certain viruses [25] [26].

In the process of *clathrin- and caveolae-independent endocytosis*, small structures referred to as ‘rafts’ occur on the plasma membrane. These rafts are small structures, 40–50 nm in diameter, that diffuse freely on the cell surface. They have a unique lipid composition that provides a physical basis for specific sorting of

membrane proteins and/or glycolipids based on their transmembrane regions. Clathrin-independent mechanisms of endocytosis also occur in neurons and neuroendocrine cells, and function in the rapid recovery of membrane proteins after stimulated secretion [27] [24] [28]. Due to the size of the rafts, it is possible for nanoparticles to enter a cell via clathrin- and caveolae- independent endocytosis.

Clathrin-mediated endocytosis, or CME, occurs in all mammalian cells, and is a process by which cells internalise molecules by the inward budding of plasma membrane vesicles containing proteins with receptor sites specific to the molecules being internalized [24]. These vesicles are approximately ~120nm in size, which suggests a possible portal of entry for nanoparticles 100nm in size or less. The process is responsible for the continuous uptake of essential nutrients, such as the cholesterol-laden low-density lipoprotein (LDL) and particles that bind to the LDL receptor. CME was previously referred to as 'receptor-mediated' endocytosis, but it is now clear that this is a misleading description, because most pinocytic pathways involve specific receptor–ligand interactions [29]. CME is crucial for intercellular communication during tissue and organ development and throughout the life of the organism, as it modulates signal transduction both by controlling the levels of surface signalling receptors, and by mediating the rapid clearance of activated signalling receptors [30] [31]. Figure 2.2 shows the process of clathrin-mediated endocytosis. Clathrin and cargo molecules are assembled into clathrin-coated pits on the plasma membrane together with an adaptor complex called AP-2 that links clathrin with transmembrane receptors, concluding in the formation of mature clathrin-coated vesicles (CCVs). CCVs are then actively uncoated and transported to early/sorting endosomes. [32].

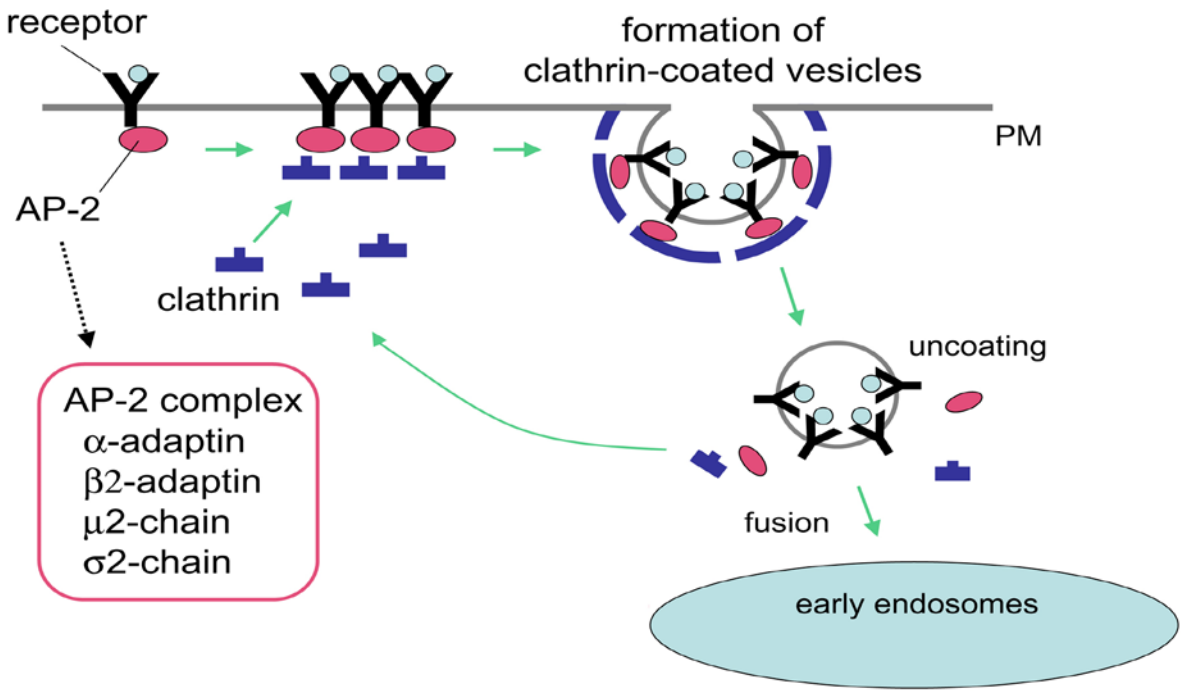

Figure 2.2 Mechanism of clathrin-dependent endocytosis.[33]

The size of the vesicles formed is different for each pathway, e.g. clathrin coated pits are approximately 120nm in diameter, caveolae generally 50 – 80m, and micropinosomes 1 – 5μm. Although the sizes of the vesicles is not definitive and there are exceptions to this general statement made, it is thought that size limits that exist act to restrict the size of the cargo that is internalised, thus introducing a form of selectivity to the endocytoic process [34]. Such pathways therefore are a likely route of uptake of nanoparticles into cells. This is also likely for nanoparticles aggregates or agglomerates that may be broken up or dispersed once entry to the cell has been gained.

It has been demonstrated that engineered nanoparticles of well-defined sizes actively interfere in the processes of regulating and modulating cellular responses [35]. One such study by Rejaman et al, 2004, demonstrated the use of intracellular potassium depletion and pre-treatment of cells with chlorpromazine to inhibit clathrin mediated endocytosis contribution to fluorescent polystyrene-based latex

microspheres. The observation of a size dependant method of uptake suggested that smaller particles (particles up to 200nm) were preferentially internalised via clatrin-mediated endocytosis (the larger of the two bulbs in figure 2.1), and larger particles (>200nm, but smaller than 1µm) via caveolin- mediated endocytosis (the smaller of the two bulbs shown in figure 2.1). Smaller particles were also observed in lysosomes [35].

While particle size has been demonstrated to influence the mechanism of particle uptake by cells, recent observations in biological systems suggest that other physical parameters of nanoparticles can affect their nonspecific uptake in cells, with potential to induce cellular responses. One such study determines the internalisation pathway of positive, negative and neutral charged 89nm and 96nm polyactide polyethylene glycol (PEG)ylated particles. It was determined that negatively charged particles were not internalised by clatherin or caveolin dependant pathways, in contrast to the positively charged nanoparticles that were internalised by these pathways in addition to a smaller contribution of macropinocytosis [36].

However, it is also worth acknowledging that different types of endocytosis can operate simultaneously [35], so that more than one type of internalisation pathway could contribute to their uptake and that if one pathway doesn’t not function, another can take over.

2.2.3 Nanoparticle-Bio Interactions

While physical characteristics have been demonstrated to have an effect on particle uptake mechanism, it is important to examine the interactions between nanoparticles and the biological interface of contact materials such as biological media. This is of particular importance when examining the uptake of nanoparticles within cells *in*

vitro. In laboratory conditions, in order to expose cells to particles, particles are generally suspended within biological media. Biological media, designed to support the growth of cells *in vitro*, is comprised of trace elements, proteins and vitamins required by cells to stay alive. It is a rich source of salts and nitrates, and has an excellent potential for any nanoparticle interaction to occur on contact. These possible interactions may have significant consequences on how a nanoparticle is presented to a cell, and therefore must be examined closely.

The 'nano–bio' interface *"comprises the dynamic physicochemical interactions, kinetics and thermodynamic exchanges between nanomaterial surfaces and the surfaces of biological components"* (for example proteins, membranes, phospholipids, endocytic vesicles, organelles, DNA and biological fluids) [37].

In vitro there are some main concerns when examining the bio-nano interface of nanoparticles suspended in biological medium. These include;

(i) The nanoparticle physicochemical surface characteristics.

(ii) The solid–liquid interface and the changes that occur when the particle interacts with components in the surrounding medium.

It had been demonstrated that physical parameters of nanoparticles can play a role in the interaction of proteins with nanoparticles [38]. It was found that both size and surface properties play a very significant role in determining the nanoparticle interactions with different biological particles such as proteins in biological media [39]. These are factors that can also influence how a nanoparticle is presented to a cell and subsequently influence the cellular uptake mechanism of particles by cells.

It is proposed that particle characteristics contribute actively to the interactions with the medium through: (i) promoting the adsorption of ions, proteins, natural organic materials and detergents; (ii) double-layer formation; and/or (iii) dissolution [40].

Quantifiable properties, such as effective surface charge (zeta potential), particle aggregation, state of dispersion, stability/biodegradability, dissolution characteristics, are all factors which determined the degree of interaction of nanoparticles and the suspending media [6]. Characteristics of the suspending media are also a factor in determining the interactions that may occur at the bio-nano interface, including the ionic strength, pH, temperature and the presence of large organic molecules (for example proteins) or detergents. Interactive forces between the nanoparticle (depending on its own properties) and biological media include long range forces arising from attractive van der Waals and repulsive electrostatic doublelayer interactions, and short range forces arising from charge and solvent interactions [40]. Media interactions (for example protein interactions) could also induce large scale changes, such as nanoparticle dissolution, ion leaching, phase transformation and agglomeration [37].

While information on biological media interaction with suspended nanoparticles could potentially provide invaluable information on how nanoparticles are taken up by cells, it is also important to consider the intracellular fate of nanoparticles upon entry to cells. After internalisation by clathrin mediated endocytosis, the endocytic vesicle delivers its contents to an early endosome (also known as a sorting endosome) [41] The endocytic vesicles fuse with an early endosome, which requires the presence of early endosome antigen -1 protein (involved in endosomal trafficking and vesicle fusion) and Rab5 (involved in the movement of endosomes along the cytoskeleton) on to early endosome membrane. These proteins allow early endosomes to

redistribute their contents to other intracellular locations [42]. For this reason, early endosomes are often called sorting endosomes [43]. The early endosome dictates the sub-cellular distribution of the internalised cargo [34], so that the vesicle is targeted to its appropriate sub-cellular destination. Such destinations include (i) delivery to late endosomes and lysosomes which subsequently target the substance for degradation, (ii) if the cargo is required by the cell it may be delivered to the endoplasmic reticulum (ER) or golgi apparatus [41] or (ii) the substance may be redirected out of the cell by exocytosis [44].

Surface-functionalisation and incorporation of nanoparticles into various organic and inorganic polymers is another area of nanoparticle-bio interaction that is of interest to nanobiologists looking at internalisation and localisation of nanoparticles within cells. Nanoparticles can be specifically functionalised to target certain cell types [45] [46] and even subcellular localisations [47]. Recent reports reveal that the functionalisation of nanoparticles with specific chemical functional groups enhances the nanoparticle functionality and efficiency. It is also reported that this fictionalisation reduces known side effects, due to properties such as targeted localisation in tumours and active cellular uptake [48]. Functionalised SERS active nanoparticles have been shown to be valuable probes of subcellular processes and protein localisation [49] [50] [51].

Current information on the intracellular transportation mechanisms of nanoparticles within cells is poor, although there are reports that nanoparticles can localise within endosomal and lysosomal compartments [52] [53] [54].

2.2.4 Mechanisms of cell death

Although intracellular tracking is important to nanobiologists, there are several substances that are known to cause toxicity at their nano size while being relatively inert in their bulk form. For example, while Zinc is a well know mineral required for healthy brain function, in its nano-sized counterpart as ZnO2 or zinc oxide, it has been found to cause toxicity to living cells [55].

The complexity of proposed mechanisms of cell death caused by nanoparticles, are beyond the scope of this thesis. However, knowing the types of cell death that may occur can give insight into the affect nanoparticles may have on cells.

The two main types of cell death processes are apoptosis (programmed cell death) and necrosis (external factors causing death) [56] [57].

Apoptosis, also known as programmed cell death (PCD), is a process whereby, cells which are no longer needed, commit suicide by activating an intracellular death program. In this process, the cell undergoes a reduction in size as its cellular components break down and condense. The breakdown of cellular components is caused by the release of specific proteins within the cell. The cell then breaks down into smaller fragments called apoptotic bodies. These fragments are enclosed in membranes so as not to harm near-by cells. The dying cell then sends signals to another type cells, known as phagocytic cells, which engulf and destroy the apoptotic bodies without causing an inflammatory reaction or harming neighbouring cells [57].

Necrosis is caused by factors external to the cell or tissue, such as infection, toxins, or trauma that result in the unregulated digestion of cell components. It is regarded as unprogrammed cell death and is less orderly than apoptos. Necrosis is

accompanied by the release of special enzymes, which are stored in the lysosomes, which are capable of digesting cell components or the entire cell itself. The injuries received by the cell may compromise the lysosome membrane, or may initiate an unorganized chain reaction which causes the release in enzymes. Unlike in apoptosis, cells that die by necrosis may release harmful chemicals that damage other cells. Necrosis caused by the exposure of living cells to nanoparticles may undergo several types of internal or cell organelle damage that lead to eventual death [58]. A possible mechanism of toxicity is proposed which involves disruption of the mitochondrial respiratory chain leading to production of (reactive oxygen species or free radicals) ROS and interruption of ATP synthesis, which in turn cause DNA damage. [59]

2.3 Polystyrene and Nanopolystyrene

2.3.1 Choice of Material

Polystyrene is a commonly used and well known polymer, with many applications in everyday life; interestingly it also has a nano-counterpart which is the primary focus of this thesis. The choice of nanopolystyrene was solely influenced by the explicit inclusion of the material in the OECD's list of nanomaterials requiring immediate investigation with respect to determining both a human and an environmental risk assessments [7]. The chosen polystyrene nanoparticles are commercially available in different sizes, surface modifications, are fluorescently labelled and are used as immunofluorescent reagents, microinjectable cell tracers as well as standards for traceability and calibration reagents for microscopy and flow cytometry [60] . The

chosen particles are therefore considered as good model particles to investigate and examine nanopolystyrene-cellular interactions.

2.3.2. Polystyrene

Polystyrene is an aromatic polymer that is made from the monomer styrene. It is a long hydrocarbon chain with every second carbon connected to the phenyl group. Styrene is an aromatic monomer, commercially manufactured from petroleum. Polystyrene is a vinyl polymer, manufactured from the styrene monomer by free radical vinyl polymerization. The attractive forces at play in polystyrene are mostly due to short range Van der Waals attractions between chains. Figure 2.3 shows the repeating monomer unit of styrene that make polystyrene.

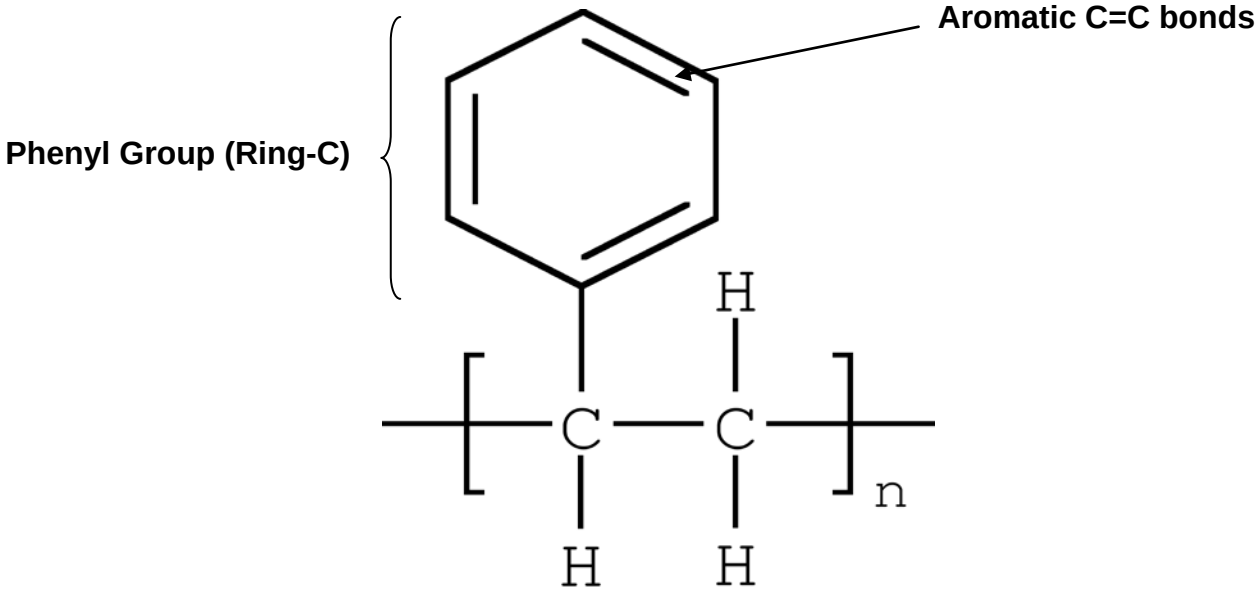

Figure 2.3 Repeating unit of Polystyrene (Styrene Monomer)[61].

Products containing styrene include insulation, fibreglass, plastic pipes, automobile parts, shoes, drinking cups and other food containers [62]. Most of these products contain styrene linked together in a long chain (polystyrene) as well as unlinked styrene. Low levels of styrene also occur naturally in a variety of foods such as fruits,

vegetables, nuts, beverages, and meats [63]. In addition, small amounts of styrene can be transferred to food from styrene-based packaging material [64]. Polystyrene is a rigid, transparent thermoplastic, which is present in solid or glassy state at normal temperature. However, once heated above its glass transition temperature, the polymer turns to a liquid state and can be moulded or extruded. Polystyrene related products are mostly everyday, widely available consumer products. The largest market for polystyrene presently is packaging, such as food and dairy containers, closures, lids, produce baskets, vending cups and fast food containers [65].

While polystyrene is widely used in an enormous variety of products, there are many styrene related products also available. For example, styrene sulfonate polymers are used in wound dressings and are used for the coating of implantable medical devices. Modern medical devices generally contain one or more polymeric region, with styrene one of the more widely used polymers in the medical device sector. Medical devices from which a therapeutic agent is released also require suitable materials for use that will typically exhibit a release profile appropriate for the disease or condition being treated. For example, numerous polymer-based medical devices have been developed for the delivery of therapeutic agents to the body. Examples include drug eluting coronary stents, which are commercially available from Boston Scientific Corp.

Polystyrene in its bulk form is non-toxic. There are currently no international bodies that define polystyrene as toxic or as having carcinogenic effects to humans [66]. While there are no reported toxic effects from polystyrene, the majority of reports published examine the toxicity of the monomer styrene. The World Health Organisation (WHO) published a report in 2003 [67] in which it revealed that it

classifies styrene to have a low acute toxicity. The report revealed that controlled laboratory studies in animals and humans have shown that uptake of styrene is rapid and that it is widely distributed to the whole body with a preference for lipids. Elimination from lipid deposits is slower (half-life 2–4 days) than from other tissues. The findings also revealed there is no tendency towards long-term accumulation. Styrene is bio-transformed mainly to styrene-7,8-oxide which occurs in the liver as well as in a number of other tissues and organs. The report also revealed that findings showed that a small percentage of the dose absorbed is excreted unchanged in the expired air in both laboratory animals and humans after exposure via various routes. More than 90% of an oral dose is excreted rapidly as metabolites, mainly via the urine. In general, the metabolites in the urine of laboratory animals and humans were found to be qualitatively the same, but the amounts were species-dependent. [67]. Other reports have also found that bronchitis, emphysema, and asthma was not associated with long term human exposure to styrene [68].

2.3.3 Nanopolystyrene

While one can conclude from findings discussed in the previous section, that polystyrene in its nano form would make an excellent candidate for therapeutic drug delivery materials or to be used in *in vivo* bioimaging or for quantitative dosage requirements, nanopolystyrene is technically a new material with little verifiable toxicological data available for it, as with most nanomaterials due to difficulties with test methods and reproducibility.

As previously discussed in Chapter 1, Section 1.3, materials with well known properties and documented toxicity values can exhibit entirely different characteristics when moving from their bulk to their nano state [69] . Modifications of

the physicochemical properties of the bulk material can create the opportunity for increased uptake and interaction with biological tissues. This combination of effects can generate adverse biological effects in living cells that would not otherwise be possible with the same material in larger form, be they desirable effects or undesirable [6]. So, while polystyrene and even styrene, in their bulk form may be non toxic, it is imperative for a full toxicological profile to be conducted for nanopolystyrene before it can be considered for use for *in vivo* development.

The nanopolystyrene particles used throughout this thesis are three types of commercially available, surface modified fluorescent and non-fluorescent nanopolystyrene beads. The properties and specifications of these nanoparticles will be discussed in Chapter 3, Section 3.1, with details of their properties and specifications. While the nanoparticles tested are of similar size (40nm, 50nm, 60nm and 100nm), the different surface charges on each particle will allow for comparison of aggregation states in different dispersants, potential toxicity to cells, internalisation and accumulation rates within cells and other properties related to surface charge.

2.4 Chapter Summary

Throughout this chapter, the discipline of toxicology, incorporating nanotoxicology, was presented. Particle uptake mechanisms were examined with recent literature results on nanoparticle uptake mechanisms also presented, describing several different methods that may be possible for nanoparticles to be taken up by cells. The nanoparticle bio-interface was examined, describing studies where the physical parameters of nanoparticles have played a role in the interaction of proteins with nanoparticles. Information on the polymer, polystyrene, used throughout this thesis, was also presented.

Nanoparticles have greater potential to travel through living cells than other materials or larger particles. The various interactions of nanoparticles with fluids, cells, and tissues need to be considered, starting at the portal of entry and then via a range of possible pathways towards target organs. The potential for significant biological response at each of these sites requires investigation. While nanotoxicology as a discipline is still in its infancy, there have been great concerns expressed at the current protocols used for nanotoxicology and the possible inaccuracies they may possess. There have been numerous reports expressing concern that new protocols should be developed for testing of all materials in the nanoscale, where there is the potential for substantial human exposure. With some known non toxic materials in their bulk form exhibiting toxic effects in their nano form, the need for nanoparticle toxicology profiling is imperative.

The following chapter will discuss the techniques used throughout this thesis as the tools used in building a physical chemical characteristic profile which will directly

allow for the production of a toxicological profile to begin. Details of techniques will be described with relevant theory provided for each section.

References

1. Brumfiel, G., *Nanotechnology: A little knowledge.* Nature, 2003. **424**(6946): p. 246-248.
2. Waldron, A., D. Spencer, and C. Batt, *The current state of public understanding of nanotechnology.* Journal of Nanoparticle Research, 2006. **8**(5): p. 569-575.
3. Wang, F., et al., *Oxidative stress contributes to silica nanoparticle-induced cytotoxicity in human embryonic kidney cells.* Toxicology in Vitro, 2009. **23**(5): p. 808-815.
4. Maynard, R., Howard B, eds., *Particulate matter: Properties and effects upon health*. 1999.: Oxford: Bios

Scientific Publishers.

5. Chen, Z., et al., *Acute toxicological effects of copper nanoparticles in vivo.* Toxicology Letters, 2006. **163**(2): p. 109-120.
6. Nel, A., et al., *Toxic Potential of Materials at the Nanolevel.* Science, 2006. **311**(5761): p. 622-627.
7. OECD, *List of manufactured nanomaterials and list of endpoints for phase one of The oecd testing programme*, in *Series on the safety of manufactured nanomaterials*

Number 6. 2008.

8. Toxicology, T.S.o. *What is Toxicology?* 2013; Available from: http://www.toxicology.org/ms/aboutsot.asp.
9. Gardner, D.E., *A Review of "Particle Toxicology".* Inhalation Toxicology, 2007. **19**(9): p. 787-788.
10. Paul, J.A.B., Wolfgang, Kreyling, *Toxicological Hazards of Inhaled Nanoparticles-Potential Implications for Drug Delivery.* Journal of Nanoscience and Nanotechnology, 2004. **4**: p. 521-531.
11. Nohynek, G.J., et al., *Grey Goo on the Skin? Nanotechnology, Cosmetic and Sunscreen Safety.* Critical Reviews in Toxicology, 2007. **37**(3): p. 251-277.
12. Wang, L., et al., *Toxicity of CdSe Nanoparticles in Caco-2 Cell Cultures.* Journal of Nanobiotechnology, 2008. **6**(1): p. 11.
13. Hussain, S.M., et al., *In vitro toxicity of nanoparticles in BRL 3A rat liver cells.* Toxicology in Vitro, 2005. **19**(7): p. 975-983.
14. Revell, P.A., *The biological effects of nanoparticles.* Nanotechnology Perceptions 2006. **2**: p. 283–298.
15. Giard, D.J., et al., *In vitro cultivation of human tumors: establishment of cell lines derived from a series of solid tumors.* J Natl Cancer Inst, 1973. **51**(5): p. 1417-23.
16. ATCC. *A549 Cell Line. Product Number CCL-185*™. 2010.
17. Borm, P., et al., *The potential risks of nanomaterials: a review carried out for ECETOC.* Particle and Fibre Toxicology, 2006. **3**(1): p. 11.
18. Donaldson, K., et al., *Combustion-derived nanoparticles: A review of their toxicology following inhalation exposure.* Particle and Fibre Toxicology, 2005. **2**(1): p. 10.
19. Buzea C, P.I., Robbie K., *Nanomaterials and nanoparticles: sources and toxicity.* Biointerphases, 2007. **Dec;2** (4): p. 17-71.
20. Carruthers, A., *Facilitated diffusion of glucose.* Physiol. Rev., 1990. **70**(4): p. 1135-1176.

21. Johannes, L. and C. Lamaze, *Clathrin-Dependent or Not: Is It Still the Question?* Traffic, 2002. **3**(7): p. 443-451.
22. May, R. and L. Machesky, *Phagocytosis and the actin cytoskeleton.* J Cell Sci, 2001. **114**(6): p. 1061-1077.
23. Tan S Y, M., JD and Dee M K*, *Elie Metchnikoff (1845–1916): discoverer of phagocytosis.* Singapore Med J, 2009. **50**(5): p. 457.
24. Conner, S.D. and S.L. Schmid, *Regulated portals of entry into the cell.* Nature, 2003. **422**(6927): p. 37-44.
25. Pelkmans, L., *Secrets of caveolae- and lipid raft-mediated endocytosis revealed by mammalian viruses.* Biochimica et Biophysica Acta (BBA) - Molecular Cell Research, 2005. **1746**(3): p. 295-304.
26. Anderson, R.G.W., *THE CAVEOLAE MEMBRANE SYSTEM.* Annual Review of Biochemistry, 1998. **67**(1): p. 199-225.
27. Edidin, M., *Shrinking patches and slippery rafts: scales of domains in the plasma membrane.* Trends in Cell Biology, 2001. **11**(12): p. 492-496.
28. Kirkham, M., et al., *Ultrastructural identification of uncoated caveolin-independent early endocytic vehicles.* The Journal of Cell Biology, 2005. **168**(3): p. 465-476.
29. Schmid, S.L., *CLATHRIN-COATED VESICLE FORMATION AND PROTEIN SORTING:An Integrated Process.* Annual Review of Biochemistry, 1997. **66**(1): p. 511-548.
30. Di Fiore, P.P. and P. De Camilli, *Endocytosis and Signaling: An Inseparable Partnership.* Cell, 2001. **106**(1): p. 1-4.
31. Seto, E.S., H.J. Bellen, and T.E. Lloyd, *When cell biology meets development: endocytic regulation of signaling pathways.* Genes & Development, 2002. **16**(11): p. 1314-1336.
32. Brodsky, F.M., et al., *BIOLOGICAL BASKET WEAVING: Formation and Function of Clathrin-Coated Vesicles.* Annual Review of Cell and Developmental Biology, 2001. **17**(1): p. 517-568.
33. Grant, B., Sato M. , *Intracellular Trafficking*, J.M.K.a.D.G. Moerman., Editor. 2006, Wormbook: Department of Molecular Biology and Biochemistry, Rutgers University, Piscataway, NJ 08854 USA.
34. Patel, L., J. Zaro, and W.-C. Shen, *Cell Penetrating Peptides: Intracellular Pathways and Pharmaceutical Perspectives.* Pharmaceutical Research, 2007. **24**(11): p. 1977-1992.
35. Rejman, J.O., Volker Zuhorn, Inge S Hoekstra, Dick, *Size-dependent internalization of particles via the pathways of clathrin- and caveolae-mediated endocytosis.* Biochem. J., 2004. **377**(1): p. 159-169.
36. Harush-Frenkel, O., et al., *Surface Charge of Nanoparticles Determines Their Endocytic and Transcytotic Pathway in Polarized MDCK Cells.* Biomacromolecules, 2008. **9**(2): p. 435-443.
37. Nel, A.E.M., Lutz Velegol, Darrell Xia, Tian Hoek, Eric M. V. Somasundaran, Ponisseril Klaessig, Fred Castranova, Vince Thompson, Mike, *Understanding biophysicochemical interactions at the nano-bio interface.* Nat Mater, 2009. **8**(7): p. 543-557.
38. Minchin, R.F. and D.J. Martin, *Minireview: Nanoparticles for Molecular Imaging--An Overview.* Endocrinology, 2010. **151**(2): p. 474-481.
39. Lundqvist. M, S.J., Elia. G, Lynch. I, Cedervall. T, and Dawson. K.A. , *Nanoparticle size and surface properties determine the protein corona with*

possible implications for biological impacts. PNAS, 2008. **105**(38): p. 14265 - 14270
40. Min, Y., et al., *The role of interparticle and external forces in nanoparticle assembly.* Nat Mater, 2008. **7**(7): p. 527-538.
41. Gruenberg, J. and F.G. van der Goot, *Mechanisms of pathogen entry through the endosomal compartments.* Nat Rev Mol Cell Biol, 2006. **7**(7): p. 495-504.
42. Liu, J. and J.I. Shapiro, *Endocytosis and Signal Transduction: Basic Science Update.* Biological Research For Nursing, 2003. **5**(2): p. 117-128.
43. Gruenberg, J., *The endocytic pathway: a mosaic of domains.* Nat Rev Mol Cell Biol, 2001. **2**(10): p. 721-730.
44. Medina-Kauwe, L.K., *"Alternative" endocytic mechanisms exploited by pathogens: New avenues for therapeutic delivery?* Advanced Drug Delivery Reviews, 2007. **59**(8): p. 798-809.
45. Weissleder, R., et al., *Cell-specific targeting of nanoparticles by multivalent attachment of small molecules.* Nat Biotech, 2005. **23**(11): p. 1418-1423.
46. Tiwari, P., et al., *Functionalized Gold Nanoparticles and Their Biomedical Applications.* Nanomaterials, 2011. **1**(1): p. 31-63.
47. Kneipp, J., et al., *In Vivo Molecular Probing of Cellular Compartments with Gold Nanoparticles and Nanoaggregates.* Nano Letters, 2006. **6**(10): p. 2225-2231.
48. Subbiah, R., M. Veerapandian, and K.S. Yun, *Nanoparticles: functionalization and multifunctional applications in biomedical sciences.* Curr Med Chem, 2010. **17**(36): p. 4559-77.
49. Schlücker, S., *SERS Microscopy: Nanoparticle Probes and Biomedical Applications.* ChemPhysChem, 2009. **10**(9-10): p. 1344-1354.
50. Qian, X., et al., *In vivo tumor targeting and spectroscopic detection with surface-enhanced Raman nanoparticle tags.* Nat Biotech, 2008. **26**(1): p. 83-90.
51. Kneipp, J., et al., *Novel optical nanosensors for probing and imaging live cells.* Nanomedicine: Nanotechnology, Biology and Medicine, 2010. **6**(2): p. 214-226.
52. Clift, M.J.D., et al., *The impact of different nanoparticle surface chemistry and size on uptake and toxicity in a murine macrophage cell line.* Toxicology and Applied Pharmacology, 2008. **232**(3): p. 418-427.
53. Li, W. and et al., *The translocation of fullerenic nanoparticles into lysosome via the pathway of clathrin-mediated endocytosis.* Nanotechnology, 2008. **19**(14): p. 145102.
54. Mukherjee. S, L.F., Garcia. A, Davorena. M, Byrne. H. J. , *Mechanistic studies of in vitro cytotoxicity of Poly(amidoamine) dendrimers in mammalian cells.* Toxicology and Applied Pharmacology, 2010. **Paper accepted. Awaiting Publication.** .
55. Li, J.-h., et al., *Toxicity of nano zinc oxide to mitochondria.* Toxicology Research, 2012. **1**(2): p. 137-144.
56. Boobis, A.R., D.J. Fawthrop, and D.S. Davies, *Mechanisms of cell death.* Trends in pharmacological sciences, 1989. **10**(7): p. 275-280.
57. Buja, L., M.L. Eigenbrodt, and E.H. Eigenbrodt, *Apoptosis and necrosis. Basic types and mechanisms of cell death.* Archives of pathology & laboratory medicine, 1993. **117**(12): p. 1208-1214.

58. Proskuryakov, S.Y., A.G. Konoplyannikov, and V.L. Gabai, *Necrosis: a specific form of programmed cell death?* Experimental cell research, 2003. **283**(1): p. 1-16.
59. AshaRani, P.V., et al., *Cytotoxicity and Genotoxicity of Silver Nanoparticles in Human Cells.* ACS Nano, 2008. **3**(2): p. 279-290.
60. Invitrogen. *FluoSpheres® Carboxylate-Modified Microspheres, 0.04 µm, Yellow-Green Fluorescent (505/515), 5% solids - azide free*. 2005; Available from: https://products.invitrogen.com/ivgn/product/F8795?ICID=search-f8795.
61. GCSE., E.C.I. 2013; Available from: https://sites.google.com/site/internationalgcsechemistry/year-11-topics/topic-5---synthetic-polymers-double-award/2---finding-the-monomer-from-the-polymer.
62. Ahmad, M. and A.S. Bajahlan, *Leaching of styrene and other aromatic compounds in drinking water from PS bottles.* Journal of Environmental Sciences, 2007. **19**(4): p. 421-426.
63. ATSDR, *TOXICOLOGICAL PROFILE FOR STYRENE*. 2007, U.S. DEPARTMENT OF HEALTH AND HUMAN SERVICES: Atlanta, Georgia.
64. Cohen JT, C.G., Charnley G, Coggon D, Delzell E, Graham JD, Greim H, Krewski D, Medinsky M, Monson R, Paustenbach D, Petersen B, Rappaport S, Rhomberg L, Ryan PB, Thompson K., *A comprehensive evaluation of the potential health risks associated with occupational and environmental exposure to styrene.* Journal of Toxicology and Environmental Health Part B: Critical Review, 2002. **5**(1-2): p. 1-265.
65. Schellenberg, J. and H.J. Leder, *Syndiotactic polystyrene: Process and applications.* Advances in Polymer Technology, 2006. **25**(3): p. 141-151.
66. Snyder, J., *Styrene Not a Human Carcinogen, Does Not Contain BPA*. 2009, Styrene Information and Research Center (SIRC),: Arlington, Va. .
67. (WHO), W.H.O., *Styrene in Drinking-water*, in *Guidelines for drinking-water quality.* , 2, Editor. 2003.
68. Welp, E., et al., *Exposure to styrene and mortality from nonmalignant respiratory diseases.* Occupational and Environmental Medicine, 1996. **53:**: p. 499-501.
69. Jones, C.a.G., D.W. , *In vitro assessments of nanomaterial toxicity* Advanced Drug Delivery Reviews, 2009. **61**(6): p. 438-456.

Chapter 3

Experimental Techniques and Procedures

Chapter 3

3.1 Introduction

This chapter further describes the general experimental techniques used in characterising and assessing the cytotoxic effects of the nanoparticles used, and briefly details the characteristics of the particles themselves. Details of microscopic and spectroscopic experimental techniques used to examine the internalisation and tracking of the nanoparticles are also discussed. A brief introduction to the underlying theory for each techniques is initially discussed, after which the general experimental arrangement and sample preparation is detailed. Further details of more specific arrangements or sample preparations will be given in the relevant results chapters as required.

3.2 The Nanoparticles

As mentioned in Chapter 2, Section 2.2, the particles chosen for this study are polystyrene based nanoparticles. The explicit inclusion of nanopolystyrene in the OECDs list of nanomaterials requiring immediate investigation was a determining factor in the choice of material used throughout this study. The choice of particle was also based on the known properties of the bulk materials, specifically the fact that polystyrene is known to be inert and has a variety of applications in consumer and medical goods, including food packaging and medical devices [1]. Significantly, polystyrene is also used as a substrate material in cell culture, were the cell adhesion on the polystyrene surface is so strong that cell detachment requires an enzymatic treatment (i.e. trypsinisation). In addition, applications of nano-polystyrene in the medical device sector are emerging [2].

In this study, bulk polystyrene obtained from Sigma Aldrich [product code 331651] was used as a control material and was subjected to the same characterisation and analysis as its nano-counterparts. The nanoparticles chosen were 40nm and 100nm carboxylated nanopolystyrene, 60nm aminated nanopolystyrene and, 50nm and 100nm neutral nanopolystyrene. The 40nm and 100nm carboxylated polystyrene, known by the trade name of *FluoroSpheres® Fluorescent Microspheres* were purchased from Invitrogen (USA) (product codes for 40nm and 100nm particles F-8795 and F-8803 respectively). They emit in the yellow-green region of the spectrum when excited using a 488nm laser line and are coated with a hydrophilic polymer containing multiple carboxcylic acid groups. The carboxylated polymer coating renders the surface effectively anionic. The 50nm and 100nm neutral polystyrene, known as *Fluorescent Microsphere Suspensions*, were purchased from Duke Scientific Corporation, now Thermo Scientific. They are internally dyed using the company's *Firefli*® process and emit in the green region of the spectrum. The 60nm aminated nanoparticles, or the polyethylenaimine polystyrene nanoparticles, were manufactured and supplied by the Centre for BioNano Interactions (UCD, Ireland). Briefly, these PEI-PS particles were synthesised from carboxylated polystyrene NPs (also manufactured by UCD), whereby the carboxylate surface group reacts with the amine of the polyethyleneimine using EDAC (N-(3-Dimethylaminopropyl)-N′-ethylcarbodiimide hydrochloride) as a dehydrating agent. These are the only nanoparticles used throughout this thesis that are not internally dyed with a fluorescent material and are not visible under a fluorescent microscope. The aminated polymer coating renders the surface effectively cationic.

The chosen polystyrene nanoparticles are commercially available in different sizes, surface modifications, are fluorescently labelled (with the exception of the aminated nanoparticles) and are used as immunofluorescent reagents, microinjectable cell tracers as well as standards for traceability and calibration reagents for microscopy and flow cytometry and are considered as excellent model particles for *in vitro* investigation. The size and chemical nature of all five particles were chosen to facilitate a comparison between the effect of size, surface charge and functionalisation on the cellular uptake of nano-polystyrene. Furthermore, literature reports indicate that particle sizes of less than 100nm are optimum for internalization [3]. While below 20nm in diameter, polystyrene particles cannot be clearly distinguished as individual particles in techniques such as confocal microscopy [4]. The particle sizes in this study therefore were chosen to fit within the range of published particle sizes optimum for cellular uptake and detection.

3.3 Nanoparticle Characterisation

All nanoparticles were characterized in-house to confirm the manufacturer's specifications and the stability of the particles. The particles were also characterised in cell culture media in order to determine the physiochemical properties of the particles in the media of exposure e.g. particle size in the media etc. This information is crucial prior to any cytotoxic testing if a valid traceable set of experiments is to be preformed [5]. As previously discussed in chapter 2, a comprehensive characterisation of the physical and chemical properties is vital in order to elucidate and interpret any adverse cellular effects. Indeed, the OECD working group on Nanomaterials, amongst others, has specified several physiochemical parameters which they recommend be tested in

advance of evaluating the toxicity of a nanomaterial [6]. However, as discussed in chapter 2, these recommendations specify a range of characterisation techniques properties which is often beyond the capabilities of any one laboratory. For this reason, this study will routinely characterize particle size, aggregation state, particle stability in solution and the fluorescence stability of the particles, in water and in culture medium, prior to conducting any cytotoxicity. The importance and relevance of the property measured will be discussed in more detail in the 4th chapter.

3.3.1 Particle sizing: Atomic Force Microscopy

The Atomic Force Microscope (AFM) is an instrument that can analyze and characterize samples at the microscopic level with a resolution of 100 μm to less than 1nm.

The AFM operates by allowing an extremely fine sharp tip to come in contact or in very close proximity to the sample that is being imaged. This tip is usually on the order of 100 μm long and less than 100Å in diameter. The tip is located at the free end of a cantilever under which the sample is scanned. Between the tip and the sample a variety of forces exist depending on the situation. For example, there can be mechanical contact forces, capillary forces, chemical bonding, or electrostatic forces acting between the sample surface and the tip. The most common contributions however are from van der Waals forces. These forces will either attract or repel the tip. The relation between the effect of forces and distance from the tip is shown in Fig. 3.1.

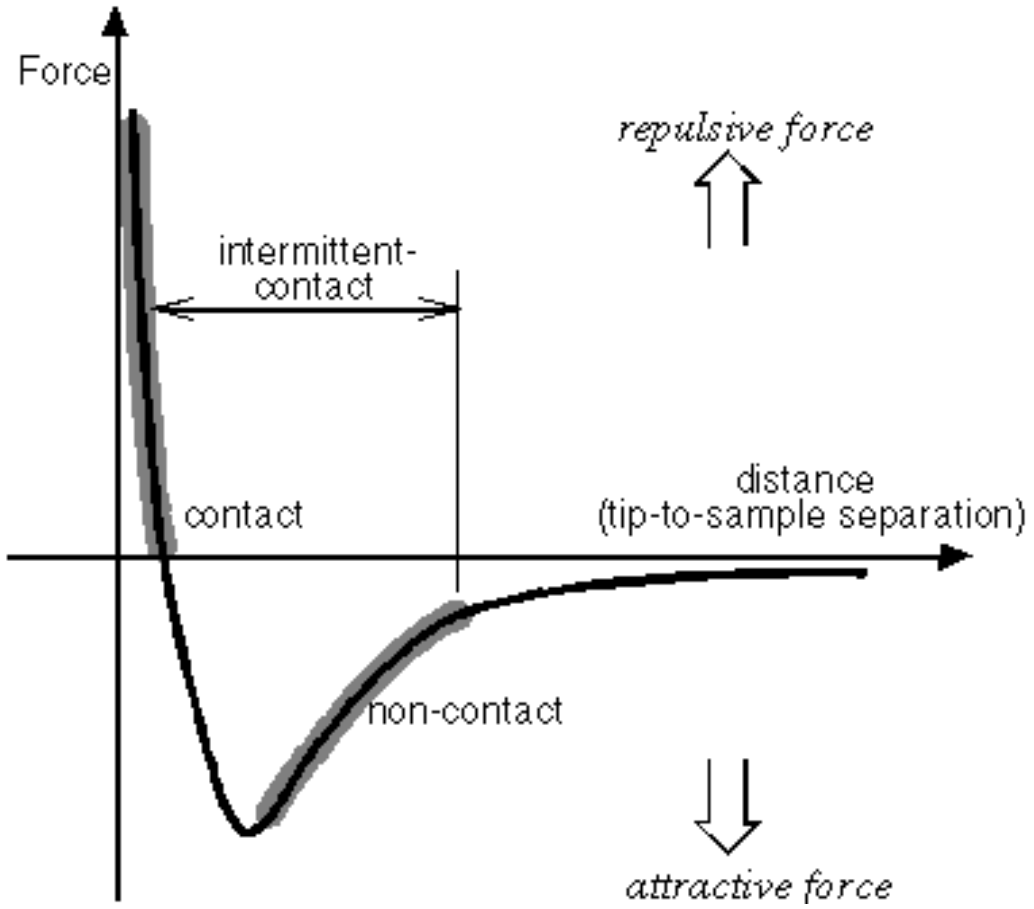

Figure 3.1 Schematic representations of force and distance in AFM measurements. Different scanning modes operate in different regions of the curve; Non–contact in the attractive region, contact mode in the repulsive and intermittent or tapping mode fluctuates between the two [7].

An AFM can be operated in a number of different modes, namely contact, non contact and tapping. In the contact mode, the cantilever is held less than a few Angstroms (10^{-10}m) from the sample surface, and the interatomic force between the cantilever and the sample is repulsive. In the non-contact mode, the cantilever is held on the order of tens to hundreds of Angstroms from the sample surface, and the interatomic force between the cantilever and sample is attractive. In tapping mode, the cantilever is driven to

oscillate near its resonance frequency by a small piezoelectric element mounted in the AFM tip holder, similar to non-contact mode. This method of 'tapping' lessens the damage done to the surface and the tip compared to the amount done in contact mode. Regardless of which mode of operation, tip deflections are recorded via a laser focused on the back of the cantilever and any variations in cantilever height are deciphered by measuring the interference it causes to the light beam. The interpretation of the interference patterns results in a topographical representation of the sample surface.

In this study, an Asylum MFP-3D BIO Atomic Force Microscope was used. It uses a He-Ne laser light source to detect any deflections. In order to measure the particles using the instrument, the nanoparticles were drop cast on to a clean silicon wafer and the solvent allowed to evaporate. All measurements were done in tapping mode.

3.3.2 Particle Sizing: Dynamic Light Scattering (DLS)

Dynamic light scattering (DLS) is a technique used for measuring the size of particles typically in the submicron region. DLS (also known as PCS – Photon Correlation Spectroscopy) measures frequency fluctuations in the interference pattern caused as a beam of light is scattered by the Brownian motion of the solvated particles. Brownian motion is the random movement of particles due to the bombardment by the solvent molecules that surround them. The larger the particle, the slower the Brownian motion. In order for the Brownian motion to be considered truly random, the temperature must be stabilised to prevent convection currents from influencing the movement. Similarly, the solvent viscosity will also play a vital role and needs to be factored into the final calculation of particle diameter. DLS does not measure actual physical particle size, but

rather the effective particle diameter in its local environment. This effective diameter, known as the hydrodynamic diameter, can be calculated from the Stokes-Einstein Equation, Equation 3.1. From the Stokes-Einstein Equation, the hydrodynamic diameters dependency on the particles translational diffusion (velocity), as well as the solvent viscosity and temperature is clear. In essence the hydrodynamic diameter refers to how a perfectly spherical particle diffuses within a fluid and in cases where the particle is non-spherical an equivalent sphere of the same diffusion coefficient is assumed.

$$d(H) = \frac{kT}{3 \times \pi \times \eta \times D}$$

Equation 3.1 Stokes – Einstein Equation

where:

d(H) = hydrodynamic diameter

D = translational diffusion coefficient

k = Boltzmann's constant

T = absolute temperature

η = viscosity

In this study, a Malvern Zetasizer Nano ZS was used for determining the hydrodynamic diameter/particle size of the polystyrene nanoparticles. The Zetasizer Nano ZS has a hydrodynamic diameter measurement range of 0.6nm to 6μm. The laser used to illuminate the sample is a red HeNe gas laser with a wavelength of 633nm. The detector

used to measure the intensity of the scattered light is an avalanche photodiode, quantum efficiency >50% at 633nm at 173° (backscatter detection). It contains automatic laser attenuation transmission, ranging from 100% to 0.0003%, to reduce or increase the intensity of scattering to be detected.

Measurements were carried out in a number of different dispersants at different time points throughout the project. Particles were gently agitated for approximately 10 seconds before being dispersed in the appropriate dispersants. The concentration of sample made up in each dispersant was 1 $x10^{12}$ particles per ml (ppml). This concentration was determined using the formula below; equation 3.2

$$\text{Number of nanoparticles / mL} = \frac{6C \times 10^3}{\rho \times \pi \times \Phi^3}$$

Equation 3.2 Nanoparticle concentration calculation

where:

C = concentration of nanoparticles in g/mL

Φ = diameter of nanoparticle in μm.

ρ = density of polymer in g/mL (1.05 for polystyrene)

The particles were measured in distilled water and 10% Foetal Calf Protein Serum supplemented cell culture medium. Measurements in both dispersants were carried out at 25°C (room temperature) and 37°C (physiological temperature). By measuring particle size at both room temperature and physiological temperature, it allows any

changes in size or any aggregation which might impact on the cytotoxicity measurements to be monitored with increasing temperature. Each sample was filtered through a 0.4µm sterile syringe filter before being measure to ensure there were no dust particles present within the sample that may lead to convection currents and interference with measurements. Measurements were taken an average of 10 times each for each temperature and dispersant. Averages were obtained and standard deviations were also calculated. All measurements were carried out in a 4 clear sided quartz cuvette.

3.3.3 Suspension Stability and Zeta Potential

Zeta potential is the measure of the stability of a colloid system [8]. When particles are suspended in a medium of different phase (e.g. solids suspended in liquid) their interaction with the medium surrounding them determines whether the particles will coagulate or stay dispersed. The interactions with the surrounding media occur in the area directly surrounding the particle. This region may be considered to consist of two separate layers, the Stern layer and the diffuse layer, figure 3.2. The innermost layer (Stern) is the region where ions suspended in the medium adhere to the particle quite strongly. The outer layer contains ions which are not as strongly bound and are said to be diffuse. The boundary of this diffuse layer has a specific potential which is known as zeta potential (ZP).

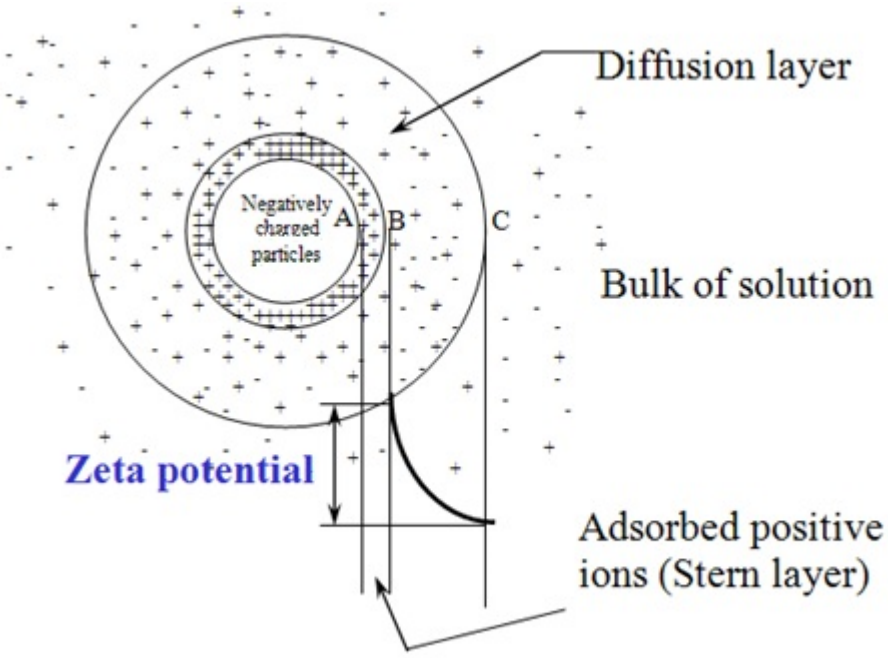

Figure 3.2 Schematic representation of Zeta Potential [9].

In general, if all particles in suspension have a large negative or positive ZP, they will tend to repel each other and there is no tendency to flocculate (process of reversible aggregation of particles). However, if particles have a low ZP value, there is no force to prevent the particles coming together and flocculating. The dividing line between stable and unstable suspensions is generally taken at zeta potentials of either +30mV or -30mV. Particles with Zeta potentials more positive than +30mV or more negative than -30mV are normally considered stable, as summarized in table 3.1.

Table 3.1 Collodial behaviour and related Zeta Potential values [9] [8]

Zeta Potential [mV]	Stability behaviour of the colloid
from 0 to ±5,	Rapid coagulation or flocculation
from ±10 to ±30	Incipient instability
from ±30 to ±40	Moderate stability
from ±40 to ±60	Good stability
more than ±61	Excellent stability

A Malvern Zetasizer Nano ZS was used for zeta potential measurements throughout this project, a schematic of which is shown in figure 3.3. The laser used to illuminate the sample is a red HeNe gas laser with a beam wavelength of 633nm. The detector used to measure the intensity of the scattered light is an avalanche photodiode, quantum efficiency >50% at 633nm at 17° (backscatter detection). It contains automatic laser attenuation transmission, ranging from 100% to 0.0003%, to reduce or increase the intensity of scattering to be detected. The light scattered at an angle of 17° is combined with the reference beam. This produces a fluctuating intensity signal where the rate of fluctuation is proportional to the speed of the particles. A digital signal processor is used to extract the characteristic frequencies in the scattered light.

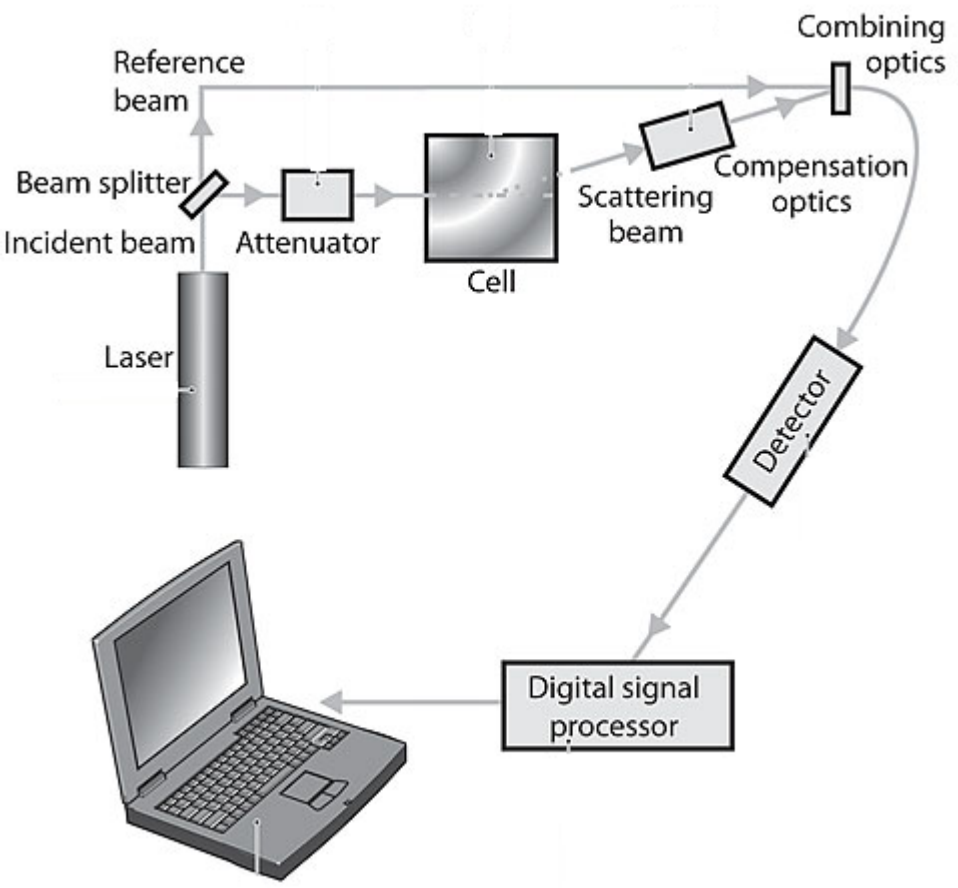

Figure 3.3 Optical configurations of the Zetasizer Nano series for zeta potential measurements [9].

As in the case of DLS, measurements were carried out in a number of different dispersants at different time points throughout the project. Particles were gently agitated for approximately 10 seconds before being dispersed in the appropriate dispersants. The concentration of sample made up in each dispersant was 1 $x10^{12}$ ppml. The particles were measured in distilled water, and 10% Foetal Calf Protein Serum supplemented cell culture medium. Measurements in both dispersants were carried out at 25°C (room temperature) and 37°C (physiological temperature). Each sample was filtered through a 0.4µm sterile syringe filter before being measure to ensure there were

no dust particles present within the sample that may interfere with measurements. Measurements were taken an average of 10 times each for each temperature and dispersants. Averages were obtained and standard deviations were also calculated.

3.3.4 Electronic Spectroscopy.

Two electronic spectroscopic techniques, namely absorption and fluorescent emission spectroscopy, were used in this research. These complementary techniques examine the optical absorption and emission characteristics of the particles. The process of optical absorption and emission of a molecule is depicted in the Jablonski diagram in figure 3.4. Absorption involves the interaction of electromagnetic radiation with the components of a molecule. S_0 is the singlet ground electronic state and S_1 is the singlet excited electronic state; with T_1 representing the triplet state. The initial absorption step takes the molecule to an excited electronic state Sn. Such a transition is denoted as a Frank-Condon transition.

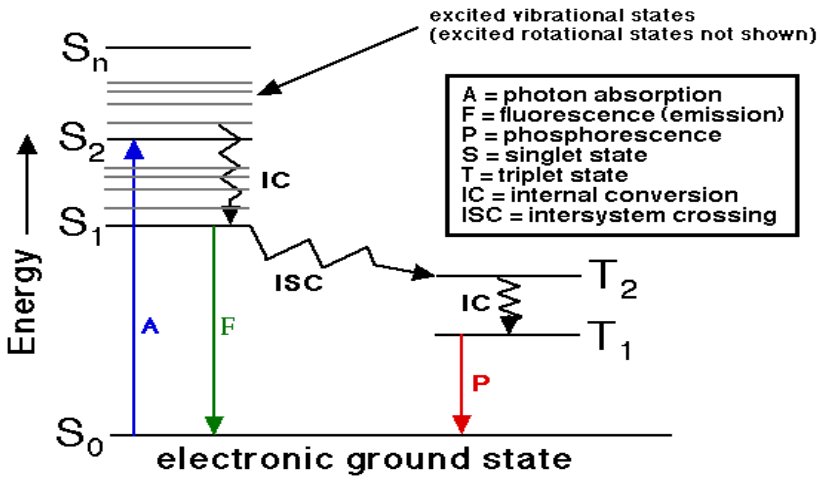

Figure 3.4 Jablonski diagram showing the sequence of steps leading to radiative decay [10]

After initial absorption, the upper excited vibrational states undergo non radiative decay or internal conversion (IC) to the lowest lying excited state S_1, by giving up energy to the surroundings. The excitation can then decay to the ground state S_0 either radiatively, resulting in fluorescence, or nonradiatively by internal conversion. Alternatively, the excitation can undergo a spin flip to a metastable triplet state, T_n, (termed intersystem crossing, ISC)) from which it can again decay nonradiatively, or radiatively resulting in phosphorescence [11].

The absorption spectrometer used to characterise the materials in this research was a Perkin Elmer Lambda 900 UV/VIS/NIR Spectrometer. The spectrometer is a double-beam, double monochromator ratio recording system with pre-aligned tungsten-halogen and deuterium lamps as sources. The wavelength range is from 175 to 3,300 nm with an accuracy of 0.08 nm in the UV-Vis region and 0.3 nm in the NIR region. It has a photometric range of $\pm$ 6 in absorbance. For all the experimental studies, the absorption was measured at all times with a reference sample in a double beam arrangement. Samples of 0.5ml of particles (approx 7.25 x 10^{13} ppml for 50nm and 7 x 10^{15} ppml for 40nm polystyrene) in 2ml dispersants of each nanopolymer in H_2O was prepared. Reference samples were blank H_2O. UV absorption was measured from 40 nm to 1000 nm in keeping within a range relavant to the reported manufacture's reported excitation maxima (447nm for 50nm polystyrene and 417nm for 40nm polystyrene). Samples were measured in a four-sided clear quartz quvette.

A Perkin Elmer LS55 luminescence spectrometer was used throughout this research to record florescence spectra. In this instrument, excitation is provided by a pulsed Xenon discharge lamp with a pulse width at half peak height of < 10 µs and pulse power 20 kW. The source is monochromated using a Monk-Gillieson type monochromator and can be scanned over the range of 200-800 nm. The luminescence is passed through a similar monochromator, which can be scanned over the range of 200-900 nm. A range of samples of different concentrations, ranging from stock solution (1.45 x10 ^{14} particles per ml (ppml) for 50nm and 1.4 x 10^{16} ppml for 40nm polystyrene) to 1.4 x 10^{11} ppml of each nanopolymer in H_2O and 10% DMEM F-12 media were prepared. This was in order to find the optimum concentration of particles per ml that would ensure optimum fluorescence reading where no fluorescence quenching would interfere with sample measurement. Reference samples were blank H_2O or 10% DMEM - F12 media. Fluorescence emission was measured from 200 nm to 800 nm in keeping within a range relevant to the reported manufacture's reported excitation maxima. Samples were measured in a four-sided clear quartz cuvette.

3.4 Cell Culture.

For this project A549 (ATCC number CCL-185) cells were used. A549 (ATCC number CCL-185) (figure 3.5) is a human epithelial cell line derived from a lung carcinoma tissue. Cells were cultured in DMEM F-12 with 10% foetal calf serum (FCS) and 5ml L-glutamine and grown in a humidified incubator at 37^{o}C (5% CO_2).

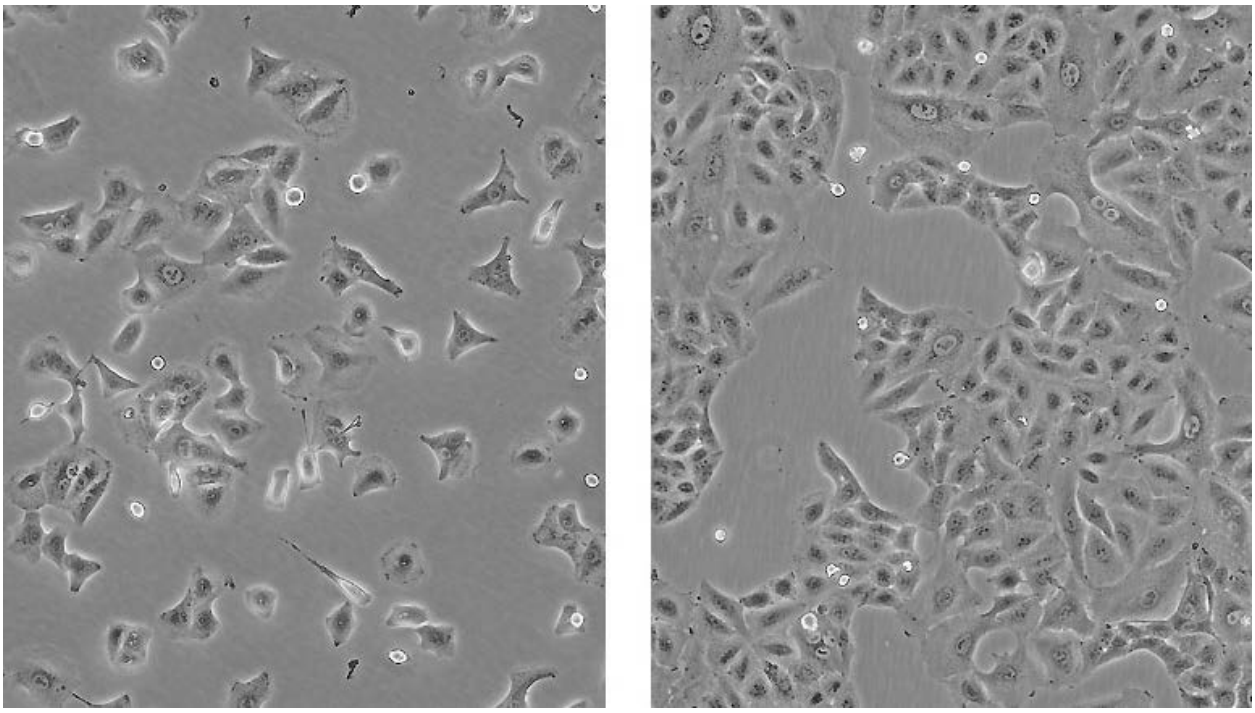

Figure 3.5 Light Microscopy images of A549 (ATCC number CCL-185) after 24hrs (approximately 25% confluence) and 4 days of culture (approximately 80% confluence).

3.4.1 Cell culture media and Reagents.

Cell viability dyes MTT and Neutral Red (NR) were purchased from Sigma Aldrich Ltd. (Dublin, Ireland). Alamar Blue™ (AB) was purchased from Biosource (UK). The carbyl-fushion staining solution was purchased from AGB Scientific (Dublin, Ireland). Cell culture media and supplements and the trypsinisation solution were purchased from Lonza (Wokingham, UK).

3.4.2 Cytotoxicity Evaluation.

To evaluate the cytotoxic response to nanoparticle exposure, cells were seeded at a density of 1 x 10^5 cells/ml for 24 hour test, 7 x 10^4 cells/ml for 48 hour test, 3 x 10^4 cells/ml for 72 hour test and 2 x 10^4 cells/ml for 96 hour test in 96- well.

3.4.3 Dispersion of nano particles in medium.

For particle size and zeta potential measurement, dispersions of nano particles were created in fresh DMEM F-12 media supplemented with 10% FCS and 5 ml L-glutamine. An initial stock concentration of 1 x 10^{12} particles per ml (ppml) was prepared for each particle by dispersing the nanopolystyrene directly into the media. Serial dilutions of the stock concentration were then made. Solutions of 5 x 10^{11}, 2.5 x 10^{11}, 1.25 x 10^{11}, 6.25 x 10^{10}, 3.125 x 10^{10}, 1.56 x 10^{10}, 7.8 x 10^{9} and 3.9 x 10^{9} ppml were then prepared from the 1 x 10^{12} ppml stock by serial dilution. Previous studies [12] have noted interactions between media components and additional supplements with carbonaceous nanoparticles. In this study, no such interactions were noted for the tested nanopolystyrene.

3.4.4 Cytotoxicity assays.

For cytotoxicity evaluation, cells were seeded in 96-well micro plates (Nunc, Denmark) in triplicate for each of the four time points studied 24, 48, 72, 96 hr. Plates were seeded at a density of 1.5 x 10^{5} cells/ml for 24hr, 5 x 10^{4} cells/ml for 48hr, 3 x 10^{4} cells/ml for 72hr and 2 x 10^{4} cells/ml for 96hr exposure. These densities were found to be optimal to achieve the desired confluence at the end of the exposure period. After an initial 24 hr of cell attachment, the medium was removed and the plates were washed with 100 µl/well phosphate buffered saline (PBS). Cells were then treated with increasing concentrations of each nanomaterial and with a positive control of a 10% dimethylsulfoxide (DMSO) 90% medium solution. The cells were then incubated for the desired time period and the cytotoxic effects evaluated. For each independent

experiment, six replicate wells were used each for negative and positive control and six replicate wells were used for each test concentration per micro plate. Fluorescence and absorbance were all quantified using a microplate reader (TECAN GENios, Grodig, Austria). Cytotoxicity was assessed using five assays as outlined below.

Section 3.4.5 Alamar Blue, Neutral Red, Coomassie Blue and MTT assays:

The Alamar Blue, Neutral Red and Coomassie Blue assays were conducted subsequently on the same set of plates. The Alamar Blue assay was performed first. The bioassay was carried out according to manufacturer's instructions. Briefly, control media or test exposures were removed, the cells were rinsed with PBS and 100 µl of an AB/NR medium (5% [v/v] solution of AB and 1.25% [v/v] of NR dye) prepared in fresh medium (without FBS or supplements) was added to each well. The plates were then incubated for 3 hours. The AB assay measures the innate metabolic activity of cells. The oxidised indigo blue, non-fluorescing form of the dye is reduced by cellular dehydrogenases to a reduced pink fluorescent form, which can be easily monitored spectroscopically [13]. Following the 3hr incubation, AB fluorescence was quantified at the respective excitation and emission wavelengths of 540 and 595 nm.

Viability determination of the cells following exposure to each chemical were then subsequently investigated using the Neutral Red and Coomassie Blue assays. The incorporation of the Neutral Red dye by the lysosomes of living cells and the quantification of the total amount of cellular proteins were performed according to Spielmann, et al, the modification of Coomassie Brilliant Blue dye being employed in place of Kenacid Blue R dye. Briefly, after measurement of Alamar Blue fluorescence,

the Alamar Blue / Neutral Red medium was discarded, the cells were washed with 100 µl PBS and the Neutral Red dye was extracted with 100 µl of an acetic acid-ethanol solution (de-staining solution). The addition of the acetic acid-ethanol solution also acts as a cell fixative step so that cell viability determinations can be conducted subsequently. The plate was shaken at 240 rpm for 10 min and the fluorescence of Neutral Red was measured at excitation and emission values of 540 and 650 nm respectively with a micro plate reader. Protein determinations were performed on the same plates immediately following Neutral Red determination. Excess Neutral Red dye was removed from the cells by washing with 100 µl de-staining solution. Coomassie Blue dye was added to each well and the plate agitated for 10 min. The dye was removed and the plate washed with an acetic acid-ethanol solution. The wash solution was discarded and the dye extracted with measuring solution (1M Potassium acetate). The plate was shaken at approximately 200 rpm for 10 min and the absorbance of the extracted dye was read at 570 nm (reference filter 340 nm) using the micro plate reader.

The MTT assay is a quantitative colorimetric method to determine cell proliferation by determining the amounts of incorporated titrated thymidine into freshly synthesized DNA. A second series of plates were set up for the MTT assay. These plates were seeded and exposed identically to the first series of plates prepared for the Alamar Blue, Neutral Red, and Coomassie Blue assays. Following the desired time point of nanomaterial exposure, control medium and test exposures were removed, the cells were rinsed with PBS and 100 µl of fresh medium (without FBS or supplements) was added to each well. Ten micro litres of MTT (1 mg/ml) was prepared in PBS were added

to each well. Plates were incubated for 3 h at 37^{o}C in a 5% CO_2 humidified incubator. After this incubation period the medium was discarded, the cells were washed with 100 µl of PBS and 100 µl of DMSO were added to each well to extract the dye. The plate was shaken at approximately 200 rpm for 10 min and the absorbance was measured at 570nm.

3.4.6 Clonogenic Assay

The procedure for the clonogenic assay was adapted from Puck and Marcus (1956) and Franken et al. (2006) and cells were treated after plating. Exponentially growing cells were harvested and seeded in 25cm^{3} closed cap cell culture flasks (Nunc, Denmark) at a density of 500 cells/ flask. Each flask contained 3ml of cell culture medium. Cells were allowed to attach for approximately 14 hours. This attachment period was shorter than the population doubling time of the cell line which is reported to be approximately 22 hours for A549 cells (ATCC, CCL-185) to ensure that single cells were present at the start of exposure. Cells were then washed with 5 ml of PBS and treated with 2 ml test solutions. Following exposure to the test solutions for 10 days, cells were washed with PBS and finally fixed and stained using a 20% carbol fuchsin in formalin solution (BDH, Poole, UK) and the number of cell colonies was determined.

3.5 Confocal Microscopy

Confocal microscopy operates on the principle that only the in-focus fluorescent light is detected, while the out-of-focus fluorescent light is blocked out. This is done with the use of a pinhole. An electronic light detector is placed behind a pinhole at the image focal point and another pinhole is placed just before the detector. By doing this, only

one point in the specimen is focused upon at any one time. An image can then be constructed of the entire specimen by scanning a laser over the entire focal plane. The mechanical movement of the specimen allows the depth of the optical plane through the specimen to be adjusted, thus, allowing for a 3D representation of the specimen to be reconstructed, with all planes in focus, in the final reconstructed image. A Zeiss LSM 510 Confocal Laser Scanning Microscope was used throughout this study, a schematic of which is shown in figure 3.6.

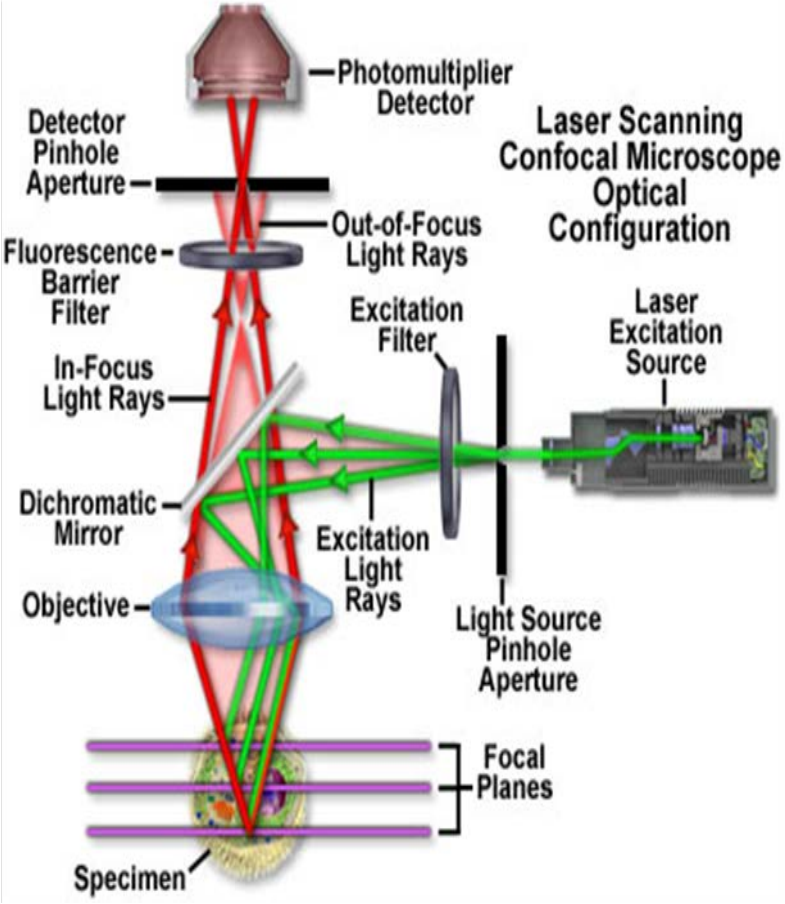

Figure 3.6 A schematic diagram of confocal instrumentation [14].

3.5.1 Sample preparation for confocal fluorescent microscopy

For the confocal studies, approximately 10,000 A549 cells (200µl of cell suspension) were seeded onto 35mm uncoated glass bottom dishes bought from MatTek Corporation, USA. Cells were allowed to attach for approx 4 hours, after which, 2mls 10% FCS DMEM - F12 media were added. Plates were incubated over night. The medium was then removed and particles (suspended in 10% FCS DMEM - F12 media) were added. Exposure times before imaging ranged from 15 minutes to 96hrs. Samples were imaged in 0.9% NaCl saline solution.

3.5.2 Imaging of A549 cells exposed to nanoparticles

Fluorescence images were captured at room temperature on an inverted Zeiss LSM510 confocal laser scanning microscope (Carl Zeiss Inc.). The excitation wavelength used was 488 nm set at 4% of laser power and the fluorescence emission was detected using a 505nm long pass filter. Images were obtained with a 63x oil immersion objective.

3.6 Raman Spectroscopy.

Raman spectroscopy is a vibrational spectroscopy where transitions between vibrational states can result from the inelastic scattering of radiation from molecules. In such scattering processes, the incident photon should be of an energy that is greater than the energy difference between the vibrational states, for example UV or visible radiation (figure 3.7). The incident photon can be scattered off the molecule in two different ways. The scattered light induces an oscillating polarisation in the scattering molecule and

when the photon exchanges energy with a quantum of vibrational energy from the molecule, then the scattered photon may have a higher (anti-Stokes) or lower (Stokes) frequency than the incident photon. The difference in energy corresponds to the energy of the vibrational mode of the molecular structure and results in a Raman shift. When the incident energy equals that of the scattered photon, the scattering is referred to as elastic or Rayleigh scattering. In Stokes Raman scattering, the molecule starts out in a lower vibrational energy state and as a result of the scattering process ends up in a higher energy state. Thus, the interaction of the incident light with the molecule creates a vibration in the material. In anti-Stokes scattering, the molecule begins in a higher vibrational energy state and after the scattering process ends up in a lower vibrational state. Thus the vibration in the material is lost as a result of the interaction. The frequency difference between Raman lines and the exciting lines are characteristic of the scattering molecule and are independent of the excitation frequency. Raman spectroscopy is analogous to Infrared absorption spectroscopy which probes transitions between the vibrational states of a material. In Infra Red spectroscopy, however, a change in dipole moment is required during the transition, whereas in Raman spectroscopy a change in polarisability is required. As polar bonds are not often very susceptible to polarisation, the two techniques are often mutually complementary

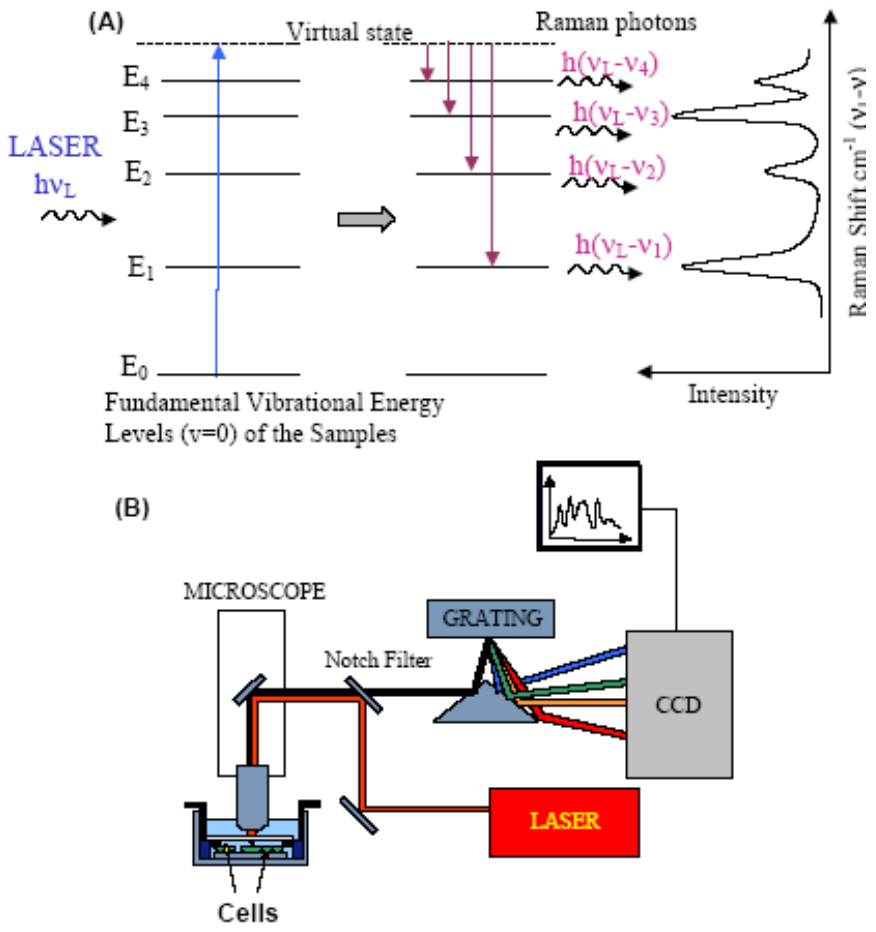

Figure 3.7.Schematic representation of (A) Raman Stokes scattering of laser photons by vibrating molecules in the sample: energy is transferred by laser photons to the molecules as vibrational energy, the energy loss correspond to the vibrational energy levels of the molecules (E1, E2, …); and (B) experimental set-up for Raman spectroscopy measurements of cells [15].

3.6.1 Sample preparation for Raman Spectroscopy

For Raman analysis, A549 cells, approximately 10,000 per substrate (200µl of cell suspension), were seeded on CaF_2 substrates (Hellma Ltd., UK) and then placed in Petri dishes (30 mm diameter, Stardest, USA). Cells were allowed to attach for approximately 4 hours, after which, 2mls 10% FCS DMEM - F12 medium was added. Plates were left to incubate over night. Medium was then removed and particles

(suspended in 10% FCS DMEM - F12 media) were added. Exposure times before imaging ranged from 1hr to 24hrs. Samples were imaged in 0.9% NaCl saline solution.

A Horiba Jobin-Yvon LabRAM HR800 spectrometer with an external 300 mW diode laser operating at 785 nm as source was used throughout this work. For all measurements, a x100 immersion objective (LUMPlanF1, Olympus) was employed which provided a spatial resolution of ~1 μm at the sample. The confocal hole was set at 100 μm for all measurements, the specified setting for confocal operation. The system was pre-calibrated to the 520.7 cm^{-1} spectral line of silicon. The Labram system is a confocal spectrometer that contains two interchangeable gratings (300 and 900 lines per mm respectively). 300 lines per mm grating was used, which gave a spectral dispersion of around 1.5 cm^{-1} per pixel. The backscattered Raman signal was integrated for 30 seconds over the spectral ranges from 400 to 1800 cm^{-1} and accumulated 3 times to improve the signal to noise ratio. The detector used was a 16 bit dynamic range Peltier cooled CCD detector. Images of the sample were acquired using a video camera within the system. Spectra were recorded from the cellular nucleus, with approximately 25 spectra recorded per substrate.

For Raman mapping, an area corresponding to the map to be acquired was defined around the cells on the optical image provided by the instrument video camera. The step between two successive measurements was set to 1.5 μm or 0.75 μm and the backscattered Raman signal was integrated for 10 seconds over the spectral ranges from 400 to 1800 cm^{-1} and accumulated twice to improve the signal to noise ratio.

3.7 Chapter Summary

This chapter presented the experimental techniques used throughout this thesis and provided relevant information and theory about each of the techniques employed.

Experimental procedures were described, with specifications and parameters used given for each relevant procedure.

The following chapter will present the results of the characterisation of 40nm and 100nm carboxylated Invitrogen nanopolystyrene and 50nm and 100nm Duke Scientific nanopolystyrene, as well as 60nm aminated nanopolystyrene (UCD). The characterisation profiling will give results obtained for a range of techniques ranging from DLS and AFM for particle sizing, zeta potential for information on particle stability in solution and electronic spectroscopy for information on the absorbance and emission properties of the fluorescent particles.

References

1. Wünsch, J.R., *Polystyrene: Synthesis, Production and Application* ed. R. Dolbey. 2000: Rapra Technology Limited
2. Balasundaram, G. and T.J. Webster, *An Overview of Nano-Polymers for Orthopedic Applications.* Macromolecular Bioscience, 2007. **7**(5): p. 635-642.
3. Rejman, J., et al., *Size-dependent internalization of particles via the pathways of clathrin- and caveolae-mediated endocytosis.* Biochem. J., 2004. **377**(1): p. 159-169.
4. Oberdörster, G., et al., *Translocation of Inhaled Ultrafine Particles to the Brain.* Inhalation Toxicology: International Forum for Respiratory Research, 2004. **16**(6): p. 437 - 445.
5. Stone, *Nanomaterials for environmental studies: Classification, reference material 3 issues, and strategies for physico-chemical characterisation.* , in *NanoImpact Net Reports* 2009: Zurich
6. OECD, *List of manufactured nanomaterials and list of endpoints for phase one of The oecd testing programme*, in *Series on the safety of manufactured nanomaterials*

Number 6. 2008.
7. Jalili, N.L., Karthik, *A review of atomic force microscopy imaging systems: application to molecular metrology and biological sciences.* Mechatronics, 2004. **14**(8): p. 907-945.
8. Hunter, R.J., *Zeta potential in colloid science: Principles and applications*. 1981: Academic Press (London and New York).
9. Malvern (2008) *Zetasizer Nano series technical note*.
10. Project, T.C.H. 2013; Available from: http://www.files.chem.vt.edu/chem-ed/quantum/jablonsk.html.
11. Wayne, R.P., *Photochemistry*. 1970, London: Butterworth and Co Ltd, .
12. Herzog, E., et al., *A new approach to the toxicity testing of carbon-based nanomaterials--The clonogenic assay.* Toxicology Letters, 2007. **174**(1-3): p. 49-60.
13. O'Brien, J., et al., *Investigation of the Alamar Blue (resazurin) fluorescent dye for the assessment of mammalian cell cytotoxicity.* European Journal of Biochemistry, 2000. **267**(17): p. 5421-5426.
14. Zeiss. *Education in Microscopy and Digital Imaging*. 2012; Available from: http://zeiss-campus.magnet.fsu.edu/articles/livecellimaging/techniques.html.
15. Notingher, I., *Raman Spectroscopy Cell-based Biosensors.* Sensors, 2007. **7**(8): p. 1343-1358.

Chapter 4

Characterisation of Nanopolymers

Chapter 4

4.1 Introduction

In the introductory chapters it was highlighted that nanotoxcity studies require special consideration of the physico-chemical properties in conjunction with the biological characterisation. Verification of internalisation of nanoparticles within cells is also paramount in order to consider nanoparticle trafficking through cells and their organelles. As discussed in Chapter 2, Section 2.1, the OECD, as well as other organisations, has highlighted several key properties which must be characterised in advance of a toxicity study being performed on a nanomaterial. Warheit *et al* has discussed this aspect in great detail and reinforced the importance and significance of such data for traceable and reproducible nanotoxicology. Indeed physiochemical parameters such as size, shape and surface characteristics, play a crucial role in the elucidation and determination of the biological properties of nano particles, often influencing how these particles interact with proteins, lipids and surfactants in the local environment [1]. As a result, such information can be used to determine how particles behave in biological media and subsequently within cells during *in vitro* studies, as performed in this thesis. Characteristics such as changes in the environment or ionic strength, or a change in the particle concentration, may result in some aggregation or a shift in the particle size distribution, which will subsequently have an effect on the manner in which the particles are presented to the cell and or cellular structures. Hence, the nature of the particles in the cell culture media is undefined making the interpretation of toxicity results with respect to the nano aspects undeterminable. The importance of ‘in-lab’ characterisation is further highlighted by Park and Grassian (2009) who showed differences between label specifications of commercial nanoparticles and

independent characterisation. Their study highlighted important insights with respect to shelf-life and stability. Again this is crucial in order to fully interpret the results of toxicity assessments [2]

In the present chapter, a number of the OECD recommended characterisation techniques were performed in advance of the cytotoxicity evaluation, particle internalisation and localisation verification studies. The properties chosen include;

- Particle size/size distribution
- Zeta Potential
- Electronic Spectroscopy

The importance and justification of these properties to nanotoxicology will be discussed within this chapter and will form the underlying theme.

This section will discuss the physico-chemical properties and material characterization and spectroscopic techniques used to create a characteristic profile of 50nm and 100nm neutral polystyrene, 40nm and 100nm carboxylated polystyrene and 60nm aminated nanopolystyrene. Characterisation was carried out throughout the project to have a complete profile of nanomaterials and to monitor any changes that may have occurred in their size, fluorescence, etc. due to aggregation.

4.2 Particle Size

Particle size is one of the main factors that affect the biological applications of nanomaterials. One of the major concerns of nanoparticles is the possible toxic effects due to the capacity of these materials to penetrate cells and potentially translocate to other cells, tissues and organs around the body. The size and shape of mammalian cells are varied, mostly related to their specific functions. A typical mammalian cell is approximately 10µm in size. It is also known that the cell membrane, which is approximately 8nm – 180nm in thickness and has an overall negative charge, allows certain substances to cross through selective permeability by processes such as diffusion, facilitated diffusion, active transport and endocytosis. Surface area, particle size, temperature, concentration and surface charge are all factors which affect particle movement across the membrane [3].

As discussed in Chapter 2, Section 2.1, there are a number pathways by which nanoparticles may cross the cell membrane, endocytosis being the most likely [4]. The size of the vesicles formed for each endocytic route is different. For example clathrin coated pits are approximately 120nm in diameter, caveolea generally 50nm – 80nm and micropinomes 1 - 5µm [4].

There is much evidence of nanoparticle size influencing cellular uptake and toxicity of particles. The uptake of fluorescent polystyrene-based latex microspheres, 50, 100, 200, 500 and 1000nm in size, by B16-F12 cells (murine melanoma cell line) was studied to investigate the size dependency of particle size uptake [5]. The study revealed that uptake of the 50nm particle was the greatest, with the degree of internalisation

decreasing as particle size increased. The authors concluded that smaller particles (up to 200nm) were preferentially internalised via clathrin-mediated endocytosis while larger particles (>200nm but not greater than 1µm) were internalised via caveolin-mediated endocytosis. Such studies provide insight into the effects of nanoparticle internalisation due to size.

Taking this information into consideration, correct and accurate particle size measurement is a critical factor for evaluating toxicity and uptake of nanoparticles. There are many recommended techniques for the measurement of particle size such as Atomic Force Microscopy (AFM), Scanning Tunnelling Microscopy (STM), Scanning Electron Microscopy (SEM), and Transmission Electron Microscopy (TEM) [1, 6, 7]. While such microscopic techniques are more modern methods of particle size measurement, there are also many older available techniques for the measurement of particle size. Dynamic light scattering (DLS), as explained in more detail in Chapter Three, is a technique used for measuring the size of particles typically in the sub micron region. DLS has the advantage that the measurements can be made in situ in the nanoparticle dispersion.

4.2.1 Particle Size Results

Size measurements were made using Dynamic Light Scattering (DLS) on a Malvern Zetasizer Nano ZS. Measurements were carried out in a number of different dispersants at different time points throughout the project. Lynch et al (2007) have argued that the representation of nanoparticles in a biological fluid is actually a representation of the nanoparticles plus the proteins associated with the nanoparticle surface, and it is the

amount and presentation of the proteins on the surface rather than the particles themselves that are the cause of numerous biological responses. It is this outer layer of proteins that is seen by the biological cells, and leads to their responses. Therefore, for this study, nanoparticles were characterised in both distilled Milli Q water and 10% FCS DMEM - F12 media. Measurements in both dispersants were carried out at 25°C (room temperature) and 37°C (physiological temperature). Measurements were taken an average of 10 x3 times each for each temperature and dispersant. Averages were obtained and standard deviations were also calculated. The results from DLS size measurements for 50nm and 100nm Duke Scientific Nanopolystyrene, 40nm and 100nm carboxylated Invitrogen Nanopolystyrene and 60nm Aminated Nanopolystyrene are reported in Tables 4.1 to Table 4.5.

Table 4.1 Size measurements for 50nm Duke Scientific Nanopolystyrene

Dispersant	**Temperature °C**	**Average Particle Size / nm**	**Standard Deviation / nm**
H_2O	25	52.05	0.29
H_2O	37	52.54	0.16
10% FCS DMEM - F12	25	49.44	0.22
10% FCS DMEM - F12	37	38.00	0.25

Table 4.2 Size measurements for 100nm Duke Scientific Nanopolystyrene

Dispersant	Temperature °C	Average Particle Size / nm	Standard Deviation / nm
H_2O	25	112.65	0.86
H_2O	37	88.36	0.35
10% FCS DMEM - F12	25	133.80	0.59
10% FCS DMEM - F12	37	102.00	0.86

As previously discussed in Chapter 3, Section 3.2.2, the Malvern Zetasizer Nano ZS measures the Hydrodynamic Radius (HR), or Stokes – Einstein Radius, from the translational diffusion coefficient. According to Malvern, the hydrodynamic size measured by Dynamic Light Scattering (DLS) is defined as “the size of a hypothetical hard sphere that diffuses in the same fashion as that of the particle being measured” [8].

Results for the 50nm and 100nm Neutral Duke Scientific Nanopolystyrene, table 4.1 and 4.2 respectively, show there are variations from the manufacturers’ specifications. The measured result of 52nm in water at 25 and 37°C, with standard deviations of 0.29 and 0.16 respectively, is above the manufacturer’s specification of 50nm ± 5nm. Similarly, for 100nm particles measured in H_2O, there is a variation in the obtained

sizes, measuring in at 112nm for particles measure at 25°C and 88nm for particles measured at 37°C, with standard deviations 0.86 and 0.35 respectively.

Measurements made in 10% FCS DMEM - F12 media, showing an apparent decrease in size, may be explained by the presence of salts in the media, which suppresses the electrical double layer, resulting in a decrease in ”apparent” hydrodynamic radius and a decrease in the overall particle measurement.

Table 4.3 Size measurements for 40nm Carboxylated Invitrogen Nanopolystyrene

Dispersant	**Temperature °C**	**Average Particle Size / nm**	**Standard Deviation / nm**
H_2O	25	78.89	2.24
H_2O	37	80.41	0.98
10% FCS DMEM - F12	25	40.55	0.24
10% FCS DMEM - F12	37	31.26	1.13

Table 4.4 Size measurements for 100nm Carboxylated Invitrogen Nanopolystyrene

Dispersant	Temperature °C	Average Particle Size / nm	Standard Deviation / nm
H_2O	25	120.96	0.69
H_2O	37	95.24	0.36
10% FCS DMEM - F12	25	180.75	1.20
10% FCS DMEM - F12	37	141.65	0.63

As can be seen from table 4.3 and 4.4, 40nm and 100nm Carboxylated Invitrogen Nanopolystyrene particles respectively show sizes which varied over a range of temperatures. The 40nm particle was observed to have twice the label value and manufacture's size specifications when measured in H_2O. In contrast, when measured in 10%FCS DMEM – F12, particle sizes were seen to return to the acceptable errors associated with the product specifications. This is not unusual for this type of measurement since it is not the physical particle diameter measured by the manufacturer. Typically, manufactures use TEM and/or calculate particle size using Brunauer–Emmett–Teller (BET) analyser rather than determining the hydrodynamic radius of the particle [9]. One explanation for the observed increase in particle sizes may be due to the fact that the hydrogen, or proton, of the -OH on the carboxylated

group can dissociate to form a hydronium ion with water if the particle containing a carboxyl group is water-soluble. A carboxyl group that has lost its -OH hydrogen due to dissociation is called a carboxylate ion. The carboxylate ion has a negative charge which is free to react with other ionic species present in the water. As previously explained, this will have an overall affect on the diffusion speed, affecting the apparent hydrodynamic radius thus affecting the overall measured particle size [10].

As can be seen from the size results obtained for the 100nm carboxylated particles, the sizes observed were considerably higher than the manufactures specification supplied with the particle. This variation of particle size results in 10%FCS DMEM - F12 media may be due to the formation of a protein corona causing aggregation [11] and the presence of salts in the medium [12]. Studies investigating the formation of a protein corona, consist of examining the effects of various nanoparticle size and surface properties in determination of their effect on the formation of the protein corona (Lundqvist et al. 2008). The study consisted of examining negatively charged (by carboxyl modification) nominally ‘‘neutral’’ unmodified polystyrene particles, positively charged (by amine modification), and the formation of the protein corona from human plasma of various sizes (50nm and 100nm). It was found that when all particles were placed into media, they increased in size, due to the number of identified proteins that were attached to each nanoparticle. Interestingly, when all of the nanoparticles (positively charged, negatively charged and neutral) were placed into H_2O and/or a buffer solution, they did in fact, also increase in size, as in keeping with the results obtained for this thesis. These results show that with commercially supplied samples, significant deviations from nominal specifications can be observed. The conformation of

surface coatings is also, as previously discussed in Chapter 2, Section 2.2, dependent on the exact nature of the dispersant media. As conformational changes occur, due to the absorption of ionic species present in the media, changes in the diffusion speed will occur, affecting the overall particle size measured.

Table 4.5 Size measurements for 60nm Aminated Nanopolystyrene

Dispersant	**Temperature °C**	**Average Particle Size / nm**	**Standard Deviation / nm**
H_2O	25	67.32	0.61
H_2O	37	50.07	0.76
10% FCS DMEM - F12	25	2425	203.33
10% FCS DMEM - F12	37	1461	205.16

The extremely high standard deviation values that can be seen in the table above, gives an indication of the wide range of particle sizes that was observed for the 60nm aminated nanoparticles when measured in complete biological media. However, while these results are largely outside of the expected size value ranges, this phenomenon has been previously observed in other studies examining the effect of surface charge on particle size. In a study to compare the abilities of ambient and manufactured nanoparticles to induce cellular toxicity, characteristics of each tested nanoparticle were

assessed in aqueous media and in complete culture medium (10%FCS RPMI). In the presence of complete medium, aminated nanopolystyrene particles showed a considerable increase in size due to agglomeration, while other nanoparticles showed smaller increases or no changes. The authors suggested that proteins in the culture media may be adsorbed onto the particle surface, leading to neutralization of charge and interference in electrostatic repulsion. [13]. Such reports suggest that the presence of protein in biological media has an effect on particle size of surface modified nanoparticles.

The above results emphasise the importance of measuring particle size in biological media for accurate toxicological assessment as this gives the most accurate apparent particle size that is being presented to the cell. The addition of surfactant should also be taken into account when examining particle sizes measure in water, as this may have a slight effect on measured size. Surfactant such as Tween, may be added to aqueous nanoparticle solutions to prevent flocculation of nanoparticles.

4.3 Atomic Force Microscopy

While DLS is an established method of particle size measurement, there are also other complementary techniques to verify particle sizes. Verification of particle size is important, particularly when examining particle size in biological media, as ionic species in the protein rich solution can have an effect on particle stability and agglomeration.

Atomic Force Microscopy (AFM) is a well documented technique for the characterisation of nanoparticles [14] [15] [16]. The technique has the capability of 3D visualization and both qualitative and quantitative determination of many physical properties including size, morphology, surface texture and roughness. A wide range of particle sizes can be characterized in the same scan, from 1nm to 8µm.

AFM was employed as a particle size verification tool. The results obtained from the AFM measurements of 40nm Carboxylated Invitrogen Nanopolystyrene and 50nm Duke Scientific Nanopolystyrene can be seen in the following section.

Details of the instrument used and the sample preparation is given in chapter 3, section 3.3.1 Particle sizing: Atomic Force Microscopy.

4.3.1 AFM Results

Figure 4.3 and 4.4 show AFM results obtained for 40nm Carboxylated Invitrogen Nanopolystyrene. Figure 4.3 is an optical image of the dropcast nanopolymer solution. The line drawn through the bright spots (particles) is an indication of the particles of which the measurements were taken. The height profile of the particles measured can be seen in figure 4.4. The height profile reveals particles to be approximately 40nm in height, as was expected. The width of the particles (x-axis) shows the particles to have a width of approximately 500nm. This can be attributed to particles clumping together on drying.

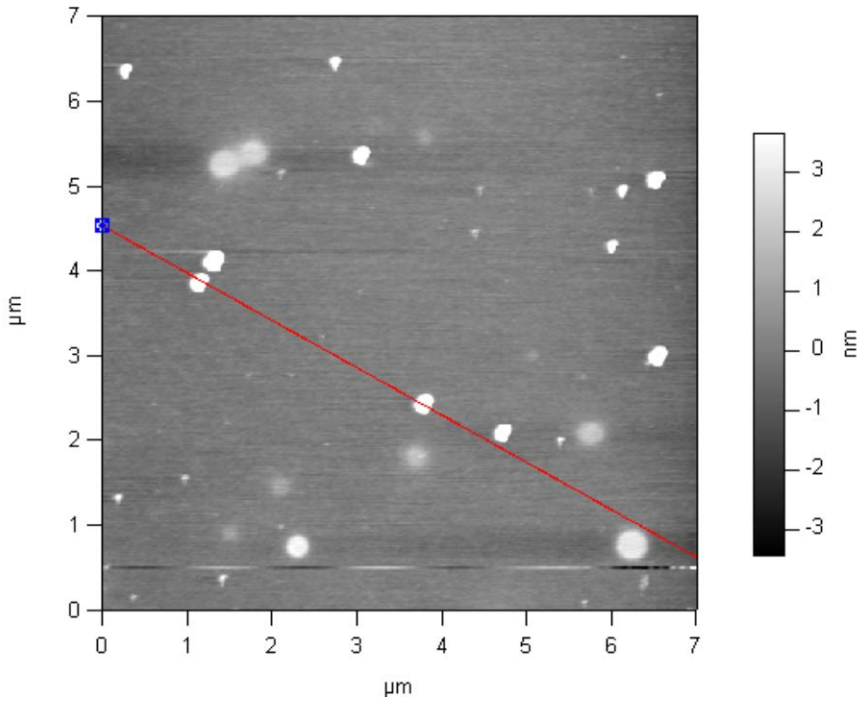

Figure 4.3 Optcal AFM image of dropcast solution of 40nm Carboxylated Invitrogen Nanopolystyrene.

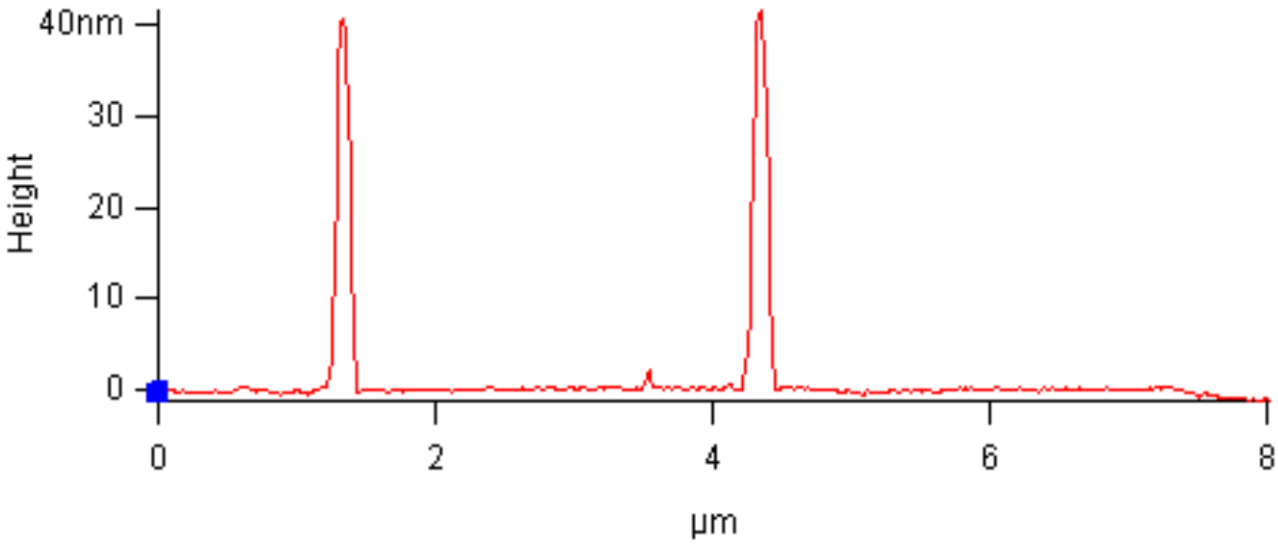

Figure 4.4 AFM Height profile measurement of 40nm Carboxylated Invitrogen Nanopolystyrene particles.

Figures 4.5 and 4.6 show an AFM optical image and a height profile measurement of 50nm Duke Scientific Nanoparticles.

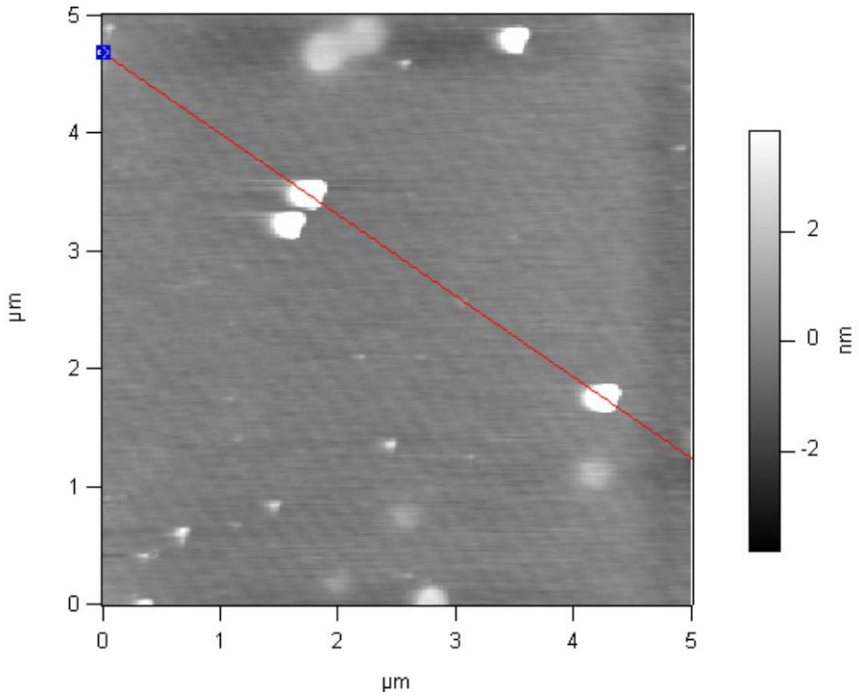

Figure 4.5 Optcal AFM image of dropcast solution of 50nm Duke Scientific Nanopolystyrene.

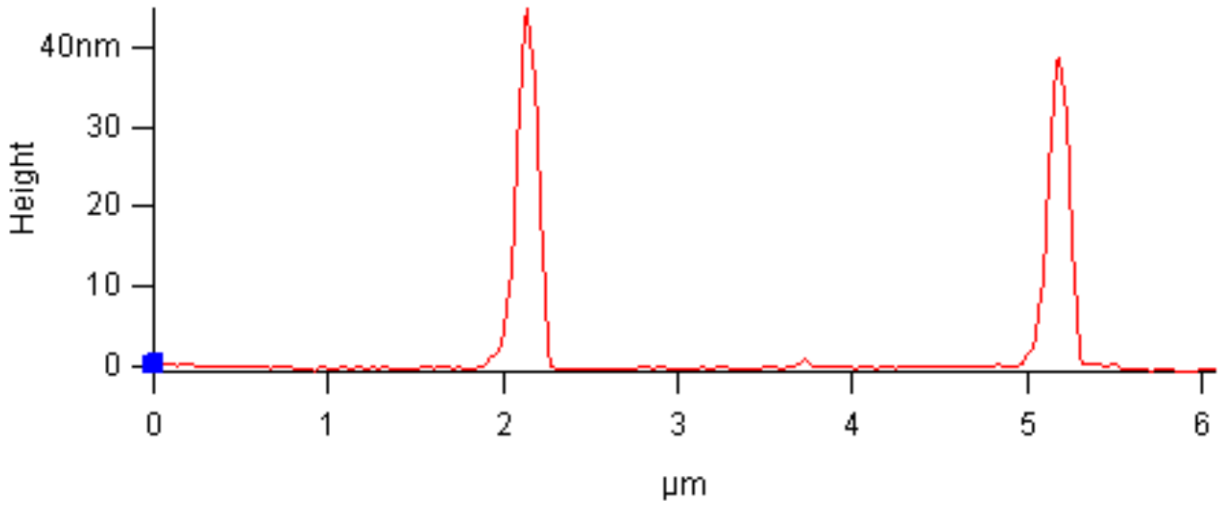

Figure 4.6 AFM Height profile measurement of 50nm Duke Scientific Nanopolystyrene particles.

The profile for the 40nm Carboxylated Invitrogen Nanopolystyrene particles revealed particles had a height of approximately 40nm when measured by AFM. 50nm Duke Scientific Nanopolystyrene particles revealed from their height profile, heights of approximately 45nm, which is within the manufacturer's specifications.

The results in both particle cases are in keeping with size values obtained by DLS, confirming particle sizes. Clumping of particles was observed, as revealed from width profile measurements. In both particle cases, images obtained were representative of the entire surface. Measurements were taken from multiple dropcast solutions, where multiple particles were detected upon the surface of the silica slides.

4.4 Zeta Potential

When examining particle characteristics in advance of any nanotoxicological study, it is imperative to know the state of the nanoparticles to be used and in particular in the appropriate test media. Surface charge is particularly important when looking at nanoparticles dispersed in biological test media. Zeta potential is considered to be an indication of the overall potential charge that a particle surface has in solution. The development of a net charge at the particle surface affects the distribution of ions in the surrounding interfacial region, resulting in an increased concentration of counter ions (ions of opposite charge to that of the particle) close to the surface. Thus an electrical double layer exists around each particle. When a particle moves (e.g. due to random Brownian motion), ions within the boundary move with it, but any ions beyond the

boundary do not travel with the particle. This boundary is called the surface of hydrodynamic shear or slipping plane. The potential that exists at this boundary is known as the Zeta potential. If all the particles in suspension have a large negative or positive zeta potential then they will tend to repel each other and there is no tendency for the particles to agglomerate. However, if the particles have low zeta potential values then there is no force to prevent the particles coming together and flocculating. This obviously has a massive influence on the measurement of the size and surface area of nanoparticles, which, depending on the dispersant, will have an effect on the actual true particle size.

Zeta potential and overall surface charge is of particular interest when looking at how particles enter the cell. As discussed in previous chapters, there are several ways for a substance to enter a cells interior. The permeability of a membrane is the ease of molecules to pass through it. Permeability depends mainly on the electric charge of the molecule and to a lesser extent the molar mass of the molecule. Electrically neutral and small molecules pass through the membrane easier than charged, large ones. Within cells, the intermediate extracellular surface of the plasma membrane is negatively charged due to the negative charge of the phospholipid heads. Therefore, the surface of the membrane could influence the way in which charged particles interact with the cell membrane. The cell uses this negative electrical membrane potential to drive the transport of the substances, often against a concentration gradient, into or out of the cell [17, 18].

Zeta potential can potentially provide information on the particle's absorbed species, such as proteins or salts. Therefore, from this information it can be concluded that it is imperative that characterization measurements, particularly surface charge and zeta potential measurements, should always be carried out in an array of different dispersants including biological media. The interaction of nanoparticles and proteins are of great interest in nanomedicine and nanotoxicology recently, in particular with the development of the idea of the nanoparticle-protein 'corona' [12].

As mention previously, a study by Lundgvist et al (2008) demonstrated the effect of surface charge in the formation of a protein corona. The report concluded that the nature of the proteins in the corona is determined by the local chemical property of the nanomaterial and differences in the particles surface charge were able to entirely change the nature of the biologically active proteins in the corona, and thereby possibly also the biological impacts. This is of particular interest to this thesis, due to the similarity of the particle surface modification examined. Specific proteomic information of the nanopolystyrene (neutral, carboxylated or aminated) bio-interface could be of huge benefit when examining particle uptake mechanisms and determining eventual nanoparticle fate within cells. Such studies highlight the need and possible invaluable importance of zeta potential measurements when building a characterisation profile of nanomaterials for toxicological assessment.

4.4.1 Zeta Potential Results

As with particle size measurements, zeta potential measurements were carried out in distilled H_2O and 10%FCS DMEM - F12 media at both 25°C (room temperature) and 37°C (physiological temperature). The average values and their standard deviations from zeta potential measurements of 50nm and 100nm Duke Scientific Nanopolystyrene, 40nm and 100nm Carboxylated Invitrogen Nanopolystyrene and 60nm Aminated Nanopolystyrene are reported in Tables 4.6 to Table 4.10. Measurements in both dispersants were carried out at 25°C and 37°C.

Table 4.6 Zeta Potential measurements for 50nm Neutral Duke Scientific Nanopolystyrene

Dispersant	Temperature °C	Average Zeta Potential / mV	Standard Deviation / mV
H_2O	25	-62.00	1.37
H_2O	37	-53.72	2.61
10% FCS DMEM - F12	25	-13.06	0.51
10% FCS DMEM - F12	37	-12.78	0.99

Table 4.7 Zeta Potential measurements for 100nm Neutral Duke Scientific Nanopolystyrene

Dispersant	Temperature °C	Average Zeta Potential / mV	Standard Deviation / mV
H_2O	25	-36.58	4.17
H_2O	37	-37.62	4.40
10% FCS DMEM - F12	25	-11.60	2.8
10% FCS DMEM - F12	37	-12.34	1.44

Table 4.8 Zeta potential measurements for 40nm Carboxylated Invitrogen Nanopolystyrene

Dispersant	Temperature °C	Average Zeta Potential / mV	Standard Deviation / mV
H_2O	25	-40.00	5.04
H_2O	37	-38.10	2.51
10% FCS DMEM - F12	25	-297.25	184.60
10% FCS DMEM - F12	37	-390.00	98.33

Table 4.9 Zeta Potential measurements for 100nm Carboxylated Invitrogen Nanopolystyrene

Dispersant	Temperature °C	Average Zeta Potential / mV	Standard Deviation / mV
H_2O	25	-40.24	2.0
H_2O	37	-38.42	5.42
10% FCS DMEM - F12	25	-12.72	5.13
10% FCS DMEM - F12	37	-11.39	1.87

Table 4.10 Zeta Potential measurements for 60nm Aminated Nanoparticles

Dispersant	Temperature °C	Average Zeta Potential / mV	Standard Deviation / mV
H_2O	25	54.28	2.24
H_2O	37	54.18	4.17
10% FCS DMEM - F12	25	-4.12	0.60
10% FCS DMEM - F12	37	-5.11	1.03

As can be seen from table 4.8, 40nm Carboxylated Invitrogen Nanopolystyrene particles were most stable in 10% FCS DMEM - F12 media. The large zeta potential value indicates that particles are highly stable in solution containing protein. The large shift in zeta potential values for particles in H_2O and 10% FCS DMEM - F12 can be attributed to the interaction between the carboxylated group on the nanoparticles and constituents in the surrounding media, effectively neutralising the surface charge of the nanopolymer, making it more stable in solution.

However, as can been seen in tables 4.6 and 4.7, 50nm and 100nm Neutral Duke Scientific Nanopolystyrene respectively, both exhibit the opposite behaviour. While the zeta potential values of the 50nm and 100nm neutral nanopolymers in H_2O reveal they are moderately stable in the aqueous solution, once placed in 10% FCS DMEM - F12, the values indicate the particles are less stable in the protein solution. The negative value obtained by these “neutral” particles may be due to the fact that although the nanoparticles are monodispered in water, there is 0.01% surfactant also in the solution (to prevent particles from aggregating). This tiny amount of surfactant may cause the “neutral” nanoparticles to have a negative zeta potential value. However, for the purpose of this thesis, they will be referred to as neutral nanoparticles. These values are in keeping with literature reports that also suggest that neutral nanopolystyrene exhibit stable zeta potential values when in aqueous media but less stable values when dispersed in protein supplemented biological media [13].

The values obtained from the zeta potential measurements of the 60nm aminated nanopolystyrene also comply with values in literature [19]. While in aqueous solution,

the particles exhibit a moderately stable state. However, once placed in complete media, the surface charge interaction with proteins can be seen to affect the stability of particles in the solution. [13].

4.5 Electronic Spectroscopy.

The use of fluorescent nanoparticles for the development of suitable labelling systems for particle penetration and translocation has been an area of investigation for a number of years [20]. Current medical and biological fluorescent imaging methods are mainly based on dye markers, which are limited in light emission per molecule, as well as photostability [21] . Nanoparticles overcome these disadvantages offering strong and stable fluorescence. A tight control of the average particle size and a narrow distribution of sizes allow the creation of very efficient fluorescent probes that emit a narrow emission wavelength band of light in a very wide range of wavelengths [21]. This helps with creating biomarkers with many and well distinguished colours. A study by Geys et al. (2006) to examine different optical techniques for measuring translocation across a cell monolayer reported that when fluorescent nanoparticles were studied, 6% transfer was observed for polystyrene nanoparticles. This work focused on the potential uptake and trafficking of nanoparticles through cells and gives a clear example of the relevance and importance fluorescent nanoparticles have in the area of nanotoxicology.

UV-Vis absorption spectroscopy was the first technique employed to verify the excitation wavelength of each particle. A solution of 40nm carboxylated nanopolystyrene particles in water was prepared and measured with the absorption

spectra obtained. The excitation maximum was revealed as 417nm, which is within the manufacturer's specifications. A second solution of 50nm nanopolystyrene particles in water was prepared and the absorption spectra of it obtained. The absorption spectrum revealed the solution of 50nm particles in water to have an excitation maximum of 447nm, which is also in agreement of the manufacturer's specification. Details of the experimental methods used can be found in Chapter 3, Section 3.2.4. Figure 4.9 shows the absorption spectra obtained for 40nm Carboxylated Invitrogen Nanopolystyrene and 50nm Duke Scientific Nanopolystyrene particles. The spectral window has been cut from 300nm – 1000nm to 375nm – 700nm for clarity.

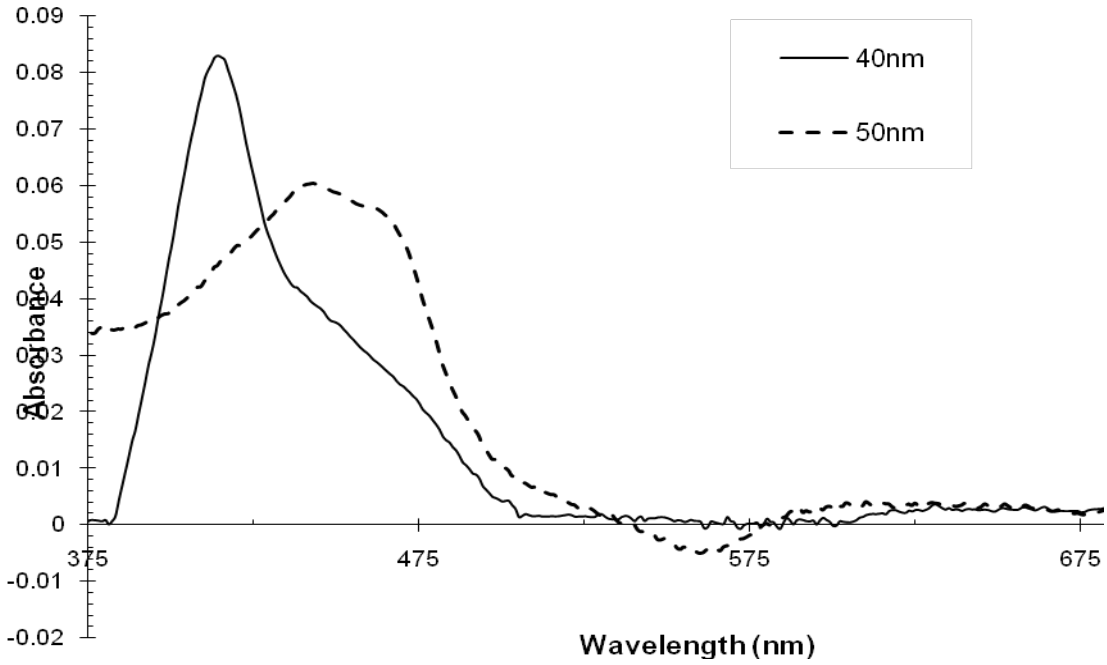

Figure 4.9 Absorption spectra of 40nm Carboxylated Invitrogen Nanopolystyrene (solid line) and 50nm Duke Scientific Nanopolystyrene (dashed line).

The excitation wavelength measured for each particle was then used to determine the optimum fluorescence emission of particles in solution at specific concentrations. The emission values obtained for 40nm carboxylated nanopolystyrene and 50nm neutral nanopolystyrene at different concentrations can be seen in figures 4.10. and 4.11, respectively.

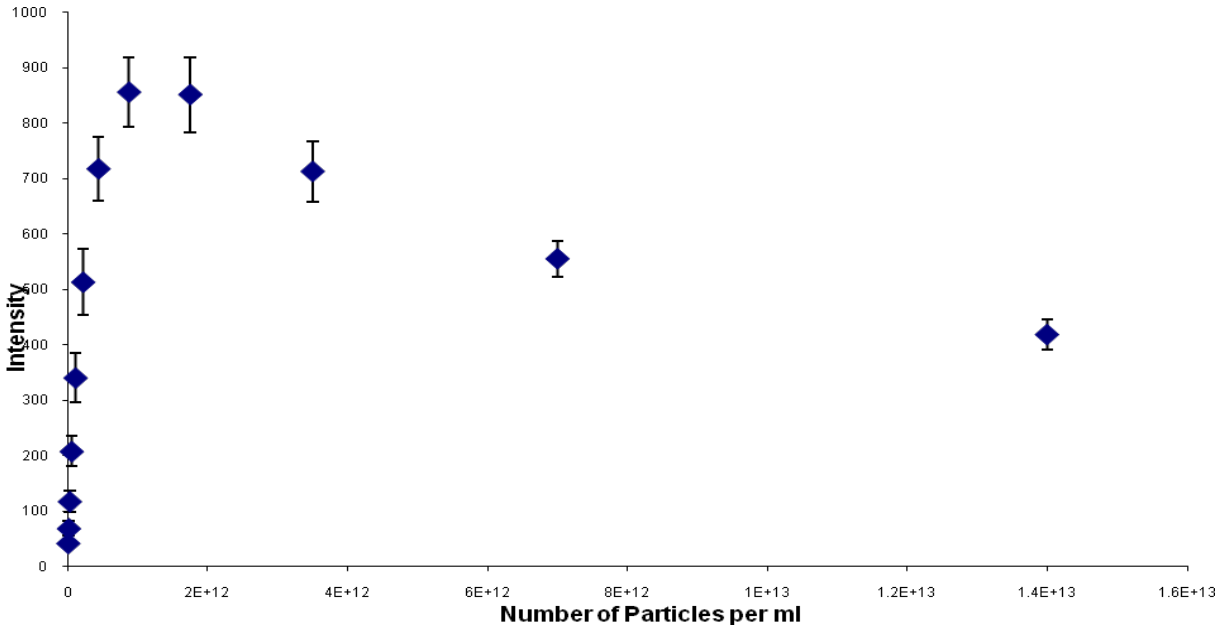

Figure 4.10. 40nm Carboxylated Invitrogen nanopolystyrene emission at 520nm by 417nm excitation as a function of nanoparticle concentration (part/ml)

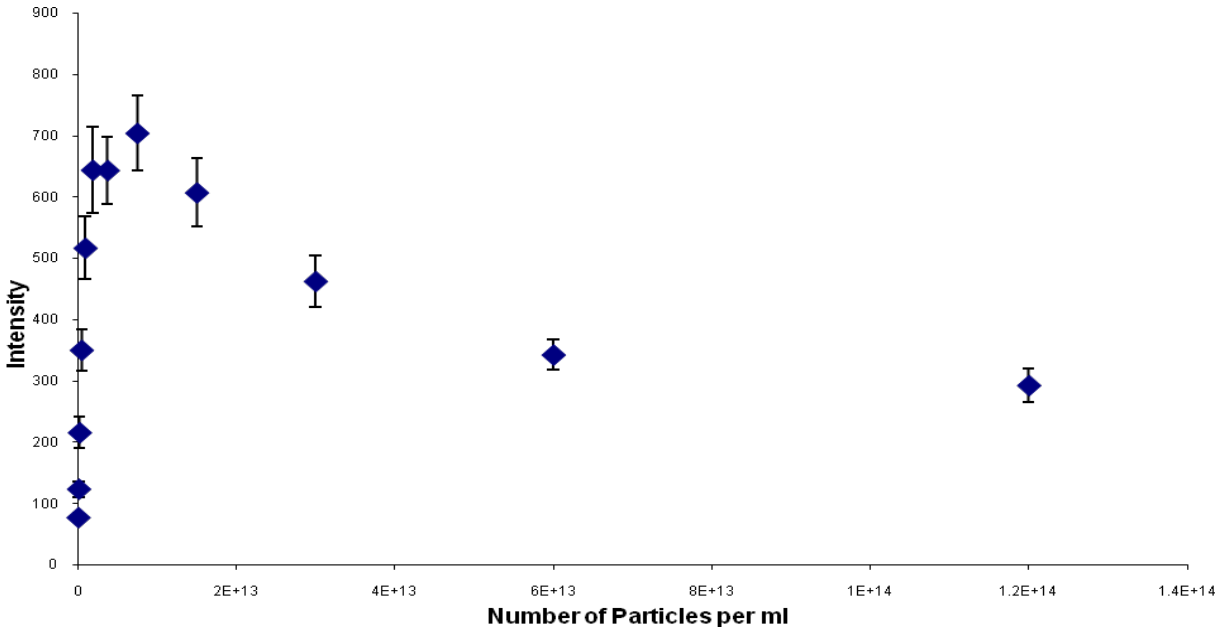

Figure 4.11 50nm Duke Scientific Nanopolystyrene emission at 508nm by 447nm excitation as a function of nanoparticle concentration (part/ml)

As can be seen from the fluorescence emission spectra obtained of both particles, the fluorescence emission reaches a maximum at a specific concentration of particles per ml, before decreasing. At these specific concentrations the fluorescence emission from the particles is at its optimum intensity. Above these concentrations, the decrease in fluorescence may be attributed to reabsorption or fluorescence quenching.

From the fluorescence emission spectrum obtained for both particles, it was concluded that optimum working concentrations of approximately 1 $x10^{12}$ particles per ml would be adapted throughout this thesis.

4.6 Chapter Summary

This chapter has presented the results of the characterisation on 50nm and 100nm Duke Scientific nanopolystyrene, 40nm and 100nm carboxylated Invitrogen nanopolystyrene and 60nm aminated nanopolystyrene. The characterisation profiling utilised a range of techniques ranging from DLS and AFM for particle sizing, zeta potential from information on particle stability in solution and electronic spectroscopy for information on the absorbance and emission properties of the fluorescent particles.

The DLS and AFM results revealed particle sizes, for 50nm and 100nm Duke Scientific Nanopolystyrene, 40nm and 100nm carboxylated Invitrogen Nanopolystyrene. The presence of surfactant may have interfered with neutral and carboxylated nanoparticles measured in water and the apparent increase in their size. The 60nm Aminated Nanopolystyrene particle was found to drastically increase in size when placed in biological media, which may be attributed to the formation of a protein corona, which would have an affect on the apparent hydrodynamic radius and thus the measured particle size. All sizes were confirmed over a range of temperatures and dispersants. Zeta potential measurements revealed that the 100nm and 40nm carboxylated particles were stable in biological media, which was most likely due to the interaction between the carboxylated surface of the nanoparticle and the ionic species found in the media, while 50nm and 100nm “neutral” particles were found to have a negative zeta potential. This may have been due to a small amount of surfactant present within the aqueous solution to prevent flocculation. However, for the purpose of this thesis they will be referred to as “neutral” nanoparticles. Both Duke Scientific particles were found to be

stable in solution over a range of temperatures, while zeta potential values showed the 60nm aminated nanoparticles to be unstable when placed in complete media. Absorbance and fluorescence emission spectroscopy revealed values which were also agreement with the supplied manufacturer's specifications. From fluorescence emission spectra obtained of both 50nm and 40nm particles, a working concentration of 1×10^{12} ppml was decided, as this concentration revealed optimum fluorescence, which will be benefit in later experimental procedures such as confocal microscopy.

The following chapter will present and discuss the results obtained of the toxicity of 50nm and 100nm Duke Scientific nanopolystyrene, 40nm and 100nm carboxylated Invitrogen nanopolystyrene and 60nm aminated nanopolystyrene. Five toxicity assays were employed, with theory and experimental results presented for each.

References

1. Warheit, D.B., *How Meaningful are the Results of Nanotoxicity Studies in the Absence of Adequate Material Characterization?* Toxicol. Sci., 2008. **101**(2): p. 183-185.
2. Park, H. and V.H. Grassian, *Commercially manufactured engineered nanomaterials for environmental and health studies: Important insights provided by independent characterization.* Environmental Toxicology and Chemistry, 2010. **29**(3): p. 715-721.
3. Nel, A.E.M., Lutz Velegol, Darrell Xia, Tian Hoek, Eric M. V. Somasundaran, Ponisseril Klaessig, Fred Castranova, Vince Thompson, Mike, *Understanding biophysicochemical interactions at the nano-bio interface.* Nat Mater, 2009. **8**(7): p. 543-557.
4. Patel, L., J. Zaro, and W.-C. Shen, *Cell Penetrating Peptides: Intracellular Pathways and Pharmaceutical Perspectives.* Pharmaceutical Research, 2007. **24**(11): p. 1977-1992.
5. Rejman, J.O., Volker Zuhorn, Inge S Hoekstra, Dick, *Size-dependent internalization of particles via the pathways of clathrin- and caveolae-mediated endocytosis.* Biochem. J., 2004. **377**(1): p. 159-169.
6. Oberdorster, G., et al., *Principles for characterizing the potential human health effects from exposure to nanomaterials: elements of a screening strategy.* Particle and Fibre Toxicology, 2005. **2**(1): p. 8.
7. Boverhof, D. and R. David, *Nanomaterial characterization: considerations and needs for hazard assessment and safety evaluation.* Analytical and Bioanalytical Chemistry, 2010. **396**(3): p. 953-961.
8. Malvern (2011) *Dynamic Light Scattering; common terms defined.* .
9. Ju-Nam, Y. and J.R. Lead, *Manufactured nanoparticles: An overview of their chemistry, interactions and potential environmental implications.* Science of The Total Environment, 2008. **400**(1–3): p. 396-414.
10. Patnaik, P., *A Comprehensive Guide to the Hazardous Properties of Chemical Substances*. 2007, John Wiley and Sons Inc.
11. Chun, A.L., *Protein corona: Particle size matters.* Nat Nano, 2011.
12. Lundqvist. M, S.J., Elia. G, Lynch. I, Cedervall. T, and Dawson. K.A. , *Nanoparticle size and surface properties determine the protein corona with possible implications for biological impacts.* PNAS, 2008. **105**(38): p. 14265 - 14270
13. Xia, T., et al., *Comparison of the Abilities of Ambient and Manufactured Nanoparticles To Induce Cellular Toxicity According to an Oxidative Stress Paradigm.* Nano Letters, 2006. **6**(8): p. 1794-1807.
14. Therrien, J., A. Dindar, and D. Smith, *AFM studies of nanoparticle deposition via electrospray ionization.* Microscopy Research and Technique, 2007. **70**(6): p. 530-533.
15. Arcoleo, V. and V.T. Liveri, *AFM investigation of gold nanoparticles synthesized in water/AOT/n-heptane microemulsions.* Chemical Physics Letters, 1996. **258**(1-2): p. 223-227.

16. X. Zeng, N.K.a.T.S., *A direct comparison of sizes characterized by TEM and AFM for Fe<INF>2</INF>O<INF>3</INF> nanoparticles prepared by laser ablation.* Applied Physics A: Materials Science & Processing, 1999. **69**(0): p. S253-S255.
17. Cooper., G., *The Cell: A Molecular Approach. Structure of the Plasma Membrane*. 2nd edition ed, ed. S. (MA). 2000: Sinauer Associates.
18. Carruthers, A., *Facilitated diffusion of glucose.* Physiol. Rev., 1990. **70**(4): p. 1135-1176.
19. McGuinnes, C., et al., *Surface Derivatization State of Polystyrene Latex Nanoparticles Determines both Their Potency and Their Mechanism of Causing Human Platelet Aggregation In Vitro.* Toxicological Sciences, 2011. **119**(2): p. 359-368.
20. Parker, J.W., et al., *Leukocyte immunophenotyping by flow cytometry in a multisite study: standardization, quality control, and normal values in the Transfusion Safety Study. The Transfusion Safety Study Group.* Clin Immunol Immunopathol, 1990. **55**(2): p. 187-220.
21. Bangs, L.B., *New developments in particle-based immunoassays: Introduction.* Pure Appl. Chem., 1996. **68**(10): p. 1873-1879.

Chapter 5

Toxicology of Nanopolymers

Chapter 5

5.1 Introduction

In the introductory chapters, Chapter 2, Section 2.1, it was highlighted that a critical issue with nanomaterials is the clear understanding of their potential toxicity. Several physico-chemical parameters have been proposed to be significant contributors in nanomaterial toxicity: size, crystalline structure, chemical composition, surface area and oxidation status [1]. However none of these parameters have been identified as being solely responsible for nanoparticle toxicity. In general, toxicity of particles is considered a consequence of a contribution of their physicochemical properties which allows them to evade or cause damage to defensive mechanisms within cells. [2].

The aim of this section is to evaluate potential toxicological effects of polystyrene on A549 cells. It has been well documented that known nontoxic materials can at nanoscale exhibit toxic effects on cells *in vitro*. In its Working Report on Nanomaterials, the OECD listed nanopolystyrene as one of the worldwide manufactured nanomaterials that is of interest, within the bio-nano area [3]. Interest generated by nanopolystyrene in the area of bio-nano applications, may be due to the lack of toxicity effects noted for its bulk form. As described in Chapter 2, Section 2.2, the toxicity of polystyrene is largely undocumented, although it is listed by The World Health Organisation (WHO) and the U.S. National Toxicology Program for Acute Toxicity Studies as having mild acute toxicity when exposed to humans or rats through various exposure routes [4]. The polymer and its associated monomer, styrene, are also listed as having no known carcinogenic effects and no endocrine disruption at the concentrations at which people are exposed to daily [5]. A report by the Health Protection Agency in the UK describe how approximately 90% of all

styrene absorbed by humans undergoes hepatic oxidation by cytochrome P450, to styrene 7,8-oxide, which is the active metabolite. Styrene 7,8-oxide is further metabolised into phenylglyoxylic acid, mandelic acid and hippuric acid which are excreted in the urine [6].

The cytotoxicity of a substance is a measure of how toxic it is to a cell. Cells treated with a cytotoxic compound can result in a variety of cell fates. There are two experimentally distinguishable mechanisms of cell death: necrosis, the “accidental” cell death that occurs when cells are exposed to a serious physical or chemical insult, and apoptosis, the “normal” cell death that removes unwanted or useless cells. Apoptosis is characterized by well defined cytological and molecular events including a change in the refractive index of the cell, cytoplasmic shrinkage and nuclear condensation. These changes may be quantitatively measured through colorimetric and luminescence based assays. There are a wide range of cytotoxicity assays that have been developed which utilise different parameters associated with cell death and interference in proliferation [1].

Although conventional colorimetric and luminescence based assays give an indication of the effect on proliferation and viability as well as organelle damage, they however, fail to recognise that although some nanoparticles may not produce immediate or semi-long term (10 days) toxic effects, nanoparticles have the ability to localise within cells and cell organelles. There is a strong likelihood that the biological activity of nanoparticles depends on physico-chemical parameters not routinely considered in toxicity screening studies. While there is an abundance of studies that examine the toxicity, accumulation and translocation of nanoparticles at short exposure times [7] [8], there is an inadequate amount of data on the long term

exposure of nanoparticles, particularly when considering the possible long term accumulation and translocation of particles around the body [9]. There is currently a lack of well characterized toxicological targets and assay methods for studying the effects of nanomaterials [1] [8]. Only recently has a working group report been published that details screening strategy for various biological targets that can be affected by nanomaterials [10].

With polystyrene in its bulk size exhibiting non-hazardous effects to humans, and the knowledge that nanoparticles can migrate to different areas of the body, the interest in nanopolystyrene as a possible potential bio-nano polymer is justified. However, as with any potential material that may be used for biological application, a full toxicological profile for the material is imperative.

While some literature presents the findings that nanopolystyrene in its cationic form can cause toxicity, and even induce cell death [11], there is however also substantial evidence that show neutral and anionic nanopolystyrene does not produce cytotoxic effects [12]. Instead, they have been shown to be taken up by cells and incorporated within cell organelles, such as endosomal, lysosomal and mitochondrial compartments of EAhy926 cells, a human umbilical vein endothelial cell line and human hepatocyte cell lines (HepG2) [13] [14]. Similar results were observed when red blood cells were used to investigate the uptake of fluorescent nanopolystyrene particles (78nm, neutral and anionic) [15]. There was no suggestion of any toxicity caused by nanoparticles, with confocal microscopy allowed for the monitoring of 78nm polystyrene to be taken up by blood cells over a period of 4 – 24 hours.

However, there are several studies that must be taken into account when examining the toxicity of charged nanopolystyrene, most notably in the case of positively

charged nanopolystyrene. For example, in a recent study conducted by Nel et al (2007), it was reported that 200nm positively charged polystyrene beads generated high levels of reactive molecules and induced oxidative stress in lung macrophages (defence cells engulf particulate matter). However, little activity was observed for negatively charged polystyrene beads, while in a previous study in 2006, Nel and colleges reported that 60nm cationic nanopolystyrene induced mitochondrial damage and cell death without inflammation. In another study, 97nm cationic nanoparticles were also found to have an immediate toxic effect at the blood brain barrier (BBB) whereas neutral and anionic nanoparticles were found to have no effect on the BBB integrity [12].

In this chapter, the direct acute cytotoxicity of 50nm neutral, 40nm carboxylated and 60nm aminated nanopolystyrene will be presented and discussed based on the use of Alamar Blue™ (AB), Neutral Red (NR), Commassie Blue (COMMASSIE) and 3-(4,5-dimethylthiazol-2-yl)-2,5-diphenyltetrazolium bromide (MTT) assays while the longer term effects will be monitored using the clonogenic assay. In all cases, data are expressed as a percentage of unexposed controls and, to verify experimental protocols, a positive control of a 10% DMSO 90% medium mixture was employed. For cytotoxicity, statistically significant differences were set at $p \leq 0.05$).

5.2 Alamar Blue Assay

The Alamar Blue™ (AB) assay is designed to quantify the proliferation, or effect or disruption on cell growth, of various cell lines and is widely utilized to measure cytotoxicity. The disruption of cell proliferation can give an indication on the effect of cell division, which may direct examination of the effect of a particle to possible DNA damage. Resazurin, a non-fluorescent indicator dye, is converted to bright red–

fluorescent, Resorufin, via the reduction reactions of metabolically active cells. Viable proliferating cells cause a reduction of the dye causing a colour change from a non-fluorescing indigo blue (oxidised) to a fluorescent pink species (reduced) (figure 5.1).

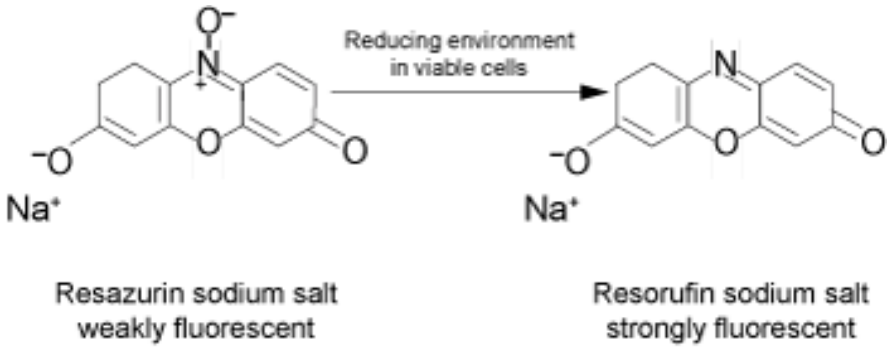

Figure 5.1 Conversion of Resazurin (oxidised form) to Resorufin (reduced form)

The amount of fluorescence produced is proportional to the number of living cells. Damaged and nonviable cells have lower innate metabolic activity and thus generate a proportionally lower signal than healthy cells. One main advantage of this assay lies in its water solubility. It requires no solvent extraction step and hence cellular viability is unaffected allowing multiple tests to be carried out on the cells. Measurements may be made by absorbance monitoring of AB supplemented cell culture medium or alternatively fluorescent measurements can be made (Biosource Inc, O'Brien et al., 2000). The absorbance spectra of the oxidised and the reduced forms overlap. Therefore, the absorbance measurements must be made at the absorbance maxima of each form, namely 570 nm and 600 nm. Fluorescent measurements can be made by exciting from 530 to 560 nm and recording emission at 590 nm (Biosource Inc, O'Brien et al., 2000).

Figures 5.2, 5.3 and 5.4 display the cytotoxic response curves obtained for 50nm nanopolystyrene, 40nm carboxylated nanopolystyrene and 60nm aminated

nanopolystyrene respectively using the Alamar Blue assay. As can be seen from figure 5.2, 50nm nanopolystyrene did not produce any cytotoxic effects over the four time points measured. When cells are metabolising they maintain a reducing environment within their cytosol and this reduced state can be measured spectrophotometrically through the conversion of Resazurin, (indicator dye), to Resorufin. From the measurement of the percentage reduction in Alamar Blue in A549 cells exposed to 50nm nanopolystyrene particles, in comparison to the control; it is evident that over the four time points (24hr, 48hr, 72hr and 96hr) there was no decrease in the number of metabolising cells. This result indicates that particles did not have an effect on the proliferation of cells. As can be seen from the graph, particle concentration also did not have an effect on proliferation, as there is no decrease in reduction of Alamar Blue dye from of Resazurin to Resorufin, indicating cells did not have a decrease in metabolic activity over all time periods and particle concentrations.

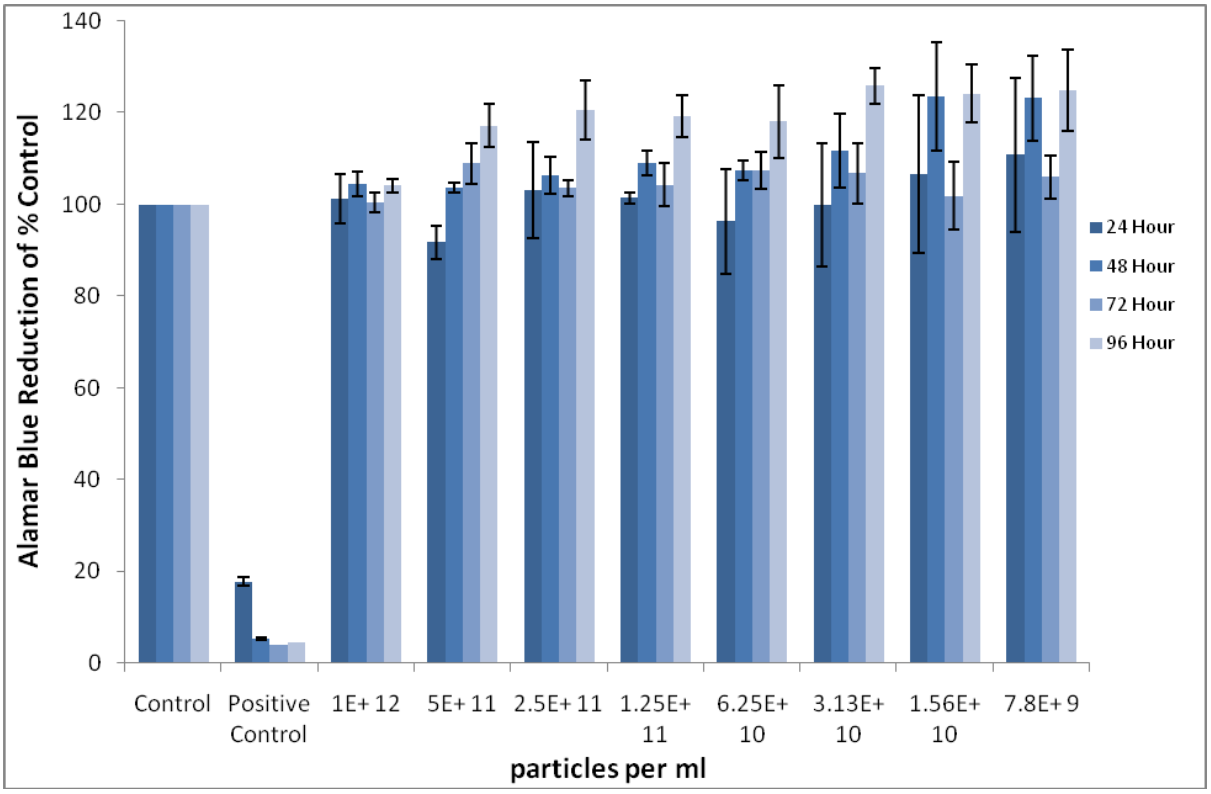

Figure 5.2 Cytotoxicity of 50 nm Duke Scientific Nanopolystyrene to A549 cells after 24, 48, 72 and 96 hour exposures determined by the AB assay. Data are expressed as percent of control mean ± SD of three independent experiments

Figure 5.3 shows the results of the Alamar Blue assay for 40nm carboxylated nanopolystyrene particles. As with the 50nm PS, the 40nm nanopolystyrene particles showed no cytotoxicity effect over the four time points measured on A549 cells. The cytotoxic response curve obtained indicates no decrease in metabolic activity with particle concentration or exposure time, with particle concentration also having no cytotoxic effect.

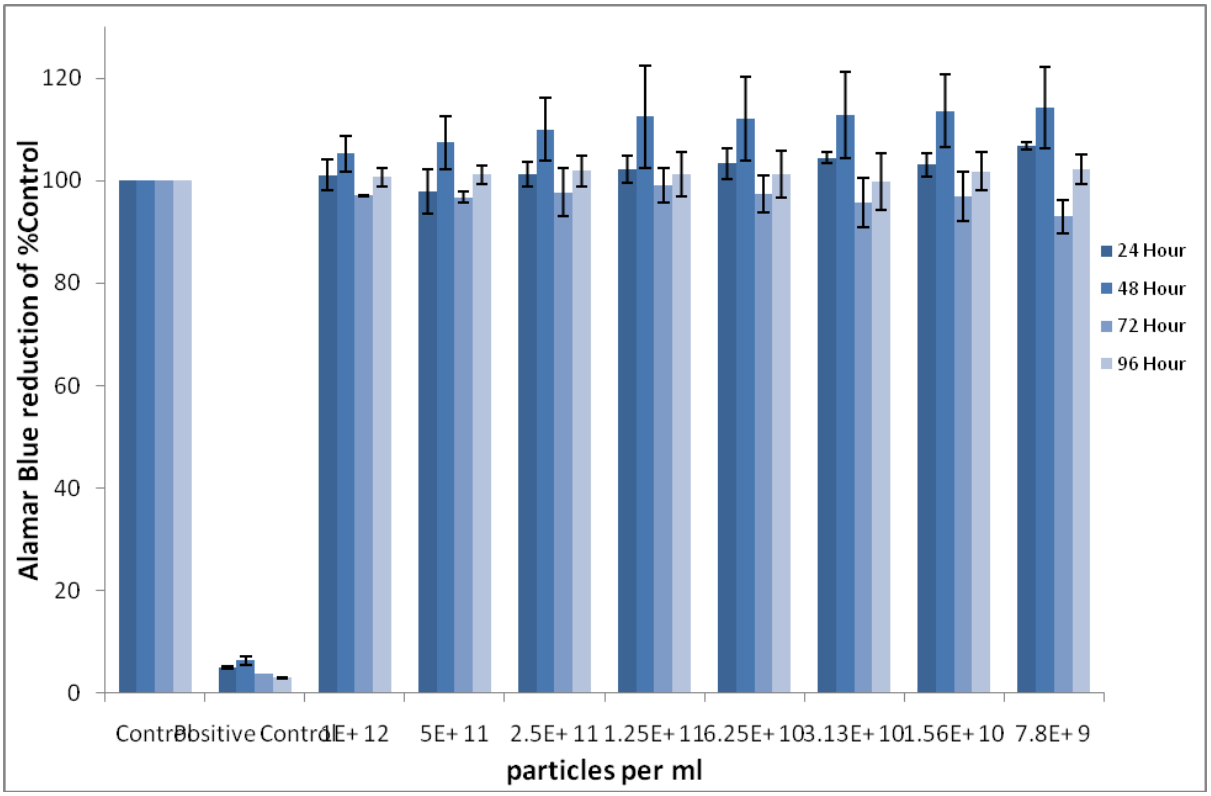

Figure 5.3 Cytotoxicity of 40nm carboxylated Invitrogen Nanopolystyrene to A549 cells after 24, 48, 72 and 96 hour exposures determined by the AB assay. Data are expressed as percent of control mean ± SD of three independent experiments.

However, there are slight increases in fluorescence reading of Alamar blue reduction in comparison of the % control in both cases. In figure 5.3 the increase can be seen particularly over the 48 and 96hr exposures. The increase for the 40nm particle is more evident during the 48hr exposure period, figure 5.3. These small increases in respect to the classical unexposed control, fall within the standard deviation errors, are generally considered to be attributed to slight variations in the seeding densities of each well or plate. The results obtained in this experiment are in keeping with literature reports by Brunsten et al, in that 50nm neutral nanopolystyrene and 40nm carboxylated nanopolystyrene does not cause any cytotoxic effects when measured using the Alamar Blue assay.

The cytotoxic response of A549 cells after exposure to 60nm aminated nanopolystyrene, measured using the Alamar Blue assay can be seen in figure 5.4. Unlike the previous two particles exposed to cells, a toxic response can be seen cause by the highest test concentration of $1x12^{12}$ particles per ml (ppml), over a range of 24 to 96 hours. A slight toxic response of cells to particles can also be seen over same time points for the second highest test concentration of $5x10^{11}$ppml.

For the highest concentration of $1x10^{12}$ ppml, it can be seen that an almost complete toxic response was observed for the 96hr exposure period. While the same concentration also caused sever cytotoxicity to cells over a 24 to 72 hour period. The number of metabolising cells observed for the test concentration $5x10^{11}$ppml, in comparison to the control, can be seen to have also sharply decreased over the test periods of 48 to 96 hour. A lesser cytotoxic response for this concentration can be observed for the 24hr exposure period. However, the remainder of the test concentration range from $2.5x10^{11}$ to $7.8x10^{8}$ppml show no cytotoxic response was observed over the time periods of 24 to 96 hours.

Toxicity results observed for A549 cells after exposure to higher test concentrations of 60nm aminated particles are in agreement with literature findings [11] .

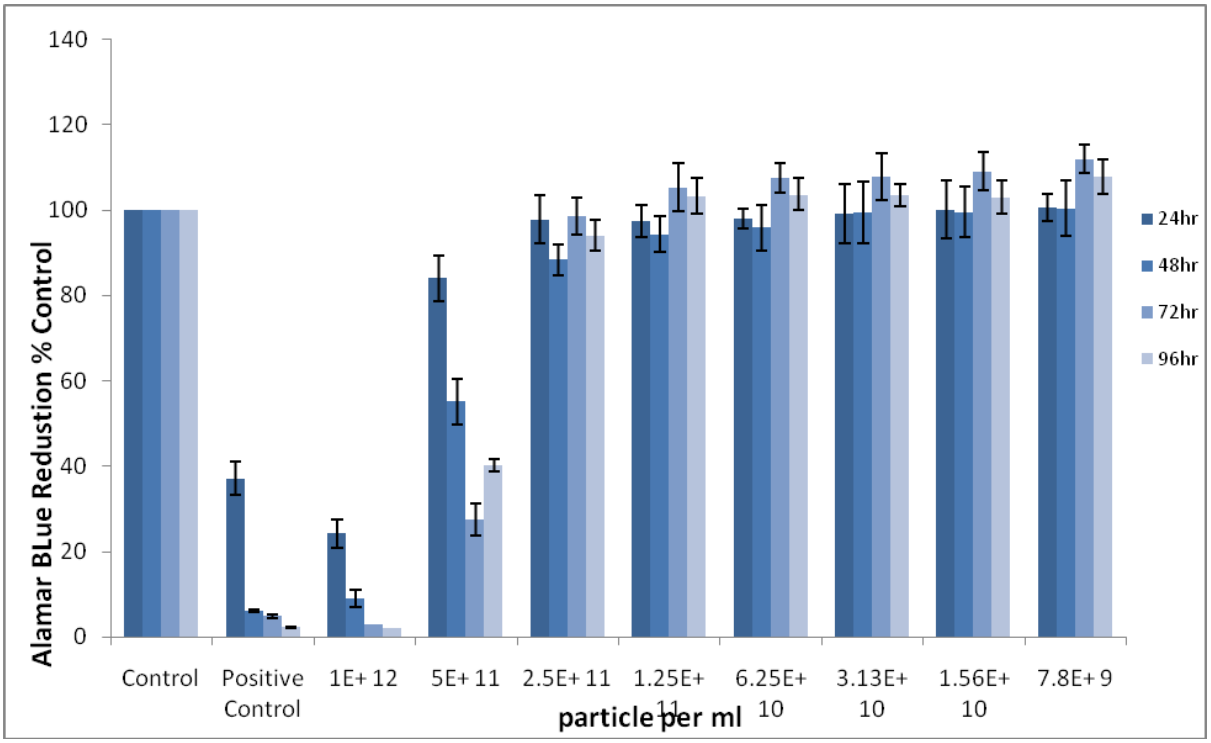

Figure 5.4 Cytotoxicity of 60nm Aminated nanopolystyrene to A549 cells after 24, 48, 72 and 96 hour exposures determined by the AB assay. Data are expressed as percent of control mean ± SD of three independent experiments.

5.3 Neutral Red Assay

The Neutral Red (NR) cytotoxicity assay is based on the ability of viable cells to incorporate and bind neutral red, a weak cationic dye, dimethyl diaminophenazine chloride, figure 5.5, that readily penetrates cell membranes by non-ionic diffusion (Borenfreund *et al*., 1984, Borenfreund *et al*., 1988). It accumulates in the lysosomes of cells where it binds to the sensitive lysosomal membrane. Cells damaged by xenobiotic action have decreased ability of taking up and binding NR, so that viable cells can be distinguished from damaged or dead cells. The dye can be extracted from intact cells using a solution of 1 % (v/v) acetic acid and 50 % (v/v) ethanol and the absorbance or fluorescence of solubilised dye can be determined (Borenfreund *et al*., 1984; Borenfreund *et al*., 1988). The uptake of neutral red depends on the cell's capacity to maintain pH gradients, through the production of ATP. At physiological pH, the dye presents a net charge close to zero, enabling it to penetrate the membranes of the cell. Inside the lysosomes, there is a proton gradient to maintain a pH lower than that of the cytoplasm. Thus, the dye becomes charged and is retained inside the lysosomes. The test is very sensitive, specific, and readily quantifiable. Cytotoxicity is expressed as a concentration dependent reduction of the uptake of the NR after chemical exposure thus providing a sensitive, integrated signal of both cell integrity and growth inhibition.

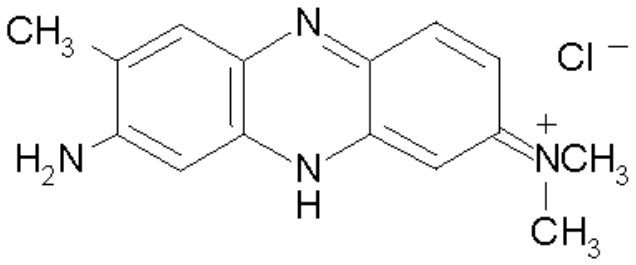

Figure 5.5 Dimethyl diaminophenazine chloride dye (Neutral Red).

Figures 5.6, 5.7 and 5.8 displays the cytotoxic response curves obtained for 50nm Duke Scientific nanopolystyrene, 40nm carboxylated Invitrogen nanopolystyrene and 60nm aminated nanopolystyrene respectively using the Neutral Red assay.

The results of Neutral Red uptake for A549 cells exposed to 50nm nanopolystyrene over time periods of 24hr, 48hr, 72hr and 96hr can be seen in figure 5.6. As with the Alamar Blue assay, particle concentration did not have an effect on the proliferation or viability of exposed cells. The exposure time of cells to particles also had no effect and did not induce toxicity over 24 – 96 hours.

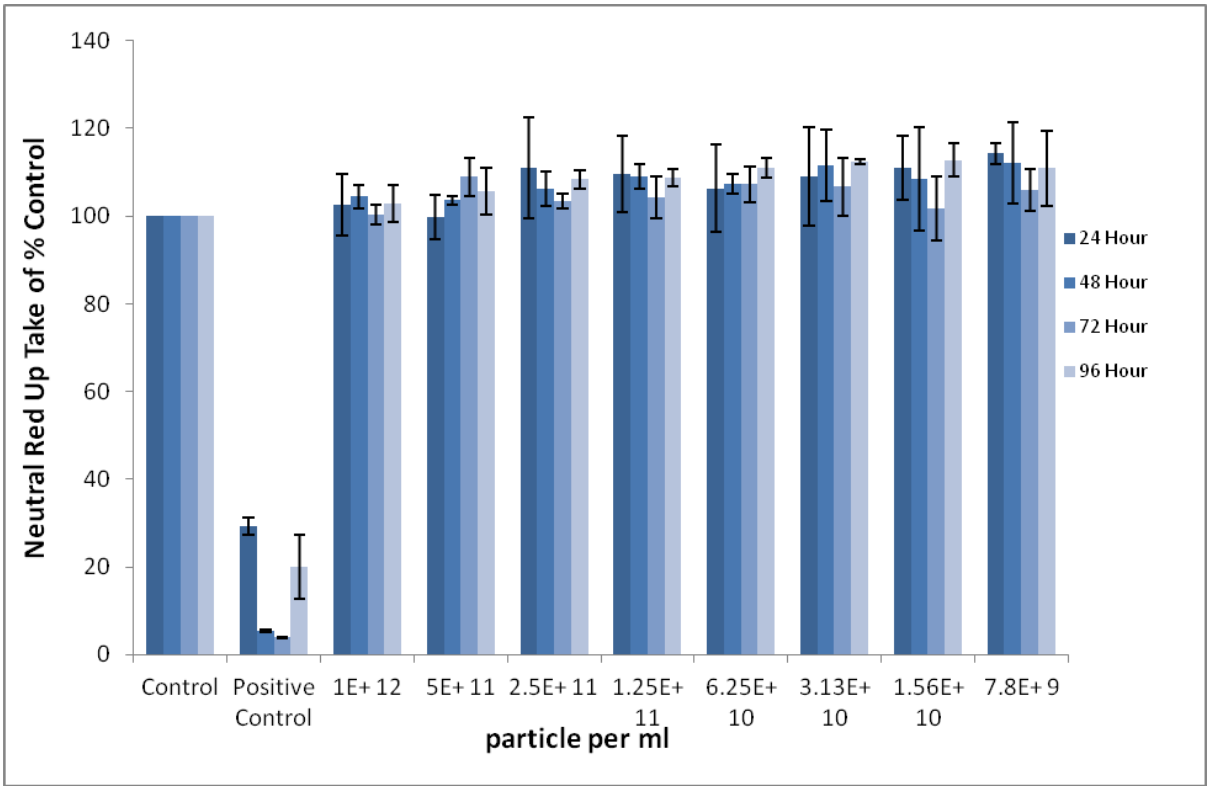

Figure 5.6 Cytotoxicity of 50 nm Duke Scientific Nanopolystyrene to A549 cells after 24, 48, 72 and 96 hour exposures determined by the NR assay. Data are expressed as percent of control mean ± SD of three independent experiments.

Figure 5.7 shows cytotoxicity results for the exposure 40nm aminated nanopolystyrene particles to A549 cells, as determined by NR assay. The results presented show there is no cytotoxic effects to A549 cells as a results of exposure to 40nm PS particles. As with the 50nm PS, the results show no cytotoxicity observed by cells as a result of exposure to particles. The results show no decrease in the uptake of NR dye over the measured time points, with particle concentration also having no effect on NR uptake by viable cells.

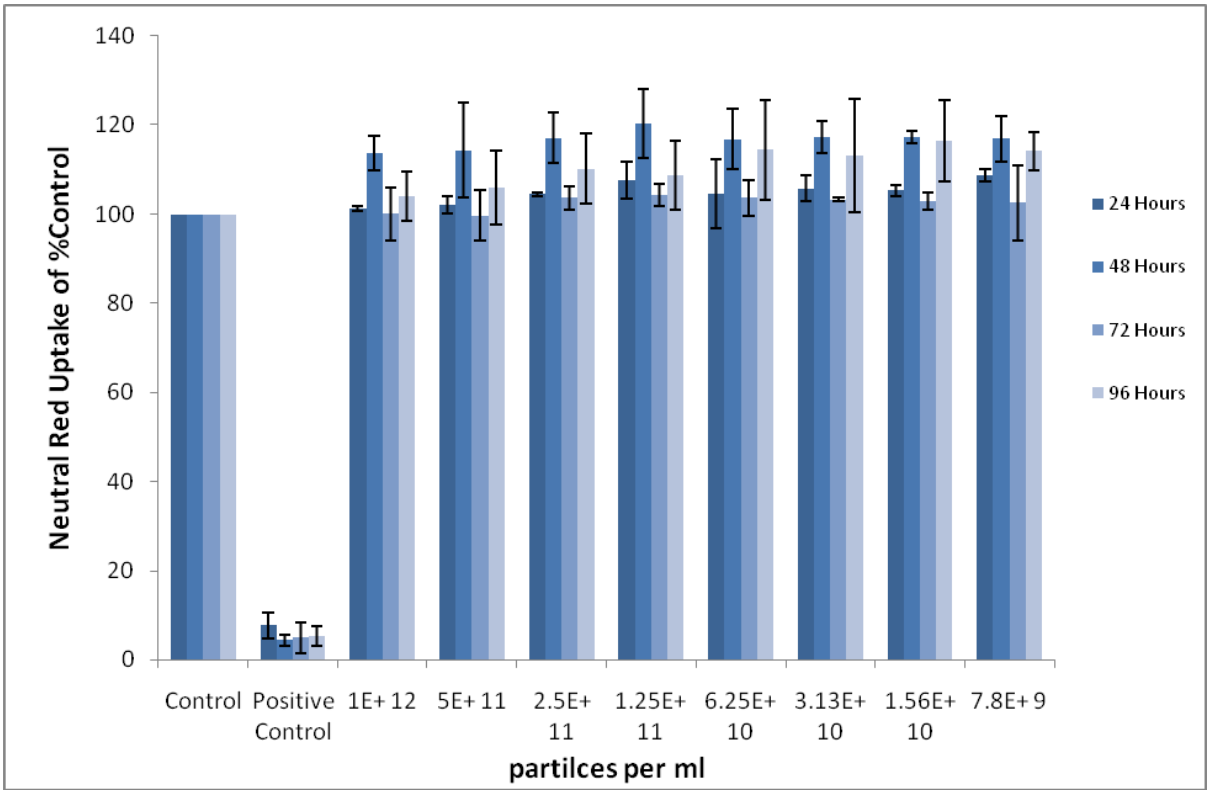

Figure 5.7 Cytotoxicity of 40nm carboxylated Invitrogen Nanopolystyrene to A549 cells after 24, 48, 72 and 96 hour exposures determined by the NR assay. Data are expressed as percent of control mean ± SD of three independent experiments.

Because cytotoxicity is expressed as a concentration dependent reduction of the uptake of NR after chemical exposure, it can be seen from the results in figure 5.6 and 5.7 that there was no decrease in the uptake of NR upon exposure, hence no alterations of the cell surface or the sensitive lysosomal membrane, resulting in no toxicity by either particle over the exposure times observed.

However, as can be seen in figure 5.8, NR uptake, within A549 cells after exposure to the highest test concentration of 60nm aminated nanoparticles, can be seen to have dramatically decreased, indicating a toxic response from cells. The $1x10^{12}$ ppml test concentration can be seen to have a toxic effect on cells after 24hr with the number of cells compared the control decreasing dramatically over the 96hr exposure period. The second highest test concentration of $5x10^{11}$ can also be seen to have a slight toxic effect on cells, with toxicity increasing over the 96hr time period. The NR uptake by healthy, viable cells is decreasing over the exposure periods suggesting that, 60nm aminated particles at a concentration of $5x10^{11}$ cause some degree of toxicity to A549 cells with increasing exposure time.

As with the previous Alamar Blue assay, the findings from this assay in also in keeping with literature reports that aminated nanopolystyrene can cause toxicity in cells.

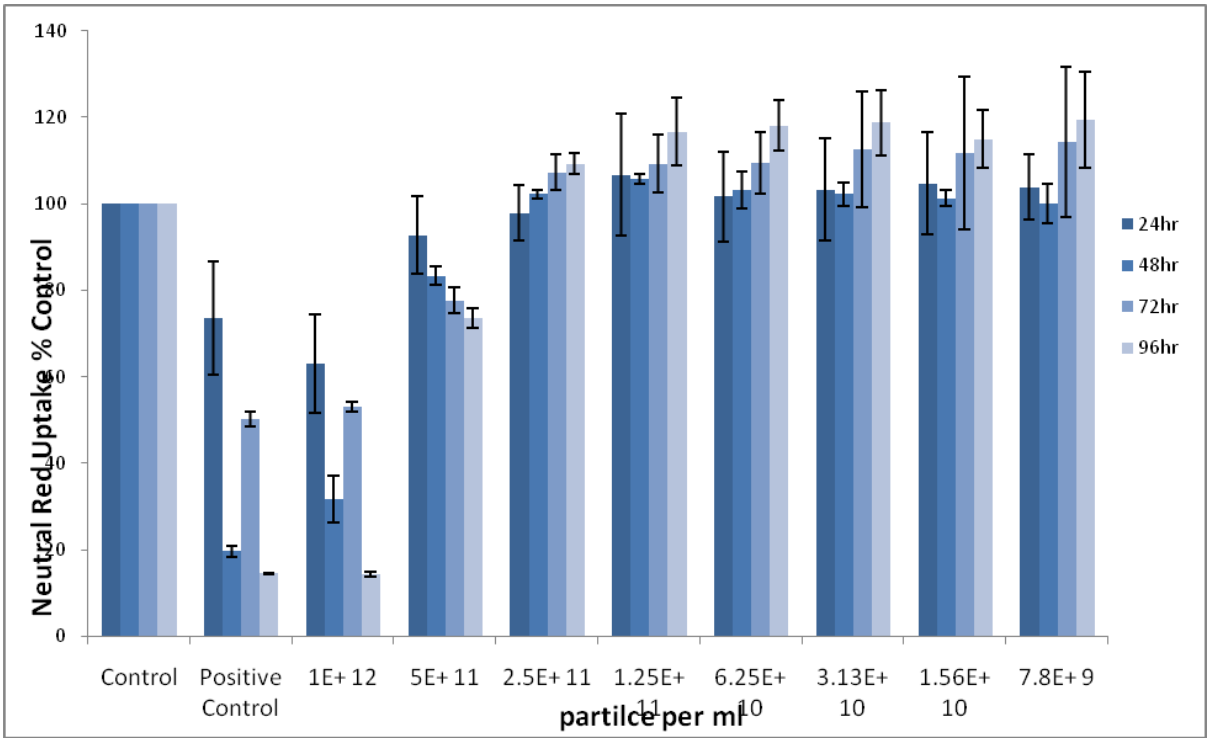

Figure 5.8 Cytotoxicity of 60nm Aminated Nanopolystyrene to A549 cells after 24, 48, 72 and 96 hour exposures determined by the NR assay. Data are expressed as percent of control mean ± SD of three independent experiments.

As previously observed with the Alamar Blue assay, there are slight increases in absorbance reading of neutral red uptake in comparison of the % control particularly over the 48 and 96hr exposures for the 40nm particle, figure, 5.7 and for the 60nm particle over 72 and 96hr periods. These are small increases in respect to the classical unexposed control, that fall within the standard deviation errors, are generally considered to be attributed to slight variations in the seeding densities of each well or plate.

5.4 Coomassie Blue Assay

The protein content of cells after exposure to a suspected toxicant is often used as a measure of cytotoxic effects *in vitro*. Different spectroscopic methods are routinely available for determination of protein concentrations, including measurement of protein's intrinsic UV absorbance, and methods generating a protein-dependent colour change, namely the Lowry assay, the Smith copper/bicinchoninic assay. The simplest and most sensitive is the Bradford assay, introduced in the mid 1970s, and is based on the equilibrium between three forms of Coomassie Blue-G250 (Coomassie) dye (figure 5.9). Development of colour in Coomassie dye-based (Bradford) protein assays has been associated with the presence of certain basic amino acids in protein, although Interactions are chiefly with arginine rather than primary amino groups; the other basic (His, Lys) and aromatic residues (Try, Tyr, and Phe) give slight responses [16].

Under strongly acidic conditions, the dye is most stable in its double protienated red state. When bound to a protein, the un-protonated blue form becomes more stable. Van der Waals forces and hydrophobic interactions also participate in the binding of the dye to proteins. The number of Coomassie dye ligands bound to each protein molecule is approximately proportional to the number of positive charges found on the protein. Free amino acids, peptides and low molecular weight proteins do not produce colour with coomassie dye reagents (Bradford, 1976).

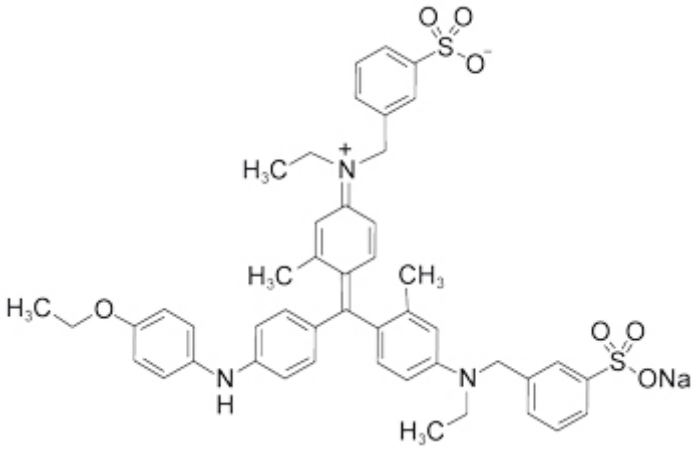

Figure 5.9 Chemical structure of Coomassie Blue G-250

When Coomassie blue G-250 (figure 5.7) binds to proteins in acid solution, it has an absorbance shift from 465 nm to 595 nm. The absorbance data can then be used in Beer's law to determine protein concentration and ultimately the actual amount of protein in a given solution.

The main disadvantage concerning this assay is the possibility to record some protein based material although no viable cells are present. The assay is very prone to influences from non protein sources, particularly detergents, and becomes progressively more non-linear at high protein concentrations (Borenfreund, 2006). The main advantage for multi-endpoint cytotoxicity studies is that after the absorbance/ fluorescence of another dye has been established, total cell protein can be measured on the same test cells using Coomassie dye.

Figures 5.10, 5.11 and 5.12 display the cytotoxic response curves obtained for 50nm Duke Scientific nanopolystyrene, 40nm carboxylated Invitrogen Nanopolystyrene and 60nm aminated nanopolystyrene, respectively using the Comassie Blue assay.

Cytotoxicity results of toxicity to A549 cells after 24, 48, 72 and 96 hour exposures of 50nm nanopolystyrene, determined by the Coomassie Blue assay, can be seen in figure 5.10. As can be seen for the diagram, particles did not induce any cytotoxic effects as measureable by the Coomassie Blue assay. As with previous assay conducted, particle concentration did not have an effect on the ability viable protein molecules within the cell to bind to the CB dye ligands. The results show that the exposure of the 50nm nanopolystyrene particles to A549 cells did not interfere with viable cells ability to produce amino acids, therefore, not having an effect on the cells function or proliferation.

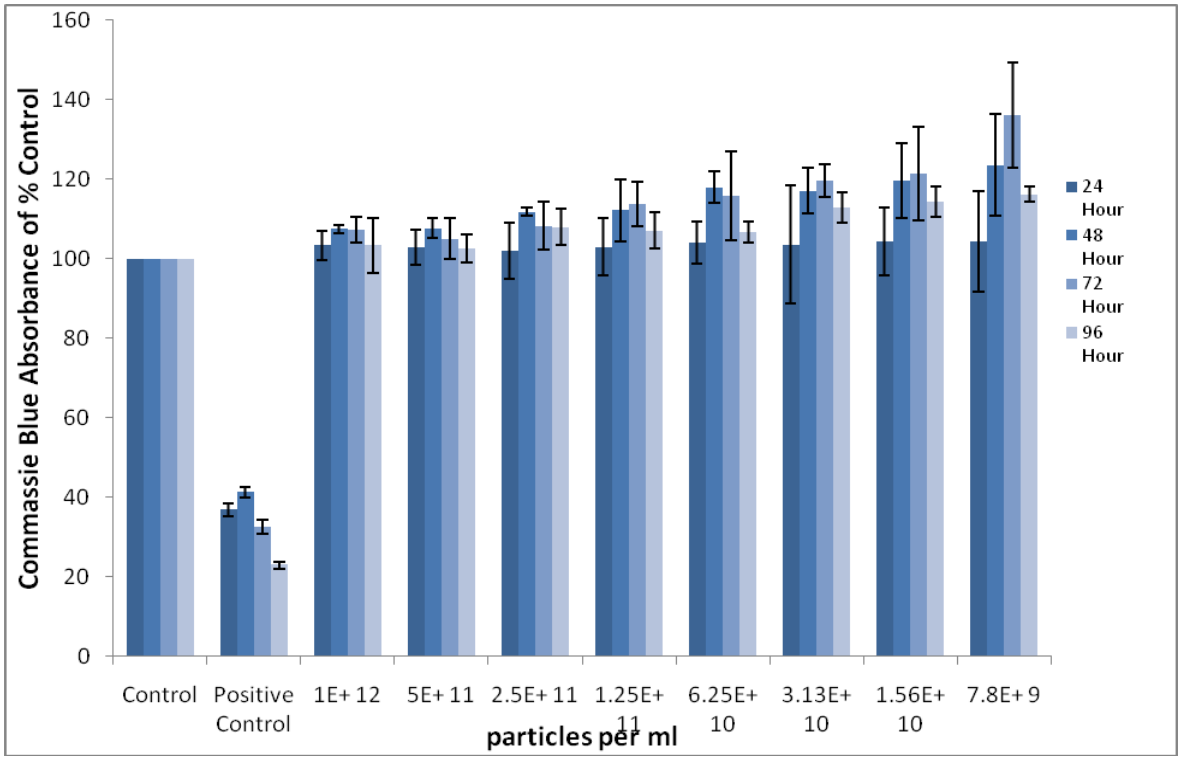

Figure 5.10 Cytotoxicity of 50 nm Duke Scientific Nanopolystyrene to A549 cells after 24, 48, 72 and 96 hour exposures determined by the CB assay. Data are expressed as percent of control mean ± SD of three independent experiments.

40 nm carboxylated nanopolystyrene exposed to A549 cells over a time range of 24 – 96 hours also produced no cytotoxicity effects as measured by the CB assay as can be seen in Figure 5.11. Amino acid production within viable cells was not disrupted. This can be seen in the absorbance values obtained. Because the number Coomassie dye ligands bound to each protein molecule is approximately proportional to the number of positive charges found on the bound protein, absorbance values obtained of cells exposed to particles in percentage comparison to control, show that a high number of proteins within the viable cells bound to the dye ligands proving that protein production was not effected and no toxicity was induced from exposure to particles.

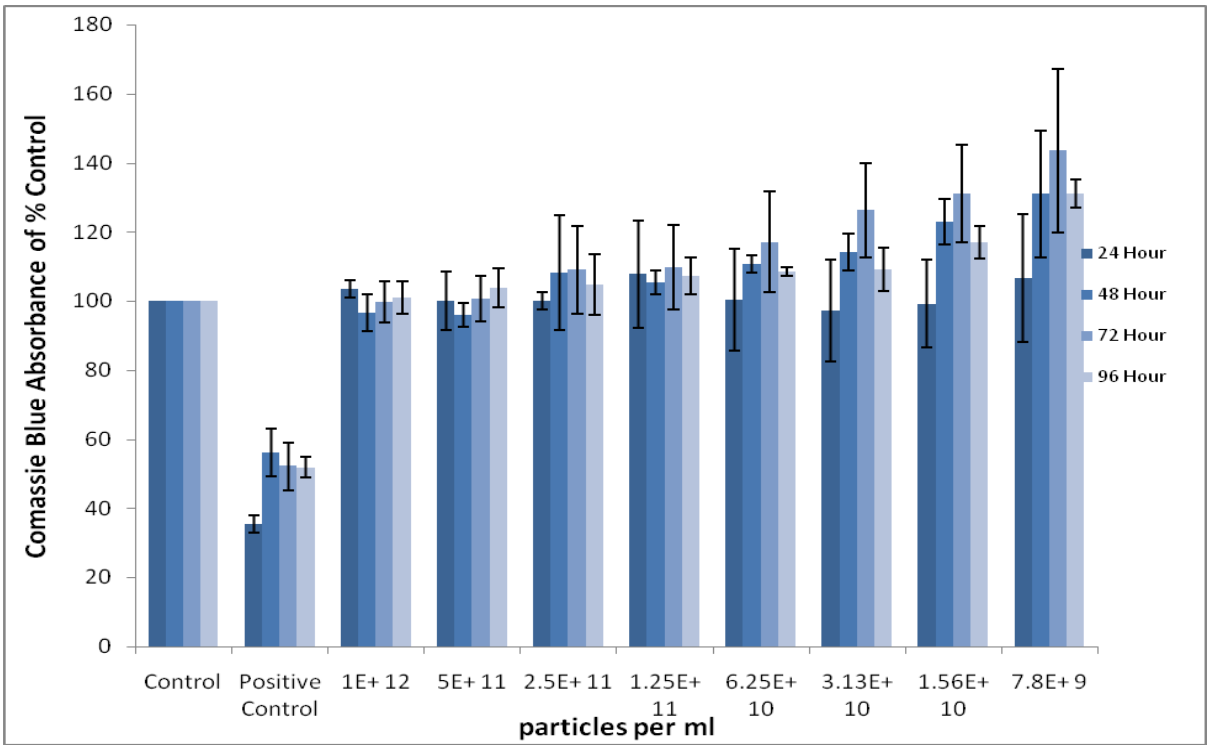

Figure 5.11 Cytotoxicity of 40nm carboxylated Invitrogen Nanopolystyrene to A549 cells after 24, 48, 72 and 96 hour exposures determined by the CB assay. Data are expressed as percent of control mean ± SD of three independent experiments.

Cytotoxicity results of toxicity to A549 cells after 24, 48, 72 and 96 hour exposures of 60nm aminated nanopolystyrene, determined by the Coomassie Blue assay, can be seen in figure 5.12.

As observed with previous assays, the highest test concentration of aminated nanoparticles is observed as causing cytotoxicity to A549 cells over a 24 to 96 hour exposure period. The concentration of $1x10^{12}$ ppml is found to induce a cytotoxic response from cells, with the highest level of toxicity found after 96 hours of exposure.

After 96 hours, it can also be observed for the concentration of $5x10^{11}$ ppml, that a slight degree of cytotoxicity is experienced by A549 cells. Due to the nature of the Coomassie Blue assay, these toxicity results show less bonding of dye ligands, indicating that protein production of viable cells after exposure has been effected.

As with the previous Alamar Blue assay, the findings from this assay in also in keeping with literature reports that aminated nanopolystyrene can cause toxicity in cells.

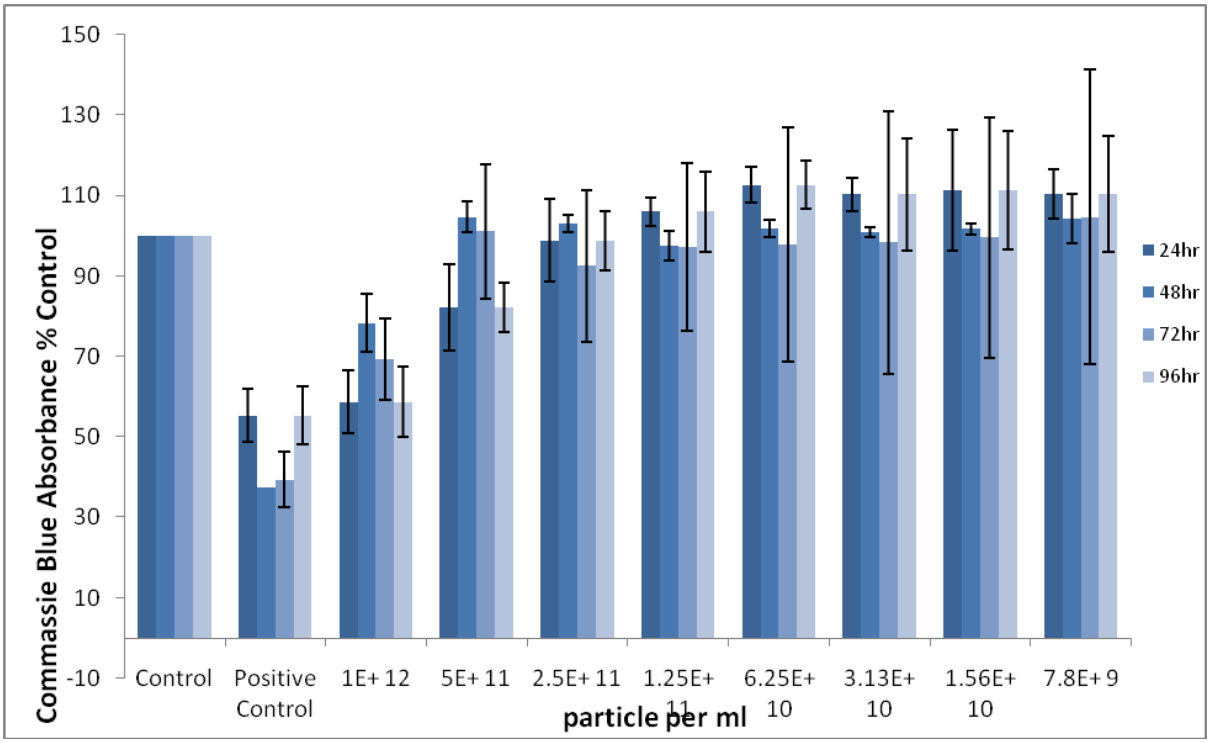

Figure 5.12 Cytotoxicity of 60nm Aminated nanopolystyrene to A549 cells after 24, 48, 72 and 96 hour exposures determined by the CB assay. Data are expressed as percent of control mean ± SD of three independent experiments

For the cytotoxicity curves obtained for all particles, the standard deviation error bars are relatively large, indicating the Coomassie Blue assay may not have been as consistently stable as other assays performed.

5.5 MTT Assay

The MTT colorimetric assay determines the ability of viable cells to reduce the soluble, yellow tetrazolium salt [3-(4,5-dimehtylthiazol-2-yl)-2,5-diphenyltetrazolium bromide] (MTT) into an insoluble, purple formazan precipitate which can be solubilised by the addition of an organic solvent and quantified spectroscopically. Tetrazolium salts accept electrons from oxidized substrates or enzymes, such as NADH and NADPH. Reduction of MTT takes place at the ubiquinone and cytochrome b and c sites of the mitochondrial electron transport chain due to succinate dehydrogenase activity, figure 5.13. [17].

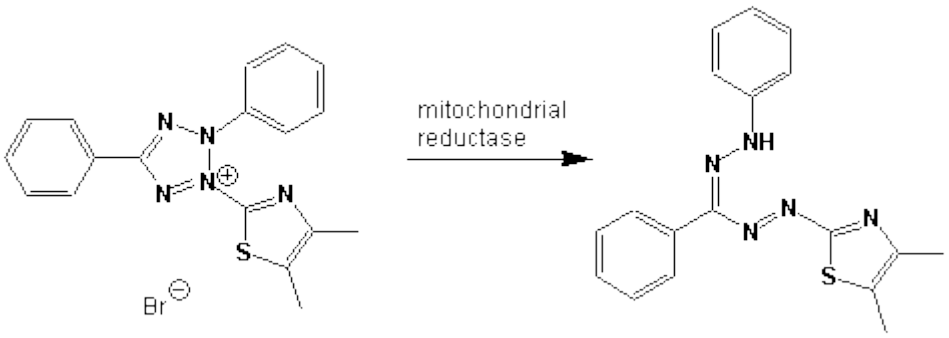

MTT (yellow tertazole salt) **Formazan**

Figure 5.13 Reduction of yellow tetrazole to purple formazan when reductase enzymes are active in living cells.

Applications for the MTT assay include drug sensitivity and cytotoxicity. The assay is considered rapid, safe, versatile, quantitative, and highly reproducible with an intra-test variation between data points of only +/- 15 percent. For each cell type, a linear relationship between cell number and absorbance can be established, enabling accurate quantification [18].

The main disadvantage to the use of tetrazolium salts are their cytotoxicity. To solubilise the formazan crystals, solvents such as dimethylsulfoxide (DMSO) or HCl/isopropanol have to be used. This treatment results in destruction of investigated cells, allowing only a single time point [19]. Addition of DMSO destroys the cell membrane and results in liberation and solubilisation of the formazan crystals. The number of viable cells is thus directly proportional to the level of the initial formazan product created and can be quantified by measuring the absorbance at 570 nm (Magrez et al., 2006).

Figures 5.14, 5.15 and 5.16 display the cytotoxic response curve obtained for 50nm Duke Scientific nanopolystyrene, 40nm carboxylated Invitrogen Nanopolystyrene and 60nm aminated nanopolystyrene, respectively using the MTT assay.

As can be seen from figure 5.14, 50nm nanopolystyrene did not induce cytotoxic effects on A549 cells after exposures between 24 and 96 hours. The reduction of MTT to formazan within cells serves as an estimate for the number of mitochondria and hence the number of viable cells after exposure to nanoparticles. 50nm particles did not interfere with the production of NADH and NADPH nor had any effect on mitochondrial electron transport chains, as is seen from the absorbance measurements made for the assay.

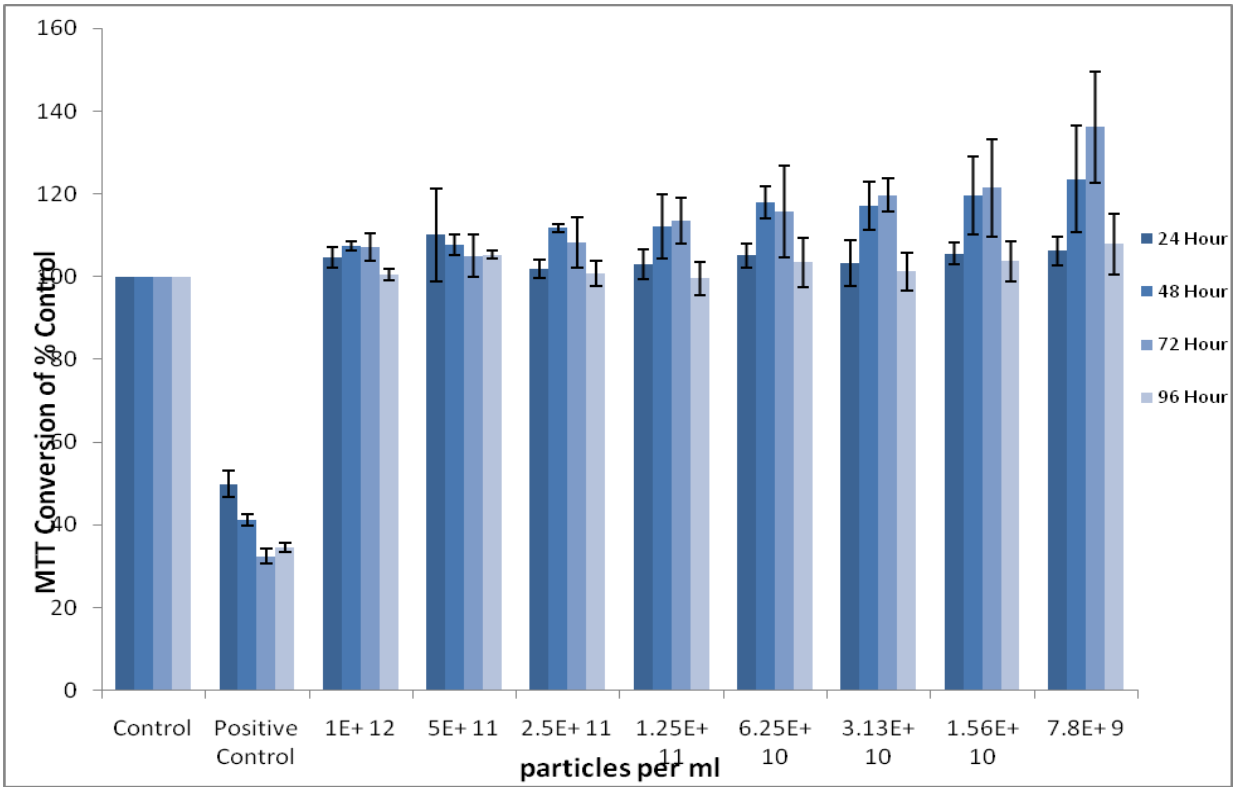

Figure 5.14 Cytotoxicity of 50 nm Duke Scientific nanopolystyrene to A549 cells after 24, 48, 72 and 96 hour exposures determined by the MTT assay. Data are expressed as percent of control mean ± SD of three independent experiments.

This is also applicable for the determination of cytotoxicity of 40nm carboxylated nanopolystyrene as can be seen in figure 5.15. The results show that A549 cells exposed to 40nm particles over exposure times of 24hr, 48hr, 72hr and 96hr were not affected and experienced no toxic effects. The tetrazolium salt is cleaved to formazan by a complex cellular mechanism that occurs primarily at the surface. This bioreduction is mostly dependent on the glycolytic NAD(P)H production of viable cells. The results show no decrease in the amount of reduced MTT to formazan dye, therefore, the absorbance of dye formed, directly correlates to the number of metabolically active cells not affected by exposure to particles.

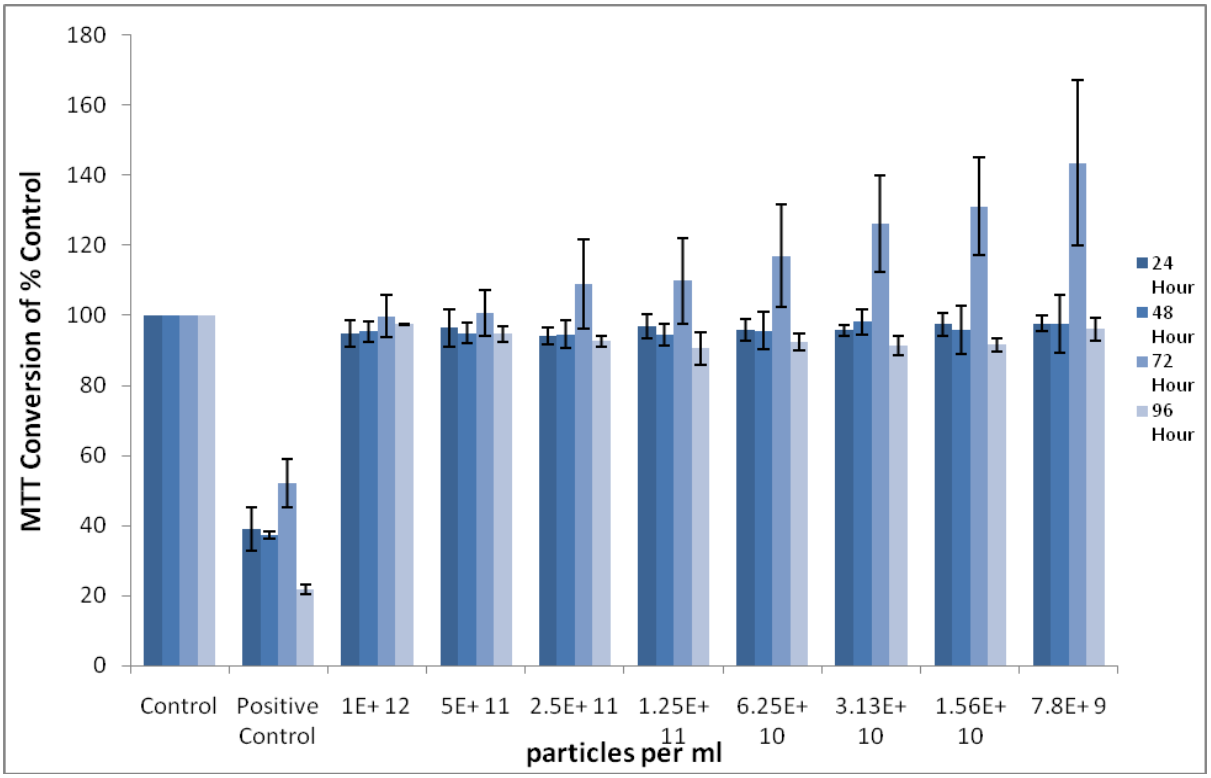

Figure 5.15 Cytotoxicity of 40nm carboxylated Invitrogen nanopolystyrene to A549 cells after 24, 48, 72 and 96 hour exposures determined by the MTT assay. Data are expressed as percent of control mean ± SD of three independent experiments.

Cytotoxicity results of toxicity to A549 cells after 24, 48, 72 and 96 hour exposures of 60nm aminated nanopolystyrene, determined by the MTT assay, can be seen in figure 5.16.

Because the amount of reduced MTT to formazan dye directly correlates to the number of metabolically active cells, it can be observed from the graph that the highest test concentration of $1x10^{12}$ ppml of 60nm aminated particles causes a reduction in the number of metabolically active cells, hence inducing a toxic response from A549 cells over the exposure period of 24 to 96 hours.

As was observed with other assays, the second highest test concentration of $5x10^{11}$ ppml also induced a lesser amount of toxicity when exposed to cells. The toxicity to

viable cells when exposed to this concentration can be seen to increase over the exposure time periods, with 96hr exposure inducing the greatest level of toxicity, at this concentration.

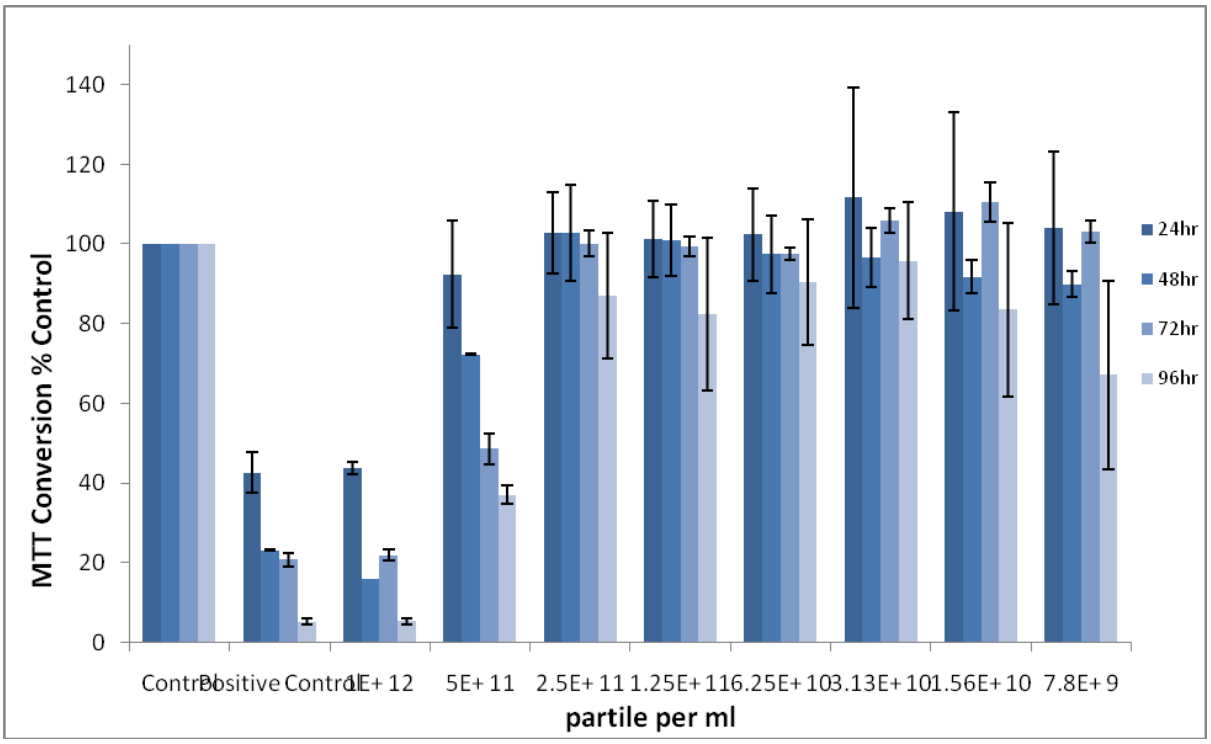

Figure 5.16 Cytotoxicity of 60nm Aminated nanopolystyrene to A549 cells after 24, 48, 72 and 96 hour exposures determined by the MTT assay. Data are expressed as percent of control mean ± SD of three independent experiments

As with all other assays performed, the results found for the highest test concentration of nanoparticle per ml were found to be in keeping with literature reports of the toxicity of aminated nanoparticles.

Cytotoxicity data obtained for 100 nm neutral nanopolystyrene and 100nm carboxylated nanopolystyrene are not presented in this chapter. The cytotoxicity data obtained revealed the same results as particles of the same surface charges with smaller sizes. It was felt it was unnecessary to present and discuss large amounts of

similar results, as to not overload the reader with data and graphs that repeat results obtained.

100nm neutral nanopolystyrene and 100nm carboxylated nanopolystryene were both found to have no cytotoxic effects on A549 cells after exposure times of 25, 48, 72 and 96 hours. This nontoxic response was confirmed through all assays performed. The cytotoxic response curves obtained indicates no effect on proliferation or cell growth (Alamar Blue assay), no effect on cell viability (Neutral Red assay), no effect on the protein content of viable cells (Coomassie Blue assay) and no decrease in metabolic activity of cells (MTT assay) with particle concentration or exposure time having no cytotoxic effect.

These findings are in keeping with literature, with neutral and carboxylated nanopolystyrene particles being reported as having no toxicity [12] [20] [21].

5.6 Clonogenic Studies

The clonogenic assay was employed as an indication of the interference of particles on single cells to form colonies. As explained in more detail in Chapter 3, Section 3.4.6, single cells were seeded and exposed to a range of concentrations of both particles and the effects monitored.

40nm Carboxylated Invitrogen Nanopolystyrene and 50nm Duke Scientific Nanopolystyrene particles were exposed to A549 cells for 10 days. The results of which can be seen in figure 5.12.The results reveal that no toxicity was induced over the period of 10 days, for either particle, and particles did not have an affect on the ability of cells to form colonies.

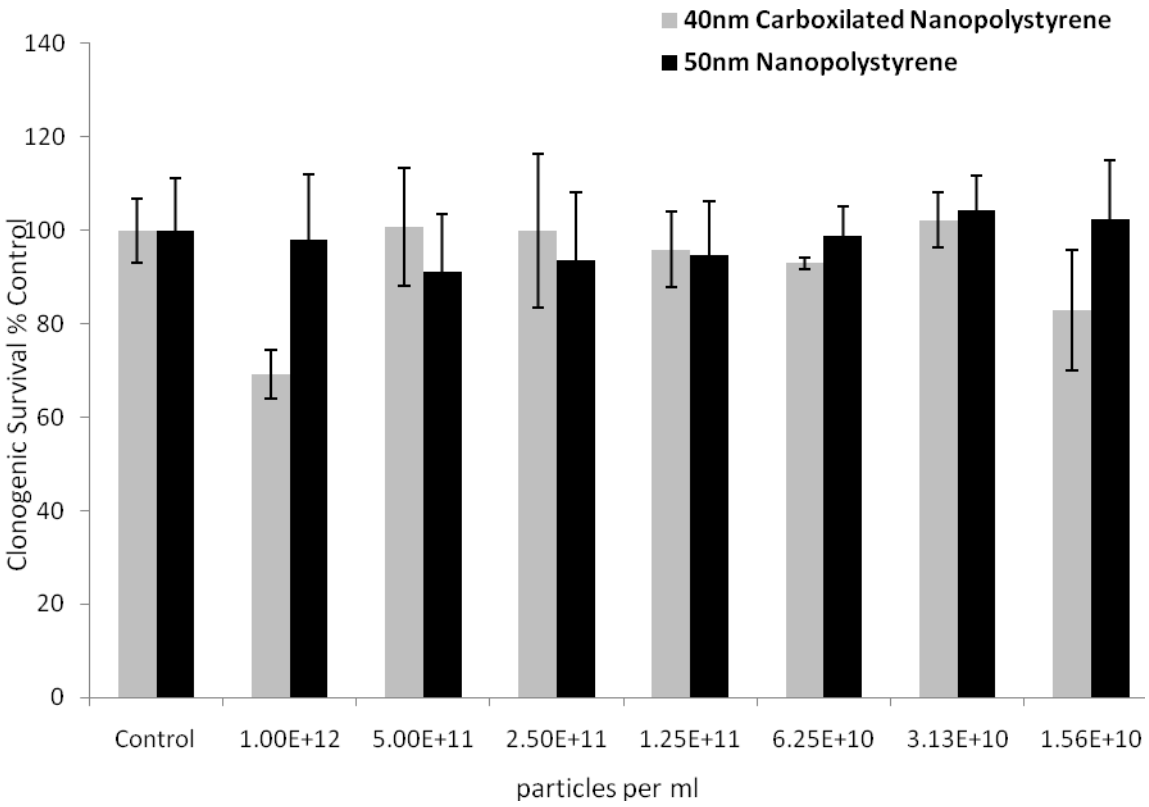

Figure 5.12 Cytotoxicity of 40nm Carboxylated Invitrogen Nanopolystyrene and 50nm Duke Scientific Nanopolystyrene to A549 cells after 10 day exposures determined by the clonogenic assay.

As can be seen from figure 5.12, 40nm Carboxylated Invitrogen Nanopolystyrene and 50nm Duke Scientific Nanopolystyrene particles did not have an effect on colony formation when exposed to A459 cell for 10days.

This clonogenic assay results provide valuable information, by verifying that the tested nanoparticles do not induce cytotoxic affects over a longer period of exposure time than other assays used.

5.7 Chapter Summary

This chapter has highlighted the results obtained for the *in vitro* cytotoxicity of 50nm neutral, 40nm carboxylated and 60nm aminated nanopolystyrene. The cytotoxicity evaluation revealed through the use of Alamar Blue™ (AB), Neutral Red (NR), Coomassie Blue (COOMASSIE) and 3-(4,5-dimethylthiazol-2-yl)-2,5-diphenyltetrazolium bromide (MTT) and clonogenic assays that the 50nm neutral and the 40nm carboxylated nanoparticles induced no cytotoxic effects when exposed to A549 cells over a range of concentration and time points. The presented results in this chapter have comprehensively confirmed, in keeping with the reported literature findings, that neutral nanoparticles, of sizes 50nm and 100nm, and carboxylated nanoparticles, of sizes 40nm and 100nm, do not induce cytotoxic effects when exposed to A459 cells over a time range of 24 to 96 hours using conventional cytotoxicity assays.

However, cytotoxicity results of A549 cells exposed to a range of concentration of 60nm aminated nanopolystyrene after 24, 48, 72 and 96 hour exposures, revealed at some concentrations, the particle does induce toxic effects on the cell. As observed throughout all assays performed, the highest test concentration of $1x10^{12}$ ppml induced toxic effects on A549 cells over the 24 to 96 hour exposure time points, with the second highest test concentration of 5x1011 ppml causing toxicity to a lesser degree. This highest test concentration of particles ($1x10^{12}$) was observed by Alamar Blue assay as having a toxic effect on the proliferation of healthy cells, with the largest degree of toxicity observed at the 96 hr time point. Similarly, the particle was found to have a toxic effect on the viability of healthy cells (NR assay), with the particle concentration also found to effect the protein production and content of

viable cells as measured by the Coomassie Blue assay. Finally, the MTT assay confirmed that $1x10^{12}$ ppml of 60nm aminated nanoparticles had an effect on the overall metabolic activity of healthy cells; hence concluding that at concentrations of $1x10^{12}$ ppml cytotoxic effects were experienced by A549 cells, with the second highest concentration of $5x10^{11}$ ppmlhaving a slightly less toxic effect on cells.

Although conventional colorimetric and luminescence based assays give an indication of the effect on proliferation and viability as well as organelle damage, they fail to recognise that although some nanoparticles may not produce immediate or semi-long term (10 days) toxic effects, nanoparticles have the ability to localise within cells and cell organelles. The ability of nanoparticles to penetrate cell membranes and translocate within cell organelles has been notably documented, which is where conventional assays fail in their attempt to give a full toxicological profile. Assays for screening on cell viability and cell number based on colorimetric, fluorescent and chemiluminescent detection may prove to be insufficient in the long term determination of nanoparticle toxicity [2]. Specific assays for membrane damage, generation of oxidative stress, mitochondrial damage, proliferation and apoptosis do allow insight into the mechanism of the toxic effect [1]. However, for nanomaterials that do not induce any of these effects short term, information about the exact migration and accumulation is imperative. Currently, there are various microscopic techniques, such as phase contrast, epifluorescence and confocal fluorescence microscopy analysis used to examine the co-localization of cell damage and particle-uptake and particle accumulation. Mapping of particles to organelles is also possible, which provides nanotoxicologists with a further understanding of nanoparticle behaviour once cell internalisation has been observed [22] [21].

The following chapter will explore the penetration and internalisation of 50nm and 100 nm nanopolystyrene, 40nm and 100nm carboxylated nanopolystyrene within A549 lung cells through various microscopy and spectroscopy techniques. Particle accumulation within cell organelles will also be examined.

References

1. Jones, C.a.G., D.W. , *In vitro assessments of nanomaterial toxicity* Advanced Drug Delivery Reviews, 2009. **61**(6): p. 438-456.
2. Nel, A., et al., *Toxic Potential of Materials at the Nanolevel.* Science, 2006. **311**(5761): p. 622-627.
3. OECD, *List of manufactured nanomaterials and list of endpoints for phase one of The oecd testing programme*, in *Series on the safety of manufactured nanomaterials*

Number 6. 2008.
4. (WHO), W.H.O., *Styrene in Drinking-water*, in *Guidelines for drinking-water quality.* , 2, Editor. 2003.
5. ATSDR, *TOXICOLOGICAL PROFILE FOR STYRENE*. 2007, U.S. DEPARTMENT OF HEALTH AND HUMAN SERVICES: Atlanta, Georgia.
6. HPA, H.P.A., *Styrene Toxicological Overview* 2007.
7. Moss, O.R. and V.A. Wong, *Alveolar macrophage accumulation rates, for 28 nm and 250 nm PSL, are mediated by separate mechanisms.* Journal of Physics: Conference Series, 2009. **151**(1): p. 012044.
8. Lanone, S., et al., *Comparative toxicity of 24 manufactured nanoparticles in human alveolar epithelial and macrophage cell lines.* Particle and Fibre Toxicology, 2009. **6**(1): p. 14.
9. Donaldson, K., et al., *Nanotoxicology.* Occupational and Environmental Medicine, 2004. **61:**: p. 727-728.
10. Oberdorster, G., et al., *Principles for characterizing the potential human health effects from exposure to nanomaterials: elements of a screening strategy.* Particle and Fibre Toxicology, 2005. **2**(1): p. 8.
11. Xia, T.K., Michael Liong, Monty Zink, Jeffrey I. Nel, Andre E., *Cationic Polystyrene Nanosphere Toxicity Depends on Cell-Specific Endocytic and Mitochondrial Injury Pathways.* ACS Nano, 2007. **2**(1): p. 85-96.
12. Lockman, P.R., et al., *Nanoparticle Surface Charges Alter Blood–Brain Barrier Integrity and Permeability.* Journal of Drug Targeting, 2004. **12**(9-10): p. 635-641.
13. Frohlich, E., et al., *Cytotoxicity of nanoparticles independent from oxidative stress.* The Journal of Toxicological Sciences, 2009. **34**(4): p. 363-375.
14. Johnston, H.J., et al., *Evaluating the uptake and intracellular fate of polystyrene nanoparticles by primary and hepatocyte cell lines in vitro.* Toxicology and Applied Pharmacology, 2010. **242**(1): p. 66-78.
15. Rothen-Rutishauser, B., et al., *Translocation of particles and inflammatory responses after exposure to fine particles and nanoparticles in an epithelial airway model.* Particle and Fibre Toxicology, 2007. **4**(1): p. 9.
16. Compton, S.J. and C.G. Jones, *Mechanism of dye response and interference in the Bradford protein assay.* Analytical Biochemistry, 1985. **151**(2): p. 369-374.
17. Mosmann, T., *Rapid colorimetric assay for cellular growth and survival: Application to proliferation and cytotoxicity assays.* Journal of Immunological Methods, 1983. **65**(1-2): p. 55-63.
18. Supino, R., *MTT Assays*, in *Methods in Molecular Biology* 1995. p. 137-149.

19. Bernas, T. and J. Dobrucki, *Mitochondrial and nonmitochondrial reduction of MTT: Interaction of MTT with TMRE, JC-1, and NAO mitochondrial fluorescent probes.* Cytometry, 2002. **47**(4): p. 236-242.
20. Rothen-Rutishauser, B.M., S.G. Kiama, and P. Gehr, *A Three-Dimensional Cellular Model of the Human Respiratory Tract to Study the Interaction with Particles.* American Journal of Respiratory Cell and Molecular Biology, 2005. **32**(4): p. 281-289.
21. Rothen-Rutishauser, B.M., et al., *Interaction of Fine Particles and Nanoparticles with Red Blood Cells Visualized with Advanced Microscopic Techniques†.* Environmental Science & Technology, 2006. **40**(14): p. 4353-4359.
22. Rejman, J.O., Volker Zuhorn, Inge S Hoekstra, Dick, *Size-dependent internalization of particles via the pathways of clathrin- and caveolae-mediated endocytosis.* Biochem. J., 2004. **377**(1): p. 159-169.

Chapter 6

Confocal Fluorescence Microscopy

Chapter 6

6.1 Introduction

One of the major concerns regarding the possible long-term toxic effects of nanoparticles is the capacity of these materials to penetrate cells and possibly translocate to other cells around the body. Conventional cytotoxicity assays do give an indication of interference to cell proliferation, viability, metabolic activity, lysosomal and mitochondrial activity. However, they fail to give a verification of internalisation of particles, or to what degree particles become internalised within cells. Penetration and internalisation of nanoparticles within cells and any associated toxicity to humans is still relatively unexplored. However, there are numerous studies that have demonstrated the ability of nanoparticles to cross membranes and internalise within many different cell types [1] [2]. A greater understanding of the migration of nanoparticles from organelle to organelle, cell to cell and essentially from one part of the body to another is needed, along with information on the translocation of nanoparticles within organelles. If information was available on the exact migration patterns of different types of nanoparticles within cells or around the body, this would be of enormous value in areas of nanomedicine and bio-nanotechnology.

In understanding possible mechanisms of nanoparticle uptake by cells, one must first examine how a cell regulates the uptake of substances. In order for a substance to enter a cell's interior, it must pass through the diffuse layer surrounding the cell and the plasma membrane which segregates the internal and external environments of a cell and regulates the entry and exit of substances into and out of the cell. The uptake mechanisms employed by cells have been discussed in more detail in Chapter 2 Section 2.2.2. It is known that size, shape and surface area all play a role

in determining the route of cellular uptake of liposomes, viruses and nanopolymers [3]. The sizes of many nanoparticles are similar to those of biological macromolecules such as proteins and DNA, as well as biological structures such as bacteria and viruses, all of which are readily taken up by cells, including lung cells. However, conventional assays do not take such physio-chemical properties into consideration and so questions remain as to what the effects are of particle accumulation within cell organelles and the subsequent effect on whole body organisms. It is thus proposed that in order to appropriately build a toxicological profile of a particle, a series of internalisation studies to both identify and assess the potential of nanoparticles to accumulate in cells and cellular structures must accompany the aforementioned cytotoxicity assays.

A number of methods exist to monitor cellular internalisation and uptake, the most commonly employed being confocal microscopy. Advances in confocal microscopy have led to the ability to monitor the internalisation of nanoparticles both *in vitro* and *in vivo* [4], using a variety of spectroscopic detectors coupled to the microscope e.g. fluorescence and Raman spectroscopy. There are however a number of limitations to the use of confocal microscopy, some of which are listed below.

1. As with conventional microscopy, confocal microscopy has inherent resolution limitations due to diffraction and the Rayleigh criterion.

2. Confocal laser microscopy works on a point by point basis rather than imaging the entire sample, thus limiting the range of visibility. Commonly confocal laser scanning instruments raster the field of view to produce an image.

3. Particles within cells must be optically active e.g. intrinsically fluorescent or fluorescently labelled for Confocal Laser (fluorescence) Scanning Microscopy (CLSM).

4. The optical sectioning capability of a confocal microscope derives from having a pinhole to reject out-of-focus light rays. As the pinhole size is reduced, so too are the number of photons that arrive at the detector from the specimen. This may lead to a reduced signal-to-noise ratio. To offset the weaker signal, more fluorescence is needed from the specimen. This usually can be done, to a limit, by raising the intensity of the excitation light. But high intensities can damage the specimen, and in the case of fluorescence, also degrade the fluorophore.

5. Among the most important aspects of confocal fluorescence microscopy is the choice of fluorophore. It is typically influenced by several factors. The fluorophore must be sensitive enough for the given excitation wavelength, the fluorescence of the emitted light must be intense enough, etc.

Throughout this study, confocal laser fluorescence scanning microscopy was employed to monitor the internalisation of 40nm and 100nm carboxylated nanopolystyrene and 50nm and 100 nm nanopolystyrene, after they have undergone exposure to A549 carcinogenic lung cells over various time points. The precise intracellular migrations of nanoparticles within specific regions of single cells were confirmed by 3D multicolour measurement, known as a Z-Stack. These single cell molecular morphology measurements provided confirmation that 40nm carboxylated nanopolystyrene and 50 nm nanopolystyrene had penetrated cell membranes and were internalised within individual cells. The 60nm aminated nanopolystyrene

particles were not available in a fluorescently labelled form and thus were not studied. However, confocal Raman spectroscopy was also used to confirm internalisation of nanopolystyrene particles within A549 lung cells, independent of any label, and will be discussed in more detail in the following chapter.

6.2 Confocal Microscopy of Nanoparticles Within Cells

Confocal microscopy was employed to investigate the internalisation of fluorescent nanoparticles within A549 cells. Confocal microscopy, along with the uses of molecular probes and biological dyes, is a conventional method in bio-imaging and has of late been extensively used in the monitoring of nanoparticle up-take by cells [5] [6]. In order to study the exact localisation and possible pathways taken by nanoparticles within cells, it is possible to expose cells to fluorescently labelled nanoparticles and track their fate after cell penetration. Co-localisation with organelle specific stains can help to identify the specific intracellular fate of the particles. It also gives the possibility to examine morphogenetic behaviours within specific cell populations of interest.

The use of confocal microscopy for the monitoring of internalisation of fluorescent nanoparticles has been widely documented. In a study to investigate the incorporation of fluorescent 20-nm polystyrene NPs into early endosomes within human hepatocyte cell lines (C3A and HepG2), confocal microscopy was extensively used for the monitoring imaging of internalisation of particles, and is a widely accepted technique for the monitoring of fluorescent imaging of cells. [1]

The imaging of polystyrene particle uptake by live A549 cells was carried out in 0.9% saline solution. The exact specifications under which images were obtained were discussed in detail in Chapter 3, Section 3.7. Intracellular accumulation of 40nm and 100nm carboxylated Invitrogen nanopolystyrene and 50nm and 100nm Duke Scientific nanopolystyrene particles after 4hr and 24 hr exposure was examined in A549 cells by imaging live cells in a 0.9% sterile saline solution. The confirmation of internalisation of 40nm carboxylated nanoparticles and 50nm nanoparticles was obtained by combining “z-stack” image series cutting through the cell in single z-steps of approximately 10 µm along with the generated orthogonal projection obtained from the z- stack image series of the cells. The 60nm aminated particles that were used throughout the rest of the study were not monitored using confocal microscopy due to the unavailability of fluorescently labelled particles within the size range and surface charge required.

6.2.1 Carboxylated Nanopolystyrene

Figure 6.1 shows an image of A549 cells exposed to 40nm carboxylated Invitrogen nanopolystyrene after a 4 hour exposure period. The image shows a fluorescent confocal image on the left and a bright-field image of the same cells showing no fluorescence on the right. After 1 hour exposure, particles were found to be aggregated upon the cell membrane with few particles present within the cell (not shown). However, the number of aggregates was observed to increase over time and accumulations of internalised particles were visible after 4 hours (figure 6.1). Surface aggregates of nanoparticles can be seen in the confocal image labelled (a) while internalised nanoparticles are labelled (b).

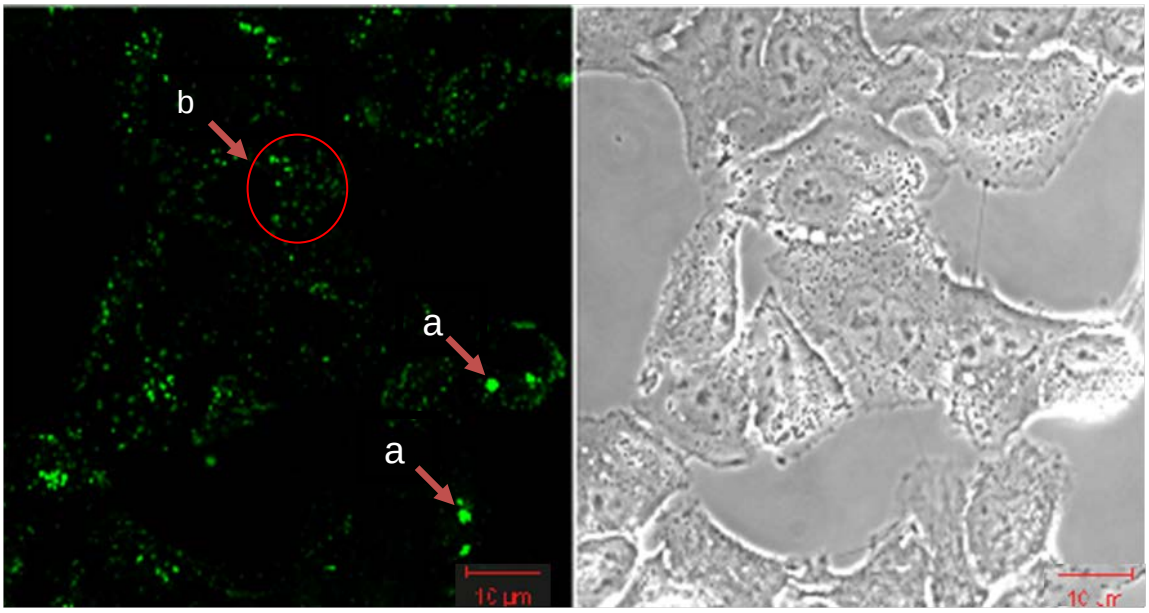

Figure 6.1 A549 cells exposed to 40nm carboxylated Invitrogen nanopolystyrene x40 magnification after 4 hour exposure. (a) Surface aggregates nanoparticles. (b) Internalised nanoparticles.

The image obtained for the uptake of 40nm carboxylated particles by A549 cells after 24hrs can be seen in figure 6.2. From the confocal image, it can be seen that the distribution of the localisation evolves over time. Nanoparticles within the cells are gathered in cluster like accumulations resembling cell organelles, such as lysosomes. As previously discussed in chapter 2 section 2.2.3, nanoparticles are taken up by the cell in a number of possible ways. Clathrin-mediated endocytosis is one such possible way in which nanoparticles have been shown to be taken up by cells [7]. Nanoparticles or macromolecules, while undergoing this form of uptake, enter the cell in clathrin-coated vesicles known as endosomes. These endosomes then fuse to form lysosomes [8]. The accumulation of nanoparticles over time within lysosomes may explain the difference in fluorescence distrubtion after different exposure times.

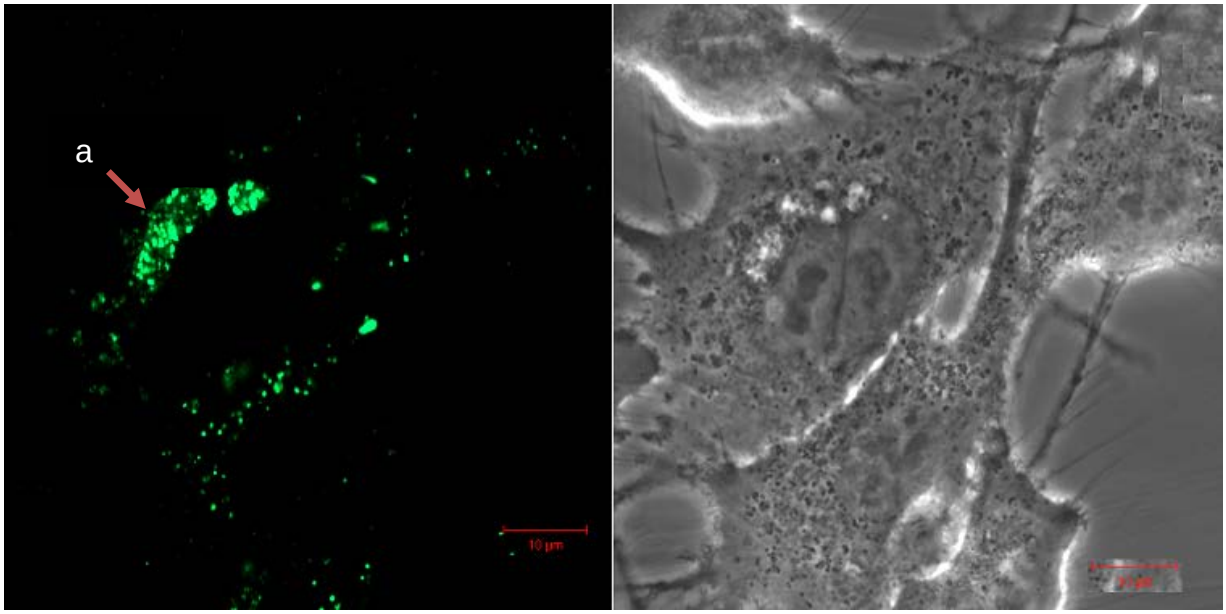

Figure 6.2 A549 cells exposed to 40nm carboxylated Invitrogen nanopolystyrene x60 magnification after 24 hour exposure. (a) Accumulations resembling possible lysosomal cell organelles

Over both exposure periods, cells observed remained healthy and regular in size. Cell membranes and nuclei could be observed. 40 nm particles were not observed within the nucleus, as can be seen in the fluorescent confocal image in figure 6.1 and 6.2, with confirmation of their absence from the nucleus revealed from the z-stack imaging (figure 6.3). Figure 6.3 shows a gallery view of confocal slices through the volume of an A549 cell exposed to 40nm carboxylated Invitrogen nanopolystyrene after 24hrs. From the images it can be seen that the fluorescence signal originates from the cell interior and not from material adhered to the surface. The optical slices reveal that the accumulation of particles is greatest within the interior of the cell.

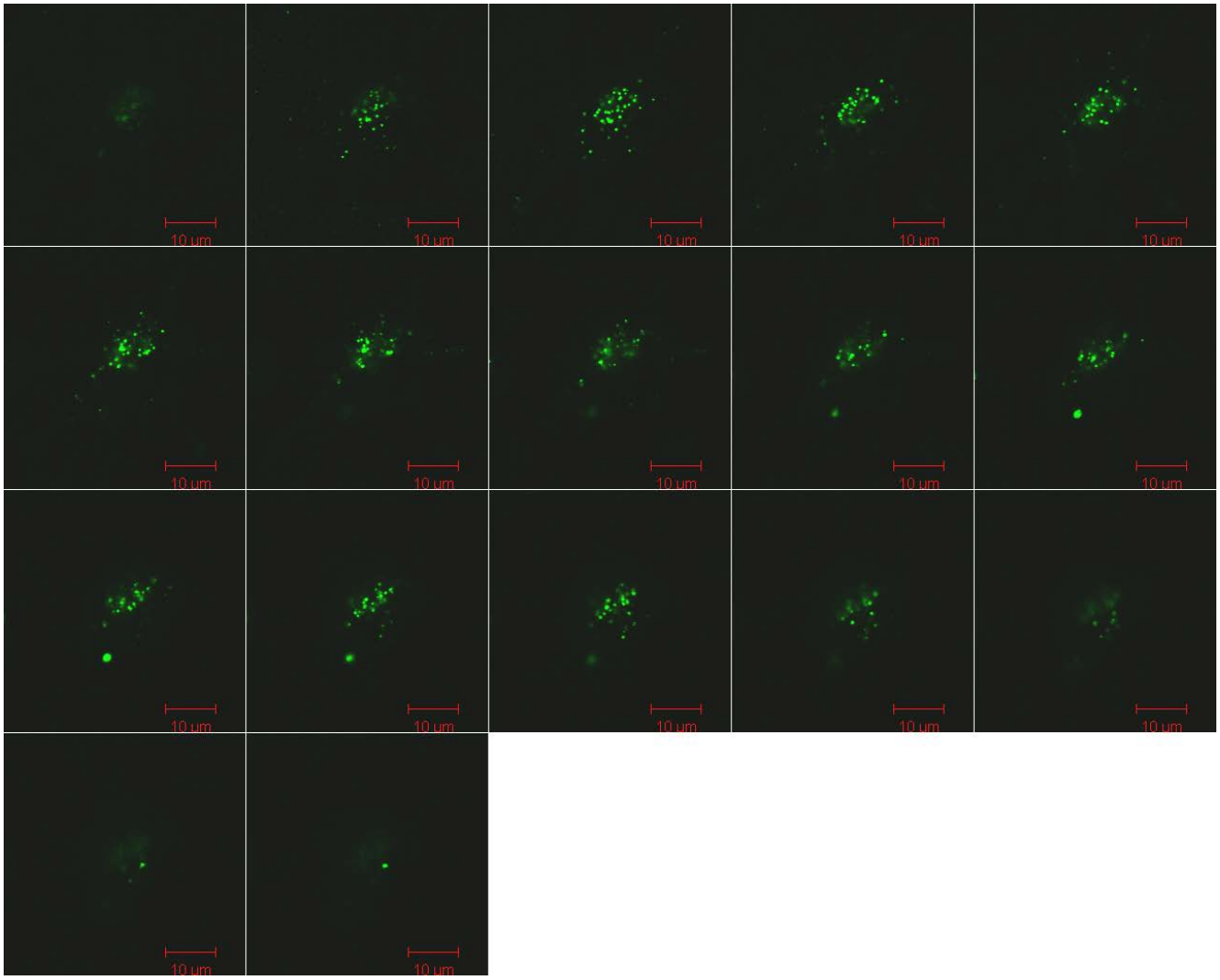

Figure 6.3 Gallery view of 24 hr exposure of 40nm carboxylated Invitrogen nanopolystyrene internalised within A549 cells from Z-stack process.

This z-stack imaging provides confirmation that the 40nm particles are internalised with the cells and have penetrated through the cell membrane. Figure 6.4 shows the *z*,*x* section (upper panel) and the *z*,*y* section (right panel) cutting orthogonally through the cell obtained from the *z*-stack image series of the cells. Nanoparticles were observed in perinuclear clusters within cells, as most of the aggregates appeared to be situated around but external to the nucleus (24hr exposure).

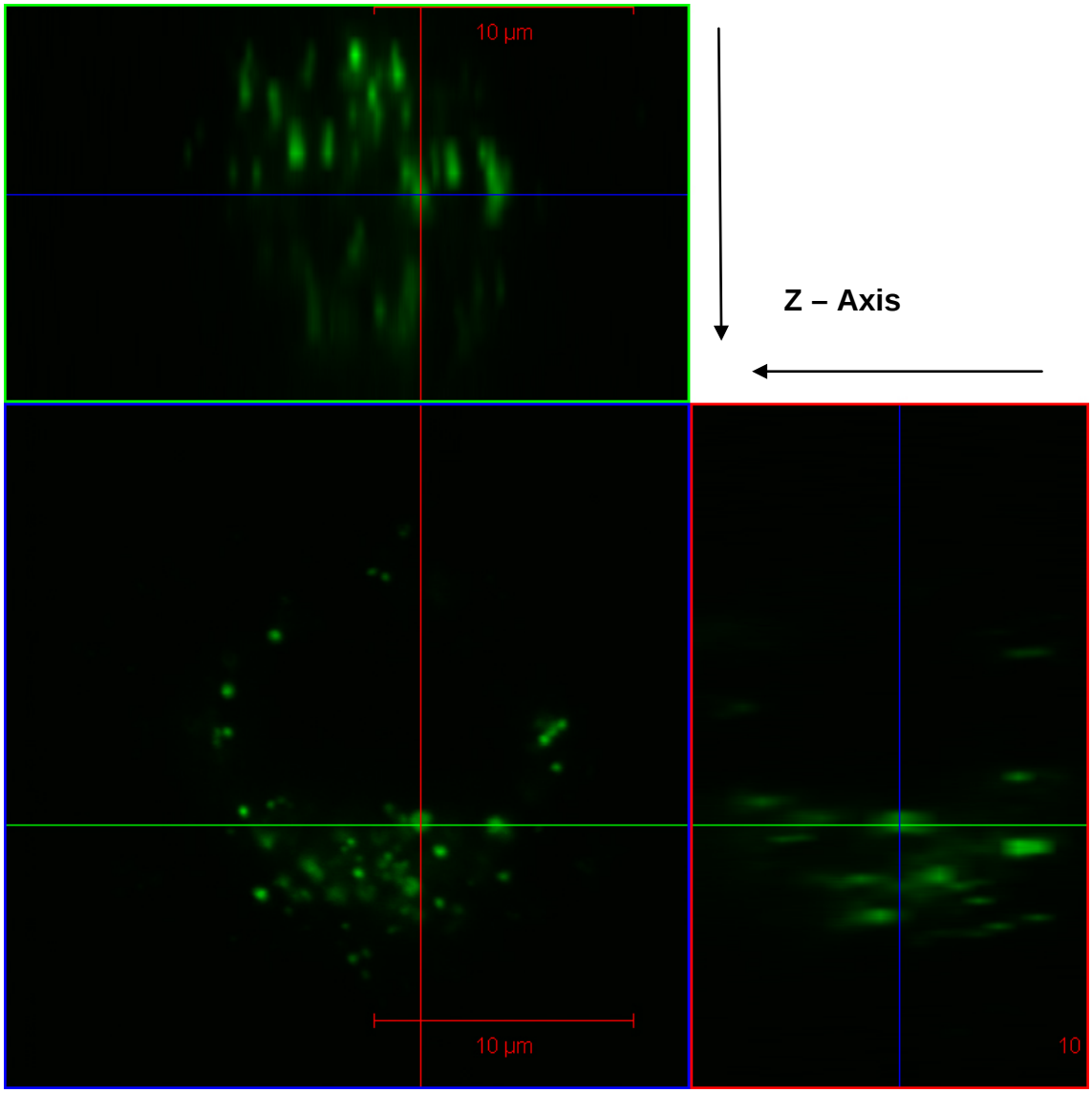

Figure 6.4 Orthogonal-view through A549 cell exposed to 40nm carboxylated Invitrogen nanopolystyrene (24hr).

This optical slicing of the 3D image of the cell represents an *x*, *y*, *z* slicing of a single cell exposed to the 40nm particles. From this image it can be concluded that particles are dispersed throughout the cell and not attached to the outer membrane. The image also gives an indication of the degree of dispersion of particles within the cell. There does not appear to be a spatially uniform fluorescence from the cells, but

rather it is concentrated in small areas, indicating that particles are compartmentalised within organelles and not just dispersed around the cytoplasm.

A similar behaviour is seen in A549 cells after exposure to 100nm carboxylated nanoparticles after 4 hours as shown in Figure 6.5. Particles can be seen to be internalised within cells. After 24 hours, the nanoparticles had internalised to a greater extent than shorter exposure times, indicated by the apparent increase in fluorescence intensity of aggregated spots that can be seen in figure 6.6.

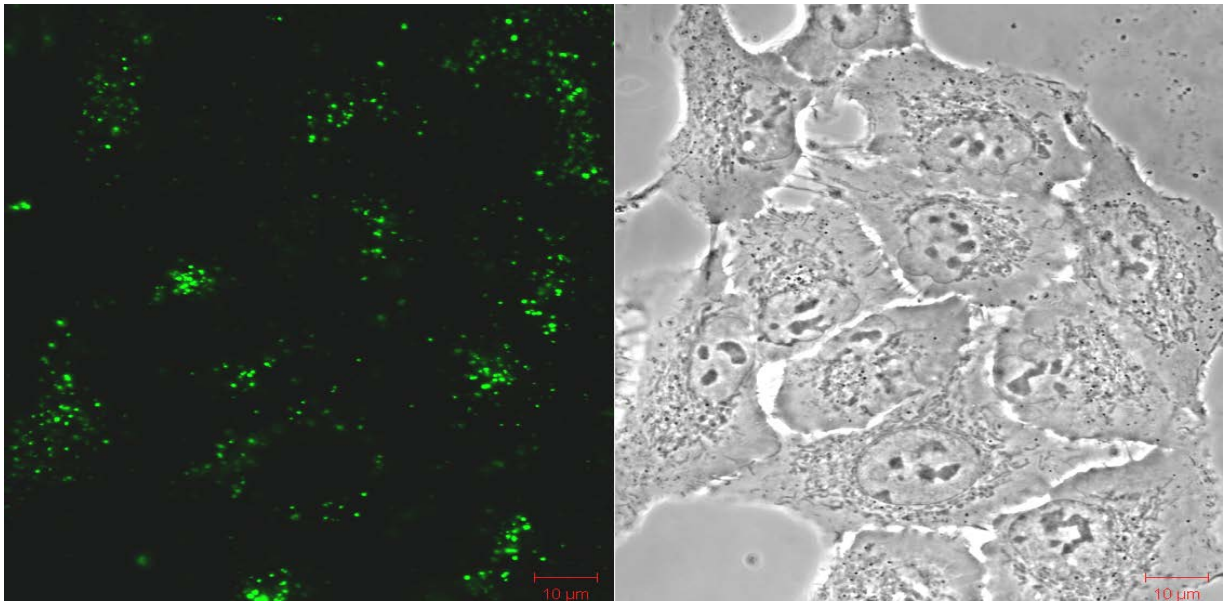

Figure 6.5 A549 cells exposed to 100nm carboxylated Invitrogen nanopolystyrene x40 magnification after 4 hour exposure.

As was observed for the 40nm particles, accumulations of the 100nm carboxylated nanoparticles appeared to be greater in, but not exclusive to, areas that resemble lysosomal cell organelles, labelled (a) in figure 6.6. The bright-field image in figure 6.6 shows circular cell organelles that resemble lysosomes or possibly the

endoplasmic reticulum. Fluorescence was not visible within the interstitial space of the cell, but rather in aggregated spots around the cell.

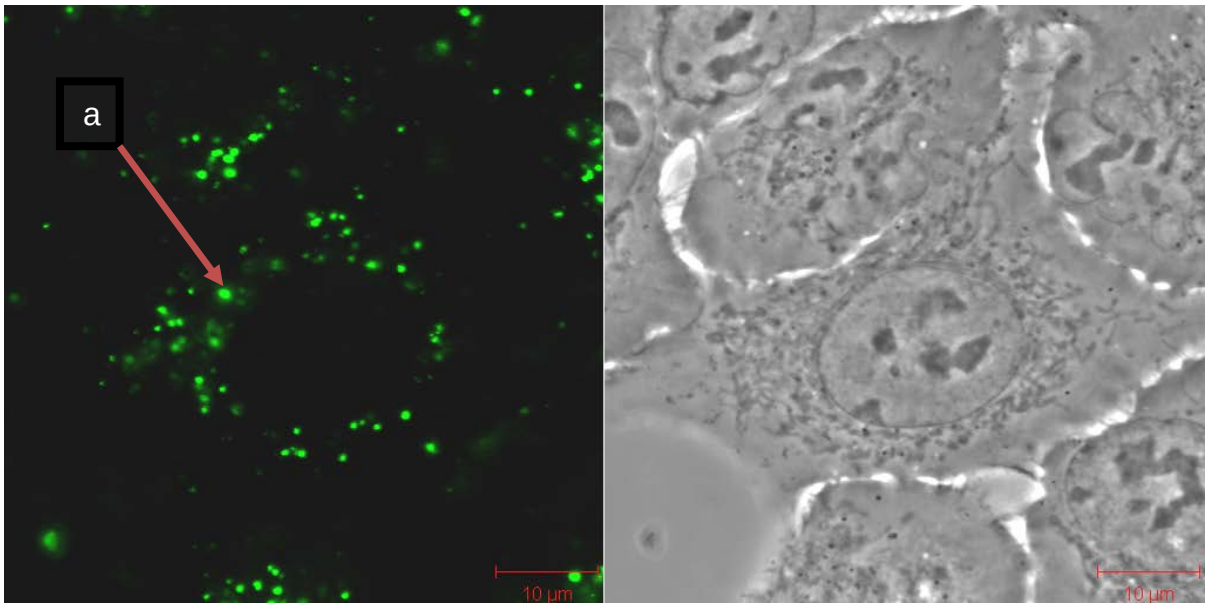

Figure 6.6 A549 cells exposed to 100nm carboxylated Invitrogen nanopolystyrene x40 magnification after 24 hour exposure. a) Accumulations resembling possible lysosomal cell organelles

As previously discussed, particles taken up by cells by possible clathrin-mediated endocytosis firstly enter the cell within endosomes, which then mature to form lysosomes [9] . Because lysosomes function as the digestive system of the cell, serving both to degrade material taken up from outside the cell and to digest obsolete components of the cell itself, it is to be expected that nanoparticles are engulfed by these organelles shortly after cellular up-take. There have been several studies to show the intracellular accumulation of polymer nanoparticles within lysosomes. A study to examine the intracellular import of polymeric nanoparticles and small molecules by Salvati at al (2011) found that nanopolystyrene was co-localised within lysosmes shortly after exposure to cells. Similarly, an examination of

the intracellular fate of hydrophobically modified glycol chitosan (HGC) nanoparticles after exposure to HeLa cells, showed co-localisation of nanoparticles within lysosomal vesicles, and eventually migration of the nanoparticles toward the perinuclear region [9]. The images presented here appear to be consistent with literature reports. However, the exact co-localisation of nanoparticles within specific cell organelles will be investigated further and discussed later in the chapter.

6.2.2 Neutral Nanopolystyrene

The confocal images of A549 cells, after exposure to 50nm, neutral Duke Scientific nanopolystyrene can be seen in figures 6.7 (4hr exposure) and 6.8 (24hr exposure). The figures show a fluorescent confocal image on the left and an bright-field image of the same cells showing no fluorescence on the right. The observations indicate that, compared to the carboxylated nanopolystyrene, 50nm neutral nanoparticles were rapidly internalised, as fluorescence could be visualised in the cytoplasm and interstitial space within 1 hour (not shown). Within 4 hours, particles were highly localised within, what appear to be, lysosomal compartments. Aggregates were observed to increase over the exposure time, with nanoparticles observed to preferentially accumulate in compartments located around the nucleus and within and between cell organelles on a timescale of 12-24hrs. Nanoparticles were present in all of the cells analysed, appearing as aggregates within the cell after 4 hours, indicating that the uptake was accomplished in a relatively short period of time. There are small concentrated areas where the fluorescence is stronger, indicating that particles are compartmentalised within organelles, such as lysosomes, as well as dispersed around the cytoplasm. The images reveal there is an overall fluorescence distribution that appears from all parts of the cell, with the exception of

the nucleus. The fluorescence observed from the particles suggest that particles have penetrated up to the nuclear membranes, which are visible, labelled (b) in figure 6.7. Notably, the fluorescence distribution of the 50nm neutral nanoparticles can be seen to be very different to that observed of the 40nm and 100 nm carboxylated nanoparticles. Unlike the 40nm and 100nm carboxylated nanoparticles, the fluorescence distribution of the 50nm neutral nanoparticles is much more diffuse, the interstitial space within cells appearing to be highly fluorescent.

From the confocal images, figures 6.7 and 6.8, it can be seen that particles within the cell are highly fluorescent. There are larger areas within the cell, labelled (a), which appear to be of greater fluorescent intensity than surrounding areas, suggesting particles are accumulated within cell organelles, such as lysosomes or the endoplasmic reticulum. The images reveal that fluorescent labelling of nuclear or vesicle membranes may have occurred (figure 6.7). In a study to evaluate the fate of TiO_2 particles within A549 epithelial cells, particles were found to be contained in membrane bound vesicles in cells (Stearns et al., 2001), suggesting the potential of nanoparticles to enter vesicle membranes. Figure 6.7 reveals the possible penetration of 50nm fluorescent particles within vesicle or nuclear membranes. However, further investigation using fluorescent specific organelle labelling kits would be needed to confirm this possibility.

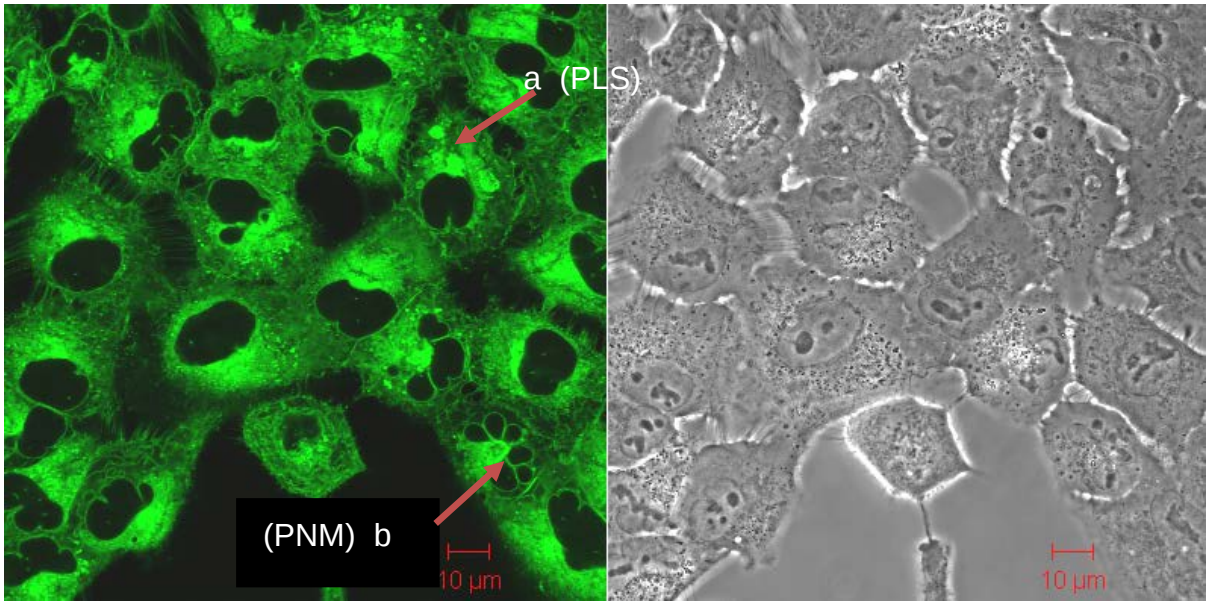

Figure 6.7 A549 cells exposed to 50nm neutral Duke Scientific nanopolystyrene x20 magnification after 4 hour exposure. (a) Possible lysosomal structure (PLS). (b) Possible labelling of nuclear / vesicle membranes (PNM).

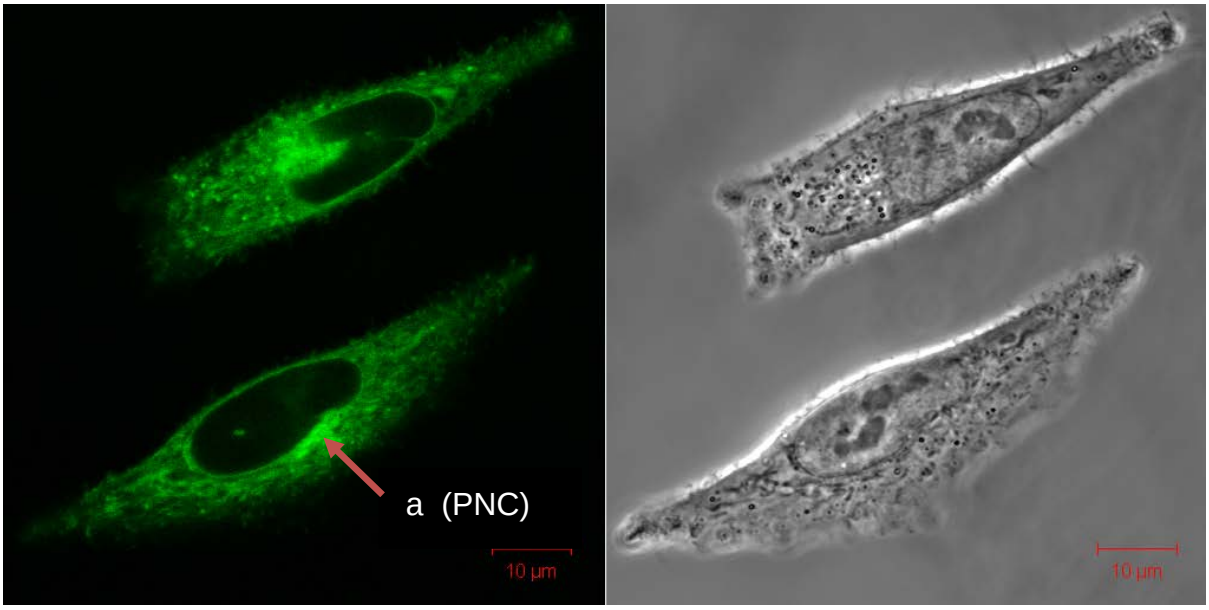

Figure 6.8 A549 cells exposed to 50nm neutral Duke Scientific nanopolystyrene x100 magnification after 24 hour exposure. (a) perinuclear clusters (PNC) of nanoparticles around nucleus.

50nm particles were not observed within the nucleus, as can be observed in the fluorescent confocal images previously shown (figures 6.7, 6.8), with confirmation of their absence from the nucleus revealed from the z-stack imaging (figure 6.9). Figure 6.9 shows a gallery view of confocal slices through the volume of an A549 cell exposed to 50nm Duke Scientific nanopolystyrene. From the images, it can be seen that the fluorescence signal originates from the cell interior and not from material adhered to the surface. The optical slices reveal that the accumulation of particles is greatest within the centre of the cell. The absence of fluorescence from the nuclear area indicates that particles did not penetrate the nuclear membrane.

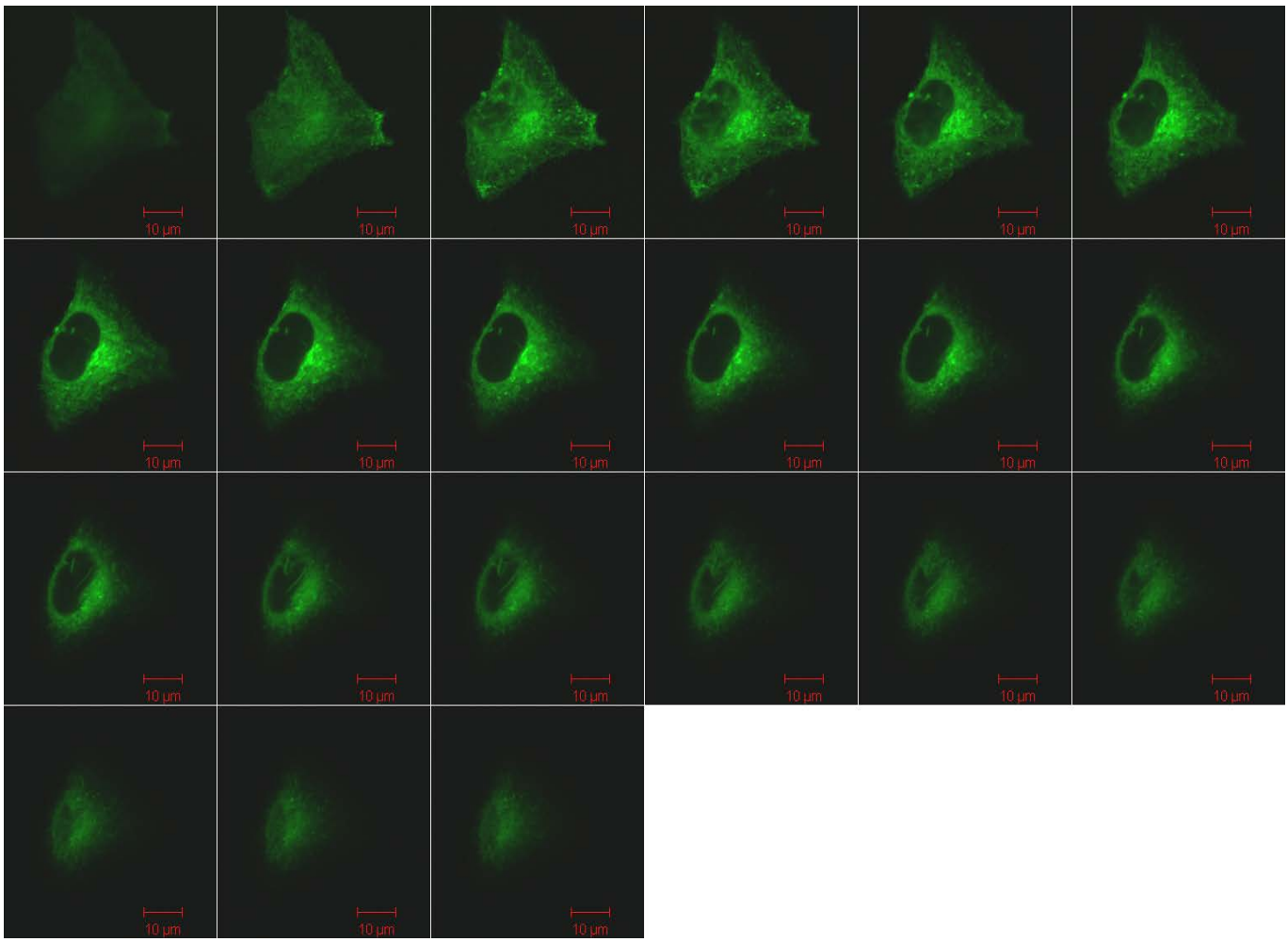

Figure 6.9 Gallery view of 50nm neutral Duke Scientific nanopolystyrene internalised within A549 cells from Z-stack process after 24hr exposure.

This z-stack imaging provides confirmation that the 50nm particles are internalised with the cells and have penetrated through the cell membrane. Figure 6.10 shows the *z*,*x* section (upper panel) and the *z*,*y* section (right panel) cutting orthogonally through the cell obtained from *z*-stack image series of the cells. Nanoparticles were observed in perinuclear clusters within cells, as most of the aggregates appeared to be situated around the nucleus. Figure 6.10 shows the *z*,*x* section (upper panel) and the *z*,*y* section (right panel), obtained from *z*-stack image series of the cells, cutting orthogonally through the cell. This optical slicing of the 3D image of the cell represents an *x*, *y*, *z* slicing of a single cell exposed to the 50nm particles, confirming that the particles are dispersed throughout the cell and not attached to the outer membrane.

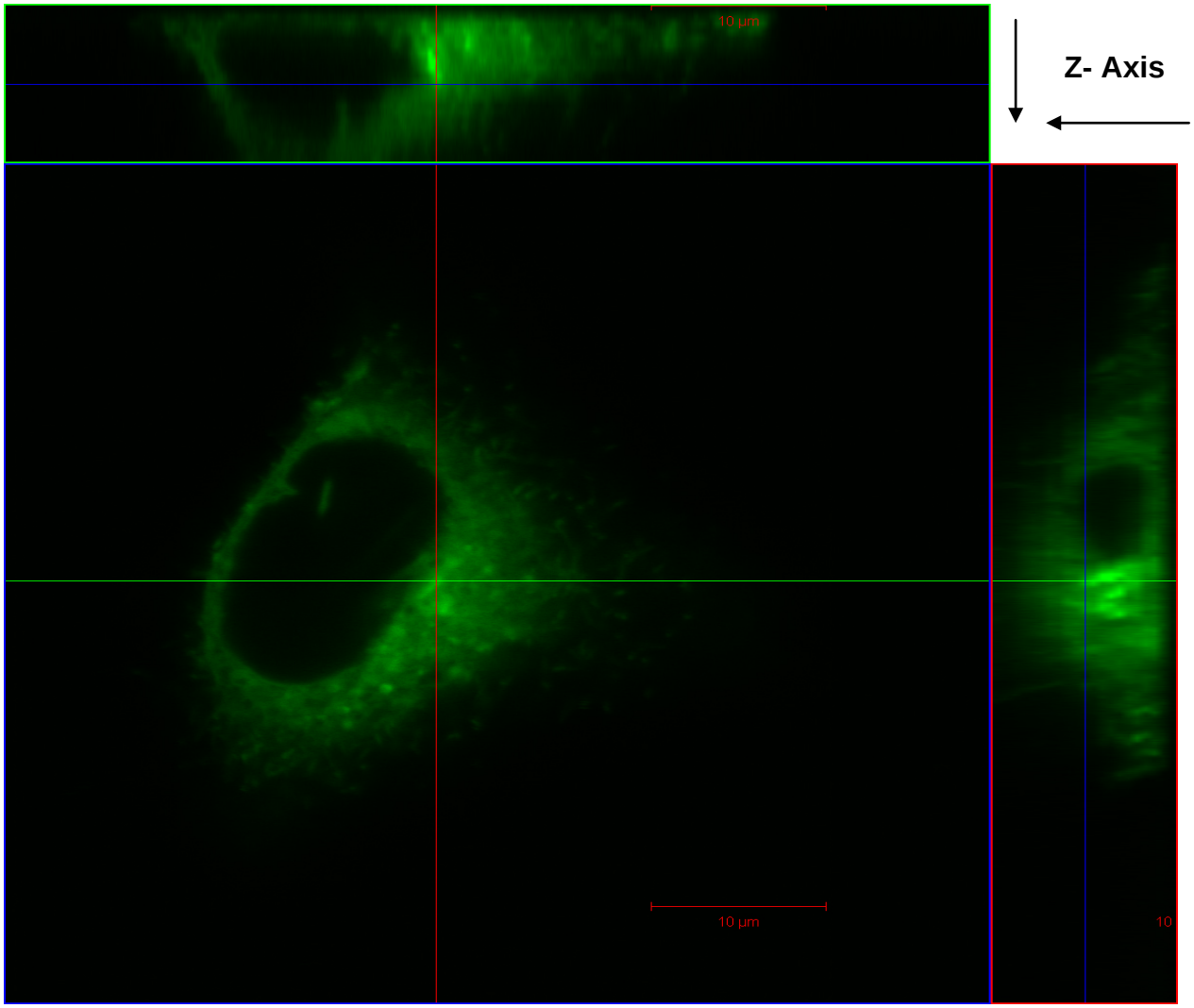

Figure 6.10 Orthogonal view through A549 cell exposed to 50nm neutral Duke Scientific nanopolystyrene after 24hr exposure.

A comparison of the z-stack images of the 40nm carboxylated nanoparticle (figures 6.3 and 6.4) and the 50nm neutral nanoparticle (figures 6.9 and 6.10) confirms a significant difference in the subcellular distribution of the fluorescence of the respective nanoparticle samples. The 50nm neutral nanoparticle z-stack images display a much more diffuse fluorescence distribution when compared to the z-stack images of the 40nm carboxylated nanoparticles, which reveal accumulations of smaller fluorescent areas within the cells.

Figures 6.11 and 6.12 show A549 cells after exposure to 100nm Duke Scientific nanopolystyrene after 4 and 24 hrs respectively. The images show a fluorescent confocal image on the left and an bright-field image of the same cells showing no fluorescence on the right. As can be seen in figures, fluorescence intensities were greatest in areas around the nucleus, labelled (a). These aggregates appeared in perinuclear clusters. The accumulations around the nucleus suggest that particles have penetrated into the endoplasmic reticulum. The observations indicate that 100nm neutral nanoparticles were rapidly internalised, as fluorescence could be visualised in the cytoplasm and interstitial space within 1 hour (not shown). As for the case of the 50nm neutral particles, however, the fluorescence is highly visible within the interstitial space of the cell, as well as in accumulated spots around the cell, as can be seen in figure 6.12. Fluorescence appeared to be more uniformly dispersed throughout the cell after the longer exposure times. The fluorescence that appears more intense in perinuclear clusters may be due to the migration of nanoparticles toward the endoplasmic reticulum after internalisation within lysosmes [9].

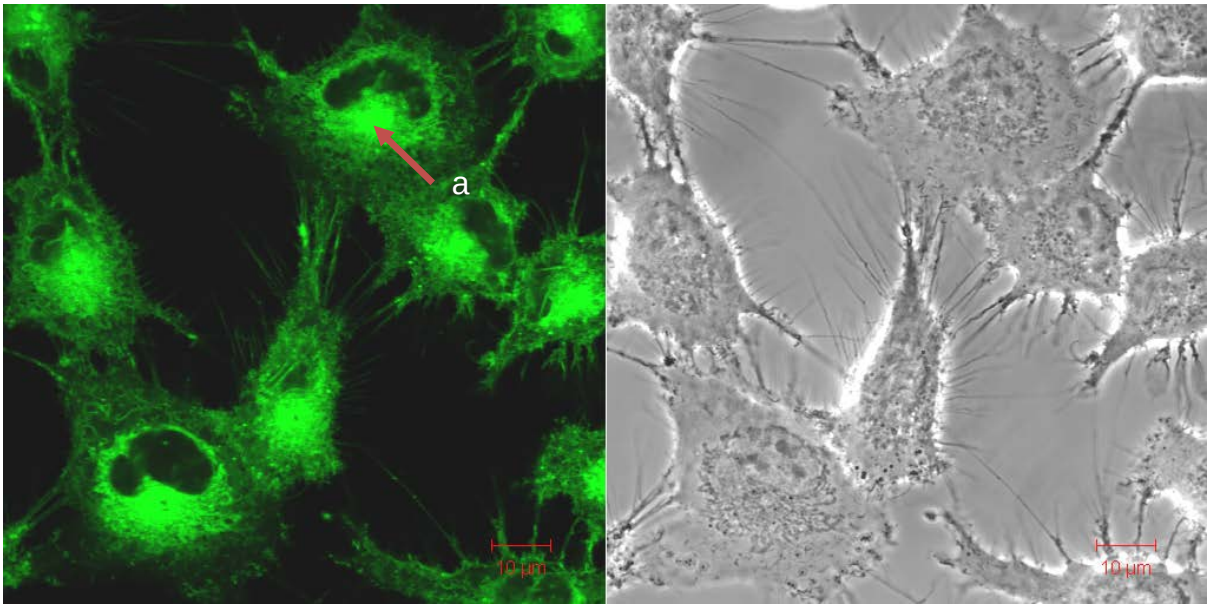

Figure 6.11 A549 cells exposed to 100nm neutral Duke Scientific nanopolystyrene x40 magnification after 4 hour exposure. (a) perinuclear clusters of nanoparticles around nucleus

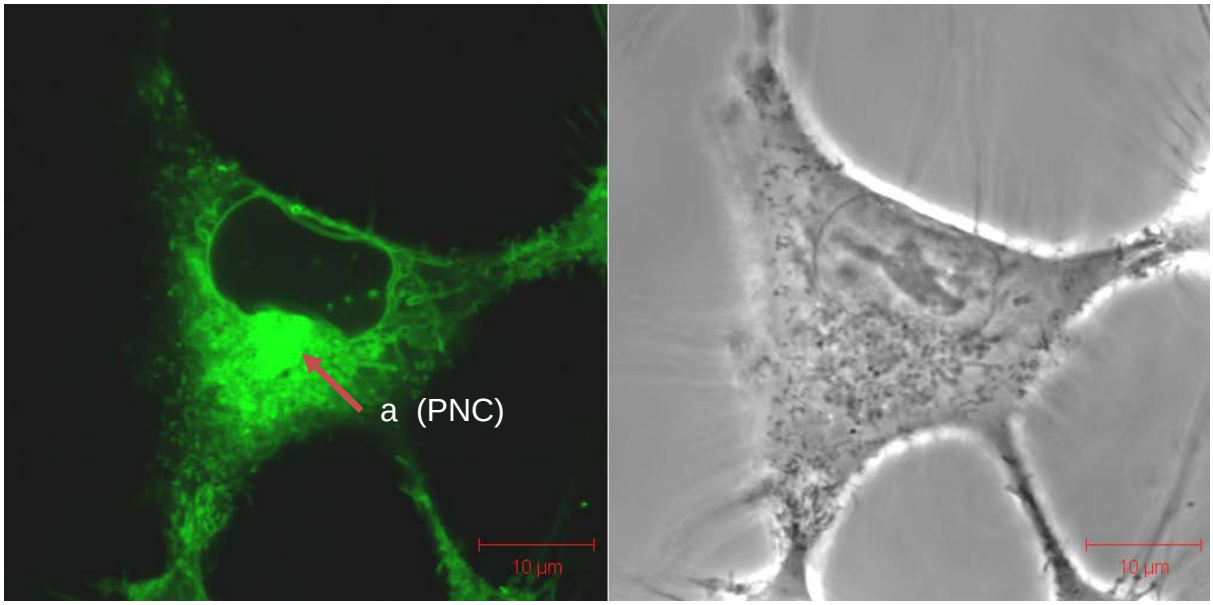

Figure 6.12 A549 cells exposed to 100nm neutral Duke Scientific nanopolystyrene x40 magnification after 24 hour exposure. (a) perinuclear clusters (PNC) of nanoparticles around nucleus.

6.2.3 Discussion

Although the confocal laser scanning microscopy studies indicated that both carboxylated and neutral polystyrene nanoparticles were readily taken up by A549 cells *in vitro*, some striking differences in the behaviour of the two nanoparticle types were apparent.

The uptake and migration time of 50nm and 100nm particles through the cell was considerably faster than that of the 40nm and 100nm carboxylated particles. Furthermore, the 50nm and 100nm neutral particles were seen result in a significantly different distribution of fluorescence than the 40nm and 100nm carboxylated particles. Whereas the latter appeared to be explusively compartmentalised, the former produced a fluorescence which was diffused over the entire cell volume, up to the nuclear membrane, in addition to a more localised fluorescence concentration.

The migration time of carboxylated nanoparticles through the cell is known to be slower than that of neutral nanoparticles, which is most likely due to their anionic surface properties [10]. The extracellular surface of the plasma membrane is negatively charged due to the negative charge on the phospholipid heads. Therefore, the surface of the membrane could influence the way in which charged particles interact with the cell membrane. However, superimposed on this is an overall intracellular negative charge, caused by unequal distribution of ions across the plasma membrane driven by the activity of ion channels and pumps. The cell uses this negative electrical membrane potential to drive the transport of substances, often against a concentration gradient into or out of the cell. These factors potentially contribute to a relatively slow uptake of the negatively charged 40nm carboxylated

Invitrogen nanopolystyrene. The negative intracellular charge would also have an effect on the transportation rates of the negatively charged 40nm and 100nm carboxylated nanoparticles around the cell, once particles have been internalised.

Neutral nanopolystyrene particles, 78nm in size, have been demonstrated to enter macrophages and red blood cells by a non-endocytic process, so that uptake may be mediated via diffusion or another unidentified mechanism [11]. Passive diffusion is usually driven by an electrochemical or concentration gradient, which results in the selective permeability of low molecular weight substances into the cells lipophylic plasma membrane. Facilitated diffusion is another form of passive transport which allows for substances to pass from an area of high to low concentration through selective membrane protein channels. No metabolic energy is required as cell entry is driven by the concentration gradient. Movement of nanoparticles into the cell via these means could explain the rapid uptake of neutral 50nm particles by cells. The cell would require no energy as particles were passively taken up, which may also explain why a larger volume of neutral Duke Scientific nanoparticles were internalised to a greater degree than carboxylated Invitrogen nanoparticles.

However, from confocal images obtained of 50nm and 100nn neutral Duke Scientific nanopolystyrene particles, the fluorescence dispersion may also indicate there is some possible leaching of dye from the particles. Intracellular fluorescence from dispersions with molecular dye (or from the labile molecular dye fraction of a nanoparticle sample) increases rapidly via conventional physical transport, and is barely energy dependent. The fluorescence is then distributed between compartments in the cell, (and for this and many other hydrophobic dyes) mostly in the endoplasmic reticulum. Fluorescence accumulation is reversible; exposure to the

dye leads to a steady state intracellular concentration, with partitioning between the compartments. [12], [13].

In a recent study by Salvati et al (2011), the uptake of labile dye from labelled manufactured nanoparticles by cells was examined. The study concluded that, for some commercially available samples, the uptake of fluorescence, for fluorescently labelled nanopolystyrene, was dominated by the presence of labile dye, rather than by the particles themselves. The authors also examined the uptake of pure fluorescent dye, concluding that fluorescence saturation is suggestive of a simple equilibration across a semi-permeable membrane. Dead and energy depleted cells were also found to reveal similar results as those for healthy cells after exposure to nanoparticles containing fluorescent dye and fluorescent dye only, suggesting that the fluorescent intensity is the result of the physiochemical process of diffusion across the cell membrane of the dye, which occurs without the cells expending energy [8].

This uniform dispersion of the fluorescent 50nm and 100nm Duke Scientific nanopolystyrene around the cell, as discussed, may thus be accounted for by the leakage of fluorescent dye from the nanoparticles. Some regions of localised fluorescence, similar to those observed for the Invitrogen nanoparticles, are observable, and may be true indications of internalised nanoparticles. The study clearly demonstrates, however, than confocal imaging of the fluorescent lables them selves is not an unambiguous confirmation of the presence and distribution of nanoparticles in cells.

6.2.4 Summary of Nanoparticles Confocal Imagary

The internalisation of 40nm and 100nm carboxylated Invitrogen nanopolystyrene 50nm and 100nm Duke Scientific nanopolystyrene into A549 lung cells was observed. Fluorescent and bright-field images revealed 40nm and 100nm carboxylated nanoparticles accumulated into cellular organelles that resemble possible lysosomes after exposure times of 24hours. 40nm carboxylated nanoparticles examined were not observed within the nucleus as was revealed by combining “z-stack” image series cutting through the cell in single z-steps of approximately 10 µm with the generated orthogonal projection obtained from the z-stack image series of the cells. 50nm and 100nm Duke Scientific nanopolystyrene were observed to accumulate within cell organelles after 1 hour exposure to A549 cells. Particles appeared to be occupying organelles that resembled lysosomes or possibly the endoplasmic reticulum surround the nucleus. 50nm particles also appeared to be contained within organelle membranes. However, after longer exposure times of 24 hours, the dispersion of the fluorescence due to exposure to 50nm particles within the cell was more uniform, with possible dye leakage attribute to the apparent dispersion of particles. 50nm Duke Scientific nanopolystyrene particles were not observed within the nucleus, as was revealed from the z- stack image series of the cells. The generated orthogonal projection obtained by combining “z-stack” image series cutting through the cell in single z-steps of approximately 10 µm with, confirmed the absence of 50nm particles from the nucleus.

Confocal images revealed that there was a difference in the dispersion of internalised nanoparticles between the different neutral and carboxlyated

nanoparticles, potentially due to their different physicochemical characteristics. Cellular up-take and migration times through the cell were observed to be slower for the carboxylated 40nm and 100nm particles, possibly due to their negative charge. While this negative charge may have affected the cellular up-take mechanism into the overall predominately negatively charged cell, it was suggested the 50nm and 100nm neutral nanoparticles may have been taken up by cells through a less energy dependant mechanism such as diffusion (dyes diffuse). However, the possibility of free dye uptake from 50nm and 100nm Duke Scientific nanoparticles could also not be ruled out. This may explain the reason as to why 50nm and 100nm neutral particles “appear” to be taken up faster and to a greater extent.

The following sections will provide the results obtained for the examination of the internalisation of nanoparticles within several specific cell organelles. From the confocal images obtained of all nanoparticles, it was concluded that three possible cell organelles may be targeted; lysosomes, mitochondria and endoplasmic reticula.

6.3 Evaluating the Internalisation of Fluorescent Nanopolystyrene into Lysosomes

Examination of intracellular localisation of 50nm and 100nm Duke Scientific nanoparticles and 40nm and 100nm carboxylated Invitrogen nanopolystyrene was carried out at room temperature using laser scanning confocal microscopy (LSM 510 Meta, Carl Zeiss Inc.) equipped with Argon (488 nm) and HeNe (543 nm) lasers. Images were acquired by multitracking (505-530nm band pass filter to collect nanoparticles fluorescence and 560nm long pass filter for the Lysosome fluorescence) to avoid bleed through between the fluorophores, and the statistical analysis was carried out using LSM 510 software.

From the examination of confocal images obtained of 40nm and 100nm carboxylated Invitrogen nanopolystyrene and 50nm and 100nm Duke Scientific nanopolystyrene within A549 lung cells in the previous section, the accumulation of nanoparticles within lysosomes was inferred. Confocal images of all particles revealed fluorescent accumulations of different sizes and distributions within the cells. As previously discussed, one of the major functions of lysosomes is the digestion of material taken up from outside the cell by endocytosis. Therefore, the incorporation of nanopolystyrene into lysosomes was considered, as these degradative organelles could represent a potential route of nanoparticle digestion or elimination from cells, subsequent to their internalisation. In the case of the 50nm and 100nm neutral nanoparticles, a more diffuse distribution of the fluorescence throughout the cell was observed, suggesting an alternative route of uptake and intracellular transport, or alternatively a release of labile fluorescent dye, resulting in a false representation of the nanoparticle distribution.

The precise cell organelle location of the accumulation of the nanopolystyrene particles will be explored through the use of commercially available transduction fluorescent staining kits, based on baculoviruses. Baculoviruses are insect cell viruses. The use of baculovirus for protein production in insect cells has been used extensively for over two decades, although its application to mammalian cells is relatively new. The utilization of baculovirus to deliver genes to mammalian cells is referred to as BacMam technology [14] [15] .

CellLight® Fluorescent Protein Constructs for Subcellular Structures *BacMam* 2.0 were purchased from Invitrogen (USA). The CellLight® reagent contains a baculovirus which, upon entry into mammalian cells, directs the expression of autofluorescent proteins that are localized in specific subcellular compartments and organelles via a signal peptide or protein fusions. The protein associated with autofluorescence is the Lysosomal Lamp1, which is a lysosomal associated membrane protein. [16]. A549 lung cells were seeded at a density of $1x10^5$ cells/ml, in glass bottom Petri dishes in 10% FBS supplemented DMEM - F12 media and incubated at 37°C in 5% CO_2 for 24hrs for cell attachment before exposure to nanopolystyrene particles of concentration 1×10^{12} particles per ml. Following the exposure period of 24 hours, the cells were washed twice with pre-warmed PBS (37°C). The appropriate volume of CellLight® reagent for the number of cells seeded was calculated by;

$$\text{Volume of CellLight® Reagent (mL)} = \frac{\text{number of cells} \times \text{desired PPC}}{1 \times 10^8 \text{ CellLight® particles/mL}}$$

Where the number of cells is the estimated total number of cells at the time of labelling, PPC is the number of particles per cell, and 1×10^8 is the number of particles per mL of the reagent. The volume of CellLight® reagent needed was added directly to the cells in complete cell medium and mixed gently. Cells were then reincubated over night in fresh media, to allow for the expression of the CellLight® fluorescent protein. The manufacturer states that there is a ~90% transduction efficiency achieved from CellLight® kits. Therefore not all cell organelles in each cell will be fluorescently transduced as the efficiency is also dependant on the number of desired transducer particles per cell,

Figures 6.15 and 6.16 display confocal images obtained of 40nm and 100nm carboxylated nanopolystyrene, respectively, within A549 cells that have also been treated with the lysosomal fluorescent staining kit. Each image consists of four sections. The section labelled (a) is a confocal image showing the fluorescence of the particles only, using the 505-530nm band pass filter. The section labelled (b) is a confocal image of the fluorescent lysosomes of the cell following transduction with the CellLight®kit using the 560nm long pass filter. Section (c) is an bright-field image of the cell showing no fluorescence and section (d) shows an image of fluorescence overlap of both the particles and the fluorescently transduced lysosomes. The fluorescence overlap, and therefore colocalisation of nanoparticles and lysosomes, is shown in a yellow-orange colour.

As can be seen in figure 6.15 (a), the fluorescent images of 40nm particles show that particles are mostly localised and accumulated in discrete regions and are not observed to occupy the interstitial space between organelles. The overlap image (d) in figure 6.15 shows the co-localisation of nanoparticles within lysosomes as an

orange fluorescence (overlap of green from particles and red from lysosomes). This orange/yellow fluorescence is visual confirmation of co-localisation of 40nm carboxylated nanoparticles within lysosomal structures.

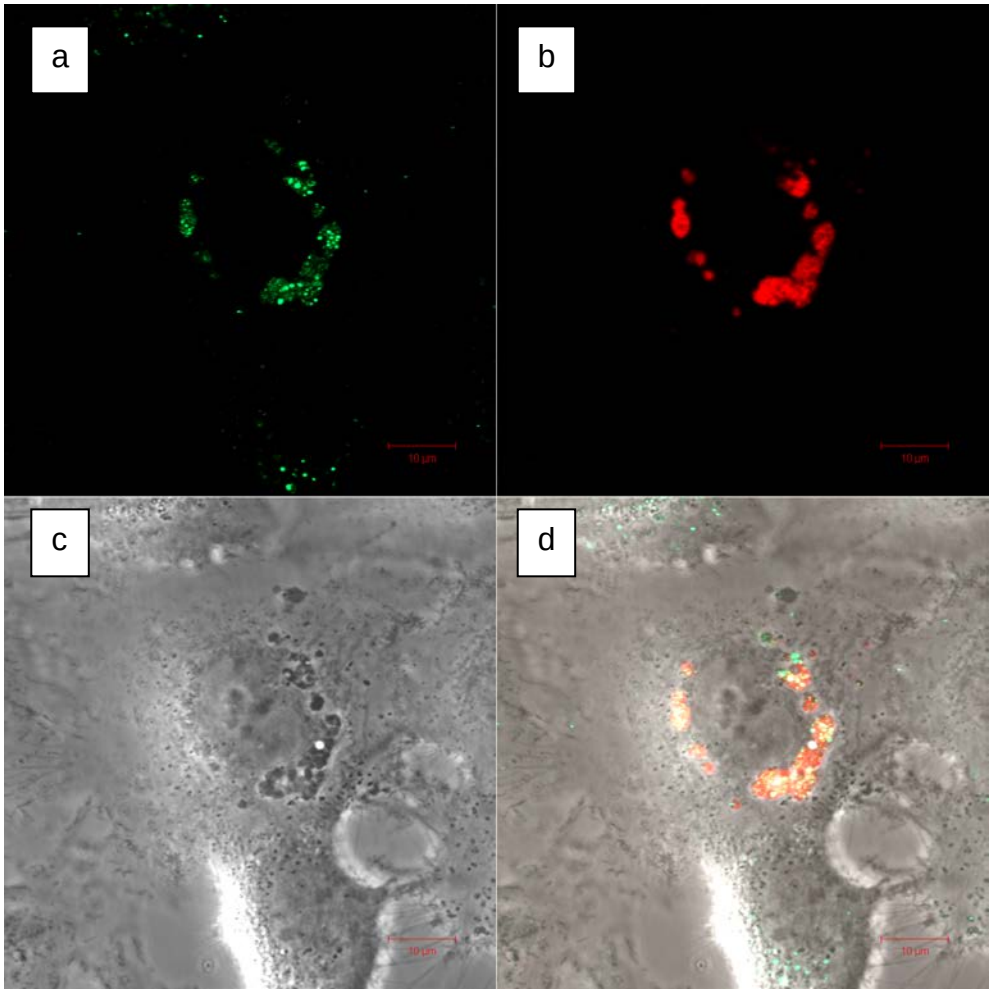

Figure 6.15 Confocal Images of 40nm Carboxylated Invitrogen Nanopolystyrene accumulated within lysosomes of A549 cells after 24hr exposure x60 magnification.

Similarly, the fluorescent overlap image (d), of figure 6.16, shows that 100nm carboxylated nanoparticles are also internalised and largely co-localised within lysosomes. The orange/yellow fluorescent accumulations within the cell also confirm the presence of lysosomes containing green fluorescent nanoparticles.

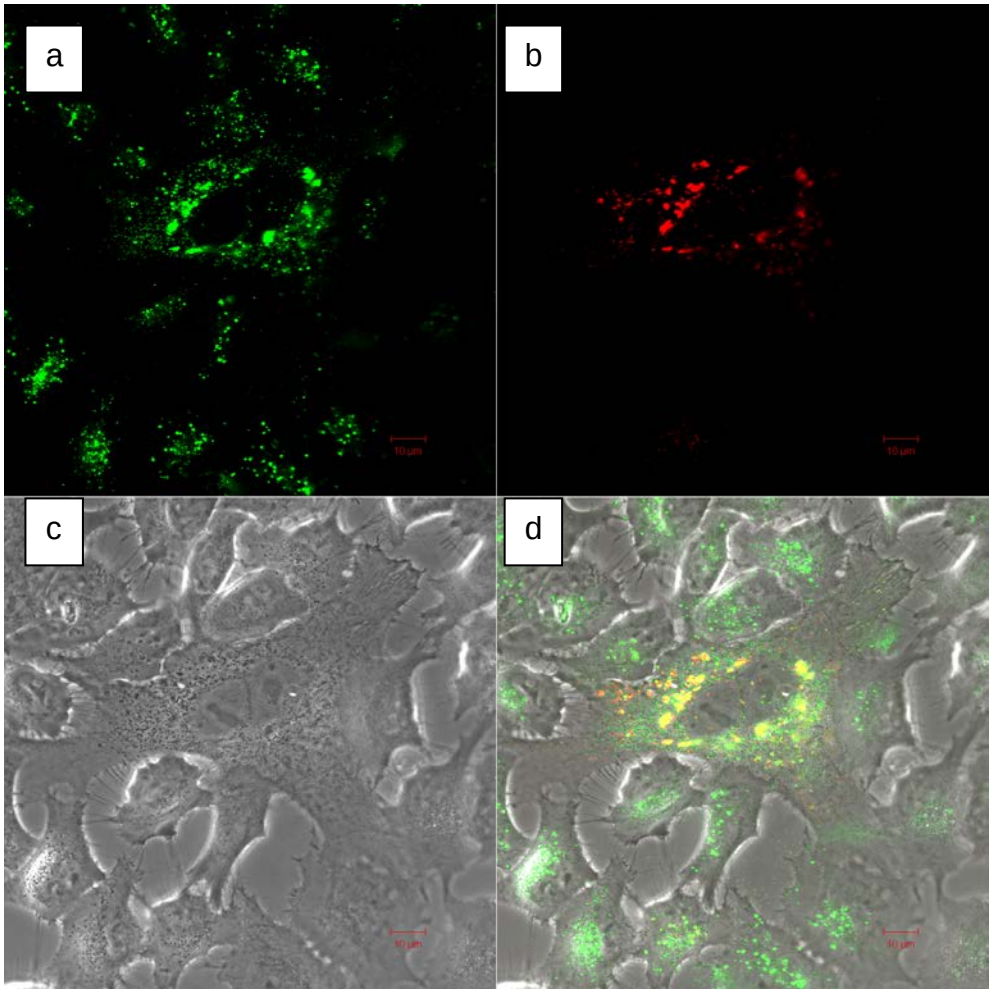

Figure 6.16 Confocal Images of 100nm Carboxylated Invitrogen Nanopolystyrene accumulated within lysosomes of A549 cells after 24hr exposure x40 mag.

Figures 6.17 and 6.18 display the confocal images obtained of 50nm and 100nm Duke Scientific nanopolystyrene, respectively, within A549 cells that have also been treated with the lysosomal fluorescent staining kit. The images each consist of four sections. The section labelled (a) is a confocal image showing the fluorescence of the particles only, using the 505-530nm band pass filter. The section labelled (b) is a confocal image of the fluorescent lysosomes of the cell following transduction with the CellLight®kit using the 560nm long pass filter. Section (c) is an bright-field image of the cell showing no fluorescence and section (d) shows an image of fluorescence

overlap of both the 50nm or 100nm particles and the fluorescently transduced lysosomes. The fluorescence overlap is shown in a yellow-orange colour.

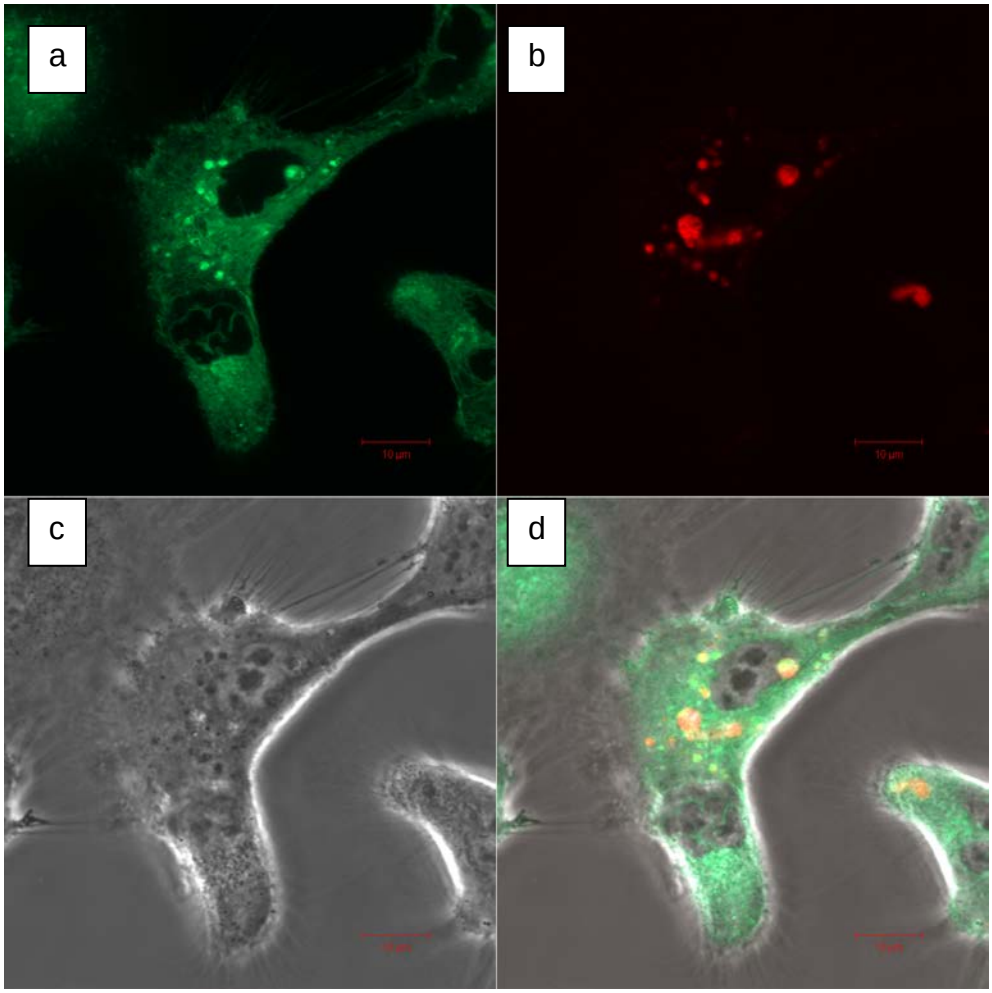

Figure 6.17 Confocal Images of 50nm neutral Duke Scientific Nanopolystyrene accumulated within lysosomes of A549 cells after 24hr exposure x60 mag.

The fluorescence overlap image in figure 6.17 displays orange/yellow fluorescent spots that correspond to fluorescent 50nm nanoparticles internalised within lysosomes. The fluorescent overlap image (d) in figure 6.18 also shows a large number of ‘spots’ around the cell that have an orange/yellow fluorescence, confirming the internalisation and co-localisation of 100nm neutral nanoparticles

within lysosomes. However, the fluorescence distribution is notably different to that of the 40nm and 100nm carboxylated nanoparticles (figures 6.15 and 6.16). As previously described in section 6.2.2, the distribution of fluorescence from the 50 and 100nm neutral nanoparticles may be due to the leakage of the fluorescent dye, which has the ability to diffuse into the cell and into organelle membranes. This molecular dye has the ability to passively diffuse into cell organelles with not much energy required (Salvati et al. 2011).

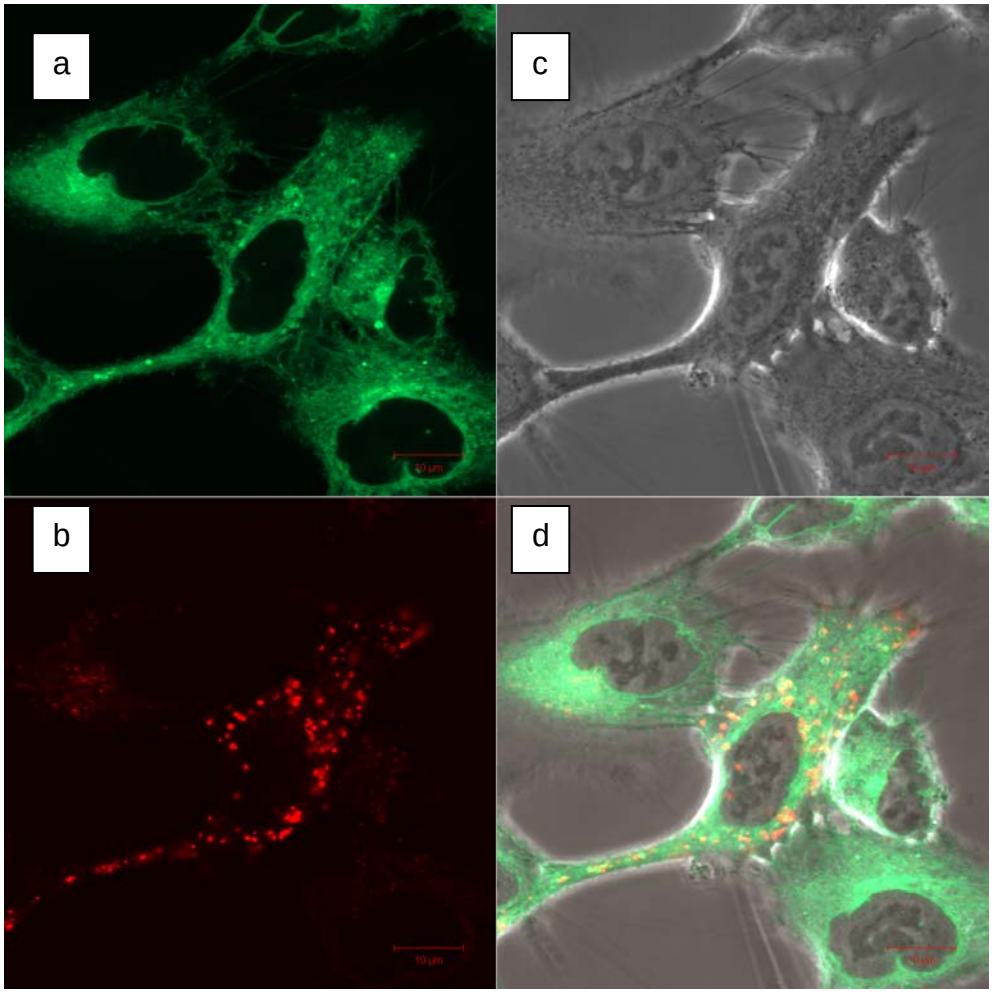

Figure 6.18 Confocal Images of 100nm neutral Duke Scientific Nanopolystyrene accumulated within lysosomes of A549 cells after 24hr exposure x60 mag.

Images 6.17 and 6.18 reveal that the 50nm and 100nm neutral nanoparticles, as well as the 40nm and 100nm (figures 6.15 and 6.16) carboxylated nanoparticles examined did in fact accumulate within lysosomes in the cell type investigated. It is expected that lysosomes could be capable of degrading polymer based nanoparticles such as those composed from polystyrene; however, it would be unlikely to occur within the short exposure times investigated.

There are reports that nanoparticles have the ability to cross cell organelle membranes, and although these nanoparticles may not cause specific cell death, there is the possibility for nanoparticles to enter organelles such as mitochondria and interfere with biochemical reactions of the organelle [17] [2]. Taking such reports into consideration, the potential of nanoparticles to penetrate into other cell organelles must be investigated.

6.4 Evaluating the Internalisation of Fluorescent Nanopolystyrene into Mitochondria

Recent reports have suggested that nanoparticle migration from lysosmes to other cell organelles, such as the mitochondria or the endoplasmic reticulum, may take place [18] [2]. In the review article "*Understanding biophysicochemical interactions at the nano–bio interface*", the authors describe a mechanism whereby nanoparticles cause lysosomal swelling as a result of the so-called proton sponge effect. This swelling eventually causes the lysosomes to rupture, which leads to particle deposition in the cytoplasm and the spillage of the lysosomal content into the cell [2]. In this instance, charged nanoparticles may undergo further interactions within the cytoplasm and therefore interfere with cellular mechanisms and subsequently have

an effect on, or enter into, other cell organelles, such as the mitochondria [17] [2] [19].

As discussed in section 6.3, the fluorescent kits used to label mitochondria within A549 cells were CellLight® Fluorescent Protein Constructs for Subcellular Structures *BacMam* 2.0. The procedure for fluorescently labelling mitochondria, as described in section 6.3, was carried out as before. The protein associated with fluorescence is a mitochondria signal sequence of E1 alpha pyruvate dehydrogenase fused to TagRFP (red fluorescent protein). All cells imaged were healthy with the nucleus visible.

Figures 6.19 and 6.20 display confocal images obtained of 40nm and 100nm carboxylated nanopolystyrene, respectively, within A549 cells that have also been treated with the mitochondrial fluorescent staining kit. The section labelled (a) is a confocal image showing the fluorescence of the particles only, using the 505-530nm band pass filter. The section labelled (b) is a confocal image of the fluorescent mitochondria of the cell following transduction with the CellLight®kit using the 560nm long pass filter. Section (c) shows an image of fluorescence overlap of both the nanoparticles and the fluorescently transduced mitochondria. Any fluorescence overlap is shown in a yellow-orange colour.

Figure 6.19 shows A549 cells after fluorescent mitochondrial staining and subsequent 24hr exposure to 40nm carboxylated nanopolystyrene. No fluorescence overlap of nanoparticles and fluorescently transduced mitochondria can be seen in the section (c). This indicates that the nanoparticles do not enter the mitochondria. Close examination reveals no orange/yellow colour that would indicate any fluorescence overlap from nanoparticles with mitochondria.

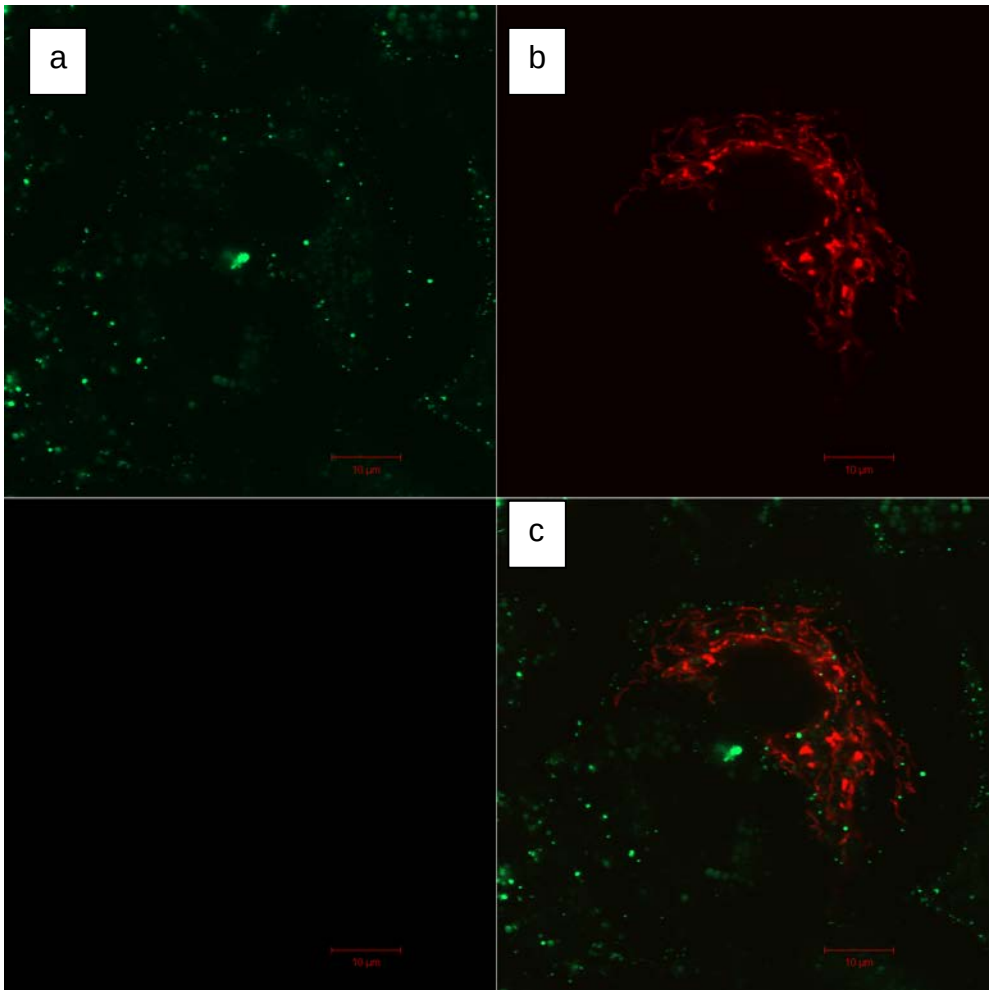

Figure 6.19 Confocal Images of 40nm Carboxylated Invitrogen Nanopolystyrene and fluorescently labelled mitochondria within A549 cells after 24hr exposure x60 magnification.

Confocal images obtained of fluorescently tranduced mitochondria within cells after 24hr exposure to 100nm carboxylated nanoparticles reveal similar results. The images obtained reveal nanoparticles accumulated in “spots” or small localised regions around the cell (section (a)). The fluorescently stained mitochondria can be clearly seen in section (b). Section (c) clearly shows no overlap in fluorescence from the nanoparticles or the fluorescent mitochondria. As previously seen with the 40nm

carboxylated nanoparticles (figure 6.19), no orange/yellow fluorescence can be observed, indicating there is no overlap in fluorescence and that nanoparticles did not enter the mitochondria.

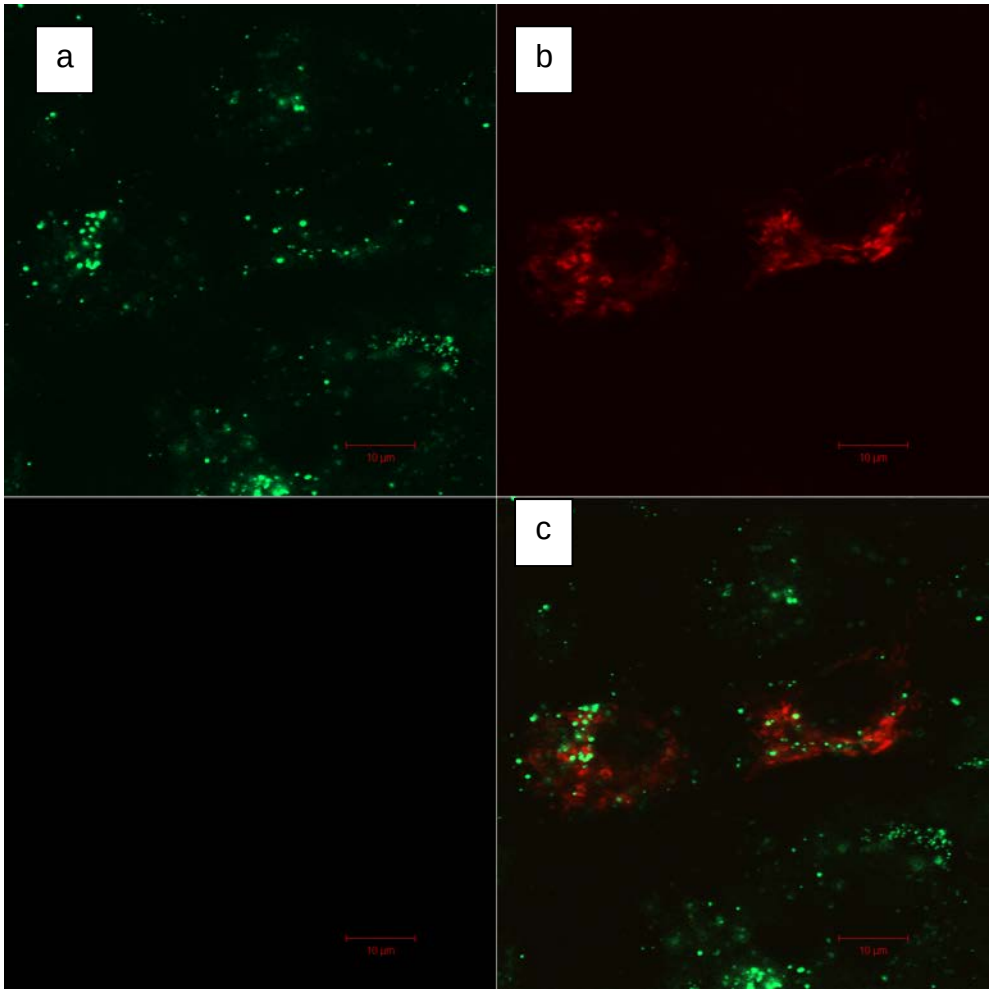

Figure 6.20 Confocal Images of 100nm Carboxylated Invitrogen Nanopolystyrene and fluorescently labelled mitochondria within A549 cells after 24hr exposure x60 magnification.

As can be seen in figure 6.21 (a), the images of 50nm particle exposed cells show that the fluorescence is widely dispersed and is not observed to be isolated to specific cell regions. The overlap image (c) in figure 6.21 indicates the co-localisation

of nanoparticles within mitochondria as an orange fluorescence (overlap of green from particles and red from mitochondria).

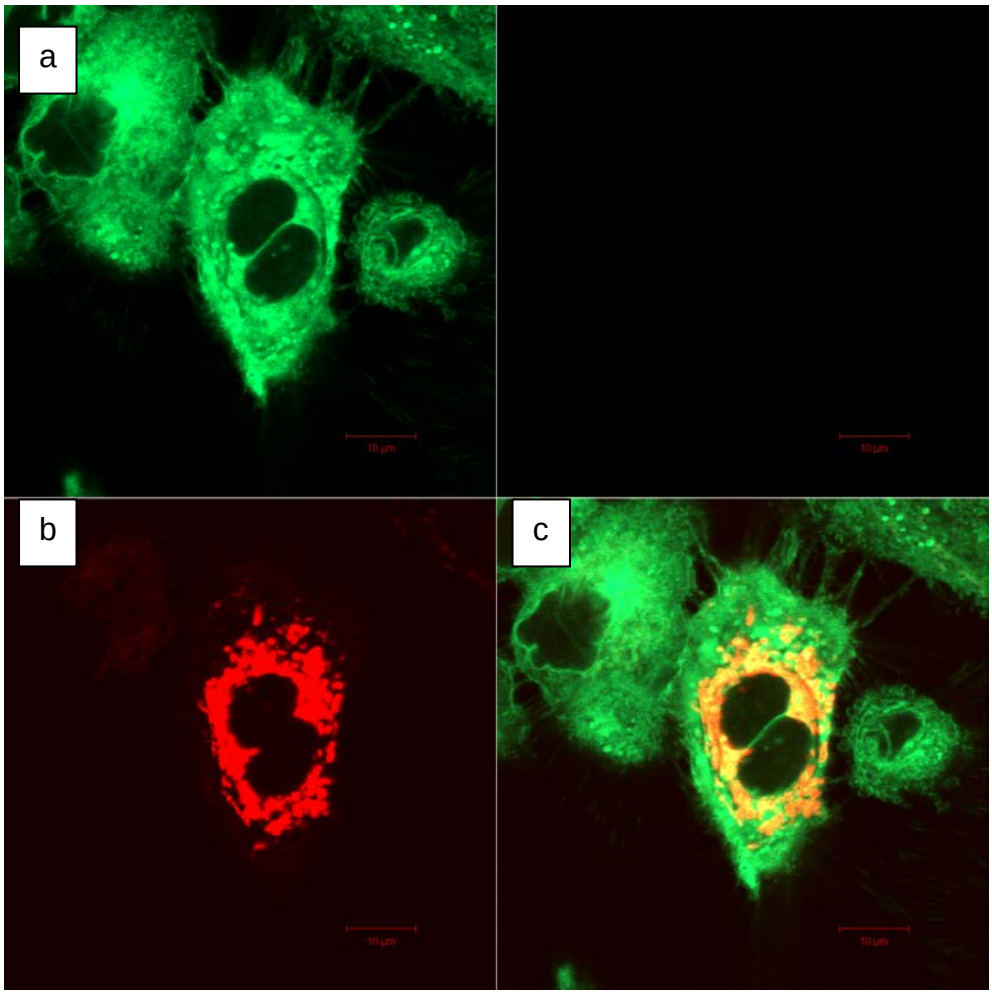

Figure 6.21 Confocal Images of 50nm neutral Duke Scientific Nanopolystyrene accumulated within mitochondria of A549 cells after 24hr exposure x60 mag.

Similarly, for the confocal images obtained for the examination of the 100nm neutral nanopolystryene particles, an overlap of fluorescence from nanoparticles and transduced mitochondria was observed. Figure 6.22, section (c) reveals a yellow/orange colour where fluorescence occurs in the same regions where there is fluorescence from stained mitochondria. As with the 50nm particle, this overlap in fluorescence suggests that the 100nm neutral nanopolystyrene particles did

accumulate with mitochondria. However, the possibility remains that the large overlap in fluorescence may be due to the presence of labile dye from the nanoparticles, which, as previously discussed, has the ability the diffuse throughout interstitial areas of the cell and various organelles.

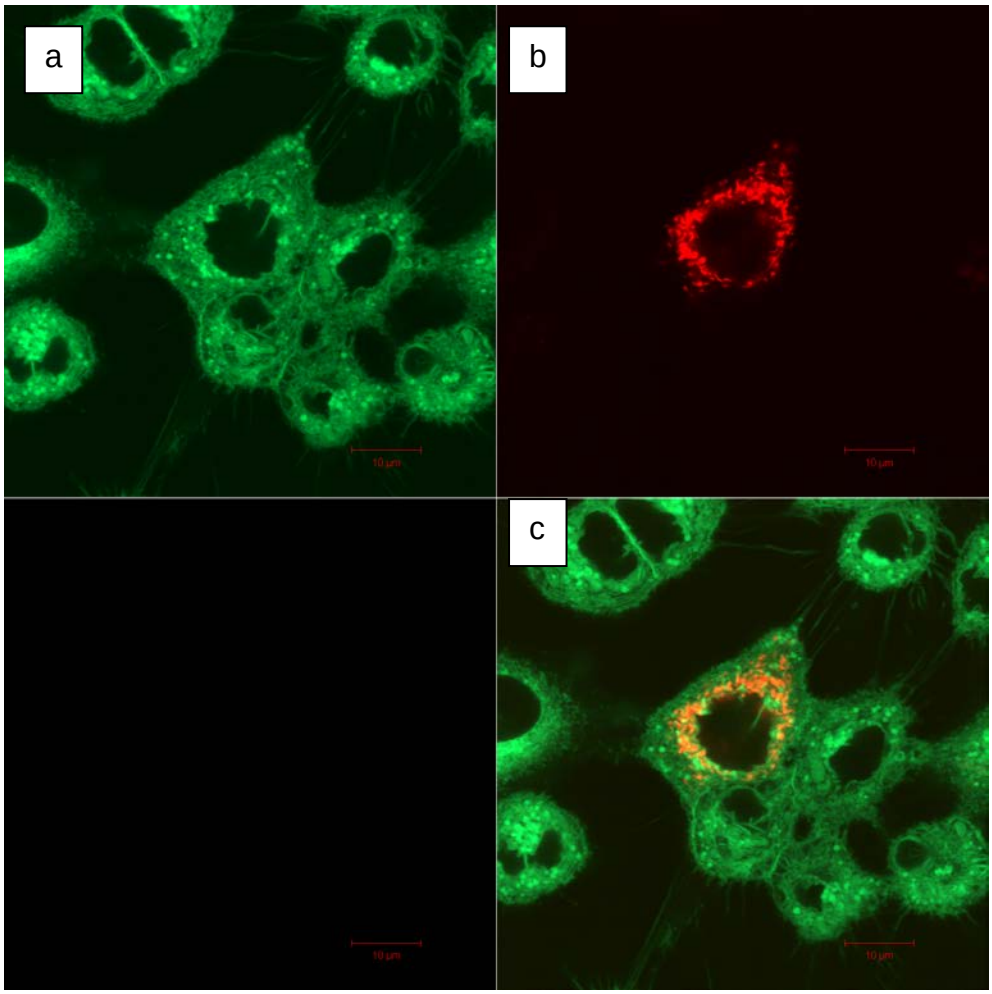

Figure 6.22 Confocal Images of 100nm neutral Duke Scientific Nanopolystyrene accumulated within mitochondria of A549 cells after 24hr exposure x60 mag.

Literature reports of the examination of nanoparticles entering the mitochondria suggest that anionic and neutral nanoparticles do not enter the mitochondria. This

may be due to the negative and neutral surface charge of the particles [2, 20, 21]. Positively charged nanoparticles have been known to have an overall effect on the proton pump of lysosomes, causing them to rupture and from there subsequently enter mitochondria. This can lead to mitochondrial damage, potentially leading to decreased ATP production and cellular apoptosis [2, 17] . However, there are no reports of anionic or neutral nanoparticles produce similar effects, and from the cytotoxicity results obtained for the nanoparticles examined (40nm and 100nm carboxylated nanopolystyrene and 50nm and 100nm neutral nanopolystyrene) and presented in Chapter 5, whereby they were found not to induce any toxic effects on cells, the results found here are more consistent with the localisation of labile dye within the mitochondria due to passive diffusion.

Salvati et al. (2011) suggested that free or liable dye from nanoparticles may be easily taken up by organelles as the molecular dye has the ability to diffuse throughout the cell, not using any energy in the process. This fluorescence diffusion can then be easily mistaken for nanoparticle accumulation. From examination of confocal images obtained of A549 cells exposed to 40nm and 100nm carboxylated nanoparticles and 50nm and 100nm neutral nanopolystyrene, it can be seen that there is greater fluorescence intensity located around the nucleus in perinuclear clusters. These observations, along with the suggestion that nanoparticles do accumulate in other organelles and that liable fluorescent dye has the ability to diffuse throughout the cell, lead to the examination of the possibility of nanoparticles entering the endoplasmic reticulum (ER).

6.5 Evaluating the Internalisation of Fluorescent Nanopolystyrene into The Endoplasmic Reticulium

While nanoparticles have been reported to accumulate in various organelles within cells [22], they have also been reported to enter the ER [23-25]. There are also reports that some substances enter cells via an unusual pathway that involves trafficking through endosomes to the ER [26, 27]. These reports, coupled with the images obtained of the fluorescent nanopolystyrene particles accumulations with A549 cells, led to the examination of nanoparticles co-localising within the ER. The images obtained of 40nm and 100nm carboxylated nanopolystryene and 50nm and 100nm neutral nanopolystyrene particles internalised within A549 cells, appear to mostly gather in perinuclear clusters after certain exposure periods (section 6.2, figure 6.2: 40nm carboxylated nanopolystyrene 24hr exposure, figure 6.4: 100nm carboxylated nanopolystyrene 24hr exposure, figure 6.10: 50nm neutral nanopolystryene 24hr exposure, figure 6.12: 100nm neutral nanopolystyrene 24hr exposure).

The fluorescent kits used to label ER within A549 cells were CellLight® Fluorescent Protein Constructs for Subcellular Structures *BacMam* 2.0. The procedure for fluorescently labelling ER, as described in section 6.3, was carried out as before. The protein associated with fluorescence is an ER signal sequence of calreticulin and KDEL (ER retention signal) fused to TagRFP (red fluorescent protein). All cells imaged were healthy with the nucleus clearly visible.

Figures 6.23 and 6.24 display confocal images obtained of 40nm and 100nm carboxylated nanopolystyrene, respectively, within A549 cells after 24 hr exposure, that have also been treated with the ER fluorescent staining kit. The image consists

of four sections. The section labelled (a) is a confocal image showing the fluorescence of the particles only, using the 505-530nm band pass filter. The section labelled (b) is an bright-field image of the cell showing no fluorescence, (c) is a confocal image of the fluorescent ER of the cell following transduction with the CellLight®kit using the 560nm long pass filter and section (d) shows an image of fluorescence overlap of both the particles and the fluorescently transduced ER. The fluorescence overlap is shown in a yellow-orange colour.

The fluorescence observed in section (d) of figure 6.23 can be considered to have no fluorescence overlap from 40nm carboxylated nanoparticles and fluorescently transduced ER. This indicates that the nanoparticles did not localise within the ER after 24hr exposure. The fluorescence image of nanoparticles only shown in section (a) of figure 6.23 reveals nanoparticles to be accumulated in small circular regions within the cells, similar to lysosmes.

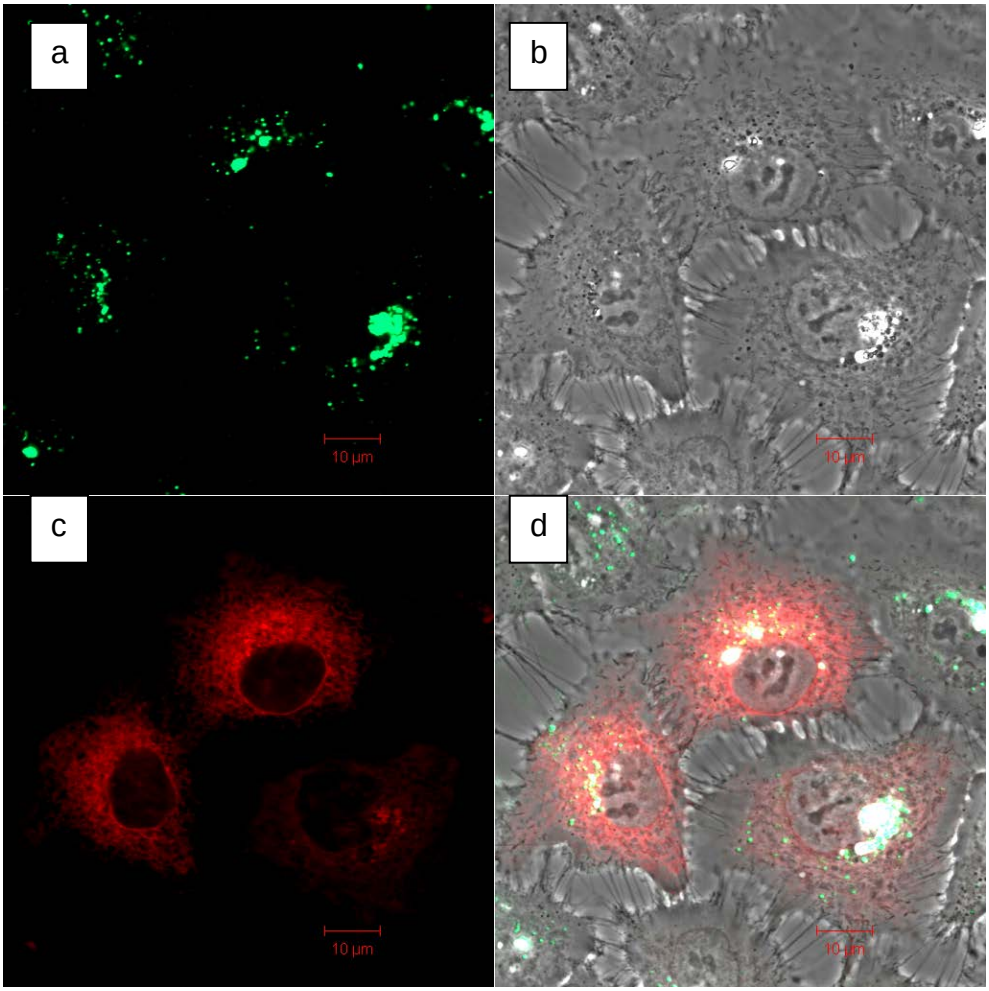

Figure 6.23 Confocal Images of 40nm Carboxylated Invitrogen Nanopolystyrene and fluorescently labelled endoplasmic reticulum within A549 cells after 24hr exposure x60 magnification.

Figure 6.24 also reveals that 100nm carboxylated nanoparticles did not internalise within the ER. Both the nanoparticles (section (a)) and the fluorescently transduced ER of the cells imaged (section (c)) can be seen clearly. While the fluorescence from the nanoparticles is localised to small circular regions resembling lysosmes throughout the cell, there appears to be no overlap with these regions and the over all fluorescently labelled ER.

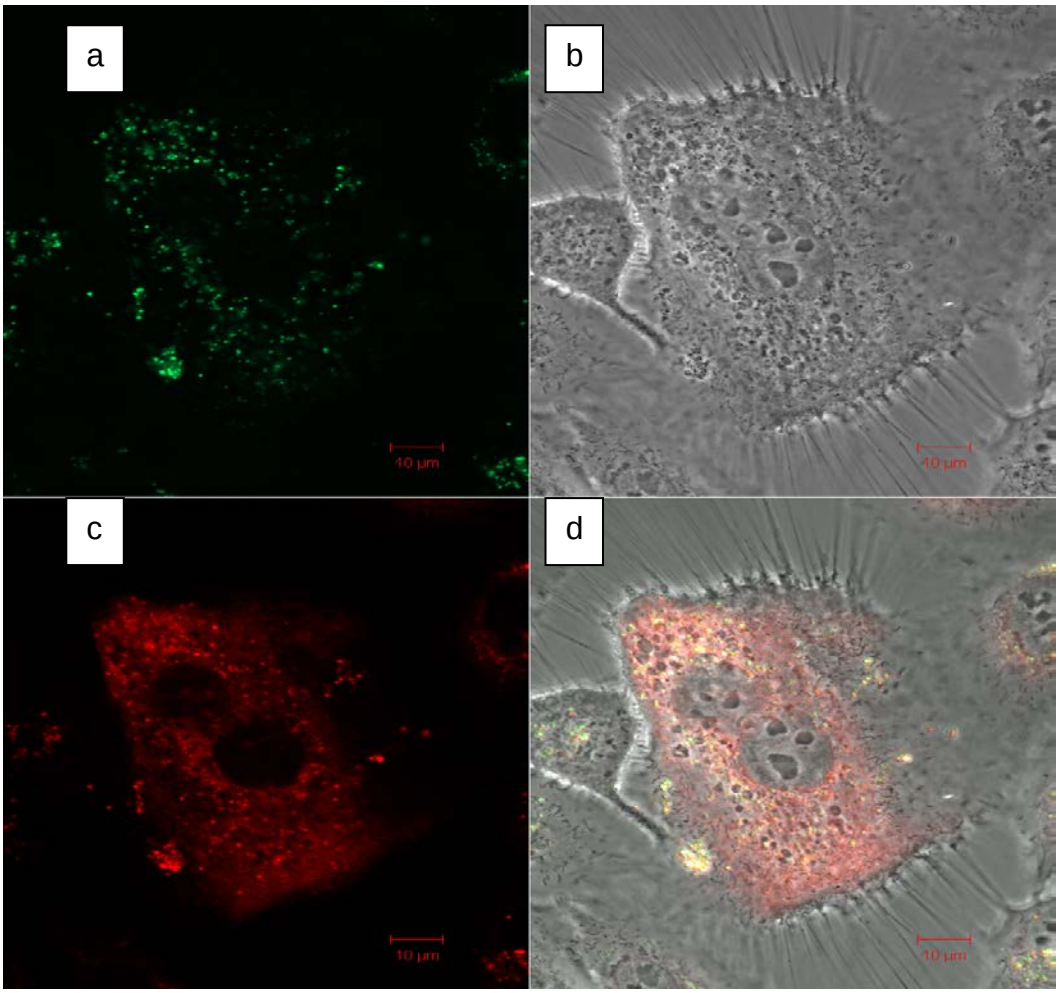

Figure 6.24 Confocal Images of 100nm Carboxylated Invitrogen Nanopolystyrene and fluorescently labelled endoplasmic reticulum within A549 cells after 24hr exposure x60 magnification.

Figures 6.25 and 6.26 display confocal images obtained of 50nm and 100nm neutral nanopolystyrene, respectively, within A549 cells after 24 hrs exposure, that have also been treated with the ER fluorescent staining kit. The image consists of four sections. The section labelled (a) is a confocal image showing the fluorescence of the particles only, using the 505-530nm band pass filter. The section labelled (b) is an bright-field image of the cell showing no fluorescence, (c) is a confocal image of the fluorescent ER of the cell following transduction with the CellLight®kit using the 560nm long pass filter and section (d) shows an image of fluorescence overlap of both the particles and the fluorescently transduced ER. The fluorescence overlap is shown in a yellow-orange colour.

Figure 6.25 represents the confocal images obtained of fluorescently transduced A549 cells and internalised 50nm neutral polystyrene after 24 hr exposure. The ER is clearly visible in section (c). The fluorescence overlap in section (d) can be seen quite strongly. While there is still dispersed fluorescence throughout the cell, the majority of the fluorescence can be seen to be localised to the perinuclear region, specific to the ER. The intensity of the yellow/orange, caused by the overlap of fluorescence from the particles and the fluorescently transduced ER, is much stronger compared to that of the previous overlap image of the 40nm and 100nm carboxylated nanopolystryene and transduced ER images. However, once again the fluorescence distribution of the 50nm neutral nanopolystryene particles throughout the cell is notably different to that of both the 40nm and 100nm carboxylated nanopolystyrene particles.

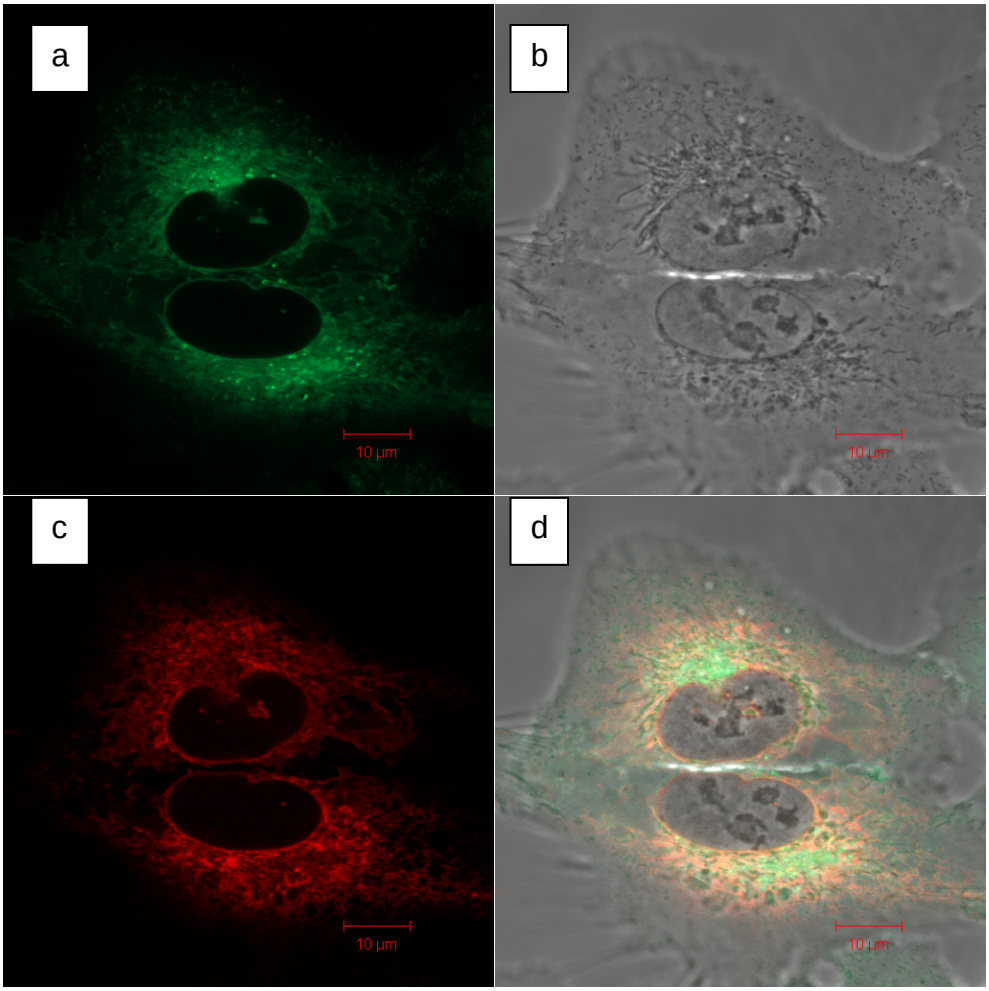

Figure 6.25 Confocal Images of 50nm neutral Duke Scientific Nanopolystyrene accumulated within endoplasmic reticulum of A549 cells after 24hr exposure x60 mag.

Similarly, for images obtained of the 100nm neutral nanopolystyrene particles, the intensity of the fluorescence overlap of the particles and the fluorescently transduced ER is strong. Figure 6.26, section (d) reveals the intensity overlap. Nanoparticle internalisation of cells can be clearly seen in section (a). From the overlap image obtained, it can be assumed that nanoparticles were internalised within the ER, however, once again, the possibility of free dye causing the intense fluorescence overlap, must be considered.

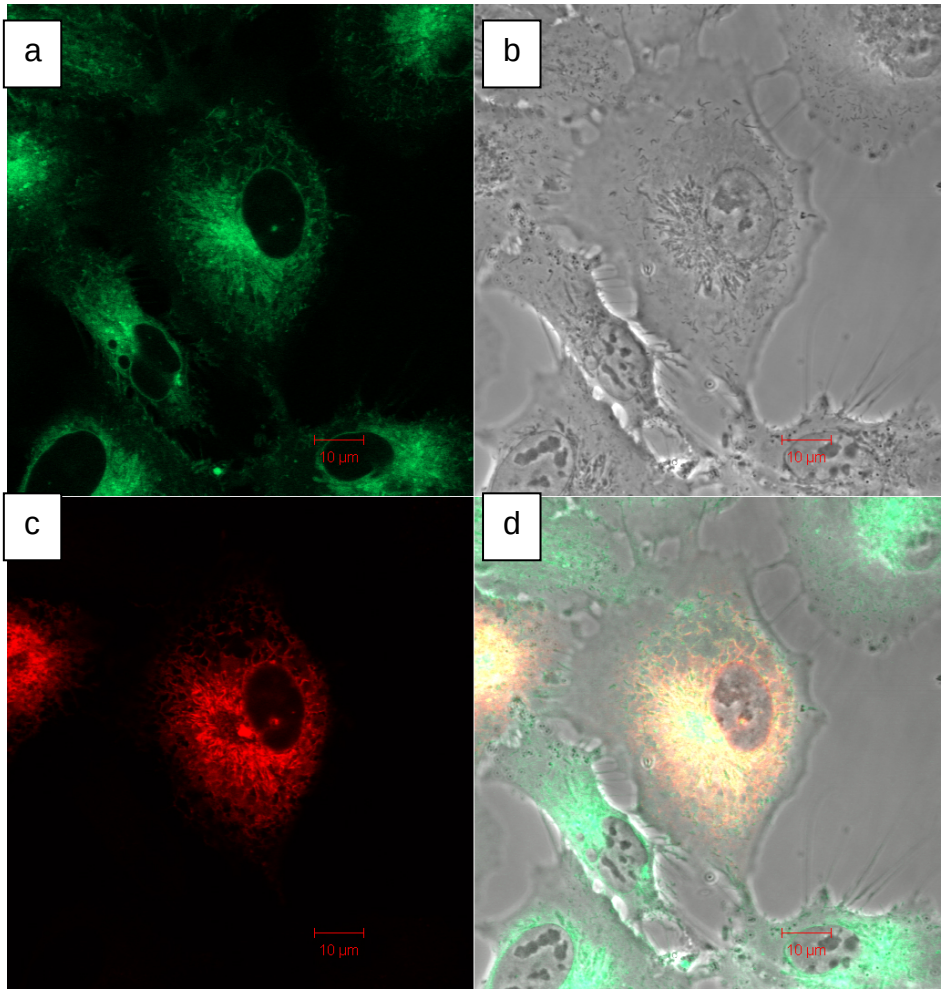

Figure 6.26 Confocal Images of 100nm neutral Duke Scientific Nanopolystyrene accumulated within endoplasmic reticulum of A549 cells after 24hr exposure x60 mag.

6.5 Summary of The Evaluation of Nanoparticles Internalisation Within Cell Organelles.

The internalisation and accumulation of 40nm and 100nm carboxylated Invitrogen nanopolystyrene particles within A549 cells was investigated. Cells were first treated with a specific cell organelle CellLight® fluorescent transduction kit, as described in section 6.3. Cells were then exposed to 40nm or 100nm carboxylated nanopolystyrene for 24hrs and the fluorescence accumulation examined using confocal microscopy.

The first cell organelle under examination for accumulation of nanoparticles was the lysosomes. From the confocal images obtained (figure 6.15 and 6.16), it was revealed that carboxylated nanoparticles, 40nm and 100nm respectively, were internalised by cells and accumulated within lysosomes. This can be seen from the fluorescent overlap images obtained (figures 6.15 and 6.16 40nm and 100nm respectively). These results are in keeping with literature reports that nanoparticles accumulate within lysosomes [8] [7, 28]. The examination of the internalisation of 40nm and 100nm carboxylated within mitochondria was next examined. As was revealed by the fluorescence overlap images in figures 6.19 (40nm) and 6.20 (100nm), carboxylated nanoparticles were not seen to be internalised within mitochondria. Similarly, 40nm and 100nm carboxylated nanoparticles were not found to be internalised within the ER upon examination of the fluorescent overlap images obtained (figures 6.23 and 6.24 respectively).

The internalisation and accumulation of 50nm and 100nm neutral Duke Scientific nanopolystyrene particles within A549 cells was investigated. As described before in section 6.3, cells were first treated with a specific cell organelle CellLight® fluorescent transduction kit. Cells were then exposed to 50nm or 100nm neutral nanopolystyrene for 24hrs and the fluorescence accumulation examined using confocal microscopy.

The examination of fluorescent overlap images obtained for the investigation of neutral nanoparticles internalised within lysosmes revealed that both the 50nm and 100nm nanoparticles were internalised within lysosomes (figures 6.17 and 6.18 respectively). However, the issue of the fluorescence distribution throughout the cell was raised. Fluorescently transduced mitochondria were also seen to have internalised 50nm and 100nm nanoparticles. The images obtained show a large degree of fluorescence overlap between the 50 and 100nm particles (figures 6.21 and 6.22 respectively) and the fluorescently tranduced mitochondria. The examination of the internalisation of the neutral nanoparticles within the endoplasmic reticulum also revealed a large fluorescence overlap between 50nm and 100nm and the fluorescently tranduced endoplasmic reticulum (figures 6.25 and 6.26 respectively). However, once again the issue of possible free or liable dye was raised as the fluorescence distribution of the nanoparticles was questionable.

While the results obtained for the internalisation of 50nm and 100nm neutral nanoparticles are in keeping with literature reports [7, 8, 28], the overall fluorescence distribution requires further investigation. The following section describes an experiment that was carried out to examine the possibility of the 50nm and 100nm neutral nanoparticles containing free or liable dye.

6.6 Fluorescence Up-take Study of Nanoparticles

The possible uptake pathways of nanoparticles by a cell were previously described in Chapter 2, section 2.2.2. One of the pathways mentioned was passive diffusion. Passive diffusion is used by the cell to allow molecules of low molecular weight to “diffuse” through the cell membrane, and is usually driven by a concentration or electrochemical gradient. Because passive diffusion requires no energy from a cell, it is possible for molecules to diffuse through the cell membrane while the cell is inactive or dormant. Cells may be incubated at 4°C where they remain viable but inactive [29].

Approximately 10,000 A549 cells (200µl of cell suspension) were seeded onto 35mm uncoated glass bottom dishes bought from MatTek Corporation, USA. Cells were allowed to attach for approx 4 hours, after which, 2mls of 10% FCS RPMI medium were added. Plates were incubated over night to ensure cells had completely attached. Cells were then removed from the incubator and placed into a fridge at 4°C overnight. After approximately 24hr, the cells were removed and the medium was replaced with fresh medium containing nanoparticles. Cells were incubated at 4°C for a further 24hr. Cells were then removed, washed with PBS then imaged in 0.9% NaCl saline solution using confocal microscopy. After images were obtained, cells were placed in fresh medium (nanoparticle free) and placed into an incubator at 37°C for 24hrs. Cells were then removed, washed with PBS then imaged in 0.9% NaCl saline solution using confocal microscopy.

The following images show the results obtained for the exposure of A549 cells to 40nm Invitrogen carboxylated nanoparticles and 50nm Duke neutral nanoparticles at 4°C.

Figure 6.27 and 6.28 display the results obtained for the exposure of A549 cells to 40nm carboxylated nanoparticles after 24hr at 4°C. As can be seen from the images, nanoparticles have not internalised within cells. Fluorescence from the particles can be seen to be accumulated on the cell membrane and not inside the cell.

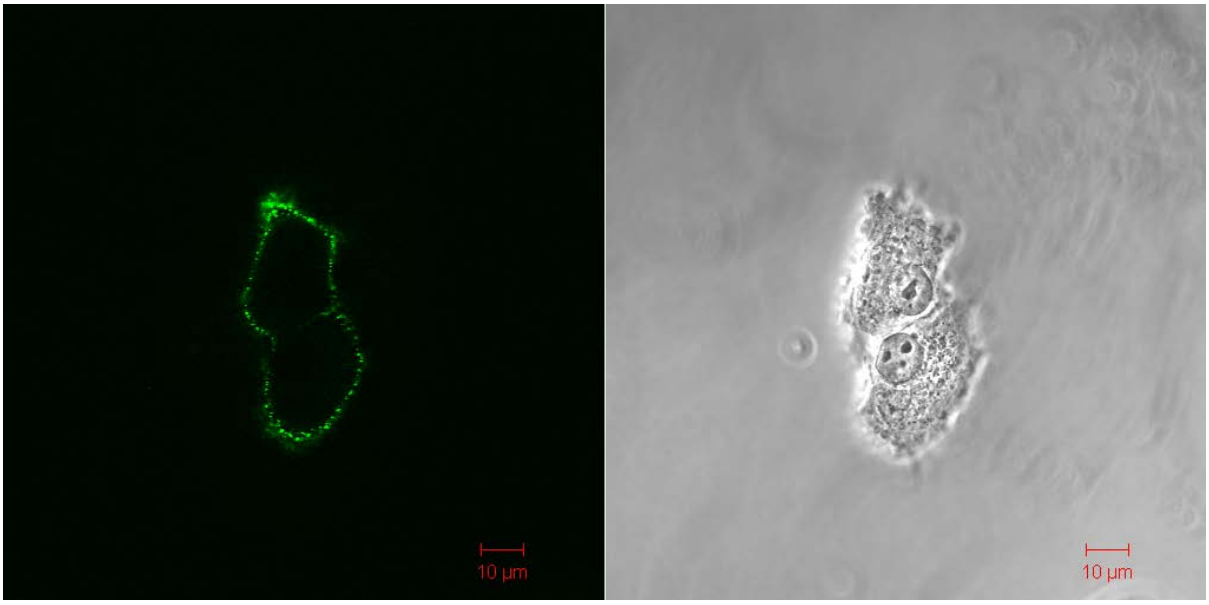

Figure 6.27 Confocal Images of A549 cells after 24hr exposure to 40nm at 4°C x60 mag

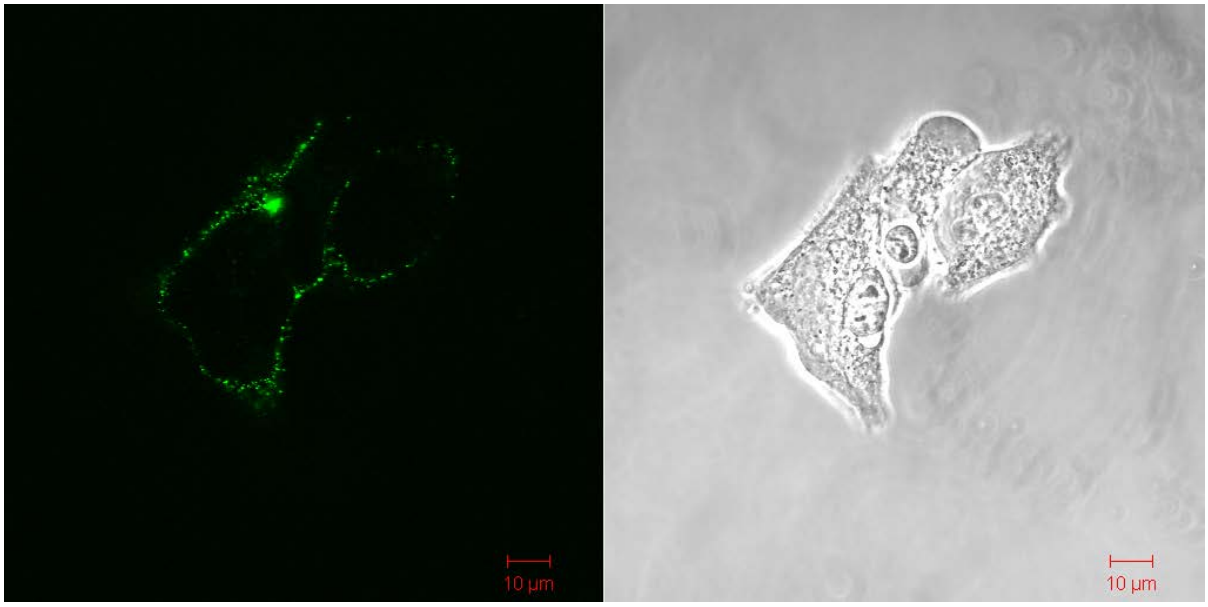

Figure 6.28 Confocal Images of A549 cell after 24hr exposure to 40nm at 4°C x60 mag

The results obtained for the exposure of A549 cells to 50nm neutral nanoparticles after 24hr at 4°C can be seen in figures 6.29 and 6.30. The images reveal that fluorescence can be seen distributed throughout the cell. The degree of fluorescence indicates that passive diffusion of free or liable dye from fluorescently labelled nanoparticles has occurred [8].

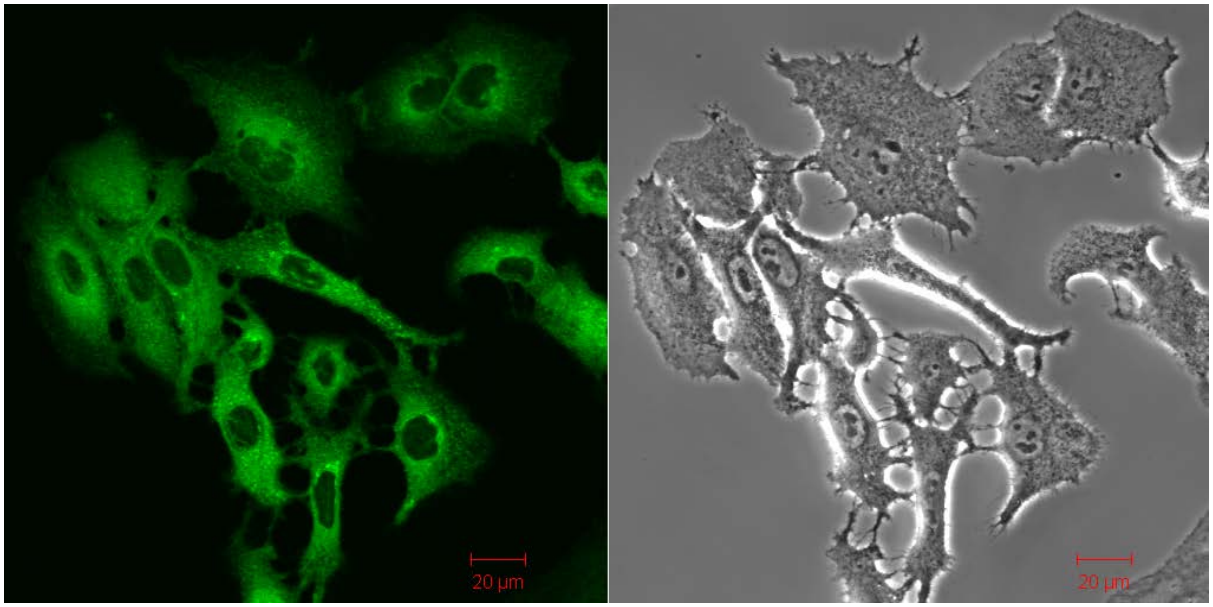

Figure 6.29 Confocal Images of A549 cells after 24hr exposure to 50nm at 4°C x60 mag

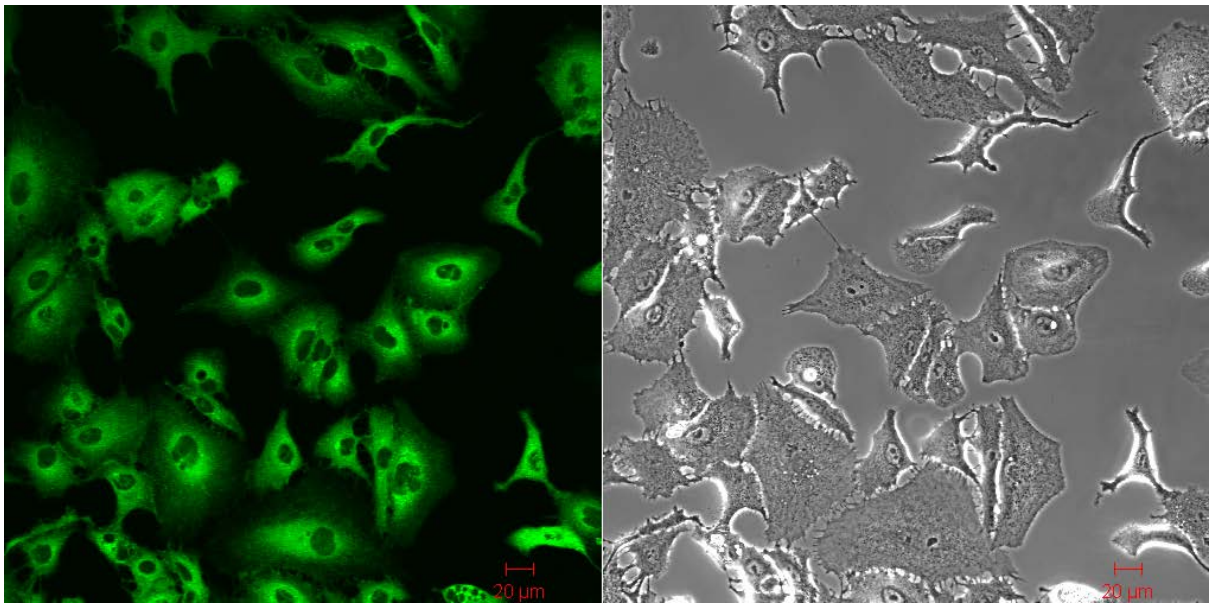

Figure 6.30 Confocal Images of A549 cells after 24hr exposure to 50nm at 4°C x60 mag

Figure 6.32 shows the Z-stack gallery of images of 50nm neutral nanoparticle fluorescent dye diffused into an A549 cells after 24hr exposure at 4°C. The Z-stack series provides confirmation that 50nm nanoparticle fluorescent dye has the capability to passively diffuse through the cell membrane.

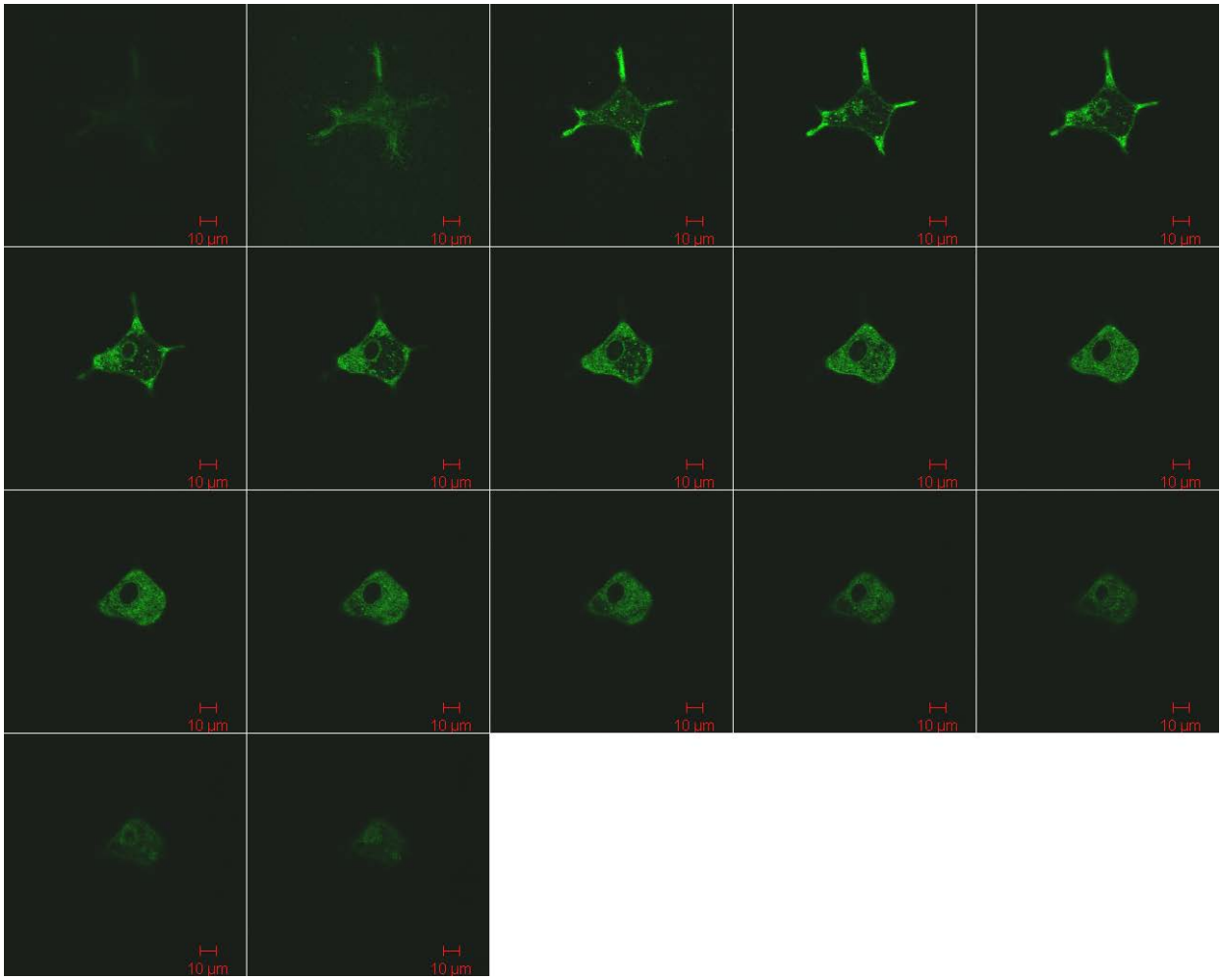

Figure 6.32 Z-stack of an A549 cell after 24hr exposure to 50nm at 4°C x60 mag

The fluorescent dye, fluorescien, used by the manufactures to fluorescently label nanoparticles has a molecular weight of 332.31 g mol^{-1} and is widely used as a biological fluorescent label. Work by Salvait at al (2012) [8] suggests that molecular dyes, such as the one used to fluorescently label nanoparticles examined, disperse throughout the cell and cellular compartments, as it is barely energy dependant. The authors also found that, when exposed to nanoparticles that were known to contain free dye, the fluorescent images of the exposed cells obtained were the same as that of cells exposed to fluorescent dye only.

The results obtained here reveal that the 50nm and 100nm neutral Duke Scientific nanoparticles examined do contain free molecular dye that diffuses through the cell membrane and into cell organelles. They also indicate that the pathway in which the 40nm and 100nm carboxylated Invitrogen nanoparticles require energy from the cell to be internalised and therefore, passive diffusion may be ruled out. This suggests that another form of active uptake is necessary for nanoparticles to be internalised or taken up by cells, such as clathrin-mediated endocytosis. Although particles were visually confirmed to have penetrated cell membranes and have internalised within cells and cell organelles through the use of confocal microscopy, the issues raised about the concerns of fluorescent dye leakage from the particles was addressed through the fluorescent uptake study. The fluorescent uptake study revealed that the actual distribution of nanoparticles may be very different to the images obtained of fluorescently labelled nanoparticles. The labelling process by each manufacturer can differ and therefore can result in the amount of free or liable dye present within the nanoparticle solution.

While the cell organelle kits demonstrated that fluorescence from the 50nm and 100nm neutral nanoparticles appear to overlap with the fluorescence from the tranduced organelle inside the cell, there is no indication that the fluorescence is in fact solely from the particles. These results reveal the necessity for a technique that can verify the internalisation of nanoparticles within cells without relying on fluorescent dyes or labels. One proposed method is that of Raman spectroscopy. Verification of nanoparticle internalisation will be addressed in the following chapter through the use of Raman spectroscopy.

References

1. Johnston, H.J., et al., *Evaluating the uptake and intracellular fate of polystyrene nanoparticles by primary and hepatocyte cell lines in vitro.* Toxicology and Applied Pharmacology, 2010. **242**(1): p. 66-78.
2. Nel, A.E.M., Lutz Velegol, Darrell Xia, Tian Hoek, Eric M. V. Somasundaran, Ponisseril Klaessig, Fred Castranova, Vince Thompson, Mike, *Understanding biophysicochemical interactions at the nano-bio interface.* Nat Mater, 2009. **8**(7): p. 543-557.
3. Chithrani, B.D. and W.C.W. Chan, *Elucidating the Mechanism of Cellular Uptake and Removal of Protein-Coated Gold Nanoparticles of Different Sizes and Shapes.* Nano Letters, 2007. **7**(6): p. 1542-1550.
4. Bharali, D.J., et al., *Organically modified silica nanoparticles: A nonviral vector for in vivo gene delivery and expression in the brain.* Proceedings of the National Academy of Sciences of the United States of America, 2005. **102**(32): p. 11539-11544.
5. Watson, P.J., Arwyn T. Stephens, David J., *Intracellular trafficking pathways and drug delivery: fluorescence imaging of living and fixed cells.* Advanced Drug Delivery Reviews, 2005. **57**(1): p. 43-61.
6. Cang, H.X., C. Shan Montiel, Daniel Yang, Haw, *Guiding a confocal microscope by single fluorescent nanoparticles.* Opt. Lett., 2007. **32**(18): p. 2729-2731.
7. Rejman, J.O., Volker Zuhorn, Inge S Hoekstra, Dick, *Size-dependent internalization of particles via the pathways of clathrin- and caveolae-mediated endocytosis.* Biochem. J., 2004. **377**(1): p. 159-169.
8. Salvati, A.A., C. dos Santos, T. Varela, J. Pinto, P. Lynch, I. Dawson, K. A., *Experimental and theoretical comparison of intracellular import of polymeric nanoparticles and small molecules: toward models of uptake kinetics.* Nanomedicine, 2011. **7**(6): p. 818-26.
9. Nam, H.Y.K., Seok Min Chung, Hyunjin Lee, Seung-Young Kwon, Seung-Hae Jeon, Hyesung Kim, Yoonkyung Park, Jae yung Kim, Joon Her, Songwook Oh, Yu-Kyoung Kwon, Ick Chan Kim, Kwangmeyung Jeong, Seo Young. , *Cellular uptake mechanism and intracellular fate of hydrophobically modified glycol chitosan nanoparticles.* Journal of Controlled Release, 2009. **135**(3): p. 259-267.
10. Harush-Frenkel, O.D., Nir Benita, Simon Altschuler, Yoram, *Targeting of nanoparticles to the clathrin-mediated endocytic pathway.* Biochemical and Biophysical Research Communications, 2007. **353**(1): p. 26-32.
11. Rothen-Rutishauser, B., et al., *Translocation of particles and inflammatory responses after exposure to fine particles and nanoparticles in an epithelial airway model.* Particle and Fibre Toxicology, 2007. **4**(1): p. 9.
12. Tsuchido, T., I. Aoki, and M. Takano, *Interaction of the Fluorescent Dye l-N-Phenylnaphthylamine with Escherichia coli Cells during Heat Stress and Recovery from Heat Stress.* J Gen Microbiol, 1989. **135**(7): p. 1941-1947.
13. Terasaki, M. and L.A. Jaffe, *Labeling of Cell Membranes and Compartments for Live Cell Fluorescence Microscopy*, in *Methods in Cell Biology*, G.A.W. Charles A. Ettensohn and M.W. Gary, Editors. 2004, Academic Press. p. 469-489.

14. Kost, T.A.C., J. Patrick, *Recombinant baculoviruses as expression vectors for insect and mammalian cells.* Current Opinion in Biotechnology, 1999. **10**(5): p. 428-433.
15. Lackner, A.G., Kathrin Koppensteiner, Herwig Herbacek, Irene Holzmann, Klaus Spiegl-Kreinecker, Sabine Berger, Walter Grusch, Michael, *A bicistronic baculovirus vector for transient and stable protein expression in mammalian cells.* Analytical Biochemistry, 2008. **380**(1): p. 146-148.
16. Invitrogen Molecular Probes SOP, *Organelle Lights™ Intracellular Targeted Fluorescent Proteins*

**BacMam 1.0*.* 2010.

17. Xia, T.K., Michael Liong, Monty Zink, Jeffrey I. Nel, Andre E., *Cationic Polystyrene Nanosphere Toxicity Depends on Cell-Specific Endocytic and Mitochondrial Injury Pathways.* ACS Nano, 2007. **2**(1): p. 85-96.
18. Mukherjee. S, L.F., Garcia. A, Davorena. M, Byrne. H. J. , *Mechanistic studies of in vitro cytotoxicity of Poly(amidoamine) dendrimers in mammalian cells.* Toxicology and Applied Pharmacology, 2010. **Paper accepted. Awaiting Publication.** .
19. Mukherjee, S.P.L., Fiona M. Garcia, Amaya Davoren, Maria Byrne, Hugh J., *Mechanistic studies of in vitro cytotoxicity of poly(amidoamine) dendrimers in mammalian cells.* Toxicology and Applied Pharmacology, 2010. **248**(3): p. 259-268.
20. Xia, T., et al., *Comparison of the Mechanism of Toxicity of Zinc Oxide and Cerium Oxide Nanoparticles Based on Dissolution and Oxidative Stress Properties.* ACS Nano, 2008. **2**(10): p. 2121-2134.
21. Marrache, S.D., Shanta, *Engineering of blended nanoparticle platform for delivery of mitochondria-acting therapeutics.* Proceedings of the National Academy of Sciences, 2012. **109**(40): p. 16288-16293.
22. Johnston, H.J., Semmler-Behnke, Manuela Brown, David M. Kreyling, Wolfgang Tran, Lang Stone, Vicki, *Evaluating the uptake and intracellular fate of polystyrene nanoparticles by primary and hepatocyte cell lines in vitro.* Toxicology and Applied Pharmacology, 2010. **242**(1): p. 66-78.
23. Christen, V.F., K., *Silica nanoparticles and silver-doped silica nanoparticles induce endoplasmatic reticulum stress response and alter cytochrome P4501A activity.* Chemosphere, 2012. **87**(4): p. 423-34.
24. Cartiera, M.S.J., Katherine M. Rajendran, Vanathy Caplan, Michael J. Saltzman, W. Mark, *The uptake and intracellular fate of PLGA nanoparticles in epithelial cells.* Biomaterials, 2009. **30**(14): p. 2790-2798.
25. Chang, M.Y.S., A. L. Chen, Y. H. Chang, C. J. Chen, H. H. Wu, C. L., *Increased apoptotic potential and dose-enhancing effect of gold nanoparticles in combination with single-dose clinical electron beams on tumor-bearing mice.* Cancer Sci, 2008. **99**(7): p. 1479-84.
26. Llorente, A.L., S. U. van Deurs, B. Sandvig, K., *Induction of direct endosome to endoplasmic reticulum transport in Chinese hamster ovary (CHO) cells (LdlF) with a temperature-sensitive defect in epsilon-coatomer protein (epsilon-COP).* J Biol Chem, 2003. **278**(37): p. 35850-5.
27. Geiger, R.L., Stefania Johnsson, Kai Greber, Urs F. Helenius, Ari, *Investigating Endocytic Pathways to the Endoplasmic Reticulum and to the Cytosol Using SNAP-Trap.* Traffic, 2013. **14**(1): p. 36-46.

28. Clift, M.J.D., et al., *The impact of different nanoparticle surface chemistry and size on uptake and toxicity in a murine macrophage cell line.* Toxicology and Applied Pharmacology, 2008. **232**(3): p. 418-427.
29. Moce-Llivina, L. and J. Jofre, *A method to maintain mammalian cells for days alive at 4 degrees C.* Cytotechnology, 2004. **46**(1): p. 57-61.

Chapter 7

Identifying and Localizing Intracellular Nanoparticles Using Raman Spectroscopy

The following chapter has been adapted from the journal article Analyst 2012 (137(5): 1111-1119).

"Identifying and Localising Intracellular Nanoparticles Using Raman Spectroscopy"

Dorney J., Bonnier F., Garcia A., Casey A., Chambers G., Byrne, H. J.

The following adaptation of the above publication addresses the issues that were raised in the previous chapter and the rationale behind the study was as a direct result of the results obtained in the previous. All work for this paper was carried out by the first named author with the exception of data processing simulations, which were run by Dr Franck Bonnier.

7.1 Introduction

One of the major concerns regarding the possible toxic effects of nanoparticles is the capacity of these materials to penetrate cells and possibly translocate to other cells around the body. Conventional *in vitro* cytotoxicity assays, such as Alamar Blue, Neutral Red, MTT, etc, provide indications of impact on cell proliferation, viability, metabolic activity, lysosomal and mitochondrial activity. However, they fail to provide a verification of nanoparticle internalisation or elucidate intracellular trafficking mechanisms and subcellular distribution within cells. Indeed, false positive results have been demonstrated due to the extracellular interaction of the nanoparticles with the cell culture medium *in vitro*, and with the cytotoxic assays themselves.[1, 2] The underlying principles of internalisation and distribution of nanoparticles within cells and any associated toxicity to humans are still relatively poorly understood. However, there are numerous studies that have demonstrated the ability of nanoparticles to cross membranes and internalise within many different cell types.[3-5]

In order to assess potential risks, but also benefits in terms of nanomedicine, a greater understanding of migration of nanoparticles intra- and inter-cellularly and essentially from one part of the body to another, along with information on the translocation of nanoparticles within organelles, is urgently required.

Among the main challenges faced by nanotoxicologists are the detection and identification of nanoparticles that have crossed the cell membrane and monitoring of their intracellular trafficking. Imaging cells exposed to fluorescently labelled nanoparticles using confocal fluorescence microscopy is one of the most common ways in which to ensure nanoparticles can be tracked and monitored as they enter and localise within cells.[6-8] However, not all nanoparticles can be easily fluorescently labelled. Furthermore, there have been reports that labelled nanoparticles can release the dye into the surrounding biological environment, and so the distribution of fluorescence within the cell does not necessarily represent the presence or subcellular distribution of the nanoparticles.[9-11] Furthermore, it is not clear that the transport mechanisms of smaller nanoparticles, fluorescently labelled with anionic moieties, are the same as their unlabelled counterparts. For example, it has been reported that extrinsic labelling of bovine serum albumin (BSA) with fluorescein-5-isothiocyanate (FITC), in a ratio of 2:1, changes its adsorption and diffusion properties.[12] Transmission Electron Microscopy can also be employed to visualise nanoparticles within cells, but significant sample processing (fixing and ultramicrotoming) is required and only particles with sufficient electronic contrast to the cellular environment can be visualised.[13, 14] Thus, there is a requirement for a sensitive technique to localise and identify nanoparticles internalised in cells, ideally based on their chemical composition, rather than fluorescence labels or electronic contrast. Identification of their local environment (e.g. endosomes, lysosomes,

mitochondria) could aid in elucidating their intracellular trafficking and interaction mechanisms, and the resulting changes in cellular metabolism.

Raman spectroscopy has been proposed as a potential technique for *in vitro* screening of the interaction of nanoparticles with cells.[15] Raman is well established for chemically fingerprinting materials, with applications in, for example, forensics and the pharmacological industry.[16-19] More recently, it has been explored for the analysis of disease and, when coupled with multivariate statistical analysis, has shown high sensitivity and specificity for diagnostic applications.[20, 21] Raman microspectroscopy also presents several advantages for the study of live cells, combining molecular analysis with optical imaging. In comparison to infrared spectroscopic analysis, the weak contribution from water offers the possibility to study the cells in an aqueous environment, maintaining viability for the duration of the measurement.[22] The specific information contained in the Raman spectrum of the cells or subcellular compartments provides a signature of the sample studied which can be related to molecular content or changes to the physiology as a result of external stimuli.[23-28] In confocal microscopic mode, the spatial resolution is of the order of ≤1 μm, depending on source wavelength, providing access to the subcellular organisation of the cells.[29, 30] Thus, Raman spectroscopy potentially offers a label free probe of nanoparticles within cells, which can potentially analyse their local environment, and ultimately changes in the cellular metabolism which can be correlated with cytotoxic responses[31], oxidative stress, or inflammation. Kneipp et al. have previously demonstrated the use of Surface Enhanced Raman Scattering from gold nanoparticles and nanoaggregates to probe the environment of the subcellular compartments through which they are trafficked.[32 33] They have also demonstrated the use of molecular labelled nanoparticles as more specific probes of the local

environment.[34-36] However, the uptake rates and mechanisms as well as the subsequent trafficking may be specific to the nanoparticle type, size and surface chemistry. Furthermore, the molecular specificity of the surface enhancement process is not well understood. Therefore, a truly label free method for monitoring and characterising the cellular uptake and subcellular localisation of nanoparticles in general is still required.

In this study, Raman spectroscopy will be evaluated for the label free detection and localisation of nanoparticles at the subcellular level. Polystyrene nanoparticles, labelled for parallel fluorescence uptake studies, are employed. Common cytotoxic assays show no observed effect over the concentration range studied. Confocal fluorescence microscopy indicates internalisation of the fluorescent label within the cells, but the spatially diffuse distribution does not allow unambiguous localisation of the nanoparticles. It is demonstrated that, based on spectroscopic fingerprint of polystyrene, Raman spectroscopy, coupled with routine multivariate analyses such as K-means clustering, is a more specific probe to detect and localise the particles. Furthermore, Principal Component Analysis can be employed to differentiate the local environment of the nanoparticles from the cytoplasm.

The importance of optimised cell culture conditions and fixation procedures is highlighted, but ultimately, this work suggests the potential of Raman spectroscopy not only to detect and identify nanoparticles within the cellular environment, but also to identify their subcellular environment and changes to the cellular metabolism which underlie toxic responses.

7.2 Materials and methods

7.2.1 Nanoparticles

"Fluorescent Microsphere Suspensions" of 50nm and 100nm polystyrene beads were purchased from Duke Scientific Corporation, (now Thermo Scientific USA http://www.thermoscientific.com). Particle size measurements and zeta potential measurements were carried out in the respective media (distilled water and cell culture medium) as described in the Supplementary Information (7S.1).

7.2.2 A549 Cell lines

A549 cells from a human lung adenocarcinoma with the alveolar type II phenotype were obtained from ATTC (Manassas, VA, USA). Cells were cultured in DMEM-F12 (Lonza, Wokingham, UK) supplemented with L-glutamine and 10% foetal calf serum (FCS, Lonza, Wokingham, UK) in a humidified atmosphere containing 5% CO_2 at 37 ^{o}C.

7.2.3 Cytotoxicity assays

A range of colorimetric cytotoxicity assays were conducted to establish the effects of exposure of the A549 cells to the nanoparticles and the details are provided in the Supplementary Information (7S.2).

7.2.4 Sample preparation for imaging

Approximately 40,000 cells were seeded onto either 35 mm uncoated glass bottom dishes (MatTek Corporation, USA) for confocal imaging or CaF_2 windows (Crystran Ltd., UK) for Raman acquisitions. The cells were incubated in 10% FCS DMEM-F12 media at 37°C for 24 hr before observation with confocal microscopy. Media was

then removed and samples were rinsed with sterile PBS and kept in 0.2 µm sterile filtered 0.9% NaCl saline solution for imaging.

Samples for confocal fluorescence imaging were obtained by seeding cells on 35mm uncoated glass bottom dishes (Mat Tek Corporation, USA) , as described above. Cells were allowed to attach for approximately 4 hrs, after which 2mls of 10% FCS RPMI media were added, containing $1x10^{12}$ nanoparticles per ml of media. Exposure times before imaging ranged from 4 hrs to 24 hrs.

For Raman analysis, A549 cells were seeded on CaF_2 windows as described above and allowed to attach for approximately 4 hrs, after which 2mls of 10% FCS RPMI media were added, containing $1x10^{12}$ nanoparticles per ml of media. Plates were left in an incubator over night for 24 hrs. Media was then removed and samples were rinsed with sterile PBS and kept in sterile 0.2 µm filtered 0.9% NaCl saline solution for imaging.

As the Raman mapping of single cells can take up to a few hours using a 785nm laser source, the cells were fixed using formalin. Thus, the stability of the sample compared to live cells is greatly improved, allowing the collection of spectra precisely from the selected area. After washing the CaF_2 windows using PBS, the samples were immersed in 10% formalin for 10 mins for fixation. After fixation, the samples were washed thrice in PBS to remove any trace of the fixative and kept in NaCl for measurement.

For comparison of cellular spectra to constituent biochemical components, five different compounds were prepared for Raman spectroscopy analysis: Raman spectra were recorded from lyophilised DeoxyriboNucleic Acid from calf thymus deposited on CaF_2 substrates. Ribonucleic acid from baker's yeast (S. cerevisiae)

was first suspended in water and deposited onto CaF_2 substrates for drying before recording. Sphingomyelin from bovine brain and L-α-Phosphatidylcholine from egg yolk were first dispersed in chloroform and then deposited onto CaF_2 substrates and left to dry before spectral acquisition. A few micro-litres of the nanoparticles suspension were deposited on a CaF_2 and air dried before recording.

7.2.5 Confocal Fluorescence imaging of cells

In order to compare the cell morphologies, samples were imaged using the white light mode of an inverted Zeiss LSM510 confocal laser scanning microscope (Carl Zeiss Inc.) equipped with an x60 oil immersion objective. For nanoparticle exposed samples, fluorescence images were captured at room temperature using an inverted Zeiss LSM510 confocal laser scanning microscope (Carl Zeiss Inc.). The excitation wavelength used was 488nm, set at 4% of laser power and the fluorescence emission was detected using a 505nm long pass filter. Images were obtained with a 60x oil immersion objective.

7.2.6 Confocal Fluorescence imaging of cell organelles

The CellLight® reagent, purchased from Invitrogen, was employed to image the subcellular components of the cells. It contains a baculovirus that, upon entry into mammalian cells, directs the expression of autofluorescent proteins that are localized to specific subcellular compartments and organelles via a signal peptide or protein fusions. The protein associated with autofluorescence is an endoplasmic reticulum (ER) signal sequence of calreticulin and KDEL (ER retention signal) fused to TagRFP (Red fluorescent protein).

A549 lung cells were seeded at a density of $1x10^5$ cells/ml, in glass bottom Petri dishes (MatTek Corporation, USA) in 10% FBS supplemented RPMI media and were

incubated at 37°C in 5% CO_2 for 4 hrs for cell attachment before exposure to nanopolystyrene particles of concentration 1 x 10^{12} particles per ml. Following the exposure period, the cells were washed twice with pre-warmed PBS (37 °C). A pre determined amount of CellLight® transduction solution was administered evenly to the Petri dishes. Cells were then incubated at 37°C in 5% CO_2 for 24 hrs. The appropriate volume of CellLight® reagent for the number of cells exposed was calculated according to the manufacture's guidelines.

Intracellular localisation of polystyrene nanoparticles was visualized at room temperature under the laser scanning confocal microscope (LSM 510 Meta, Carl Zeiss Inc.) equipped with Argon (488nm) and HeNe (543nm) lasers. Images were acquired by multitracking (505-530nm band pass filter to collect nanoparticles fluorescence and 560nm long pass filter for the cell organelle kit fluorescence) to avoid bleed through between the fluorophores, and the statistical analysis was carried out using the LSM 510 software.

7.2.7 Raman spectroscopic measurements

A Horiba Jobin-Yvon LabRAM HR800 spectrometer with an external 300 mW 785 nm diode laser as source was used throughout this work. For all measurements, a x100 immersion objective (LUMPlanF1, Olympus) was employed to reduce the spectral background.[37] The confocal hole was set at 100 µm for all measurements, the specified setting for confocal operation. The system was pre-calibrated to the 520.7 cm^{-1} spectral line of silicon. The Labram system is a confocal spectrometer that contains two interchangeable gratings (300 and 900 lines/mm respectively). In the following experiments, the 300 lines/mm grating was used, which gave a spectral dispersion of around ~1.5 cm^{-1} per pixel. The detector used was a 16-bit dynamic

range Peltier cooled CCD detector. Images of the sample were acquired using a video camera within the system.

For Raman mapping, an area corresponding to the map to be acquired was defined around the cells on the optical image provided by the instrument video camera. The step between two successive measurements was set to 1.5 µm or 0.75 µm [38] and the backscattered Raman signal was integrated for 10 seconds over the spectral ranges from 400 to 1800 cm^{-1} and accumulated twice to enable an automatic software elimination of any spurious peaks.

7.2.8 Data Analysis

The different data analysis steps were performed using Matlab (Mathworks, USA). Before statistical analysis, a Savitsky-Golay filter (5^{th} order, 7 points) was applied to smooth the spectra and the reference spectrum constituting the background signal was subtracted.

K-means clustering analysis was utilised for initial analysis of the spectral maps. It is one of the simplest unsupervised learning algorithms used for spectral image analysis. It groups the spectra according to their similarity, forming clusters, each one representing regions of the image with identical molecular properties.[39] The distribution of chemical similarity can then be visualised across the sample image. The number of clusters (k) has to be determined *a priori* by the operator before initiation of the classification of the data set. K centroids are defined, ideally as far as possible from each other, and then each point belonging to a data set is associated to the nearest centroid. When all the points have been associated with a centroid, the initial grouping is done. The second step consists of the calculation of new centroids as barycentres of the clusters resulting from the previous step. A new

grouping is implemented based on the same data points and the new centroids. These operations are repeated until convergence is reached and there is no further movement of the centroids. Finally, k clusters are determined, each containing the most similar spectra from the image. From here, colours can be attributed to each cluster and false colours maps can be constructed to visualise the organisation of the clusters in the original image.

As K-means cluster analysis groups and represents similar spectra by their mean, Principal Component Analysis (PCA) was employed to further analyse the grouped spectra. PCA is a method of multivariate analysis broadly used with datasets of multiple dimensions[40]. It allows the reduction of the number of variables in a multidimensional dataset, although it retains most of the variation within the dataset. The order of the PCs denotes their importance to the dataset. PC_1 describes the highest amount of variation, PC_2 the second greatest and so on. Therefore, var (PC_1) ≥ var (PC_2) ≥ var (PC_p), where var (PC_i) represents the variance of PC_i in the considered data set. Generally, the 3 first components represent more than 90% of the variance. This statistical method was preferred for this study to highlight the variability existing in the spectral data set recording during the different experiments. The other advantage of this method is the derivation of loadings which represent the variance for each variable (wavenumber) for a given PC. Analysis of the loadings of a PC can give information about the source of the variability inside a data set, derived from variations in the chemical components contributing to the spectra.

7.3 Results and Discussion

7.3.1 Particle Characterisation

Full details of the results of the physico-chemical characterisation of the nanoparticle samples are provided in the Supplementary Information (7S.1). In summary, the sizes of the nominally 50nm and 100nm nanoparticle samples were found to be somewhat dependent on the suspension medium and temperature, and the zeta potentials similarly varied, potentially consistent with interactions of the nanoparticle surface with the molecular components of the cell culture medium.[2] Despite the variation in the exact nanoparticle sizes, for the purpose of brevity, the nanoparticles will be referred to as 50nm and 100nm particles throughout the manuscript.

7.3.2 Cytotoxicity of Nanoparticles.

For all assays employed, at all time points, no significant cytotoxicity was observed over the concentration range employed for both 50nm and 100nm polystyrene nanoparticles (see Supplementary Information 7S.2). The observations are consistent with previous reports of exposure to neutral nanoparticles [41] and indicate that the labelling of the nanoparticles with the fluorescent moiety does not impact significantly on the toxic response.

7.3.3 Confocal Fluorescence Microscopy

Figure 7.1 shows a confocal fluorescence and white light microscopic image of A549 cells after exposure to 50nm neutral nanopolystyrene particles for a time of 24 hrs at a dose of $1x10^{12}$ particles per ml of media. The images are typical of a range of doses and time points for both nanoparticle sizes. The fluorescence is observed to be spatially diffuse throughout the subcellular environment, and no specific subcellular localization of nanoparticles is inferred.

The observations are not consistent with the increasingly accepted mechanisms of particle uptake by endocytosis and trafficking of nanoparticles through endosomes to lysosomes.[14, 42] Such a diffuse distribution of fluorescence in cells exposed to labelled nanoparticles has recently been reported, however, and the phenomenon has been attributed to the uptake of labile fluorescent moieties, which become detached from the nanoparticles in the culture medium and are internalized in the cellular environment by passive molecular diffusion. Thus, the spatial distribution of the fluorescence profile does not reflect the subcellular[9] distribution of the nanoparticles in the cells. The work of Salvati et al.[9] highlights the importance of a complete screening of the nanoparticles employed for such studies in order to confirm the stability of the labelled nanoparticle and thus the validity of such fluorescent imaging procedures. For the purpose of this work, however, the observations of figure 7.1 highlight the importance of an independent technique to verify and profile the spatial distribution of nanoparticles in cells. Fluorescence microscopy identifies the distribution of the label, but notably is not chemically specific, and so is ineffective in independently and unambiguously locating the distribution of polystyrene.

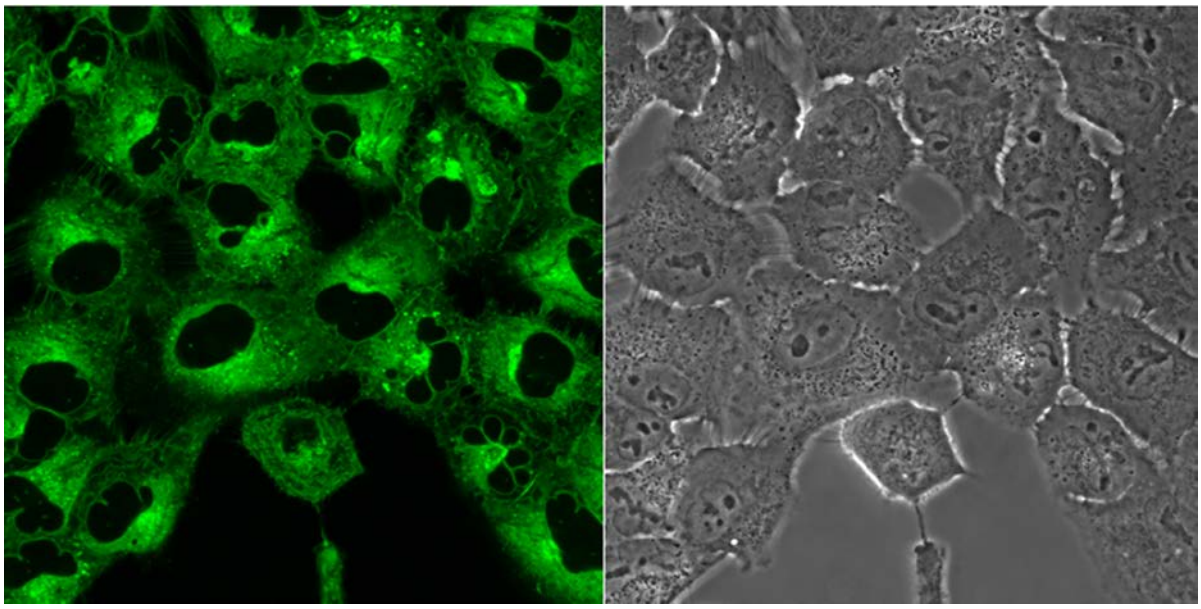

Figure 7.1 A549 cells exposed to 50 nm polystyrene nanoparticles x20 magnification after 24 hour exposure.

7.3.4 Raman Spectroscopy

The literature contains many examples of works based on cell analysis using Raman spectroscopy[43-46]. In general, however, many problems arise due to substrate contributions, spectral background and poor signal to noise. Sampling in a confocal mode can minimize contributes due to substrates, and the use of substrates, such as CaF_2, which have minimal contribution to the Raman spectra in the region of interest, improves matters further. In tissue samples, it has been demonstrated that working in immersion significantly reduces the spectral background[37], and for the case of cell cultures on collagen gels, measured in immersion, the background has been shown to be reduced to that of the surrounding water [47].

Although progress has been made in the measurement techniques, little attention has been paid to the quality of the cellular samples. The aim of this work is to detect and localize nanoparticles within the cytoplasm of the cells without the use of a

specific label. In order to achieve this goal, it is crucial to first optimise the sample preparation techniques to reduce as much as possible variations related to the cell handling. A full description of the optimization of the cell culturing and fixation process is provided in the Supplementary Information (7S.3).

As the fixation process was shown to have negligible effect on the Raman spectra, A549 cells exposed to 100nm polystyrene nanoparticles at a concentration of $1x10^{12}$ nanoparticles per ml of media for a period of 24 hrs were formalin fixed in CaF_2 substrates and were mapped for their Raman spectral profile.

The two main factors influencing the time needed to map a full cell are the step size and the acquisition time. Using a 785nm laser as source, a 10 s acquisition gives a signal to noise ratio more than acceptable for the identification of the different spectral features present.[22, 38] However, two accumulations are required by the software to remove any spurious spikes in the spectra recorded, and thus the total acquisition time per spectrum was 20 s. A mild smoothing was applied to further improve the spectral quality, as described in Section 7.2.8. The instrument software allows the selection of customised areas for mapping, as presented in figure 7.2A, considerably reducing the measurement time, and a step size of 1.5 μm has been used in order not to exceed ~4 hrs per cell, a timescale which is most feasible for maintaining sample integrity and stable conditions for spectral mapping. After completion of the spectral recording, the map was exported to Matlab for analysis using K-means clustering. For cells exposed to nanopolystyrene, it is expected that the K-means clustering will be able to localise the nanoparticles within the cellular environment.

Using a 100x objective, the visible image obtained from the cells is rather detailed (Figure 7.2A). The nucleus is clearly identifiable and the nucleoli can also be seen. The membrane of the cells is well defined and the cytoplasm presents different structures and the region containing the endoplasmic reticulum can be easily recognised. Figure 7.2B presents the results obtained using 10 different groups for the K-means cluster analysis. Increasing the number of groups to 10 allows consideration of the variability existing in the spectra recorded from the edge of the cells which have a lower intensity and therefore a weaker signal to noise ratio. A cluster has been formed corresponding to the nuclear area (cluster 1) but the analysis does not discriminate between the nucleus and nucleoli. Similarly, distinct clusters are assigned to the cytoplasm and membrane.

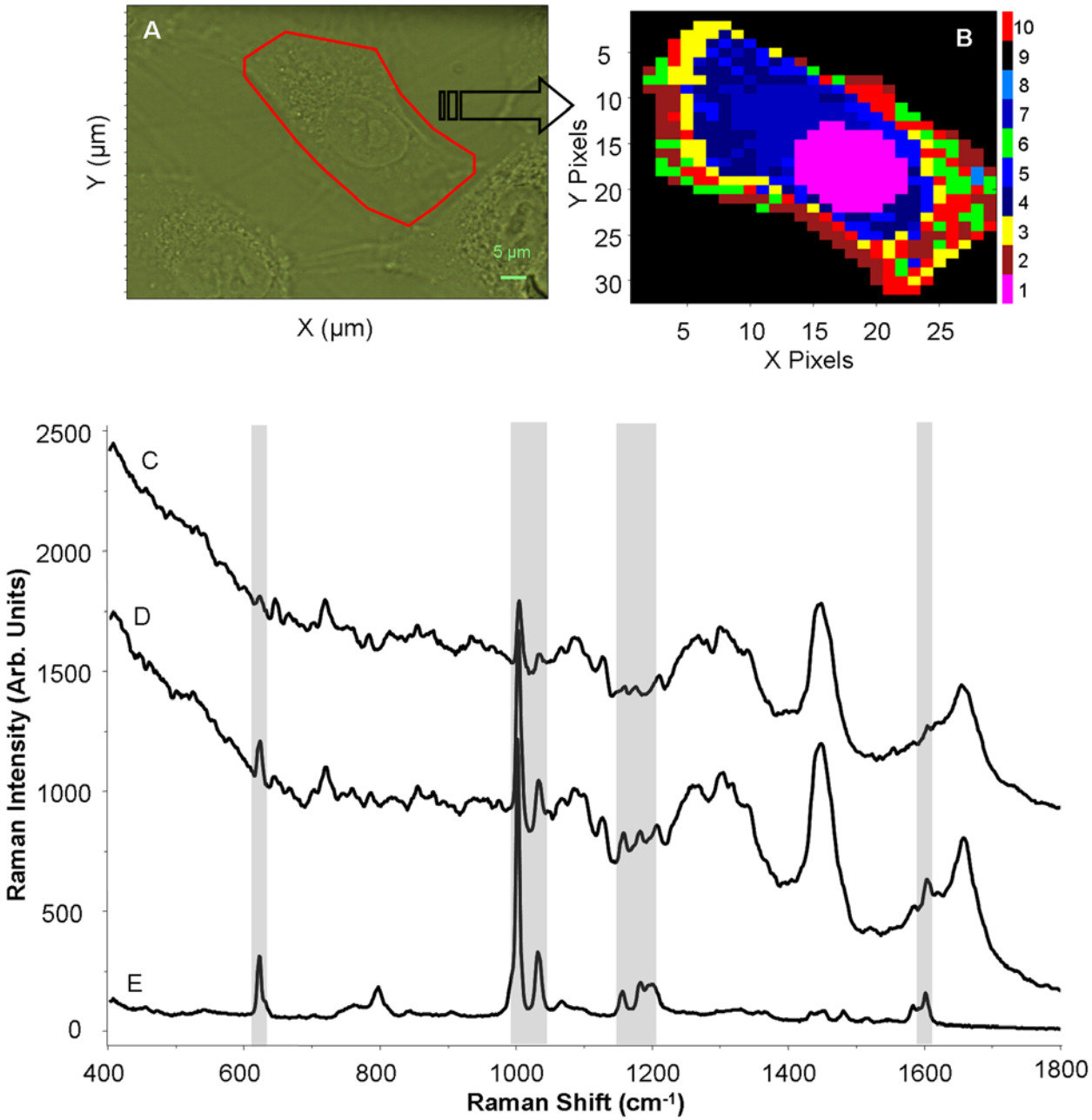

Figure 7.2 Top; (A) Microscopic image of an A549 cell, showing the area identified for spectral mapping. (B) K-means cluster map of the Raman profile of the same cell. **Bottom**; Raman spectra of (C) cytoplasm, (D) cytoplasm showing the contribution of spectral features of (E) polystyrene nanoparticles. Grey shading is a guide to identification of characteristic Raman features of polystyrene. Spectra are offset for clarity

Notably however, none of the 10 clusters identified by the analysis exhibit clear signatures which can be associated with polystyrene (figure 7.2 bottom). It is

expected that the nanoparticles will be predominantly localised within the cytoplasmic region, but there is no evidence of specific polystyrene peaks in the spectrum of the cytoplasm (Figure 7.2C). Although it overlaps with the strong and sharp phenyl group of aromatic amino acids in cells, the best indicator of the presence of nanopolystyrene in the spectra recorded remains the intensity of the strong 1004 cm^{-1} peak. Based on this observation, it has been possible to manually screen the map and identify the presence of these features in individual Raman spectra (figure 7.2D). The manually identified polystyrene spectra are, however, sparsely located throughout the cell, a strong indication that the fluorescence map of figure 7.1 is not representative of the distribution of polystyrene nanoparticles within the cell. Although Raman spectroscopy can detect the presence of nanoparticles in the cells, the K-means clustering analysis does not group their signature as a spatially defined cluster.

The use of a 100x objective provides maximum lateral resolution and helps to obtain visible images which detail the cell morphology. However, the focal depth is minimised and, in an automated map, it is difficult to optimise acquisition conditions over the spatial extent of the cell. The visible image in figure 7.2A highlights this phenomenon, as, although the focus is optimised for the nucleus, the edge of the cell remains blurry. This difference is enough to create a loss in the Raman intensity when recording spectra on the outer parts of the cells, reducing considerably the signal to noise ratio. For this reason, the area selected for spectral mapping was reduced, as indicated in figure 7.3 IA. Moreover, scanning a smaller area allows a decrease of the lateral step size to 0.75 µm without increasing the overall acquisition time. Thus, the definition of the map recorded is improved and a more precise localisation of the nanopolystyrene can be achieved.

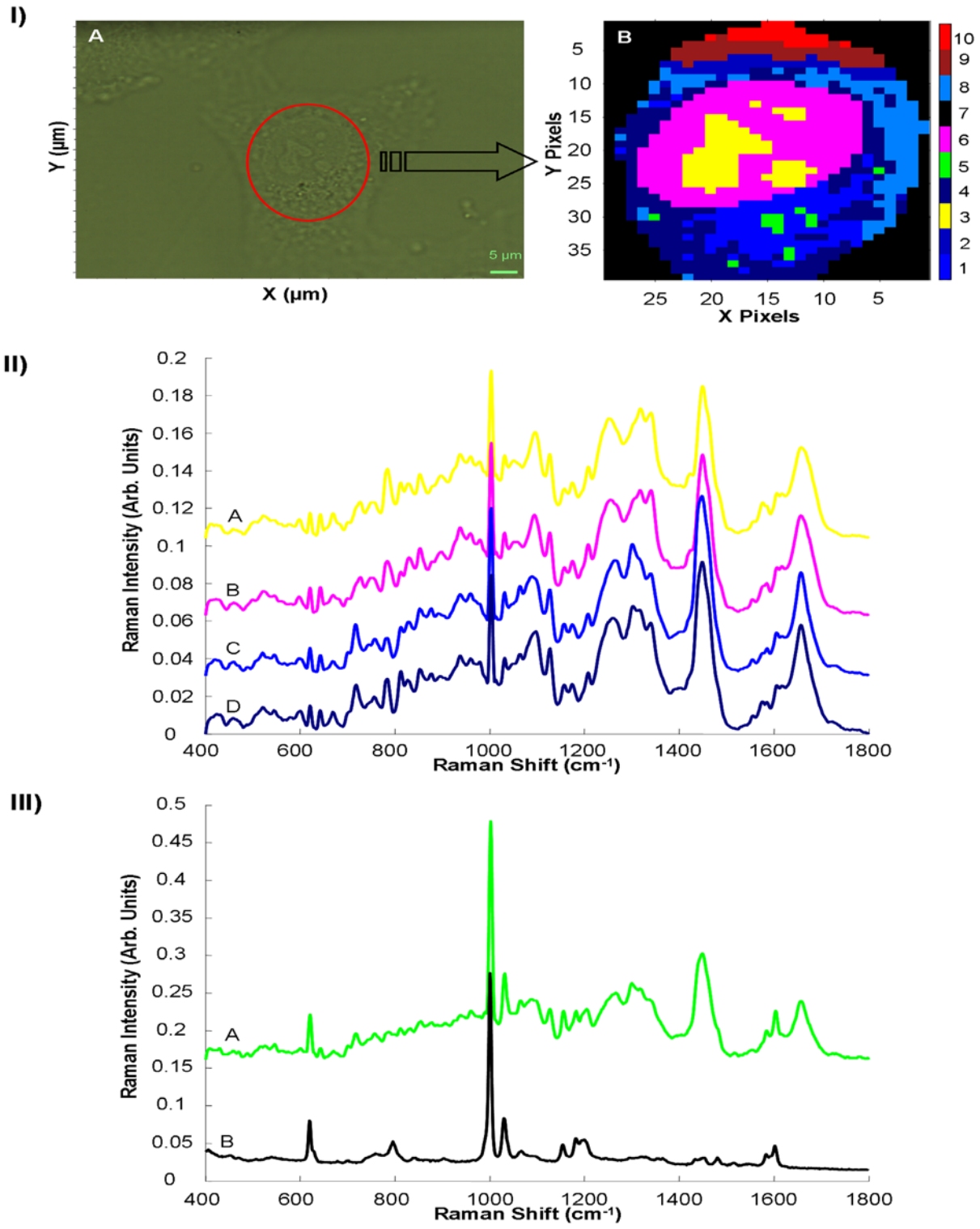

Figure 7.3: I; (A) Microscopic image of an A549 cell, showing the reduced area identified for spectral mapping. (B) K-means cluster map of the Raman profile of the same reduced area. **II**; K-means spectra of clusters 3 (A – representing nucleoli), 6 (B – representing nucleus), 1 and 4 (C and D, both from the cytoplasm). Spectra are offset for clarity. **III**; K-means spectrum of Cluster 5 (A), compared to the Raman spectrum polystyrene nanoparticles (B). Spectra are offset for clarity

Under these conditions, the K-means clustering analysis run using 10 groups yields more specific clusters, as shown in figure 7.3 IB. The nucleoli spectra form a specific group (cluster 3), distinct from the nucleus (cluster 6). The corresponding mean spectra are displayed in figure 7.3 II. The cytoplasm is represented by a number of different clusters (1, 2, 4, 8, 9, 10). Notably, nanopolysterene can now be localised in the cytoplasm according to cluster 5, the corresponding mean spectrum of which is presented in figure 7.3 IIIA. Although some cellular features clearly contribute to the cluster spectrum, it is dominated by specific features originating from polystyrene. Notably, in comparison to figure 7.1, figure 7.3 IB gives a map of the distribution of the fingerprint of the molecular structure of polystyrene, rather than the fluorescent label.

K-means cluster analysis yields the average spectra for the identified clusters. These average spectra can contain contributions from points on the boundaries between the cellular regions and a direct comparison does not always easily facilitate identification of the differences in the biochemical composition. Cluster 5 clearly identifies the presence of polystyrene nanoparticles localised in the cytoplasm, but the averaged spectrum also exhibits clear contributions of the biological environment. PCA can be employed to highlight the biochemical differences between the subcellular regions.[48] In figure 7.3 IB, cluster 5 is predominantly surrounded by cytoplasmic regions grouped within cluster 1.

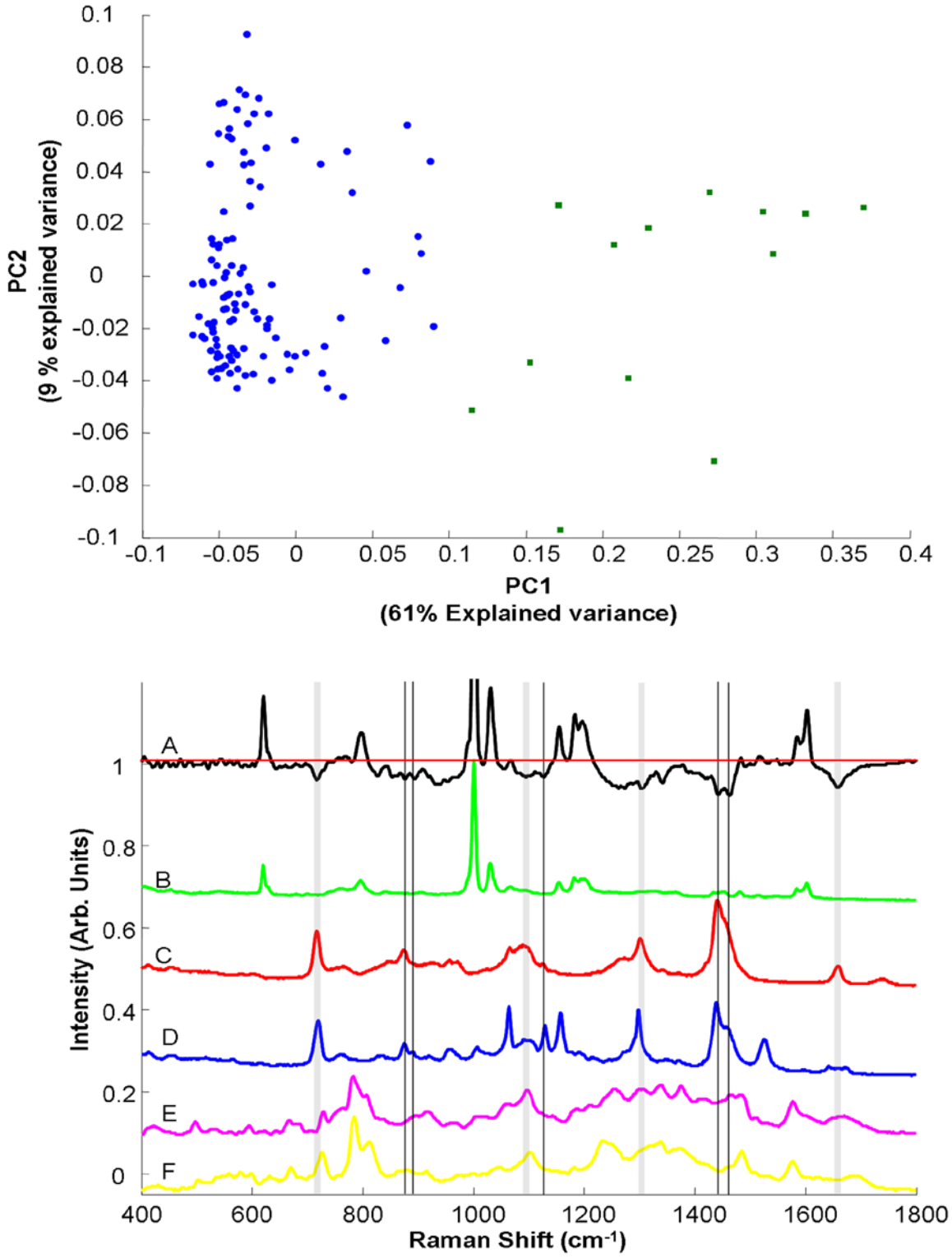

Figure 7.4 Top; Scatter plot of the PCA of spectra associated with clusters 1 (Blue) and 5 (Green). **Bottom**; (A) Loading of PC1 (B) Raman Spectrum of polystyrene nanoparticles (C) of L-□-Phosphatidylcholine, (D) of Sphingomyelin, (E) of DNA and (F) of RNA.

Figure 7.4 (top) is a scatter plot of the PCA of spectra associated with K-means clusters 1 and 5. For visualisation purposes, spectra associated with cluster 1 are coloured blue, while those from cluster 5 are coloured green, and although the data is rather dispersed, some differentiation between the two clusters according to PC1 is apparent. PC1 accounts for 61% of the variance and, as shown in the loadings plot of figure 7.4 (bottom), it is dominated by positive contributions of polystyrene (figure 7.4 B). Notably, the negative contributions of PC1 match well with the Raman features of lipids such as L-α-Phosphatidylcholine (figure 7.4 C) and also sphingomyelin (figure 7.4 D). For comparison, the Raman spectra of DNA (figure 4 E) and RNA (figure 7.4 F) are also shown, and it is clear that they exhibit few or no similarities with PC1. High loadings of PC1 for cluster 5 are therefore an indication of the dominance of polystyrene. Positive loadings of PC1 for some of Cluster 1 may indicate regions of overlap between the localised nanoparticles and the surrounding cytoplasm, which, although they have significant polystyrene contributions, are represented in the K-means cluster analysis by the average spectrum of cluster 1.

An established mechanism for the transport of nanoparticles in cells is via endosomes and later lysosomes.[42] A number of studies have also demonstrated that, in the later stages of trafficking, individually endocytosed nanoparticles accumulate in larger multivescular bodies [33] and they have also been seen to be localized in the endoplasmic reticulum and Gogli apparatus.[49] Notably, in figure 7.3 IA, the majority of the nanoparticles, identified in green as cluster 5, are surrounded by cytoplasmic regions of cluster 1, which is relatively spatially extensive, particularly compared to typical sizes of lysosomes (1-2μm). In the white light image of figure 7.3 IB, this region can be identified as the ER, which may be expected to be rich in lipidic compounds, and a PCA of the different regions of the cytoplasm, as shown in the

scatter plot of figure 7.5 (top) and the corresponding loadings of figure 7.5 (bottom), confirms this. Cluster 4, on the other hand is relatively rich in nucleic acids, which may be due to the presence of mitochondria.

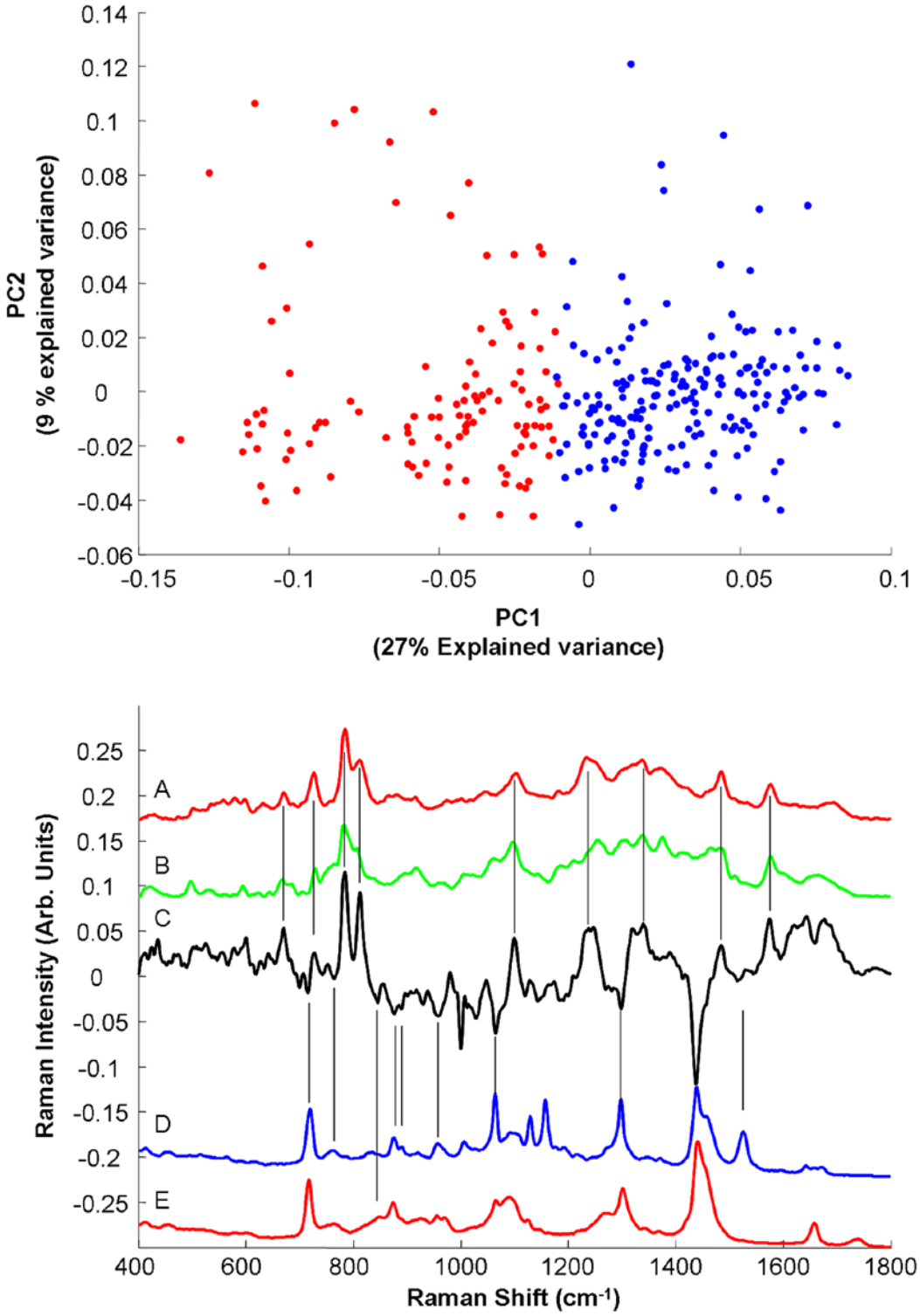

Figure 7.5 Top; Scatter plot of the PCA of spectra associated with clusters 1 (red) and 4 (blue). **Bottom**; (A) Raman Spectrum of RNA (B) Raman Spectrum of DNA (C) Loading of PC1, (D) Raman spectrum of Sphingomyelin, (E) Raman spectrum of L-□-Phosphatidylcholine.

Figure 7.6 shows an image of A549 cells exposed for 24 hrs to 50 nm fluorescently labelled polystyrene nanoparticles, also stained for ER, as described in section 7.2.6. Although, as outlined in relation to Figure 7.1, the fluorescence distribution is diffuse and therefore not exclusively attributable to the presence of nanoparticles within the cell, the confocal image indicates a strong correlation between the ER stain and the fluorescence of the nanoparticle label, and any locally concentrated fluorescence which may be indicative of encapsulated nanoparticles is contained within the ER, clearly visible in the white light image of figure 7.6B. The analysis supports the attribution of the subcellular environment of K-means cluster 1 as endoplasmic reticulum.

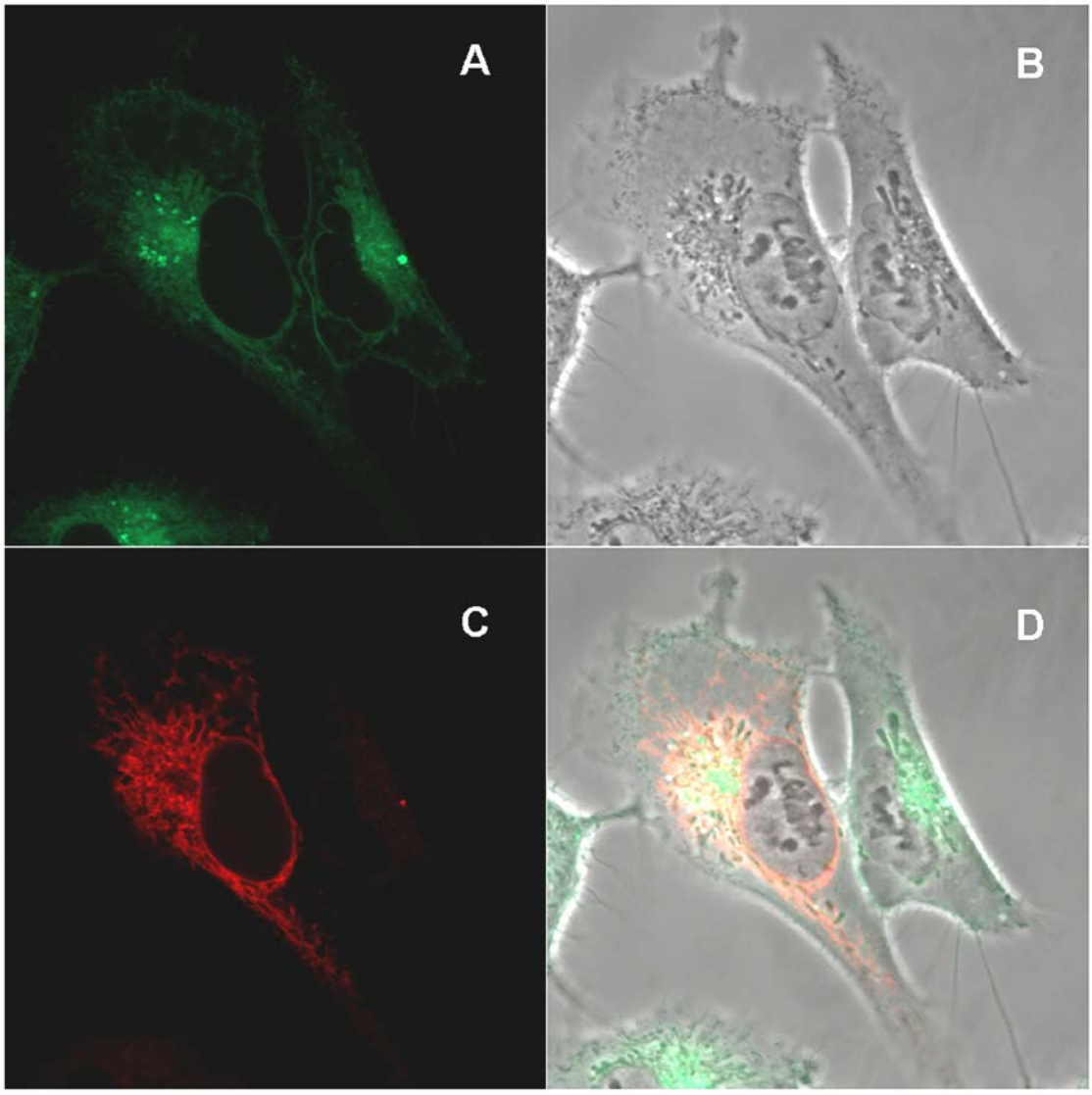

Figure 7.6 Confocal microscopic images obtained of 50 nm polystyrene nanoparticles within A549 cells that have also been treated with CellLight® Endoplasmic Reticulum staining kit. **(A)** Confocal image showing the fluorescence of the particles only, using the 505-530 nm band pass filter. **(B)** Optical image of the cell showing no fluorescence. **(C)** Confocal image of the fluorescent endoplasmic reticulum of the cell following transduction with the CellLight® kit using the 560 nm long pass filter and **(D)** Image of fluorescence overlap of both the 50 nm particles and the fluorescently transduced ER. The fluorescence overlap is shown in a yellow-orange colour.

7.4 Discussion

The work presented here represents an initial proof of concept, to demonstrate the potential use of Raman spectroscopy to identify and locate nanoparticles in cells and to probe their subcellular environment. No attempt has, as yet, been made to quantify the amount of nanoparticles located or the sensitivity and detection limit of the technique. Instrumentally, the spatial resolution can be improved by moving to lower wavelength sources, although the excitation of any fluorescence from the nanoparticles and the cell constituents should be avoided. However, as it scales linearly with wavelength, a move from 785nm to 473nm should result in an improvement in lateral resolution by a factor of ~1.7. Ultimately, the confocal mode of operation can provide 3D localisation of the nanoparticles at submicron resolution.

Fixed cells were employed in this work to facilitate prolonged mapping. However, the technique can be applied to live cells[38], and the identification of a characteristic spectral marker for the nanoparticles or a cell metabolite could ultimately facilitate real time monitoring. The subcellular environment of the cell is complex, and differentiation of the subcellular environments based on characteristic Raman spectra is best facilitated using multivariate statistics, two examples of which are illustrated here. A range of other data mining techniques are available, however, which could improve the molecular sensitivity of the technique.

It is notable that the initial attempts to locate the nanoparticles within the cell, using a 1.5 μm step size over the whole cell area proved inconclusive. The mapping conditions also failed to identify the nucleoli within the nucleus, however. In the automated mapping protocol, no adjustment of the focussing conditions was performed, and, using the x100 objective in a confocal geometry, the focussing

conditions, optimised in the region of the nucleus, are less well optimised over the extent of the whole cell. Therefore, the variability of spectra from the outer part of the cell is significantly higher than the variability which should differentiate the spectra containing polysterene from those containing only cellular features. An increase of the number of clusters resulted only in the creation of more clusters in the membrane region of the cells. Restricting the mapping to the centre part of the cells provides a more consistent signal without adjustment of the focus. In this case, both K-means clustering and PCA differentiate regions with clear contributions of polystyrene to the spectra. Improved automated mapping protocols which include auto-focusing could improve the routine application of the technique.

Polystyrene nanoparticles are emerging as potential standards for nanotoxicity, notably in their aminated form. The aromatic styrene unit is a relatively strong Raman scatterer, and thus they are particularly suitable for Raman mapping. The example of fluorescently labelled nanoparticles which potentially lose the label, with the result that fluorescence microscopy does not unambiguously identify the nanoparticles within the cells, highlights the potential of the technique as a label free probe applicable to a broad range of nanoparticles. To demonstrate the universality of the technique, the study will be extended in the future to a broader range of both organic and inorganic nanoparticles.

7.5 Conclusion

This study demonstrates the ability of Raman microspectroscopy to localise nanoparticles in the subcellular environment, based on their chemical structure. The measurements also indicate that the technique can be employed to identify the subcellular environment. Raman has previously been employed to monitor changes in the metabolism of cells, particularly due to external agents, and thus this label free, non invasive tool can potentially simultaneously, locate and identify nanoparticles, probe their local environment and ultimately changes to the metabolism of the cell due to cell-nanoparticle interactions.

7.6 Acknowledgements

This research was supported by the Integrated NanoScience Platform, Ireland, and the National Biophotonics and Imaging Platform (NBIP) Ireland, both funded under the Higher Education Authority PRTLI (Programme for Research in Third Level Institutions) Cycle 4, co-funded by the Irish Government and the European Union Structural fund.

7.7 References

1. Berntsen P, Park CY, Rothen-Rutishauser B, Tsuda A, Sager TM, Molina RM, Donaghey TC, Alencar AM, Kasahara DI, Ericsson T, Millet EJ, Swenson J, Tschumperlin DJ, Butler JP, Brain JD, Fredberg JJ, Gehr P, Zhou EH, Journal of The Royal Society Interface, 2010, **7**, S331-S340.
2. Lundqvist M, Stigler J, Elia G, Lynch I, Cedervall T, Dawson KA, Proceedings of the National Academy of Sciences, 2008, **105**, 14265-14270.
3. Clift MJD, Rothen-Rutishauser B, Brown DM, Duffin R, Donaldson K, Proudfoot L, Guy K, Stone V, Toxicology and Applied Pharmacology, 2008, **232**, 418-427.
4. Rejman J, Oberle V, Zuhorn IS, Hoekstra D, Biochem. J., 2004, **377**, 159-169.
5. Rothen-Rutishauser B, Muhlfeld C, Blank F, Musso C, Gehr P, Particle and Fibre Toxicology, 2007, **4**, 9.
6. Naha PC, Bhattacharya K, Tenuta T, Dawson KA, Lynch I, Gracia A, Lyng FM, Byrne HJ, Toxicology Letters, 2010, **198**, 134-143.
7. Roy I, Ohulchanskyy TY, Bharali DJ, Pudavar HE, Mistretta RA, Kaur N, Prasad PN, Proceedings of the National Academy of Sciences of the United States of America, 2005, **102**, 279-284.
8. Cang H, Xu CS, Montiel D, Yang H, Opt. Lett., 2007, **32**, 2729-2731.
9. Salvati A, Aberg C, Dos Santos T, Varela J, Pinto P, Lynch I, Dawson KA, Nanomedicine, 2011, **7**, 818-826.
10. Suh H, Jeong B, Liu F, Kim SW, Pharmaceutical Research, 1998, **15**, 1495-1498.
11. Yin Win K, Feng S-S, Biomaterials, 2005, **26**, 2713-2722.
12. Gajraj A, Ofoli RY, Langmuir, 2000, **16**, 8085-8094.
13. Davoren M, Herzog E, Casey A, Cottineau B, Chambers G, Byrne HJ, Lyng FM, Toxicology in Vitro, 2007, **21**, 438-448.
14. Shapero K, Fenaroli F, Lynch I, Cottell DC, Salvati A, Dawson KA, Molecular BioSystems, 2011, **7**, 371-378.
15. Bouwmeester H, Lynch I, Marvin HJ, Dawson KA, Berges M, Braguer D, Byrne HJ, Casey A, Chambers G, Clift MJ, Elia G, Fernandes TF, Fjellsbo LB, Hatto P, Juillerat L, Klein C, Kreyling WG, Nickel C, Riediker M, Stone V, Nanotoxicology, 2011, **5**, 1-11.
16. Hodges CM, Akhavan J, Spectrochimica Acta Part A: Molecular Spectroscopy, 1990, **46**, 303-307.
17. Kneipp K, Kneipp H, Itzkan I, Dasari RR, Feld MS, Chemical Reviews, 1999, **99**, 2957-2976.
18. Vankeirsbilck T, Vercauteren A, Baeyens W, Van der Weken G, Verpoort F, Vergote G, Remon JP, TrAC Trends in Analytical Chemistry, 2002, **21**, 869-877.
19. Wilson AS, Edwards HGM, Farwell DW, Janaway RC, Journal of Raman Spectroscopy, 1999, **30**, 367-373.

20. Lyng FM, Faoláin EÓ, Conroy J, Meade AD, Knief P, Duffy B, Hunter MB, Byrne JM, Kelehan P, Byrne HJ, Experimental and Molecular Pathology, 2007, **82**, 121-129.
21. Byrne HJ, Sockalingum GD, Stone N.in Biomedical Applications of Synchrotron Infrared Microspectroscopy: A Practical Approach, David M, RSC Analytical Spectroscopy Monographs 2011,11, 105-143
22. Draux F, Jeannesson P, Beljebbar A, Tfayli A, Fourre N, Manfait M, Sule-Suso J, Sockalingum GD, Analyst, 2009, **134**, 542-548.
23. Mariani MM, Day PJ, Deckert V, Integr Biol (Camb), 2010, **2**, 94-101.
24. Matthaus C, Chernenko T, Newmark JA, Warner CM, Diem M, Biophys J, 2007, **93**, 668-673.
25. Meister K, Schmidt DA, Brundermann E, Havenith M, Analyst, 2010, **135**, 1370-1374.
26. Notingher I, Hench LL, Expert Rev Med Devices, 2006, **3**, 215-234.
27. Notingher I, Verrier S, Haque S, Polak JM, Hench LL, Biopolymers, 2003, **72**, 230-240.
28. Yu C, Gestl E, Eckert K, Allara D, Irudayaraj J, Cancer Detect Prev, 2006, **30**, 515-522.
29. Puppels GJ, de Mul FF, Otto C, Greve J, Robert-Nicoud M, Arndt-Jovin DJ, Jovin TM, Nature, 1990, **347**, 301-303.
30. Puppels GJ, Garritsen HS, Segers-Nolten GM, de Mul FF, Greve J, Biophys J, 1991, **60**, 1046-1056.
31. Knief P, Clarke C, Herzog E, Davoren M, Lyng FM, Meade AD, Byrne HJ, Analyst, 2009, **134**, 1182-1191.
32. Kneipp K, Haka AS, Kneipp H, Badizadegan K, Yoshizawa N, Boone C, Shafer-Peltier KE, Motz JT, Dasari RR, Feld MS, Appl. Spectrosc., 2002, **56**, 150-154.
33. Kneipp J, Kneipp H, McLaughlin M, Brown D, Kneipp K, Nano Letters, 2006, **6**, 2225-2231.
34. Kneipp J, Kneipp H, Rajadurai A, Redmond RW, Kneipp K, Journal of Raman Spectroscopy, 2009, **40**, 1-5.
35. Kneipp J, Kneipp H, Rice WL, Kneipp K, Analytical Chemistry, 2005, **77**, 2381-2385.
36. Kneipp J, Kneipp H, Wittig B, Kneipp K, The Journal of Physical Chemistry C, 2010, **114**, 7421-7426.
37. Bonnier F, Mehmood A, Knief P, Meade AD, Hornebeck W, Lambkin H, Flynn K, McDonagh V, Healy C, Lee TC, Lyng FM, Byrne HJ, Journal of Raman Spectroscopy, 2011, **42**, 888-896.
38. Bonnier F, Knief P, Lim B, Meade AD, Dorney J, Bhattacharya K, Lyng FM, Byrne HJ, Analyst, 2010, **135**, 3169-3177.
39. MacQueen JB.in Proceedings of 5-th Berkeley Symposium on Mathematical Statistics and Probability, Berkeley, University of California Press, 1967,1, 281-297
40. Varmuza K. 2009. Introduction to multivariate statistical analysis in chemometrics. New york: CRC Press.

41. Ryman-Rasmussen JP, Riviere JE, Monteiro-Riviere NA, J Invest Dermatol, 2006, **127**, 143-153.
42. Nel AE, Madler L, Velegol D, Xia T, Hoek EMV, Somasundaran P, Klaessig F, Castranova V, Thompson M, Nat Mater, 2009, **8**, 543-557.
43. Draux F, Gobinet C, Sule-Suso J, Trussardi A, Manfait M, Jeannesson P, Sockalingum GD, Anal Bioanal Chem, 2010, **397**, 2727-2737.
44. Mariani MM, Lampen P, Popp J, Wood BR, Deckert V, Analyst, 2009, **134**, 1154-1161.
45. Miljkovic M, Chernenko T, Romeo MJ, Bird B, Matthaus C, Diem M, Analyst, 2010, **135**, 2002-2013.
46. Nawaz H, Bonnier F, Knief P, Howe O, Lyng FM, Meade AD, Byrne HJ, Analyst, 2010, **135**, 3070-3076.
47. Bonnier F, Meade AD, Merzha S, Knief P, Bhattacharya K, Lyng FM, Byrne HJ, Analyst, 2010, **135**, 1697-1703.
48. Bonnier F, Byrne HJ, Analyst, 2012, **137**, 322-332.
49. Chang MY, Shiau AL, Chen YH, Chang CJ, Chen HH, Wu CL, Cancer Sci, 2008, **99**, 1479-1484.

7S Supplementary Information

7S.1 Physico Chemical Characterisation of the Nanoparticles

Physico-chemical characterization of the particles was performed by dynamic light scattering using a Malvern Zetasizer ZS. A HeNe laser with a wavelength of 633nm and an avalanche photodiode detector, Q.E. >50% at 633nm at 173° (backscatter detection) was used. Particle size measurements and zeta potential measurements were carried out in the respective biological media at a concentration of $1x10^{12}$ particles per ml at 37° C. The number of particles per ml of suspension may be determined from the following equation, as specified by the supplier:

$$\text{Number of particles/ ml} = \frac{6C \times 10^{12}}{\rho \times \pi \times \Phi}$$

Where: C = Concentration of suspended beads in g/ml

ρ = Density of polymer in g/ml

Φ = Diameter of suspended particles in μm.

The size and zeta potential of both the nominally 50nm and 100nm sized particles differed slightly according to the medium in which they were suspended, when measured by dynamic light scattering. Nominally 50 nm particles were found to have an average particle size in H_2O at 25°C and 37°C of 52 nm and 53 nm, respectively, while 50nm particles in 10% FBS RPMI media at 25°C and 37°C were determined to have particle sizes of 49 nm and 38 nm respectively. The average particle sizes for the 100nm samples in H_2O at 25°C and 37°C were found to be 169nm and 138nm respectively, while average particle sizes for 100nm samples measured in medium at

25°C and 37°C were found to be 149nm and 116nm respectively. Zeta potential measurements of the 50nm samples revealed that particles dispersed in H_2O at 25°C and 37°C were found to be -62 mV and -53 mV respectively, and in media at 25°C and 37°C to be -13 mV and -12 mV indicating that the solution was moderately stable at the temperatures measured. 100nm particles were found to have zeta potential values, in H_2O at 25°C and 37°C, of -18.62 mV and -15.09 mV respectively. Similarly, zeta potential measurements of 100nm particles in H_2O at 25°C and 37°C were found to have values of -42.32 mV and -38.27 mV respectively, also indicating the solution was moderately stable at both temperatures. Changes in zeta potential between H_2O and cell culture medium are well documented and are proposed to result from the interaction of the nanoparticle surface with the molecular components of the cell culture medium [1]. Despite the uncertainty in the exact nanoparticle sizes, for the purpose of brevity, the nanoparticles will be referred to as 50nm and 100nm particles throughout the manuscript.

7S.2 Cytotoxicity Assays

The cytotoxicity assays employed during this experiment were Alamar Blue™ (AB), Neutral Red (NR), Coomassie Blue (CB) and 3-(4,5-dimethylthiazol-2-yl)-2,5-diphenyltetrazolium bromide (MTT). For cytotoxicity evaluation, cells were seeded in 96-well micro plates (Nunc, Denmark) in triplicate for each of the four time points studied 24, 48, 72, 96 hr. Plates were seeded at a density of 1.5×10^5 cells/ml for 24hr, 5×10^4 cells/ml for 48hr, 3×10^4 cells/ml for 72hr and 2×10^4 cells/ml for 96hr exposure. These densities were found to be optimal to achieve the desired confluence at the end of the exposure period. After an initial 24hr of cell attachment, the media was removed and the plates were washed with 100 µl/well phosphate buffered saline (PBS). Cells were then treated with increasing concentrations of each

nanomaterial and with a positive control of a 10% DMSO 90% media solution. The cells were then incubated for the desired time period and the cytotoxic effects evaluated. For each independent experiment, six replicate wells were used for control, six replicate wells were employed for the positive control and six replicate wells were used for each test concentration per micro plate. For cytotoxicity evaluation, fluorescence and absorbance were all quantified using a microplate reader (TECAN GENios, Grodig, Austria). Further details for each of the assays performed can be found in [2].

For all assays employed, at all time points, no significant cytotoxicity was observed over the concentration range employed for both 50 and 100 nm polystyrene nanoparticles. As an example, Figure 7S.1 shows the MTT response to exposure of 50nm polystyrene nanoparticles. The observations are consistent with previous reports of exposure to neutral nanoparticles [3] and indicate that the labelling of the nanoparticles with the fluorescent moiety does not impact significantly on the toxic response.

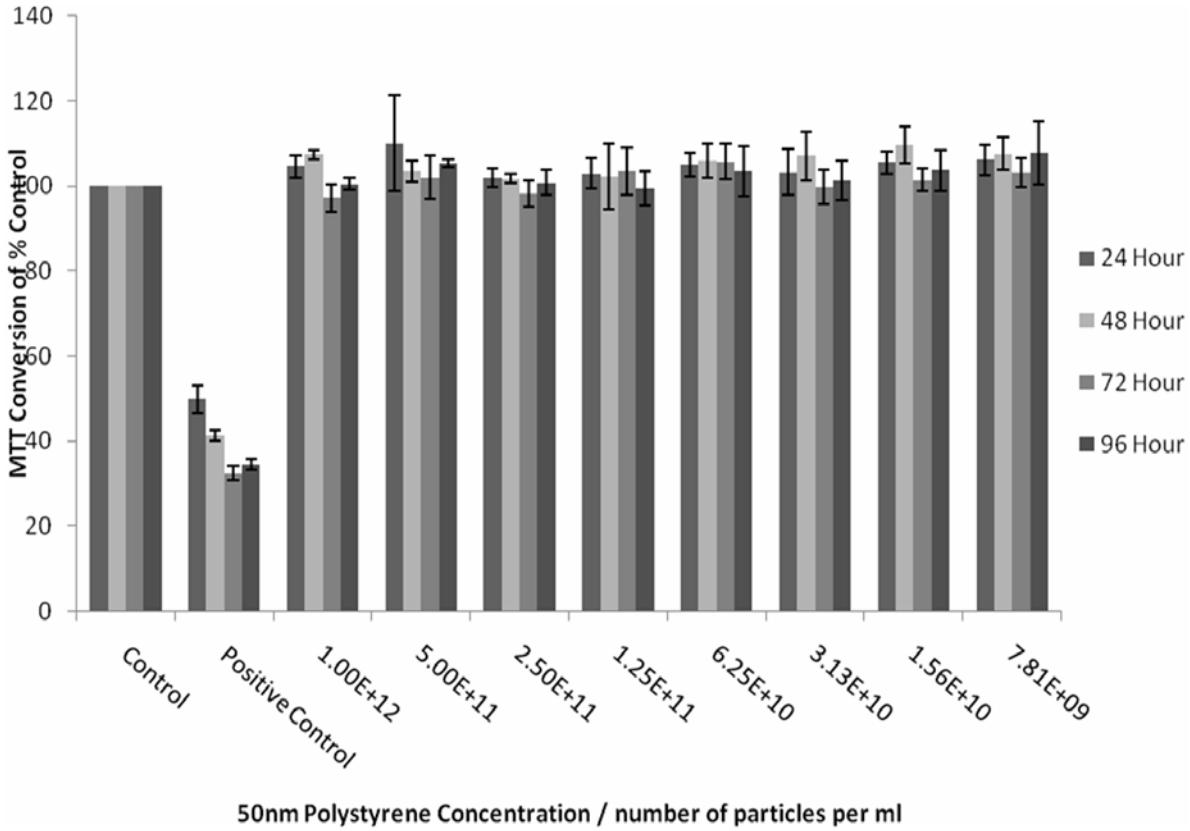

Figure 7S.1: Cytotoxicity of 50nm Duke Scientific Nanopolystyrene after 24, 48, 72 and 96 hour exposures determined by the MTT assay. Data are expressed as percent of control mean ± SD of three independent experiments.

7S.3 Sample Preparation and Cell Morphology

When working with A549 cells, the first observation made was the inconsistency of the cell morphology while preparing the samples. The cells were seeded on CaF_2 substrates, left overnight in the incubator and used for Raman analysis the next day for both live cell and fixed cell analysis. The protocols used were standard, but still the cells could exhibit particular characteristics and “stressed” samples seemed to be regularly observed. The main characteristic of these cells was the presence of microscopic “droplets” (~1-5 μm) in the cytoplasm. Their number was seen to vary considerably from sample to sample and thus the ability to resolve different

structures present in the cytoplasm varied significantly. This phenomenon is independent of the cell fixation using formalin as the features can be seen in both live cells (figure 7S2.A) and fixed cells (figure 7S2.B). The droplets are observed to exhibit consistent Raman spectra which vary little in fixed (figure 7S2.D) compared to live cells (figure 7S2.C), and comparison with spectra of common lipids such as phosphatydylinositol (figure 7S2.E) and phosphatydyl-L-serine (figure 7S2.E) confirms that they are lipidic in structure, an obvious candidate being peroxisomes. Regardless of their origin, the main concern was the strong Raman scattering of these droplets and therefore the probable interference with the detection of nanoparticles in the cells. It was therefore deemed imperative to optimize the protocols for the cell sample preparation and to reproducibly obtain cells with similar morphologies.

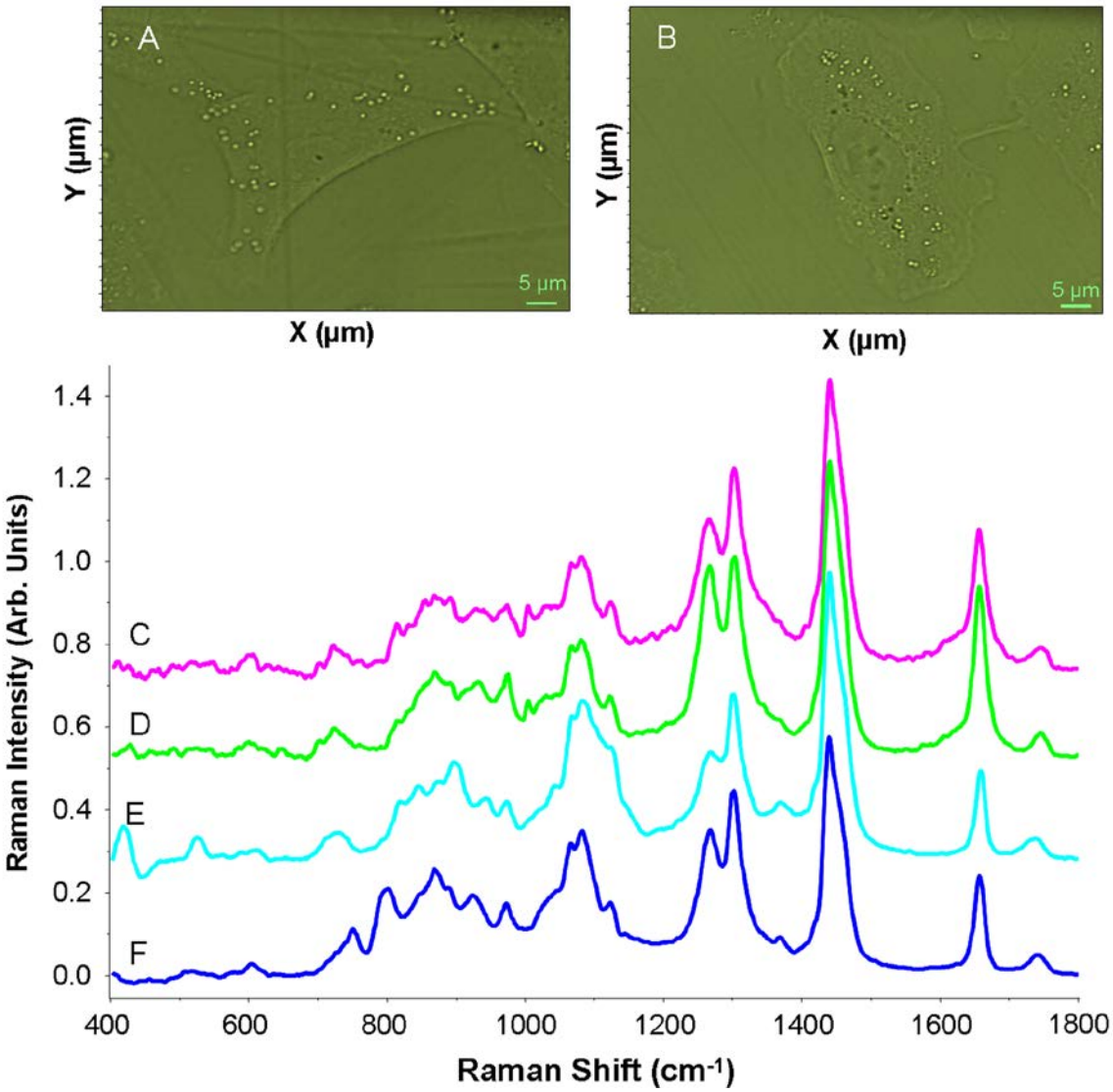

Figure S2 Microscopic images of live (A) and formaline fixed (B) A549 cells with "stressed" morphologies. Raman Spectra of droplets in (C) live cells (D) fixed cells compared to (E) phosphatidylinositol and (F) Phosphatidyl-L-serine. Spectra are offset for clarity

Different parameters have to be taken into consideration during the cell culture and the preparation of the samples. The cells are commonly split when they have reached between 80-85% of confluency in the cell culture flasks. However, performing a splitting when the cells were only about 60% confluent greatly diminished the number of the droplets per cell. Under such conditions, after several

splits, almost no droplets can be seen in cells either in the cell growth flasks or on the substrates used for confocal imaging or Raman mapping. Subsequently, the temperature of the PBS solution used to wash the cells has to be 37 °C, and it was further noted that the quality of the fixation can be affected by the temperature of the formalin used. Although, the formalin is usually kept at room temperature, warming to 37 °C before fixation showed a better conservation of the cell morphology after fixation. Once the sample preparation procedures have been optimised, cells of consistently “unstressed” morphology can be routinely obtained, as shown in Figure 7S3. Fewer vacuoles or lipid droplets are evident, and there is a better definition of the endoplasmic reticulum (marked with arrows in figure 7S3).

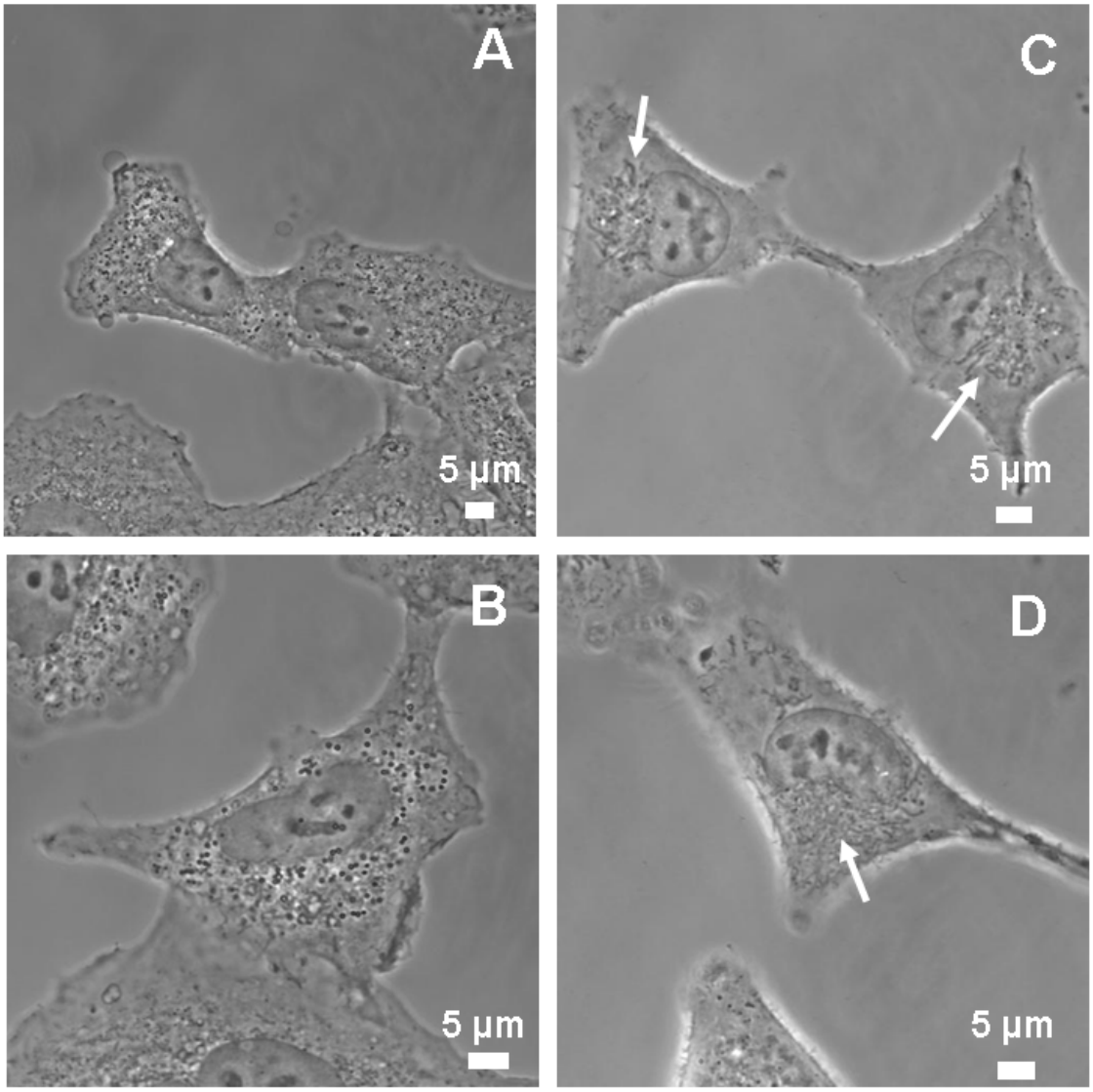

Figure 7S3 Microscopic images of cells with “stressed” (A, B) and “unstressed” morphology (C, D).

7S.4Effect of Cell Fixation on Raman Spectra

Mapping of single cells using Raman spectroscopy can be time consuming and, depending on the quality of spectra required, many hours are usually needed to complete a single map. As the viability of cells removed from an incubation environment is compromised, fixation of cells remains a popular option for extended measurements. Different approaches to fixation can be employed, including dry

fixation, alcohol fixation or formalin fixation. These different methods have been recently compared by Raman spectroscopy [4-6]. In order to preserve the cell morphology, dry fixation has been excluded for this study, as the modification in the cell shape and thickness due to the drying will make comparison with live cells difficult. Formalin fixation is the more promising approach, as the cells are maintained in a hydrated state and, therefore, as close as possible to the living state [4]. Based on the observations made above, the protocols for cell fixation were optimised and the sample preparation standardised. Under these conditions, the localisation of the different subcellular organelles can be precisely visualised and Raman spectra recorded from similar structures more accurately. Figure 7S4 presents spectra recorded from the nucleus and cytoplasm from live and formalin fixed cells. The spectra exhibit similar intensities and no contribution from the CaF_2 substrate can be seen. The spectral signatures obtained after fixation using formalin are identical to those recorded from the live cells. Using adapted protocols for the cell culture and fixation, the effect of the fixatives used can be greatly reduced.

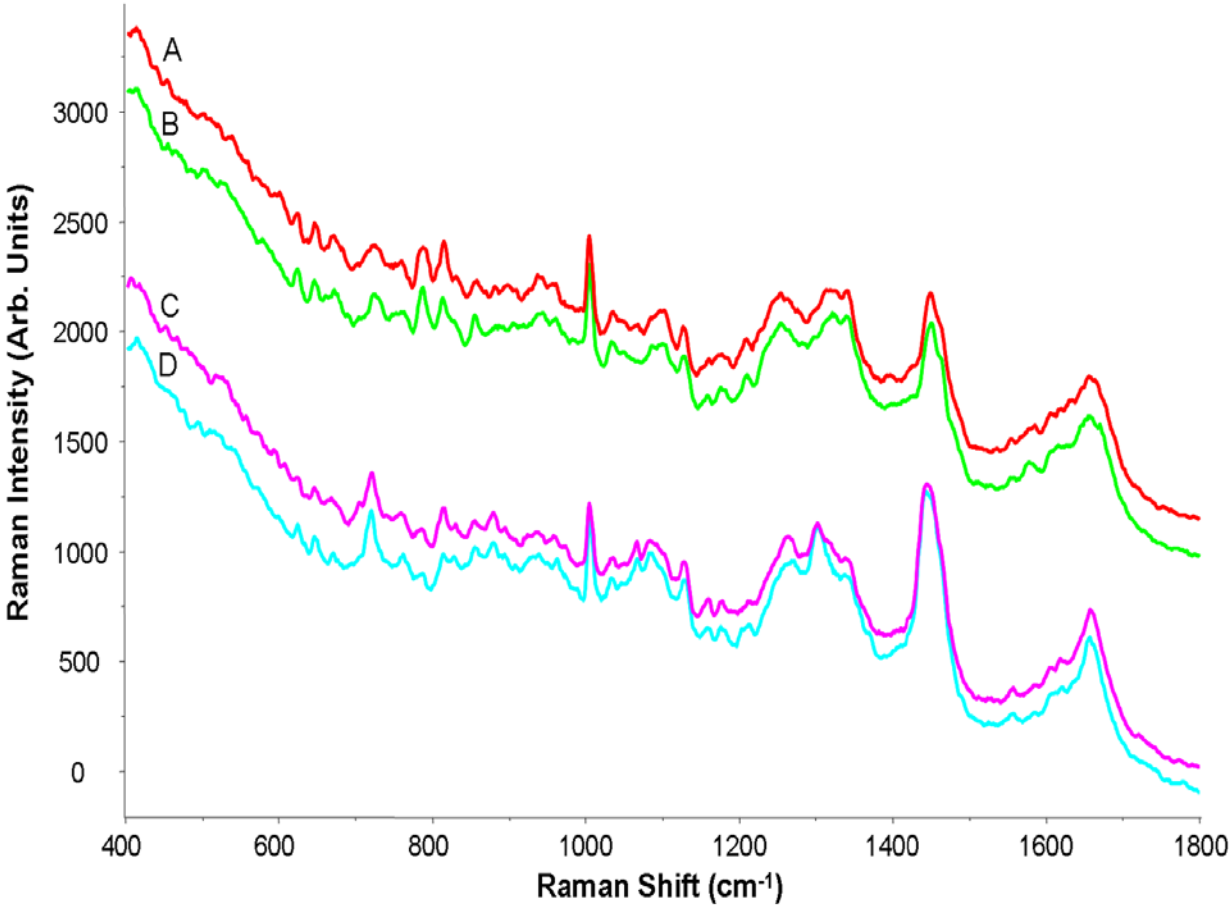

Figure S4 Raman spectra of the nuclear region of fixed (A) and live (B) cells and the cytoplasmic region of fixed (C) and live (D) cells. All Spectra have been recorded using the 785 nm laser source and are the result of two accumulations of 20 seconds per spot. Spectra are offset for clarity

Bibliography:

1. Lundqvist M, Stigler J, Elia G, Lynch I, Cedervall T, Dawson KA, Proceedings of the National Academy of Sciences, 2008, **105**, 14265-14270.
2. Davoren M, Herzog E, Casey A, Cottineau B, Chambers G, Byrne HJ, Lyng FM, Toxicology in Vitro, 2007, **21**, 438-448.
3. Ryman-Rasmussen JP, Riviere JE, Monteiro-Riviere NA, J Invest Dermatol, 2006, **127**, 143-153.
4. Meade A, Clarke C, Draux F, Sockalingum G, Manfait M, Lyng F, Byrne HJ, Analytical and Bioanalytical Chemistry, 2010, **396**, 1781-1791.
5. Draux F, Gobinet C, Sule-Suso J, Trussardi A, Manfait M, Jeannesson P, Sockalingum GD, Anal Bioanal Chem, 2010, **397**, 2727-2737.
6. Mariani MM, Lampen P, Popp J, Wood BR, Deckert V, Analyst, 2009, **134**, 1154-1161.

Chapter 8

Discussion and Conclusions

8.1 Summary of Findings

Over the course of this thesis, several different commercially available nanopolystyrene particles of different sizes and surface charges were examined. The nanoparticles chosen were; 40nm and 100nm carboxylated Invitrogen nanopolystyrene, 60nm aminated nanopolystyrene (UCD) and, 50nm and 100nm Duke Scientific (now Thermo Scientific) neutral nanopolystyrene.

In Chapter 4, the results of the characterisation of 40nm and 100nm carboxylated nanopolystyrene, 50nm and 100nm nanopolystyrene, and 60nm aminated nanopolystyrene were presented. DLS investigation confirmed neutral and carboxylated nanoparticle sizes to increase in water, possibly due to the presence of surfactant, which would interfere with the measurement of the apparent hydrodynamic radius. However, all particles differed in size when placed in biological media. In particular, the 60nm aminated nanopolystyrene particle was found to significantly increase in size when placed in biological media, which may be attributed to the formation of a protein corona, which would have an effect on the apparent hydrodynamic radius and thus the measured particle size. Zeta potential measurements revealed that the 100nm and 40nm carboxylated particles were stable in biological media, which was most likely due to the interaction between the carboxylated surface of the nanoparticle and the ionic species found in the media. Both neutral particles, 50nm and 100nm, were found to be stable in H_2O over a range of temperatures and less stable when placed in biological media. However the “neutral” nanoparticles were found to have an overall negative zeta potential, which again, may possibly be attributed to the presence of surfactant within the aqueous solution. While zeta potential values showed the 60nm aminated nanoparticles to be unstable when placed in complete media. Absorbance and fluorescence emission

spectroscopy revealed values which were also in agreement with the supplied manufacturer's specifications. From fluorescence emission spectra obtained of both 50nm and 40nm particles, a working concentration of 1 x 10^{12} ppml was chosen, as this concentration revealed optimum fluorescence.

The results obtained and presented in Chapter 5, of the toxicity of 50nm and 100nm Duke Scientific nanopolystyrene, 40nm and 100nm carboxylated Invitrogen nanopolystyrene and 60nm aminated nanopolystyrene, were much in keeping with literature findings on the toxicity of nanopolystyrene. Five toxicity assays were employed, with experimental results presented for each. The cytotoxicity evaluation revealed, through the use of Alamar Blue™ (AB), Neutral Red (NR), Coomassie Blue (COOMASSIE) and 3-(4,5-dimethylthiazol-2-yl)-2,5-diphenyltetrazolium bromide (MTT) assays, that the 50nm and 100nm neutral and the 40nm and 100nm carboxylated nanoparticles induced no cytotoxic effects in A549 cells over a range of concentration and time points. However, cytotoxicity results of A549 cells exposed to a range of concentration of 60nm aminated nanopolystyrene after 24, 48, 72 and 96 hour exposures, revealed, at some concentrations, that the particle does induce toxic effects in A549 cells. As observed throughout all assays performed, the highest test concentration of 1x10^{12} ppml induced toxic effects on A549 cells over the 24 to 96 hour exposure time points, the second highest test concentration of 5x10^{11} ppml causing toxicity to a lesser degree.

Chapter 6 presented the results obtained for the examination of the internalisation of 50nm and 100nm nanopolystyrene and 40nm and 100nm carboxylated nanopolystyrene within A549 lung cells through the use of confocal microscopy. Fluorescent and optical images revealed 40nm and 100nm carboxylated nanoparticles were taken up by cells and accumulated into cellular organelles, which

resembled lysosomes, after exposure times of 24hours. 50nm and 100nm Duke Scientific nanopolystyrene were observed to be rapidly taken up by cells and accumulate within cell organelles after 1 hour exposure to A549 cells. 50nm particles also appeared to be contained within organelle membranes. However, after longer exposure times of 24 hours, the dispersion of the fluorescence within the cell was widely distributed throughout the cell.

From the z- stack image series of the cells, it was revealed that neither 40nm carboxylated or 50nm neutral nanoparticles were found in the nucleus. The generated orthogonal projection obtained by combining “z-stack” image series cutting through the cell in single z-steps of approximately 10 µm width, confirmed the absence of 40nm carboxylated and 50nm neutral particles from the nucleus.

Confocal images revealed that there was a difference in the degree and dispersion of fluorescence between the different neutral and carboxylated nanoparticles, potentially due to their different physiochemical characteristics. Cellular up-take and migration times through the cell were observed to be slower for the carboxylated 40nm and 100nm particles. It was suggested the 50nm and 100nm neutral nanoparticles may be taken up by cells through a less energy dependant mechanism such as diffusion. However, the possibility of free dye uptake from 50nm and 100nm Duke Scientific nanoparticles could also not be ruled out. The diffusion of free dye into cells was suggested as the reason as to why 50nm and 100nm neutral particles “appear” to be taken up faster and the observation that the fluorescence within the cell was distributed to a greater extent, rather than contained within isolated organelles.

From the confocal images obtained of all nanoparticles, it was concluded that three possible cell organelles may have been targeted by nanoparticles; lysosomes, mitochondria and endoplasmic reticulum. The first cell organelle examined for accumulation of nanoparticles was the lysosomes. From the confocal images obtained, it was revealed that carboxylated nanoparticles, 40nm and 100nm respectively, were internalised by cells and accumulated within lysosomes. These results are in keeping with literature reports that nanoparticles are endocytosed and that early stage endosomes evolve into lysosmes [1, 2] The internalisation of 40nm and 100nm carboxylated within mitochondria was examined next. As was revealed by the fluorescence overlap images, carboxylated nanoparticles were not seen to be specifically internalised within mitochondria. Similarly, 40nm and 100nm carboxylated nanoparticles were not found to be internalised within the endoplasmic reticulum upon examination of the fluorescent overlap images obtained.

The examination of fluorescent overlap images obtained for the investigation of neutral nanoparticles internalised within lysosmes revealed that both the 50nm and 100nm nanoparticles have a large fluorescent distribution and appear to have been internalised within lysosomes. However, the issue of the degree fluorescence distribution throughout the cell was raised once again. Fluorescently transduced mitochondria were also seen to have internalised 50nm and 100nm nanoparticles. The images obtained show a large degree of fluorescence overlap between the 50 and 100nm particles and the fluorescently tranduced mitochondria. The examination of the internalisation of the neutral nanoparticles within the endoplasmic reticulum also revealed a large fluorescence overlap between 50nm and 100nm and the fluorescently tranduced endoplasmic reticulum. However, once again the issue of possible free or liable dye was raised as the fluorescence distribution of the

nanoparticles was questionable. While the results obtained for the internalisation of 50nm and 100nm neutral nanoparticles are in keeping with literature reports, the overall fluorescence distribution required further investigation.

Although 50nm and 100nm neutral nanoparticles were visually confirmed to have penetrated cell membranes and have internalised within cells and cell organelles through the use of confocal microscopy, the issues raised about the concerns of fluorescent dye leakage from the particles were addressed through the energy dependent uptake study. Quenching the cellular energy revealed that the actual distribution of nanoparticles may be very different to the images obtained of fluorescently labelled nanoparticles. 40nm carboxylated nanoparticles and 50nm neutral nanoparticles were exposed to A549 cells which had been incubated at 4°C. Because cells are “inactive” at 4°C, only passive diffusion of substances through the cell membrane may occur, as this requires no energy from the cell. At 4°C, 40nm carboxylated nanoparticles were not found to have diffused through the cell membrane. Particles were observed to “sit” on top of the cell membrane, but were not internalised within cells. However, cells incubated at 4°C which were exposed to 50nm neutral nanopolystyrene particles were found have exhibit internal fluorescence, indicating that free or liable molecular dye from the nanoparticles had diffused through the cell membrane into the cells. The results obtained in the energy dependent uptake study revealed that fluorescently labelled nanoparticles produced from different manufacturers exhibit different characteristics, with dye leakage a possible factor which impacts on fluorescent imaging results.

While the issue of possible fluorescent dye leakage from nanoparticles was addressed in the energy dependent uptake study, the question was then raised as to whether nanopolystyrene was actually entering the cell. Raman spectroscopy was

then proposed to identify and locate nanoparticles in cells. Chapter 7 was adapted from the published paper **"Identifying and Localising Intracellular Nanoparticles Using Raman Spectroscopy".** The fixation process of cells was examined and was shown to have negligible effect on the Raman spectra of A549 cells exposed to nanopolystyrene particles. The results of K-means cluster analysis of Raman maps of the cells confirmed that 50nm neutral nanopolystyrene particles were in fact internalised and are predominantly localised within the cytoplasmic region and the endoplasmic reticulum region. Several spectra in these regions were dominated by the sharp and strong peak of the polystyrene phenyl group. Principal components analysis of several of the K-means clusters revealed that the nanopolystyrene particles were located in a lipidic rich environment, such as that of the ER. This study demonstrated the ability of Raman microspectroscopy to locate and identify nanoparticles in the subcellular environment, based on their chemical structure. The results obtained also indicated that the technique can be employed to identify the subcellular environment.

8.2 Future perspectives

With the number of engineered nanoparticles being produced annually having risen to an estimated 11 million tonnes, [3] the need for toxicological information about these novel materials is of utmost importance for both general health and safety of the public who may come in contact with these material and also for the ecological impact that such materials may have on our environment. The potential use of nanoparticles within various areas of science and engineering is boundless. However, in order for nanoparticles to fulfil their full potential in areas such as nanomedicine, nano-drug delivery, etc., it is imperative that a full risk assessment profile of nanoparticles first be constructed. While the continual research in this area

should focus predominately on the building of toxicological profiles of nanomaterials, there are some other issues which need to be addressed.

The development of additional toxicological assays which are specifically designed with nanoparticle testing in mind, to accompany traditional assays, is an area that should be fully explored. Regardless of the toxicity of nanoparticles, the capability of these materials to penetrate cell membranes and cell organelle membranes raises many questions about the potential long term effects of the accumulation of nanoparticles within cells, as well as raising questions as to their potential use in drug delivery and nanomedicine.

Commercially manufactured nanoparticles, specifically those containing fluorescent labels, may be unreliable when using conventional methods of monitoring fluorescent materials, such as confocal microscopy. Ideally, label free methods to locate nanoparticles, probe their local environment and the overall effects on the cell should be investigated. From the work produced in this thesis, Raman spectroscopy is one such proposed method. The capability of Raman spectroscopy to not only locate nanoparticles within cells, but also to probe the local environment of the nanoparticle and the ability of detect any changes in the local environment or within the cell, offers a label free method for the tracking of nanoparticles within cells and the monitoring of the internalisation of nanoparticles within cell organelles.

While in this thesis, spontaneous Raman spectroscopy was proposed as a label free method for the monitoring of nanoparticles within cells, there are other forms or Raman spectroscopy which may potentially add to the list of label free methods. Surface Enhanced Raman Spectroscopy or SERS is one such possible method. The enhancement process of Raman intensities can be achieved using a number of

substrates including roughened metallic surfaces, structured metal arrays and specially imprinted surfaces. The effect has largely been attributed to an electronic enhancement due to local fields generated by surface plasmon resonances at the metal surface. SERS has been applied to many different applications including a number of biological scenarios, which include diagnostic studies *in vitro*, *ex-vivo* and *in-vivo* [4] [5] [6] , novel bio assay as well as cellular studies [7] . The proposal of SERS to probe the chemical nature of the subcellular environment and the intracellular distribution of biomolecules also makes it an ideal method for the investigation of nanoparticle internalisation within cells [8] [6].

Coherent anti-Stokes Raman spectroscopy or CARS is also another method proposed for the monitoring of internalisation and localisation of nanoparticles within cells. CARS employs two laser beams, which are used to generate a coherent anti-Stokes frequency beam. The anti-Stokes signal can be then enhanced by resonance. CARS allows the enhancement of the weak Raman signal by means of nonlinear excitation, enabling imaging to speed up to video rate. The nonlinear CARS signal is generated only at the focus where the excitation intensities are the highest. This leads to 3D sectioning capability, which is essential for imaging cells and cellular structures. CARS has notably been used for the monitoring of intracellular trafficking, drug delivery, as well as nanoparticle uptake by living organisms. With promising results, CARS is another viable potential method for the investigation of internalised nanoparticles within cells.

Raman spectroscopic methods hold the potential to supply nanotoxicologists with intracellular and environmental information about the interaction of nanoparticles with cells, but areas such as proteomics should also be investigated to give a complete understanding of nano-bio interactions. Spectroscopic and proteomic data could feed

directly into the development of a risk assessment method for nano-safety, as well as helping to validate alternative toxicity screening methodologies which could reduce the cost and complexity of nanoparticle safety screening, reducing the reliance on animal tests and enabling high-throughput screens to emerge.

8.3 Concluding Remarks

Over the course of this thesis, the reliability of commercially manufactured fluorescently labelled nanopolystyrene was questioned. Fluorescently labelled nanoparticles from one manufacturer were shown to contain free or liable dye which inhibited the accuracy of localisation results using conventional fluorescent microscopy methods. Raman spectroscopic analysis revealed that there was a significant difference between the apparent fluorescence distribution of nanoparticles and the actual distribution of nanoparticles within cells. It is concluded that liable dye within commercially manufactured nanoparticles can in fact hinder the monitoring of nanoparticle trafficking within cells.

The results presented have raised a very important question; as to whether fluorescently labelling of nanoparticles reliable for correct, accurate intercellular monitoring and trafficking of nanoparticles within cells? Furthermore, can conventional fluorescent microscopic techniques be relied upon for the most accurate and reproducible data needed by nanotoxicologists to build the necessary toxicological profile required for the safe us of these novel materials?

The answer to these questions, undoubtedly, like nanotoxicology, is complicated. It is the general consensus of researchers in the field of nanotoxicology, that if it is to move forward as a discipline and reach the overall goal of providing reliable toxicological data on the ever increasing range of engineered nanoparticles then it

will rely heavily on the collaboration of materials and biological scientists. Collaborations of this manner will facilitate all the contributing factors to nanoparticle toxicity, from both physical/chemical and biological viewpoints, to be identified and classified in order of toxicological relevance. Nanotoxicology does not necessitate a new toxicological science as such, but it does demand the communication between different disciplines of science as was seen throughout his thesis which employed both physical/chemical and biological techniques to assess the internalisation of nanopolystyrene particles.

References

1. Clift, M.J.D., et al., *The impact of different nanoparticle surface chemistry and size on uptake and toxicity in a murine macrophage cell line.* Toxicology and Applied Pharmacology, 2008. **232**(3): p. 418-427.
2. Rejman, J., et al., *Size-dependent internalization of particles via the pathways of clathrin- and caveolae-mediated endocytosis.* Biochem. J., 2004. **377**(1): p. 159-169.
3. Commission, E., *http://europa.eu/rapid/press-release_MEMO-12-732_en.htm#PR_metaPressRelease_bottom*. 2012.
4. O'Neal, D.P., et al. *Surface-enhanced Raman spectroscopy for the in-vitro and ex-vivo detection of excitatory amino acids*. 1999.
5. Yigit, M.V. and Z. Medarova, *In vivo and ex vivo applications of gold nanoparticles for biomedical SERS imagingi.* Am J Nucl Med Mol Imaging, 2012. **2**(2): p. 232-41.
6. Kneipp, J., et al., *In Vivo Molecular Probing of Cellular Compartments with Gold Nanoparticles and Nanoaggregates.* Nano Letters, 2006. **6**(10): p. 2225-2231.
7. Schlücker, S., *SERS Microscopy: Nanoparticle Probes and Biomedical Applications.* ChemPhysChem, 2009. **10**(9-10): p. 1344-1354.
8. Kneipp, J., et al., *Novel optical nanosensors for probing and imaging live cells.* Nanomedicine: Nanotechnology, Biology and Medicine, 2010. **6**(2): p. 214-226.